DISCRETE PARTICLE SIMULATION OF SOLID SEPARATION IN A JIGGING DEVICE

Stephen VIDUKA

A thesis submitted in the fulfilment of the requirements
for the degree of Doctor of Philosophy

Monash Advanced Particle Engineering Laboratory
Department of Chemical Engineering
Faculty of Engineering
Monash University

CSIRO Mathematics, Informatics, and Statistics
The Commonwealth Scientific and Industrial Research Organisation

November 2012

CERTIFICATE OF ORIGINALITY

I hereby declare this submission is my own work and that, to the best of my knowledge it contains no materials previously published or written by another person,, nor material which to a substantial extent has been accepted for the award of any other degree of diploma at Monash University or any other educational institution, except where due acknowledgement is made in the thesis. Any contribution made to the research by others, with whom I have worked with at Monash University or elsewhere, is explicitly acknowledged in the thesis.

I also declare that the intellectual content of this thesis is the product of my own work, except to the extent of assistance from others in the project's design and conception, or in style, presentation and linguistic expression which is duly acknowledged.

Stephen Viduka

(Signed) _____.

ABSTRACT

This project presents a numerical study of solid separation in a jigging device, which is a high yield and high recovery gravity separation device widely used in ore processing. The mathematical model adopted is a combination of computational fluid dynamics (CFD) for the liquid flow and discrete element method (DEM) for particle motion.

In the numerical model the motion of individual particles is 3 dimensional (3D) and the flow of continuous liquid is 2 dimensional (2D), considering the bed thickness is $1/3^{rd}$ of the bed width, and one CFD computational cell is used through the thickness. Periodic boundary conditions are applied on the front and rear walls to emulate a bed of larger thickness using a relatively small number of particles. The initial packing conditions consist of a binary-density particle system where the light particles and heavy particles, have respective densities of 2540 (glass) and 4630 (ceramic) kg/m^3. There are 1130 particles each 1 cm in diameter.

A comparison between numerical and physical experiments was conducted, and particle fluid interaction forces were examined. The importance of various particle fluid interaction forces were analysed in order to elucidate their influences on the bulk behaviour of the particle system. The lubrication, Magnus, Saffman, virtual mass, and inertial forces are investigated, and quantitatively compared to the drag force which is assumed dominant in the system.

Stratification is heavily dependent on fluid motion through the jig. The study explores 5 different pulsation profiles. The profiles studied include: sinusoidal, triangular, sawtooth-backward, sawtooth-forward, and trapezoidal. As an initial comparison, all simulations are conducted using a fixed peak-peak amplitude and pulsation period. Their relative performances are compared in terms of solid flow patterns, separation kinetics, energy, mean particle position, coordination number, and concentration profile. The underlying mechanisms are explained in terms of particle-fluid interaction force. These quantitative comparisons demonstrate significant differences

in the segregation rate and energy used for various pulsation profiles. An extensive understanding is developed of internal processes in jigging.

Further, a parametric study is conducted using variations in jigging cycle frequency and amplitude with particular consideration to boundaries of operation. Quantitative comparisons demonstrate significant differences in separation time, concentration mechanics, and energy consumption over varying parameters, and find different particle flow phenomena at the operational limits. This study has raised awareness for potential improvement and hence optimisation of jigging. Details of two separate methods to reduce segregation time and energy used per cycle are explained.

Finally, given insight by means of the numerical model two original propositions are made for the future operation and design of jigs. These include an operational method of reducing energy consumption per jigging cycle. In addition to a novel jig design mechanically capable of executing an alternative optimum jigging profile.

ACKNOWLEDGEMENTS

This work was carried out under the supervision of Dr. Yuqing Feng, Assoc. Prof. Karen Hapgood, and Dr. Phil Schwarz. They have added considerable expertise and experience to the project. I would also like to acknowledge the members of the CMIS Fluids Process Modelling research group, past and present, for providing helpful discussions and a pleasant study environment. Finally, I thank the Australian government and CSIRO Office of the Chief Executive (OCE) for providing funds for this postgraduate scholarship.

TABLE OF CONTENTS

LIST OF FIGURES

CHAPTER 4

CHAPTER 5

LIST OF TABLES

CHAPTER 1

INTRODUCTION

The Australian minerals industry is integral to the nation's economy contributing 8% percent to the gross domestic product (GDP) in 2007–08 and 51.4% to the total value of exports from 2008–09 (ABS, 2010). The mineral process of jigging is a method of gravity separating and is one important type of many mineral processing techniques. A diaphragm type jig (the Pan-American Placer) is shown in Figure 1–1.

Figure 1–1. Pan-American Placer.

Jigging is a gravity separation method commonly used by the minerals industry to separate coal, iron ore, diamonds and other minerals on the basis of particle size and/or density. Jigging units characteristically dilate the particle bed by an upward blast of water and particles of different size and densities settle at different velocities. By repeating this operation particles will segregate and eventually meet product requirements. Jig separation is one of the oldest methods of gravity separation and is still widely used owing to its high separation precision, easy maintenance, cost-effectiveness and high throughput rate (Kelly and Spottiswood, 1982; Wills, 1992).

Much of the published research performed in jigging has been experimental. Commercial jigs date back as far as the Neil Jig (1914) (Burt, 1984); and the first reported jigging device for the beneficiation of metal ores was used in the 1560s (Agricola, 1950). It is reasonable to assume many jigs historically were designed principally with the aid of experiments and also analytical expressions in the absence of computational capabilities. Past experimental techniques have involved full scale, currently out-of-date, or bench scale jigs. While experiments help understand how the feed material macroscopically responds to various operating conditions e.g. amplitude, feed characteristics, frequency of pulsation, and hutch water flow, they do

not elucidate on the intricate transient behaviour of both fluid and particles. The key to better stratification of particles lies with the understanding gained by analysing particle scale information, e.g. solid flow patterns and mixing kinetics, which in turn control the bulk behaviour of the system.

Modern investigations of jigging phenomena using numerical simulation techniques has shown to be a fast growing area. Various modelling techniques implemented have included: single phase computational fluid dynamics (CFD), discrete element model (DEM) coupled with simplified fluid models, and the Lagrange-Euler (DEM-CFD) model. Other notable models used to investigate jigging include Potential energy, Potential energy-Monte Carlo, Artificial Neural Network (ANN), Statistical, and Unsteady-fluidisation. Possible future numerical techniques capable of jigging simulation which have not been used are Direct Numerical Simulation-DEM, and Lattice Boltzmann-DEM. Among the models mentioned, the DEM-CFD approach remains the most attractive due to its ability to capture particle scale information while requiring less computing facilities.

This project proposes to build on the current knowledge of wet jigging using a DEM-CFD model to establish further understanding, optimisation, and a new design/operation approach for jigging. In the literature it is found that experimental validation has been performed on a combined DEM and simplified fluid model. However, discrepancies between the numerical and experimental results exist. Further, a one-way coupled DEM-CFD model without consideration of the numerous non-drag forces present in this system has been used for experimental validation for a single ‘base’ case. Qualitatively the results are comparable although differences of up to 30% are present. It is unknown how this model compares with empirical data in multiple scenarios. This thesis seeks to improve validation by using a two-way coupled DEM-CFD jigging model and including relevant particle fluid forces. In addition, no numerical modelling studies have investigated how the jigging inlet velocity profiles such as sinusoidal or sawtooth compare in terms of jigging performance and the reasons behind this. This study will delve into evaluating numerous jigging profiles.

Chapter 2 gives a review on the minerals industry, jigging, previous work in this area, together with DEM-CFD and relevant particle physics theory. A brief introduction on the importance of the minerals industry to the world and in particular Australia is made in terms of modern society and economics. An introduction to jigging is presented together with an explanation of the principles of gravity separation and jigging theory. Jigging is one of the oldest methods of mineral processing; a thorough historical background on jigs is presented and the various types of jigs are explained. Jig design, operation and control systems are detailed. Previous studies on particle segregation behaviour using jigging are reviewed. Here both experimental and numerical techniques and studies are explored with a particular focus on DEM-CFD. Finally, DEM-CFD and particle motion in fluids theory is detailed.

Chapter 3 outlines the simulation method in this project; presents an experimental validation study; and examines particle fluid interaction forces present in jigging. Here the governing equations implemented in this project of both DEM and CFD are discussed along with the coupling scheme implemented. Simulation conditions are detailed explaining the approach used to model a jigging system; this includes boundary conditions, mesh topology, particle and fluid properties, and pulsation profiles. Simulation validity is sought using experimental data of a laboratory jig. Under comparable conditions, the experimental average bulk density values taken along the particle bed height are compared with simulation values. Lastly, non-drag particle fluid interaction forces are modelled and their relative importance are discussed.

In chapter 4, DEM-CFD modelling has been used to study the segregation behaviour of five pulsation profiles. This chapter presents a comparison study of the following pulsation profile shapes: sinusoidal, triangular, sawtooth-backward, sawtooth-forward and trapezoidal, respectively. All five profiles were compared by holding the shape and cycle periods (T) of 2 seconds (30 cycles/min) constant and using 3 variations of volumetric water input. These are 1.5, 2.25 and 3 litre water amplitudes. The amplitudes are represented in litres not distance as the water/air free surface is not resolved (i.e. the domain at anytime is completely filled with water), otherwise the amplitudes would be equivalent to 0.2, 0.3 and 0.4 cm. The particles were processed using 12 seconds of jigging. The initial packing conditions consist of a binary-density

particle system, where the light particles and heavy particles have respective densities of 2540 (glass) and 4630 (ceramic) kg/m^3. There are 1130 particles each 1 cm in diameter. A quantitative analysis is carried out for an extensive understanding of the process. Various useful data analysis methodologies are employed to achieve this goal including: population averaging of various quantities including both particle-fluid interaction and particle-particle forces; statistical distributions of particles such as mean particle positions and velocity, coordination numbers and concentration profiles; and additionally instantaneous values of pressure drop, power, and cumulative energy. It is shown that each profile displays different particle transport phenomena with varying degrees of either fluidization, slugging or complete transport. Significant differences are found in segregation rate and energy used across the variety of profiles. Moreover, an extensive understanding is developed of internal processes in jigging. It was found that the particle-fluid interaction force, porosity and expansion duration are key variables in achieving segregation and have an intricate relationship.

Chapter 5 presents a comprehensive comparison between the profile types, and a profile optimisation study. Here a further study is performed with variations in both amplitude and frequency values. The particles were processed using 60 seconds of jigging concluding with 1 second of settling after the last jigging cycle. The underlying separation mechanisms of jigging of the binary particle system were analysed for each profile shape and setting. The profile variants are compared to elucidate on differences in jigging performance using numerous quantitative criterions including: energy consumption, separation time, and cycle numbers. The study is subsequently extended to establish and investigate operational boundaries in terms of amplitude and frequency and concentration mechanics are investigated in these regions. The examination of profiles shapes in Chapter 4 and more so this chapter has raised awareness for potential improvement and hence optimisation of jigging. This chapter details two methods to reduce segregation time and energy used per cycle.

In chapter 6 design and operation recommendations are discussed. The results and information in previous chapters have given rise to insights and new ideas for jig operation and engineering design. Here novel methods along with practical

descriptions of jig control are established with an aim to reduce energy consumption and utilize the entire processing time by jig cycle modification.

Chapter 7 summarises the work in this thesis, highlights difficulties in the numerical modelling of jigging, and future research is proposed.

CHAPTER 2

LITERATURE REVIEW

2.1 AUSTRALIAN MINERALS INDUSTRY ECONOMICS

The world's minerals industry is critical for the quality of human life. It was estimated by the Minerals Information Institute (2011) that every American born will need 2.96 million pounds of minerals, metals, and fuels in a life time.

Australia is a modern trading nation which trades in a diverse range of high quality goods. Trade is a vital component in Australia's economic prosperity. The Australian minerals industry is in the top five producers of most of the world's key mineral commodities. The sector is integral to the nation's economy contributing 8% to the gross domestic product (GDP) in 2009–10. In the same period mining exports made up 48% of the total export value. A strong future is envisioned with a record $6 billion invested in 2008–09 on mineral exploration which is 116% higher than in 2004–05. (Minerals Council of Australia, 2010)

Australia's Minerals industry continues to grow. In 2008–09, merchandise exports increased 27% and minerals contributed to 27.2% of this growth. In this year four of the seven major commodity movements were minerals driven (including coal): the biggest driver coal (+123.6%, up 30.2 $Ab), second iron ore (+67.0%, up 13.7 $Ab), third natural gas (+72.3%, up 4.2 $Ab), forth gold (+40.2%, up 4.8 $Ab). (DFAT, 2009)

Breaking down the total exports in order of monetary contribution we quickly see the most economically influential minerals of 2009–10: coal & uranium $35.6 billion, iron ore $29 billion, other minerals $44.4 billion, mining services & equipment $2.5 billion, with a total of $111.5 billion. However, other ores are also very lucrative exports including: gold, alumina, copper, and nickel. (Minerals Council of Australia, 2010)

Another indicator of the importance of minerals to the Australian economy is the level of mining investment which continues to grow strongly in Australia. The minerals industry is a highly capital-intensive industry, between 2005–2010, capital expenditure rose 258%, and accounted for two-thirds of the increase in total new

private capital expenditure in the Australian industry (Minerals Council of Australia, 2011).

Given the large influence and strength of the Minerals industry in Australia it must be well equipped to take full advantage of the opportunities. This includes every stage of mining including: mineral exploration, deposit evaluation, mine planning, mine construction, operations, and mine closure. Of particular interest in this PhD thesis is the area of 'operations' and more specifically mineral processing.

Most ores require mineral processing by physical or chemical methods before they can be converted to useful metals or final mineral products. Mineral processing also adds great value to the ore and it is beneficial for any organisation or nation to contribute their efforts in this area. In 2003 the value of raw mineral mined in the U.S was $47 billion, but after processing the value became $418 billion, which contributed significantly to the U.S GDP (Mining Eng., 2003).

2.2 JIGGING

2.2.1 Principles of gravity concentration

Gravity concentration methods separate minerals of different specific gravity (i.e. density) by their relative movement in response to gravity and one or more other forces, the latter often being the resistance to motion offered by a viscous fluid, such as liquid or gas—usually water or air—on a particulate solid in a suspension. The key fluid properties are density and viscosity, and the relevant forces are buoyancy and upward impulse. These processes rely on the gravity to impart a force and direction to particles and then a medium to offer a resistance force which results in different penetration rates for particles of different size, shape and density. In other gravity processes friction between the particles and solid supporting surface are an important element to the particle movements. (Taggart, 1967)

Considering solely density the *concentration criterion* provides an idea of the effort required for separation (Wills, 1992):

$$C = (D_h - D_f)/(D_l - D_f) \tag{2–1}$$

where, D_h is the specific gravity of the heavy mineral, D_l is the specific gravity of the light mineral, and D_f is the specific gravity of the fluid medium. This quotient neglects the presence of particle size, viscosity of medium and mechanism employed. Generally a negative or positive number greater than 2.5 will result in easy separation down to the finest sands (below 200 mesh). At 1.75 the lower limit is 100 mesh, at 1.5 about 10 mesh, and at 1.25 only gravel sizes can be treated.

The weight of a particle is an important factor in its motion and this is related not only to the density but also the size of the particle. A particle of a given high specific gravity of small size will have the same motion in a fluid medium as a large particle with low specific gravity. Hence, the size distribution of a particle mixture must be size controlled in order for specific gravity differential behaviour to exist (Taggart, 1967). Figure 2–1 below illustrates the optimum size range for various gravity separation techniques.

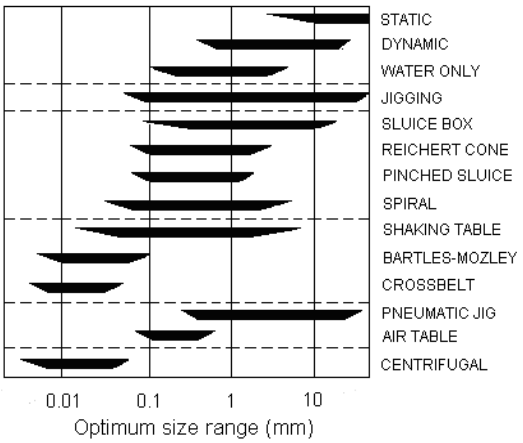

Figure 2–1. Optimum size range for various gravity separation techniques (Anderson, 2010).

2.2.2 Introduction to jigging

Jigging is one of many mineral processing techniques which uses gravity to separate minerals. Mineral processing techniques are usually part of a chain of processes which gradually refine the mining yield. Figure 2–2 illustrates a typical mineral processing flow chart outlining the various stages. Jigging is one of the potential options in the 'Separation' step.

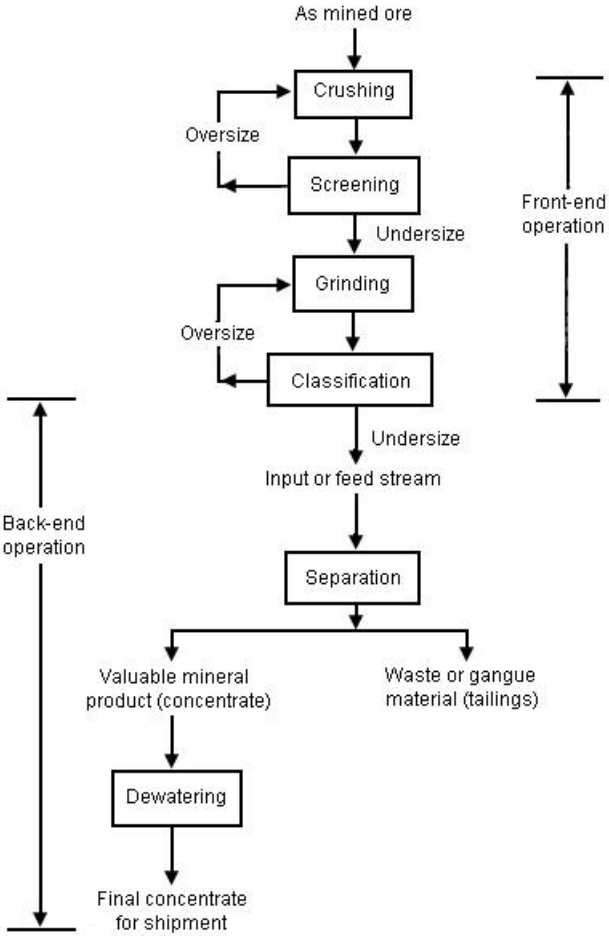

Figure 2–2. Sequence of mineral processing flow sheet (Gupta, 2003).

This density-separation process is widely used for the beneficiation of ore and washing coal, but there are other popular applications such as recycling. It is one of the oldest methods of gravity separation and is still widely used owing to its high separation precision, easy maintenance, cost-effectiveness, and high throughput rate

(Kelly and Spottiswood, 1982; Wills, 1992). Its popularity dwindled slightly as newer technologies came into existence which produced higher separation efficiency, including dense media cyclones and heavy media baths. The salvation of jigs has been their associated low operating costs and ease of operation which has recently resulted in usage in the Indian iron ore industry (Mukherjee et al., 2006). Although the technology dates back to the early ages, jigging even today is not clearly understood. To maintain competitiveness and remain a viable option a current research focus has emerged towards improving jig separation efficiency.

Jigs are most effective for relatively coarse materials typically of 0.5–200mm in diameter (Gupta, 2003). There are different types: wet and dry; semi-continuous and continuous feed; non-centrifuge and centrifuge; and magnetic. The precision of separation depends on the size ratio and density ratio of the materials being separated. The closer the ratio the less effective jigging becomes (Gupta, 2003). Magnetic and centrifuge jigs are used for the finest particle separation (Lin et al., 1997). Table 2–1 lists materials and their specific gravities which can be processed using jigs.

Table 2–1. Table of materials processed using jigs.

Materials Treated by Jigging and Specific Gravities			
Metallic		*Non – Metallic*	
Platinum	21.51	Cassiterite	6.6 to 7.0+
Gold	19.3	Barite	4.5
Silver	10 to 12	Garnet	3.8 to 4.3
Copper	8.9+	Diamonds	3.5
Iron	7.85	Gravel	1.52 to 2.4
Manganese	7.44	Gypsum	2.3+
Tin	7.3	Coal	0.83 to 1.51
Chromium	7.1		
Magnetite	5.1+		
Pyrite	5.1+		

The basic operation of a jig is cyclic and consists of four stages: inlet, expansion, exhaust, and compression. A basic jig construction is shown in Figure 2–3. At the

inlet stage the water is driven using a pulsation device through a stationary perforated screen and imparts a force on the mineral bed which raises the particles. During expansion or dilation the bed is fluidized. Here the bed is loosened and the particles rise and fall at different rates depending on their individual properties including density and size. The denser and larger particles form the lower layers and the finer and lighter particles concentrate on top. The expansion stage can be supplemented with additional hutch water to extend the dilation period allowing additional time for the particles to independently move through the mass. The exhaust stage consists of the withdrawal of pulsation, and is followed by compression where the particles resettle through the fluid and the bed collapses back to its original volume. This cycle is a rate process and repeated continually inducing separation across the bed height. The final product concentration is realized after a certain time. The dense materials can be collected either by continuously removing the heavy tailing on the stationary screen or below the screen depending on aperture size. Alternatively the tailing of lighter particles can be removed from the top of the bed. Once a sufficient amount of concentration has accumulated it can be removed either manually or automatically. (Gupta, 2003; Nagaraj, 2005)

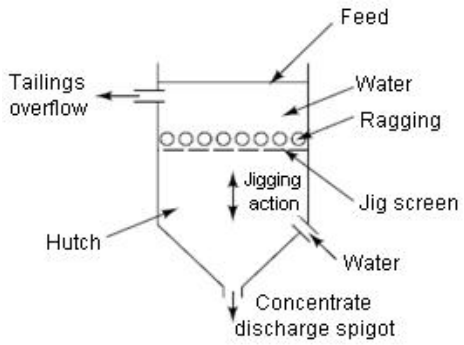

Figure 2–3. Basic jig construction
(Nagaraj, 2005).

Ragging is used in the case where the entire concentrate is collected in the hutch and fine particles are captured. Ragging is a heavy coarse layer of material which acts as an artificial bed and must be heavy enough to retain its position on the bottom of the bed but light enough to fluidize. The size of the material must be large enough to block the apertures in the screen and also able to provide enough space to allow fine

particles to travel between the ragging and down into the hutch. Ragging can be made of steel shot, lead shot, coarse galena, or some other heavy material. (Nagaraj, 2005)

Commercial jigs come in a variety of designs. Different methods of pulsation can be used to induce motion in the particles. A movable-screen lifts the particles without the need of pulsating water flow. The plunger and diaphragm jigs impart force and movement to the water using a translating solid component. Air pulsation displaces water by injecting air and creating a growing cavity which pushes the fluid. A more recent design uses solely air pulsation whereby no liquid is used in the system. Extending jigging to finer sizes the centrifugal Kelsey jig feeds material at the centre which flows radially over the jig bed and exits at the circumference. Further, collection of the concentrate can be made through the screen as shown in Figure 2–3 or over the screen. The range of jigging designs will be discussed in section 2.2.4.

2.2.3 Theory of Jigging

Even though jigging has been practiced for probably some 1000 years there is no single theory which can characterize the process. Lyman (1992) stated after a comprehensive review of jigging theories that even though “the modern era of jigging began approximately 100 years ago..”, over this time jig theory has remained mainly as conjecture and not moved into the realms of science. The theories fail in connecting operating parameters to stratification performance which is still the situation in the present day.

Three important mechanisms in jig stratification from classical theory are: differential acceleration, hindered settling and interstitial trickling. These mechanisms occur in various magnitudes depending on the jig cycle employed (Burt, 1984). These are detailed in this section and illustrated in Figure 2–4.

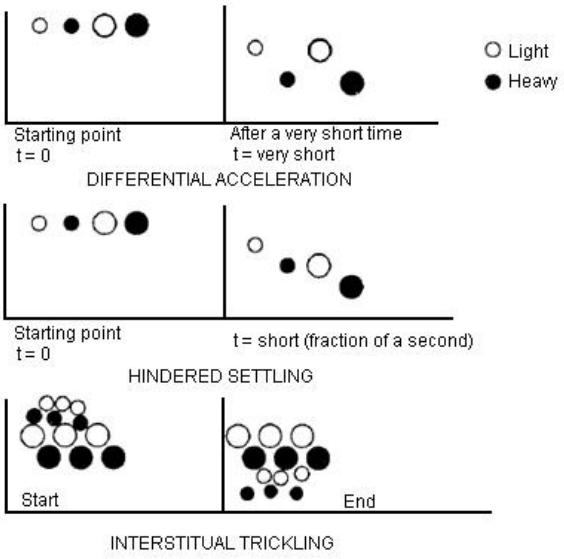

Figure 2–4. The three Mechanisms of jigging individually shown (Burt, 1984).

An alternative concept which is note worthy is the potential energy theory by Mayer (1964). Mayer's theory explains that the water pulsion is purely to open the bed and release the potential energy of the particle bed. While the bed is open stratification occurs and the particle bed centre of gravity is lowered. This theory is not popular due to the lack of explanation of how particles rearrange themselves in mid flight and without contact.

2.2.3.1 Differential acceleration

Fundamentals on jigging theory are detailed by Gupta (2003). In order to understand the principle of separation by jigging, the motion of a particle settling in a viscous fluid must be visited. The equation of motion of a particle settling in a viscous fluid is given as:

$$m\frac{d\mathbf{v}}{dt} = m_p\mathbf{g} - m_f\mathbf{g} - \mathbf{f}_{drag} \qquad (2\text{–}2)$$

where m_p is the mass of the particle, $d\mathbf{v}/dt$ is its acceleration, $\mathbf{g}$ is the acceleration due to gravity, m_f is the mass of the fluid displaced, and $\mathbf{f}_{drag}$ is the drag force resulting

from the fluid resistance opposing the downward movement of the particle. At the onset of particle settling the velocity is small and $\mathbf{f}_{drag}$ which is a function of velocity can be disregarded. The equation of motion then simplifies to the following:

$$\frac{d\mathbf{v}}{dt} = \left(\frac{m_p - m_f}{m_p} \right) \mathbf{g} \tag{2–3}$$

Since the volume of the particles is equal to the volume of the fluid displaced the following is the final relationship:

$$\frac{d\mathbf{v}}{dt} = \left(1 - \frac{\rho_f}{\rho_p} \right) \mathbf{g} \tag{2–4}$$

where ρ_p and ρ_f are the respective specific gravities of the particle and fluid. This expression shows that unlike terminal velocity of the particle, the initial acceleration is independent of particle diameter, and dependent on the densities of the particle and fluid. This type of low velocity acceleration explained through formulae is termed *differential acceleration*. If the repetition of the fall is frequent enough and duration of the fall short enough, the distance travelled by the particle will be influenced by specific gravity alone and not particle size.

2.2.3.2 Hindered settling

After more time the particles will reach 'terminal velocity' where the particle has ceased accelerating and separation enters the *hindered settling* phase. Here the drag force and weight become relevant which are dependent on the particle diameter. All regions of the standard drag curve, omitting the boundary layer separation region (not applicable here) are dependent on particle diameter. The Stoke's law region (approx $\mathrm{Re} \leq 0.3$) is proportional to the particle diameter, and the Newton's law region (Re~500 to 2×10^5) is proportional to the square root of the diameter (Rhodes, 2008). As the terminal velocity varies directly with the ratio of weight to drag, particle separation becomes dependant on particle diameter rather than solely specific gravity.

Differential acceleration dominates in dilute slurries but it is opposed by hindered settling. In concentrated slurries, the voidage in the bed is relatively small and neighbouring particles interfere with each other decreasing the effect of differential acceleration. Hindered settling favours heavy particles and introduces particle size as a factor which contributes to particle movements. (Burt, 1984)

2.2.3.3 Interstitial trickling

At the end of the down stroke, the bed begins to compact and *interstitial trickling* occurs. The large particles are wedged between each other and cannot move while smaller particles are able to trickle down between the interstices under the influence of gravity. This leads to the recovery of fine particles in the final concentration. If this stage is long enough it can support the recovery of heavy fines significantly by adding to their total bed penetration and complimenting the differential acceleration phase. (Burt, 1984)

2.2.3.4 The Jig Cycle

Jigging is a cyclic process of particle bed dilation and compaction. Figure 2–5 shows an idealized jigging cycle of a plunger jig—the sinusoidal motions are of the fluid not the particle bed. Variations of this motion can control the concentrating mechanisms. This simple example is helpful in elucidating the fundamentals. Wills (1992) explains the fundamentals of the jigging cycle as follows. The vertical speed of the flow through the bed is proportional to the speed of the piston. When this speed is greatest the speed of flow through the bed is also greatest.

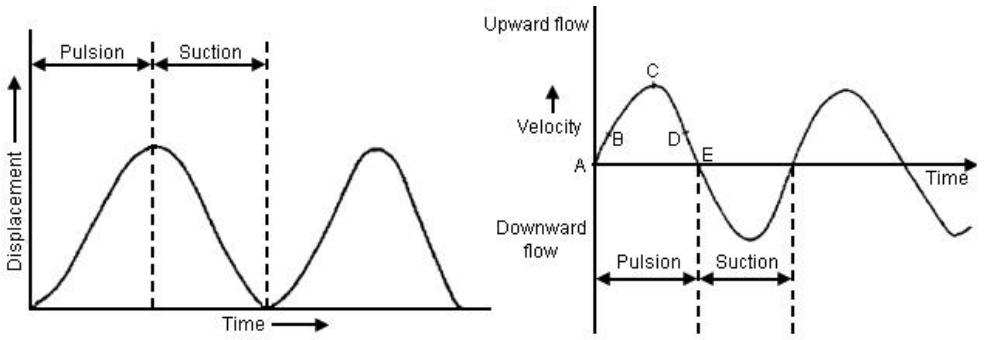

(a) (b)

Figure 2–5. Harmonic motion cycle of a plunger type jig
(a) fluid displacement (b) fluid velocity (Wills, 1992).

In the beginning of the cycle at point ‘A’ the piston moves from its lowest position upwards accelerating the fluid flow and raising the bed. At point ‘B’ the rate of acceleration lessens and the bed loosens (i.e. expands) from the bottom, total bed expansion follows via a loosening wave spreading upward through the bed.

Between points ‘A’ and ‘B’ hindered settling is present in the upward flow. The heaviest particles travel the least distance while the lightest including dense and light fines are at their greatest chance at point ‘C’ of being lost to the top layer and being carrying out with the tailings.

From point ‘C’ to ‘D’ the upward velocity decreases and displacement levels. By about point ‘D’ differential acceleration prevails as each particle begins to reverse direction and begin to fall. The particles continue to fall between point ‘D’ and ‘E’ by the mechanism of hindered settling.

At point ‘E’ the suction phase begins pulling the particle downwards. The large dense particles having been displaced upwards the shortest distance and moving downwards at the greatest velocity arrive first. They are followed by the coarsest lights and other dense particles, and then lastly the fine lights. As the bed compacts the slower moving particles continue to settle by the mechanism of interstitial trickling. During the suction phase new feed enters the hutch. Extending this phase will increase the

capacity of the jig. Figure 2–6 illustrates the jigging process and the separation mechanisms.

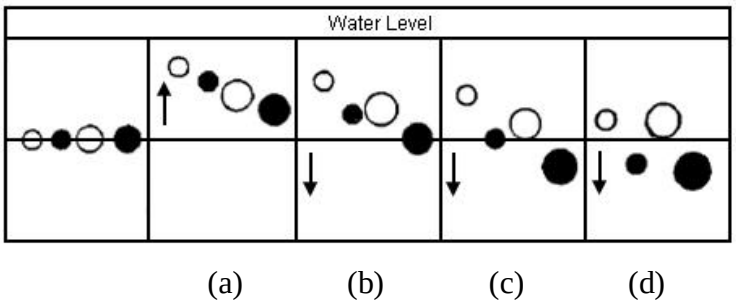

Figure 2–6. Diagrammatic representation of the jigging cycle
(a) pulsion (b) differential acceleration (c) hindered settling (d) interstitial trickling (Burt, 1984).

A constant supply of hutch water is needed for the jig to operate. Adding more water will modify the jig cycle by reducing suction and increasing pulsion (see Figure 2–7). Reducing suction decreases the compaction of the bed which aids jigging as the coarse ore will penetrate the bed more easily. Increasing pulsion improves horizontal transport of the feed over the jig by increasing the volume and height of water, but this also increases the loss of fines due to a faster movement of the top flow reducing settling time. The use of *hutch water addition* is an important way to control the jigging cycle and improve separation performance. (Burt, 1984)

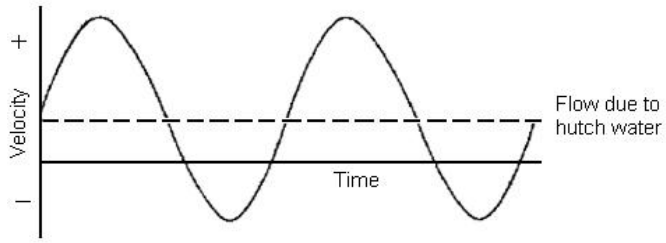

Figure 2–7. Fluid velocity with added hutch water
(Burt, 1984).

2.2.3.5 Layers of operation

Jigs comprise of three operational layers, top layer, roughing layer and separating layer (see Figure 2–8). Each layer contains particles of different size and density and assists the particles to pass through either the tailing or concentrate chute, and if applicable the middling's chute. (Taggart, 1967)

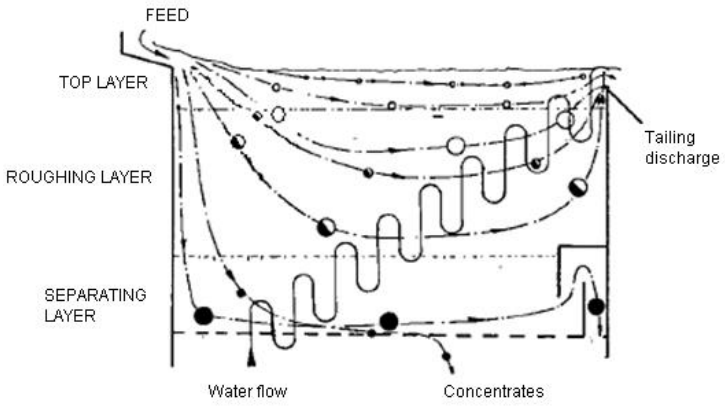

Figure 2–8. Flow and solids distribution in a loaded two mineral jig (Burt, 1984).

In the beginning particles pass into the top layer which is relatively thin and dilute. The top layer has the following three functions: spread the feed entering the jig allowing it to pass onto the roughing layer below; immediately discard slimes (i.e. viscous matter unprocessable using jigs) to the tailing; and discard fine light particles to the tailing. (Burt, 1984)

Underneath the top layer is the roughing layer. Light particles that dip into this layer will immediately be rejected back to the top layer and exit the tailing chute, whilst heavier particles will pass down to the separating layer. The separating layer divides heavy concentrates passing them through the screen, and heavy middling's (partially refined ore) passing them through a chute on the right hand side.

Two techniques are used for removing concentrates which are referred to as 'jigging through-the-screen' and 'jigging over-the-screen'. Jigging through-the-screen involves concentrates falling through perforations in the jigging screen and then being

collected. Jigging over-the-screen involves concentrates passing through a chute positioned above the jigging screen before being collected. The position of a middling chute depends on the mineral application and jig design. The number of middling chutes is determined by how many degrees of middling are desired. Jigging for valuable fine particles that are a low percentage of the mining yield e.g. diamonds, a through-the-screen method is suitable owing to its low throughput giving more time for enrichment. Alternatively, a high throughput over-the-screen chute would collect far too much gangue mixed in with the concentrates leading to a relatively poorly segregated final product. Jigging over-the-screen for example is suitable for iron ore which abundant in a mining yield and segregation is easier. (Burt, 1984)

2.2.4 Types of jigs

The type of jig depends upon the mineralogy and size distribution of the ore, and upon the product requirements and separation efficiency desired (Taggart, 1967). Since the antiquated hand jig, jigging has been used and developed over time where different operating principles have been discovered and have manifested in numerous types of jigs. Due to the vast models of jigs the various types will be introduced but only one example will be given. A complete list of jigs over the entire history of their application and also the most popular modern day jigs has been compiled (refer to Appendix A, Table A–1 and Figure A–1).

Jigs can be partly classified according to their mechanical method of pulsation and whether the concentrate falls through or over the screen (Burt, 1984). The mechanical method of pulsation is chosen based partly on the material being processed but almost completely on operating cost. Some methods are less expensive to operate and hence favourable, others have greater accuracy in separation and consequently are costly.

Firstly, there are two broad classifications of pulsation method which are *fixed screen* and *movable screen*. In a fixed screen jig the mineral bed is propelled upwards by a periodic rush of water passing through a fixed screen. In a moveable screen jig instead of water transporting the particles the screen is not fixed and moves vertically driving the particle bed upwards. The fixed screen jig classification can be subdivided into the

fixed screen *mechanical* and *pulsator*. The fixed screen mechanical types are divided into, *plunger* and *diaphragm*, while the pulsator types are divided into, *air*, *solely air*, *water* and *vane*. Figure 2–9 helps illustrate the breakdown of types of jigs.

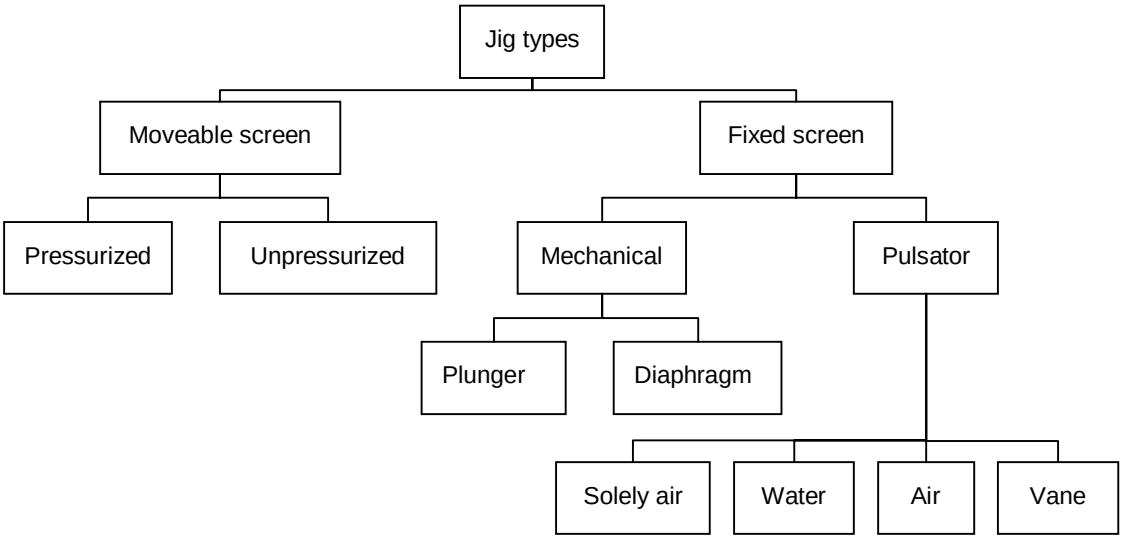

Figure 2–9. A breakdown of the numerous types of jigs.

2.2.4.1 Moveable screen unpressurized and pressurized pulsion

Figure 2–10 shows an image of the run-of-mine (ROM) moveable screen jig and the InLine Pressure Jig. Moveable screen jigs treat low grade sulphide ores e.g. iron, copper, lead, nickel, and zinc, and produce a relatively high grade concentrate (Burt, 1984). The pitfall of this type of jig is maintenance due to the high number of moving parts, high stresses, and high power consumption. The relatively newly invented pressurized InLine Pressure Jig has proven to be viable. This jig is used for very high recovery of precious materials from low grade ore e.g. gold and diamonds, and uses a pressurized hutch to prevent fines being rejected in the top layer. This jig is claimed by Gekko Systems (2003) to offset operational costs by reducing water consumption by up to 90% and may be the future technology for similar operations.

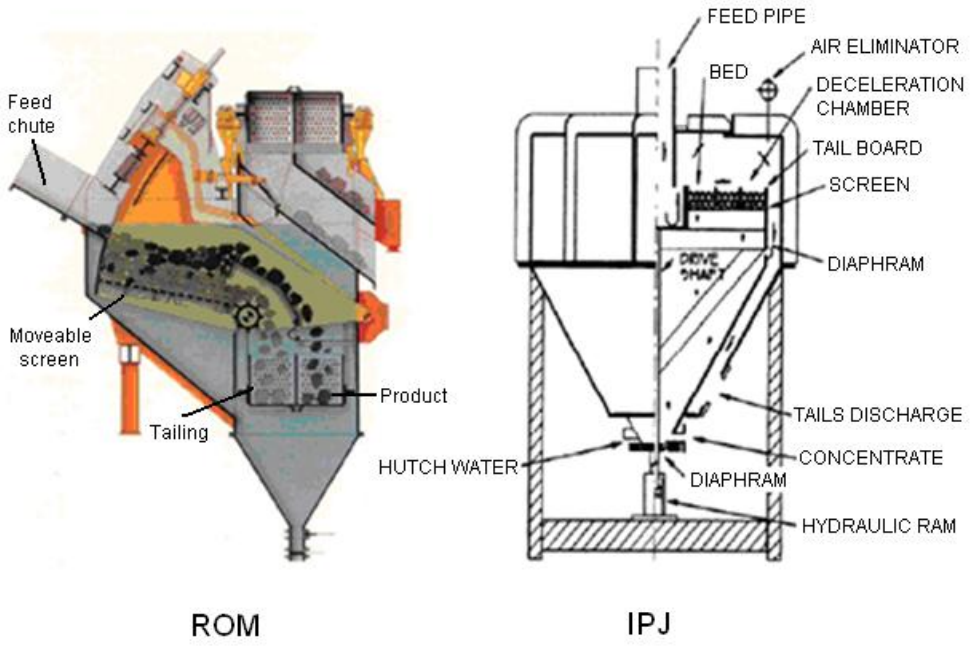

Figure 2–10. The moveable screen ROM and the InLine Pressure Jig (Gray, 1997; Humboldt-Wedag, 2009).

2.2.4.2 Plunger and Diaphragm pulsion

The plunger jig (see Figure 2–11 for an example) is the oldest mechanical type jig and uses a plunger driven by an eccentric motor to impart water motion. The plunger is tightly sealed against the surface of a cylinder and pushes down displacing water through the jigging screen fluidizing the particle bed. Plunger jigs are becoming obsolete due to durability issues of piston seals; and uneven stratification accompanied with a loss of efficiency due to hydrodynamics of the liquid flow travelling in a U-shape before reaching the bed (Taggart, 1967). Other concentration devices do a superior job (Han and Fuerstenau, 2003). The drawbacks found in plunger jigs were overcome by using diaphragms (Burt, 1984). Diaphragm type jigs use a moveable lower conical section connected to the hutch (see Figure 2–11). The conical section is mechanically displaced upwards by mean of eccentric motor pushing water upwards through mineral bed. The diaphragm jig is popular and currently used. An operational limitation of both the plunger and diaphragm jigs are their mechanical linkages which generally create a fixed harmonic motion. Consequently, the jigging cycle cannot readily and easily be modified.

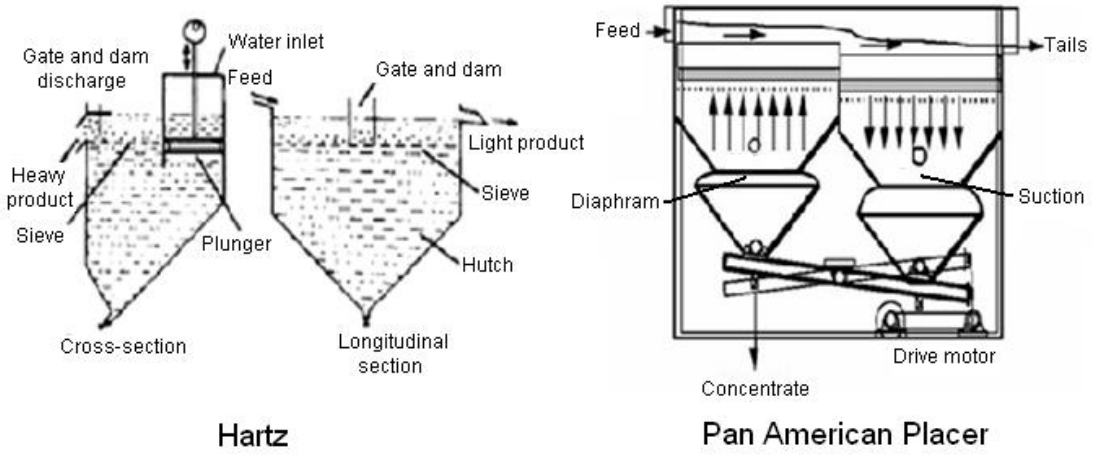

Figure 2–11. The plunger type Hartz jig and diaphragm type Pan–American placer jig (Coggin, 2006; Wills, 1992).

2.2.4.3 Air, solely air, water, and vane pulsion

Jigs characterized by pulsion only and not suction were showed to be superior in separating closely sized feeds at a higher rate (Richards, 1894, 1896). The vane method of pulsion is outdated and will not be discussed in detail. This method employs a vane which fans water side-to-side causing a simple harmonic motion which is very inefficient. Joining the obsolete vane pulsator is the water pulsator. This technique injects solely water into the hutch to induce bed movement, either by a revolving water valve, or water triggered spring pressure valve. This system has been superseded by the less power intensive, more uniform, and precise air pulsed devices. (Burt, 1984)

Air pulsion devices have been commonly applied to coal separation. Until recently the high price of coal has justified finer separation through dense media separation techniques. Air pulsed jigs are also applied to iron ore and other mineral projects.

The two broad configurations have either an air chamber situated on one side of the jigging vessel and an air valve, or any number of small air chambers beneath the jigging screen with accompanying air valves. Figure 2–12 illustrates the former with the Baum jig and later with the Batac jig. This system works by air valves releasing air under pressure and creating an air cavity which grows and imparts force on the

water moving it upwards and dilating the mineral bed. The air is then released to the atmosphere and the bed begins to fall under the influence of gravity. An important design consideration in the side pulsed jig is the width of the bed; because the water flows around a U-bend uneven stratification occurs which is proportional to the screen width. This problem is overcome by the under-bed method or narrowing of the screen width. A great advantage of using electronically controlled air valves is they have sharp cut-off pulsation points which are infinitely variable with regard to speed and length of stroke. This allows tailoring of the pulsation cycle according to varying ore characteristics and product requirements. As a result of jig cycle flexibility the Batac jig was reported to separate both coarse and fine sizes well (Chen, 1980), and also lump ore which cannot be upgraded by heavy-medium techniques (Hasse and Wasmuth, 1988; Miller, 1991). Air pulsed jigs also have the benefit of low maintenance as there are no moving parts except for air valve actuators. (Burt, 1984)

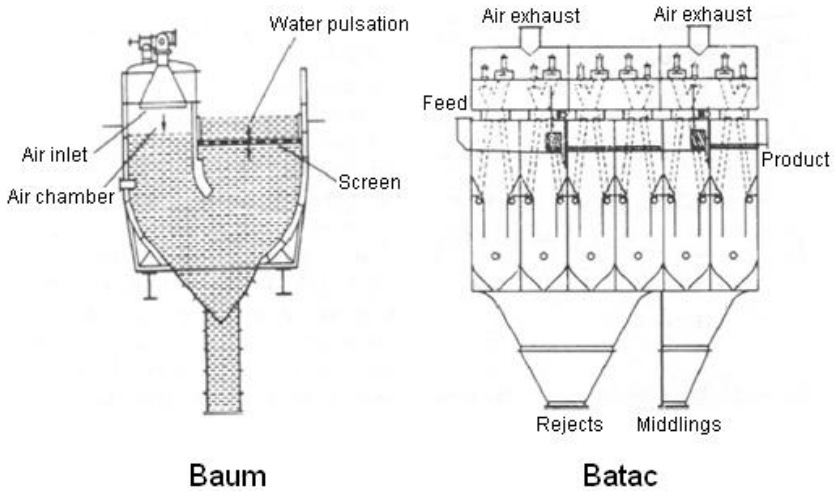

Figure 2–12. Baum side pulsed and Batac under bed pulsed (Wills, 1992).

There are many advantages of dry jigging technology using solely air for pulsion (Richards and Richard, 2007). The first is the absence of process water as mining is often performed in areas with a lack of, or no water. Eliminating the need for water also takes away the need for slurry confinements. Dry processing does not wet the product which then avoids having to dry the material which requires significant energy input and can have significant delays in processes such as coking. Minerals

can also breakdown with exposure to water. As the waste or refuse is a dry and stable material it can easily be returned to the mine and covered by subsequent open cast mining operations. These jigs also have limitations and can only be used in relatively low near-gravity applications—which generally means high specific-gravity separations—and small particles between 0.5μm and 50mm. The Allair jig is an example of a modern solely air operated jig (see Figure 2–13).

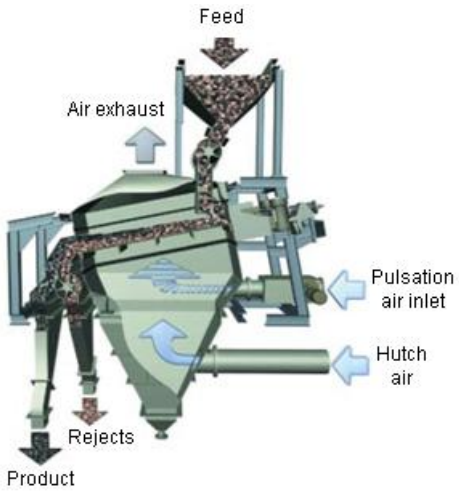

Figure 2–13. Allair jig uses pulsated airflow rather than water (Richards and Richard, 2007).

2.2.5 Design and Operation of Jigs

Jigs remain poorly understood, physically non-transparent, and are hydrodynamically highly complex devices. Experiments have attempted to elucidate jigging phenomena but have the handicap of not being able to visualize the inner workings or measure particle scale fluid and solid kinetics. An experimentalist thus can only examine input and output data and pass on this empirical knowledge. Alternatively, numerical modellers have struggled to develop the required sophistication to sufficiently simulate such complex multiphase flows.

2.2.5.1 The Jig cycle

There has been no agreement on which of the many jigging profiles is optimum for beneficiation. Numerous jigging profiles have been created each with the inventor's theory on how they perform. However, no independent study together with published data exists which has tested each type of jigging profile—therefore one can not definitively select a profile for optimum processing. A study on jigging profiles would go a very long way in understanding and building the knowledge base for this equipment. Among the pulsation waveforms presently available, the differences between each wave form are clear. They attempt to accentuate, attenuate, or eliminate the mechanisms of either differential acceleration, hindered settling, or interstitial trickling. Table A–2 in the Appendix A summarises all the present and past jigging profiles together with associated particle bed behaviours.

Aside from the shape of the jigging profile, the amplitude and frequency is an important aspect on how efficient the jig segregates. If the amplitude is too small the bed may not fully dilate thereby not allowing rearrangement of the particles. Conversely, over dilation using excessively high amplitudes can cause mixing to occur by fluidization slugging, and departure from the original jigging cycle movement (Rasul et al., 2000). Further, adopting high amplitudes or high frequencies can prevent the mineral bed settling by not allowing enough time for the falling particles to rest and the interstitial phase will be eliminated.

Feeds that are closely sized and tightly packed do not need high amplitudes to dilate the bed because the feed has less voidage and therefore experiences higher drag and is fluidized at lower amplitude. Close sized coarse feeds with a high proportion of heavies require a high amplitude and long cycle time. Broad sized feeds separate more easily so it is advantageous to used a high frequency and increase the throughput rate. Coarse feeds that result in loosely packed high porosity beds need large amplitudes to invoke enough drag to lift the mineral bed. Light fine feeds do not require high amplitude to lift the bed but faster stratification will occur with an increase in frequency. A slow stroke, particularly one with slow acceleration will not create back pressure rapidly enough and will lose fluid energy through interstices and fail in

producing satisfactory bed dilation; alternatively, a sharp stroke with rapid acceleration will lift the bed as a whole. (Burt, 1984)

An important tool for the operator is the control of hutch water (i.e. water residing in the hutch which is continually replenished). Adding a large amount of hutch water can completely eliminate suction or accentuate the upward pulsation. Hutch water control is important to fine tune the operating parameters especially if the jig cycle profile is relatively fixed. (Wills, 1992)

2.2.5.2 Ragging

As mentioned previously ragging is used in the case where the entire concentrate is collected in the hutch and fine particles are captured. Ragging must be the same specific gravity or slightly lighter than the concentrate. If heavy ragging is used a greater upward force is needed to lift the ragging and once raised will overly fluidize the mineral bed causing slugging. Alternatively, a light ragging will either be lost to the tailing or bank-up toward the tailing board. Adopting a ragging on the heavier side will move upwards only slightly on pulsion and allow less room for concentrate to get under and pass through. A coarser ragging provides ample size interstices and less friction providing an easy avenue for particles. An important operation problem is a blocked bed that exists when random heavy mineral particles fall to rest under the ragging and prevent any minerals to pass through, and consequently causes a particle build up on the jigging screen. (Burt, 1984)

2.2.5.3 Jigging screen

The jigging screen design must endeavour to have the least influence possible on the fluid flow and avoid irregular flow and slugging (Taggart, 1967). To achieve a uniform flow the screen must be rigid and not flex with changes in the direction of water, or bow with the weight of the particle bed. The apertures need to be uniform throughout the jigging screen and the screen material (such as wire) must be thin to reduce drag and deformities in the flow.

The type of jig screen depends on whether the operation is of the over-the-screen or through-the-screen type. When jigging over-the-screen, the apertures must not permit particles to pass through and hence their size must be smaller than the smallest particle. For jigging through-the-screen, the aperture needs to be smaller than the ragging but larger than the maximum size of the heavies. (Burt, 1984)

2.2.5.4 Feeding

Jigging equipment operate more efficiently on prepared feeds. Jigging feeds usually go through a process removing detritus, oversize particles, and by low pressure cyclones the rejection of fines and slimes. The key principles of feeding a jig are to keep the feed rate regular and spread the mineral over the full area of the screen. Mineral beds respond slowly to increases in feed rate and consequently much of the valuables will not have time to penetrate to the separating layer and will be rejected in the tailings. If the feed is spread unevenly part of the screen will be under-worked reducing the capacity of the jig. (Taggart, 1967)

2.2.5.5 Jig dimensions

Hutch shape is an important consideration hydrodynamically. In the early square tank design, the bed was treated very unevenly as the inner part was too active and the outer stagnated. A rounded tubular tank was an improvement but was costly to manufacture. The bend was replaced by a straight partition which was cheaper and improved performance. Subsequently, the importance of elevating the jigging screen some distance above the bottom partition and also depressing the plunger below the sieve was discovered. The depth of the hutch is also important as the particle action of a shallow jig is uneven due to the pulse being too strong next to the partition and weak on the farther side. (Richards et al., 1909)

Conventional over-the-screen mineral jigs consist of square or rectangular tanks. This configuration accelerates the particles over the screen and reduces residence time of the particle bed, giving less time for stratification. In addition, the drag associated with the side gates and the slurry creates a build up of fines and a low pressure area which reduces the effect of jigging. A circular configuration avoids these problems, as

the slurry flows rapidly to the centre and slows as it approaches the tailings launder at the periphery of the unit. In the fast section of flow the heaviest particles are concentrated while progressively finer particles are collected near the overflow. Another advantage of the circular jig is its large capacity. (Taggart, 1967)

The jig compartment is often subdivided into numerous sub-compartments to collect different degrees of middling in through-the-screen jigging. The tailing launder can also have various gates and associated compartments beneath the screen for over the screen middling capture.

2.2.6 Jigging control

Jigging control has been an explored area. Lyman (1992) provided a thorough review of jigging principles and control. The author mentioned "..the control of the process is still quite rudimentary" even though "the modern era of jigging began approximately 100 years ago..". Moreover, Lyman (1992) stated after a comprehensive review of jigging theories that over this time jig theory has remained mainly as conjecture and not moved into the realms of science. The theories fail in connecting operating parameters to stratification performance which is still the situation in the present day.

The Lyman (1992) review placed emphasis on coal washing jigs. The methods fall into two categories. The first method of control seeks to regulate the amplitude and frequency of the jigging cycle automatically to ensure a desirable hydrodynamic condition in the bed. While the second aims for regulation of jig discharge. These techniques are in response to information attained from sensing conditions in the bed using a float, or stand pipe, or radioisotope density gauge.

Float systems involve a float inside the particle bed changing position in accordance to the average bed density around the float and the effective density of the float. The position of the float is transmitted by either electronic or mechanical means. The float position signal is used to control the reject gate, which depending on the jig mechanism either: changes position, opens and closes, or increases in rotation etc.

Pressure based systems are also used for refuse discharge control. The ACCO system uses a stand-pipe which resides in the middle of the bed, just below the jigging screen and stands vertically up through the bed (Lyman, 1992). The stand pipe contains only a float and is absent of particles. The float will rise in accordance to peak pressure below the jigging screen. As the bed grows dense the float will move upwards and activate a valve which vents a chamber and activates the discharge section of the jig causing particles to exit. When not vented pulsation is damped and particles in the lower portion of the bed will not exit. In the McNally jig (Lyman, 1992), the float position regulates the strength of the pulsation cycle over the entire bed. The float has been known to be replaced by pressure sensor.

Pressure sensors at different levels of the bed itself have been used to regulate air supply pressure (Remennyi and Levchanko, 1972). The sensors measure the pressure drop through the bed. Once the resistance of the bed to flow changes, the jigging stroke is altered.

The “Autovibrational” cycle control method developed by Vinogradov (1968) sets jigging conditions individually for each compartment of a subdivided jig. Each compartment of a jig may have different bed compositions and resistance to flow thus require individual treatment. Here an air valve is opened when a probe above the jig detects water. The duration the valve is opened controls the admission of air an intern bed dilation.

A radioisotope method of control found by Bartelt (1962) uses a radiation beam to measure the average wet bulk density of the jig bed. The system applies control using electronic density signals which alters the reject gate position according to bed density.

The patented control device JIGSCAN has given considerable improvement for jig control. It adopts a nucleonic density gauge to monitor bed density, and pressure transducers to record pressure variations in the jig pulse. This technology controls both the reject gate position in addition to the amplitude a frequency of the jigging profile (Jonkers and Lyman, 1997; Lyman, 1992).

The most sophisticated controller used for the automation of electromechanical processes is the programmable logic controller (PLC). Mishra and Chakroborty (1995) explored the fuzzy logic controller (FLC) numerically using a DEM jigging simulation. However, this has not yet been tested outside a simulation setting.

Other methods of jig control do not probe the inner workings of the jig, rather, they focus on particle feed and output. Mukherjee et al. (2007) explain that optimising the feed grade can improve jigging performance. The authors explain that treating feed of higher or lower grade than the equipment is designed for causes yield loss. Hiens et al. (2006) reviewed measurement systems for gravity separation circuits to modulate mineral processing equipment (including jigs) for optimum separation. These included: float and sink tests, tracers (density, magnetic, x-ray fluorescent, and radio frequency identification).

Thus far, neither of the jigging control techniques have optimised profile shape beyond frequency and amplitude selection. Further, little emphasis has been placed on reducing energy consumption; aside from energy efficiency being a by-product of time efficient separation. Potential for improvement in jigging control may exist within these areas and is studied in this PhD project.

2.3 EXPERIMENTAL AND NUMERICAL STUDIES

2.3.1 Experimental techniques

Until recently, experimentation has been the sole method of evaluating and extracting knowledge from jigs. Over the long history of jigs, several cases have been found where researchers conducted and published experimental jigging studies with the aim of understanding the fundamentals of jigging (Clarke et al., 1997; Das et al., 2007; Hentzschel, 1958; Jinnouchi et al., 1984; Jong et al., 1996; Kellerwessel, 1998; Mukherjee et al., 2006; Mukherjee et al., 2005; Mukherjee and Mishra, 2006, 2007; Schubert, 1994). Manufacturers also perform experiments to enhance and evaluate their designs or develop operational policies but for the most part develop

unpublished work. The work that is published by manufacturers maybe biased and/or partially withheld which limits usefulness for this thesis. Operators additionally perform unpublished experiments which aim to maintain product requirements by regularly recalibrating jigging devices and quantifying their results using metallurgical assays.

Although this thesis has a focus on numerical simulation, a high emphasis is placed on empirical studies as they provide a wealth of information on jigging mechanisms which can be drawn on in the numerical model analysis. This section will summarise the key findings of published experimental studies by the scientific community.

Mukherjee et al. (2005) studied the movement of water and particle separation in an air pulsed, 15cm diameter U-tube, batch scale pilot jig. The pilot jig was employed to allow obtrusive measurements of the velocity profile which could not be done using available commercial equipment. A nucleonic density gauge was used to record the variation in slurry density. The main limitation was that the pulsation profile studied was reasonably asymmetrical even after corrective modifications. Test results showed three types of water displacement profiles could be obtained. Type-I the up-stroke was much higher than the down-stroke and hence with successive strokes water level in the jig rises. Type-II jigging profile corresponded to approximately equal pulsation and suction stroke. In the Type -III jigging profile, the pulsation stroke was less than the suction stroke leading to a fall of water level over successive jigging cycles. Type-II was preferred and closest to a sinusoidal profile. When applying the Type-II jigging profile to a binary size particle system, Mukherjee et al. (2005) found that particle stratification generally increases with the amplitude of pulsation. Further, it was found that a combination of high frequency and amplitude was detrimental for stratification.

Mukherjee et al. (2006) conducted a study using a two-chamber Denver plunger jig with sinusoidal wave pattern and iron ore feed material of -10.0mm. An investigation was performed to understand the behaviour of various size fractions of the feed material during jigging. Coarser feeds needed higher maximum water velocity for better jigging efficiency. As a result, it was suggested the maximum water velocity of a feed must be matched to the largest size particles present in the feed. Further, even at optimal maximum water velocity different size fractions of feed respond differently

and ideal separation is not reached. Therefore, the final conclusion was that jigging efficiency could be improved by narrowly sizing the feed and subsequently optimizing the maximum water velocity. It was also found that if the optimal maximum water velocity is exceeded, the separation efficiency declines. The same authors later confirmed this using a Baum jig (Mukherjee and Mishra, 2007). The second part of the study found there was a favourable size ratio for each density ratio. Adopting a pseudo-binary study, the iron ore feed with a density ratio of 1.5 was found to have a favourable size ratio of 0.44 or above. Feeds with a density ratio below 0.44 would mix during jigging. Another size ratio consideration is the theoretical limit for interstitial trickling given by a size ratio of 0.41 and found through simple geometric analysis (Rowe et al., 1972).

In a subsequent paper Mukherjee and Mishra (2006) postulated that segregation in the jig bed is a direct consequence of resonance of the particles which is influenced by the frequency of pulsation. To validate this theory, they used a Denver plunger jig with different size classes of the feed material and varying pulsation frequencies. Their analysis suggested that the alignment of the pulsation frequency with the particle natural frequency will improve density classification of particles of that type. For example, if the applied pulsation frequency is close to that of the fine lighter particles natural frequency it is likely to improve segregation in the finer light particles class, and more generally, the fine size class. They concluded that in a jigging system, first the frequency of pulsation should be optimised based on particle type, and of secondary importance the amplitude of water pulsation should be adjusted for maximum water velocity.

Focusing on single particle trajectory. Schubert (1994) explains using particle tracking radiometric data that particles can move in fluctuating leaps—in particular low density particles—due to circulation flows, turbulence, and particle collisions which are stochastic effects that contribute to mixing. Further, it is shown that if bed expansion is low, the high density particles move downwards slowly. Alternatively, if expansion is high, low density particles can penetrate into the lower layers due to mixing motions. Kellerwessel (1998) verified this experimentally with radioisotope tracers, and showed that particles in the jig bed not only follow the vertical motion of the fluid, but also perform circulatory motion. Subsequent evidence of this has been

found by following the trajectories of particles using a positron emission particle tracking technique (Clarke et al., 1997). Therefore, the current jigging theories based simply on upward and downward motion are lacking in complexity.

The motion of a tracer particle penetrating a jig bed was studied by Jong et al. (1996) using a plunger type bench scale jig with a sinusoidal wave pattern. Particle trajectories were measured by a CCD video camera. It was found that an optimum jigging frequency existed when the maximum particle jump length (i.e. distance the particle moves vertically with pulsation) was considered. At higher frequencies the average particles jump length increases and the height at which the maximum jump length occurs reduces.

Particle bed dilation phenomenon was studied by Hentzschel (1958). Particle beds comprised of monodisperse particles of the same density and polydisperse particles of the same or different density were examined. In all particle systems studied, when the particles are lifted as a whole during pulsion they begin to drop from the bottom as a loosening front of higher porosity—also known as particle *erosion*—which travels upward through the bed. Below the loosening behaviour, a fluidization layer was identified. An exception was found with particles of a polydisperse system having the same density—if size segregation takes place and there are large size differences dilation can proceed from the top to the bottom. It was concluded that fluidization behaviour should be reduced and the period of loosening extended. Jinnouchi et al. (1984) obtained dilation jigging data using coal and a TACUB jig. Initially it was shown the bed begins to dilate from the top layer and expands slowly, then once maximum upward water velocity is reached another larger expansion begins in the bottom layer propagating to the top.

As mentioned previously jigging is analogous to a fluidization and defluidization process, therefore similar phenomena may be applicable especially when segregation is considered.

Rasul et al. (2000) used experimental methods to study inversion phenomena in fluidization. They defined a boundary which subdivides binary particulate systems into mixing and segregation type depending on particle size and density ratio.

Additionally, a third type is mentioned by Mukherjee and Mishra (2007) which is an intermediate group of particles that can segregate or mix. Mukherjee and Mishra (2007) performed an experimental binary-fluidization study and suggested that although it is widely believed that separation efficiency is controlled by the size and density ratio of particle components, their results demonstrated that fluid velocity during fluidization can exert an overriding influence to improve separation efficiency. It is clear that during fluidization that the ratio of size and density of the particle components and fluid velocity are all important factors of separation efficiency, although the work by Mukherjee and Mishra (2007) is restricted to fluidization phenomena which may be limited in jigging.

Particle velocities where examined by Handley et al. (1966) who found downward particle velocities in a homogenous fluidised bed to be higher than their freefalling velocity, also noted by Kmiec (1978) and Jong et al. (1996). Handley explained this effect by the presence of back mixing streams in the liquid. The present jigging theory used today does not account for local variations in fluid and particle velocities.

2.3.2 Numerical techniques

Many numerical techniques are well poised at simulating the jigging process but few are practical. Some numerical models are very computationally time consuming while other more easily calculable models lack in flow physics resolution.

2.3.2.1 Single phase flow

The single phase flow technique is a computational fluid dynamic (CFD) method which resolves the fluid flow using the Navier-Stokes and Continuity equation, and if required additionally the Energy and Turbulence equations. The fluid flow is based on the concept of continuum while advancing the solution through space and time to obtain the numerical description of the complete flow field at a local average level.

Solnordal et al. (2009) applied this technique in a transient simulation to investigate the flow of a water based slurry containing gold in an InLine Pressure Jig. The main

limitation of this model is the treatment of the slurry as a single phase. As a result the thick particle bed is simulated using a static area of porosity which does not move during the pulsation cycle. Being unaware of the actual distribution of the solid bed at any time introduces an error and it is unknown how this affects model performance.

2.3.2.2 Two fluid Model

When using a CFD Two Fluid Model (TFM) for a fluid-solid system both phases are treated mathematically as interpenetrating continua. The solid phase—which is in fact discrete—is considered as a continuum under the concept that an infinitesimally small element can be treated as a sufficient number of particles representing fluid behaviour, for which can be applied a mean velocity, mean kinetic energy and pressure (Anderson and Jackson, 1967). The TFM model couples the phases by incorporating the concept of phase volume fractions, interfacial forces, and a momentum exchange term. The volume fractions represent the space occupied by each phase, and the laws of mass and momentum conservation are satisfied by each phase individually. The momentum exchange term is an empirically specified interphase momentum transfer coefficient between both phases. Interfacial forces include drag force, lift force, and virtual mass force, etc. Closure of the solid phase momentum equation requires a description of the solid phase stress which is a challenging topic. Many studies have been done to obtain constitutive equations of the solid phase, e.g. the kinetic theory for granular flow, (Ding and Gidaspow, 1990; Jenkins and Savage, 1983; Lun et al., 1984). By introducing the concepts of solid "pressure" and "viscosity", the well-known granular kinetic theory has been established and is now being widely employed for the solid stress calculation (Du et al., 2006). The TFM approach is advantageous for practical applications of complex multiphase flows as both solid and fluid phases are described at a local averaged cell scale, which makes large scale study possible.

The limitation of this technique is that the discrete nature of the solid phase is not recognized and the solid phase is treated as a whole—no part of which can be distinguished from neighbouring parts. Therefore, individual particle-particle and particle-fluid interactions are not resolved. Further, there is a difficulty in obtaining closure laws for the interaction of particles belonging to different classes (Feng,

2004). The TFM technique has not been used in numerical studies of jigging to date owing to more favourable methods.

2.3.2.3 DEM-Simplified fluid model

Various discrete elements method (DEM) models coupled with Simplified fluid models have been used with the view of achieving quantitative results but to-date these have yielded only qualitative data. DEM is adopted to simulate any problem involved with the discontinuum behaviour of particle systems. Superseding the continuum two-fluid model, DEM results give better insight into micro-mechanical processes at the particulate level. Very briefly, in DEM the position of each particle is tracked incrementally by applying Newton's second law of motion and a force displacement law. The effect of fluid on the motion of particles is computed in a simplified manner. When the particle enters the fluid, the drag force is determined either by an analytical drag force equation or a drag force correlation.

Beck and Holtham (1993) along with Mishra and Mehrotra (1998) made early attempts modelling a jig using two-dimensional DEM models with a drag coefficient determined using the Abraham equation and drag force using the Bernoulli equation. Extending the model spatially Srinivasan et al. (1999) made a three-dimensional (3-D) DEM model investigating stratification. This model predicted a considerably higher degree of lift of the bed that could not be explained with empirical data. It was determined that the interaction of the fluid with the particle did not take into account bed porosity and the resulting drag force behaviour. The porosity issue was addressed by Mishra and Mehrotra (2001) improving the 3-D model by using the Di Felice (1994) drag force correlation which takes into account the effect of bed porosity. However, experimental validation performed by the authors yielded poor correlations. Mukherjee and Mishra (2006, 2007) also adopted this approach and extended the model to multi-sized particles. A problem of this multisized particle model is that it attempts to distribute the drag calculated using Di Felice's drag force correlation evenly over different sized particles, even though the small particles in reality experience less drag due to their form and lower surface area.

The models mentioned above are limited as they assume a uniform fluid field and do not account for the effect of non-uniform fluid velocity on the particle drag force. The presence of non-uniform particle distribution will also change the fluid velocity field.

2.3.2.4 DEM-CFD

The Lagrange-Euler (DEM-CFD) model was first proposed by Tsuji et al. (1993). It remains the most attractive technique because of its superior computational convenience, as compared to the high resolution but time consuming Direct Numerical Simulation-DEM or Lattice Boltzmann-DEM models, and is capable of capturing the flow physics as compared to DEM-Simplified fluid models.

This model calculates the fluid flow in an Eulerian frame and the particles are moved in Lagrangian coordinates. The fluid phase is treated as a continuous phase and utilizes Computational Fluid Dynamics solving the Navier-Stokes and continuity equations in terms of local mean variables over a computational cell. The solid phase is treated as a discrete and dispersed phase where the motion of individual particles is solved using Newton's second law of motion. Coupling between each phase at each time step is achieved by calculating the particle fluid interaction force for individual particles which is then used in the fluid phase through a local averaged scheme. This approach can generate detailed information about the trajectories of particles and the transient forces between two particles and between particles and fluid. A more detailed review of DEM-CFD will be given in section 2.4.

Many studies of particle-fluid flow phenomenon have been researched using multiple time and length scales. These investigations range from atomic/molecular scale to process equipment scale (see Figure 2–14). A quantitative description of particle scale phenomenon has been the research focus of the past decade using techniques such as DEM-CFD. This focus is driven to establish a general theory for reliable scale-up to assist in unit process design and control. Through knowledge gained by analysing particle scale information e.g. solid flow patterns and mixing kinetics it is possible to understand the bulk behaviour of the system which is a culmination of micro-mechanical processes. Figure 2.14 illustrates the approaches at different time and length scales.

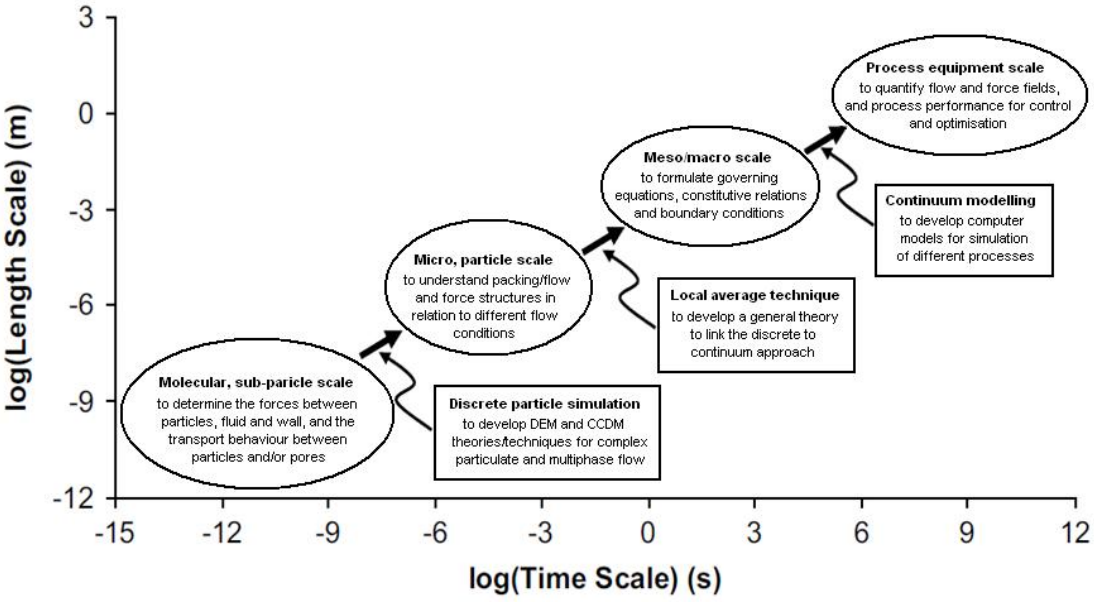

Figure 2–14. Numerical modelling approaches at different time and length scales (Zhu et al., 2007).

Reviews of DEM-CFD major applications and findings along with theoretical developments have been published by Zhu et al. (2007, 2008). These include examples of complex flows, heat transfer, chemical reactions, and a multitude of particle-fluid applications.

Jig models generally involve particles motions in liquid, which is a highly dense and viscous medium compared to gas and various physical forces become relevant to jigging models.

These forces include the virtual mass force (or Added mass force), which is the inertia added to a system because an accelerating or decelerating body must move some volume of surrounding fluid (Odar, 1966a; Odar and Hamilton, 1964a). Closely linked is the Basset force which describes the force due to lagging boundary layer development with a change in a bodies acceleration (Basset, 1961). The Magnus force (see Figure 2–18) is a slip-rotation lift force caused by an induced faster flow due to rotation around one side of the particle and a slower flow around the other (Rubinow and Keller, 1961). The Saffman force (see Figure 2–19) is the lift experienced by a

particle in a shear field perpendicular to the direction of flow originating from inertial effects in the viscous flow (Saffman, 1965, 1968). The lubrication force (see Figure 2–20) arises from the hydrodynamic pressure created by interstitial fluid being squeezed out from the space between two solid surfaces, including particle-particle and particle-wall. Lubrication forces also explain viscous interactions for the motion of neighbouring surfaces transverse to the line of centres due to shear and rotation (Derksen and Sundaresan, 2007). Finally, there is the force due to carrier phase acceleration, known as the inertial force (or pressure gradient force) due to acceleration. These forces related to particle motion in a fluid may or may not be influential on the overall behaviour depending on the system. These forces are detailed and discussed in section 2.4.5 and 2.4.6.

Only four jigging studies have adopted DEM-CFD (Asakura et al., 2007; Dong et al., 2009; Xia et al., 2007; Xia and Peng, 2007).

Xia and Peng (2007) developed a two-way coupled two-dimensional (2D) column model. The study considered drag on each particle individually and did not consider porosity by adopting Ergun, Wen and Yu, Di Felice or other drag force correlations for porous media. This model implemented forces including: drag force, pressure gradient force due to acceleration, virtual mass force, Magnus force and Saffman force. Interestingly, this study analysed the importance of different forces acting on particles in jigging performed for monosize particles with the same densities in a sinusoidal pulsion. However, the results appear to have been taken not with a pulsated flow as mentioned by the author but with a constant fluid velocity. This becomes apparent as the drag force added with buoyancy force, and pressure gradient forces values appear identical. The pressure gradient force due to fluid acceleration should generally be vastly different in magnitude—in practice usually relatively small and hence commonly neglected. Alternatively, if the values given are total pressure gradient force values, having an identical appearance to the drag force indicates a constant inlet velocity, and is unhelpful in the “analysis of the importance of the different forces acting on a particle in jigging”. In addition, the values for other forces i.e. Saffman, Virtual mass, and Magnus, plotted against increasing particle size or density, display frequent random large outlier data points several magnitudes larger

than closely neighbouring values. No explanation is offered for these inconsistencies thus one may deduce these forces have potentially been improperly implemented.

The results by Xia and Peng (2007) show that the drag force, pressure and buoyancy force are dominant and increase linearly with monosize particles and increasing particle density. Other forces show little impact and a weak horizontal trend. The virtual mass force and the Magnus force are almost two orders smaller than drag force, while the Saffman force is even weaker. Increasing particle size whilst keeping particle density constant, the same forces are dominant however exponentially increased with size. Other forces behave similarly with a weak horizontal trend (i.e. consistently low force values) and low impact although some higher values appear.

Additionally, the authors use both the particle diameter (D_{50}) and specific gravity (SG_{50}) cut-points metrics to quantify stratification. The cut-point value indicates which particle size or density will separate with 50% efficiency. Sizes or densities larger than the cut-point will be recovered with greater efficiency and smaller or less dense particles will be recovered with lower efficiency. Interestingly, it was found the SG_{50} is inversely proportional to particle diameter. This implies that fine particles have higher dense clean coal recovery than coarser particles. Further, to achieve high density separation from a multisize system, density cut-points of the various sizes need to be similar. As the relationship between SG_{50} and size is steep and linear, preparation of the feed into narrow size distributions and processing separately would ensure similar cut-points and good gravity separation. Other results indicate that the best stratification is achieved at intermediate frequency and amplitude values. The sharpness of separation is evaluated by using *Ecart probable (Ep)*. Which is defined as one half the specific gravity interval corresponding to recovery values of 25% and 75%. *Ep* is found to be influenced more by frequency than amplitude.

Further, in the same year Xia et al. (2007) used the same model and highlighted that the fluid is highly dynamic and influenced by the presence of particles confirming the simplified idealized flow behaviour as assumed in DEM-simplified fluid models does not exist. However, neither Xia et al. (2007) nor Xia and Peng (2007) attempted to experimentally validate their numerical model.

Asakura et al. (2007) went a step further including the Basset force—thus the full Basset (1888), Boussinesq (1885) and Oseen (1927) (BBO) equation—and a three-dimensional (3D) column model. No analysis of the importance of forces was attempted as did Xia et al. (2007). This would have been particularly revealing and interesting, especially due to this being the first time the Basset force had been introduced into a jigging model and also the associated high level of complexity in doing so. Similarly to Xia et al. (2007) this study was two-way coupled and did not consider porous drag phenomenon. The study included a monosize mixture of particles with small differences in density in a sinusoidal pulsation. The amplitude of pulsation was varied and fractions of low density particles were measured over the height of the bed. Different separation rates were clearly present although little explanation as to why with the authors concluding "trial and error experiments in actual operation is necessary to find effective conditions for separating". The study similarly analysed a system which aimed to eliminate the effects of terminal velocity. A particles system of size and density ratios of 0.62 and 0.875 respectively, and with identical terminal settling velocities showed that although the particles have the identical terminal velocity segregation is present. They concluded that further investigation of particle fluid interactions is necessary to understand this behaviour. Although this is true, one would suspect that with an absence of hindered settling and interstitial trickling—since the size ratio >0.41—segregation is primarily caused by differential acceleration (see section 2.2.3.1). The authors made an attempt to seek an explanation through analysing particle response time. A trapezoidal pulsation profile with only one particle was simulated then repeated and compared to other particles with the same terminal velocity but different physical characteristics. It was found that the particles were lifted almost to an identical height and descended at different rates showing potential for segregation. Interestingly, it was shown in the middle of the jig cycle, when the carrier flow velocity is zero the particles travel at the same velocity downwards—which is the terminal velocity—as suction begins particles descend at different rates until again reaching the same velocities. This is a particle response time effect (i.e. different Stokes number) and *not* differential acceleration as the particles are already in fast motion. This phenomenon promotes segregation. Finally, Asakura et al. (2007) have not pursued in experimentally validating this model.

Dong et al. (2009) produced a one-way coupled three-dimensional model of the laboratory-scale moveable-screen InLine Pressure jig (IPJ). Instead of two-way coupling, a fictional static porous region above the bed is used to emulate fluid flow influences caused by particles. The region does this by the addition of volumetric particle-fluid forces using the Ergun equation to the standard momentum equations of the fluid. Hence, Dong et al. (2009) considered fluid flow as the dominant factor in the jig, as one-way coupling does not accurately account for the influence of local particles and porosity distributions on the fluid. However, porosity was factored into particle drag force calculations using the Di Felice correlation. However, this equation is based on a monosize particle drag force system which the authors applied with an *ad hoc* approach to a multisize system. Further, their model does not include the range of fluid-particle forces as used by previous authors (Asakura et al., 2007; Xia et al., 2007; Xia and Peng, 2007), only drag and buoyancy forces were implemented.

Dong et al. (2009) investigated particle separation within the context of an IPJ, adopting a sawtooth-forward profile and a simplified polydisperse particle distribution. The study focused on effects of vibration frequency, amplitude, along with the size and density of ragging particles on flow separation. Interestingly, their results revealed that not only jigging but also elutriation contribute to separation of lighter particles in the IPJ. A strong radial fluid velocity from the feed bowl outward to the walls can cause lighter particles to by-pass and flow over the particle bed and through apertures in the wall before discharging. Further, the particle-fluid and gravity forces were found to be almost balanced, therefore, it was inferred that particle-particle collision forces are responsible for particle separation—which solely is not a conventional jigging separating mechanism i.e. unlike differential acceleration. Validation of the numerical model was attempted using experimental particle recovery values. For the single 'base' case used for experimental validation, qualitatively the results were comparable although differences of up to 30% were present.

2.3.2.5 Other numerical modelling techniques

A review by Zhu et al. (2007) details many of the computational modelling techniques applicable to jigging and their suitability. The existing approaches to modelling

particle flow can be classified into two approaches, discrete: Molecular Dynamic Simulation (MDS), Lattice Boltzmann (LB), Pseudo-particle methods (PPM); or continuum: Direct Numerical Simulation (DNS), Large Eddy Simulation (LES) and Two Fluid Model (TFM). Theoretically they can all be combined with DEM to describe coupled particle-fluid flow. Examples of coupled models are LB-DEM (Cook et al., 2004), PPM-DEM (Fernandez et al., 2011; Ge and Li, 2003), DNS-DEM (Hu, 1996; Pan et al., 2002), and LES-DEM (Zhou et al., 2004).

Other notable models used to investigate jigging which do not give particle scale and fluid flow field information although have had success include: Potential energy (Mayer, 1964; Tavares, 1999; Tavares and King, 1995), Potential energy-Monte Carlo (Tavares, 1999), Artificial Neural Network (ANN) (Panda et al., 2012; Sun et al., 2005), Statistical (Ahmed, 2011), Unsteady-fluidisation (Jinnouchi and Kawashima, 1979), and Mathematical (Dieudonne et al., 2006).

Table 2–2 outlines the key features and relative merit of typical models used for particle-fluid flow. It can be seen in the fourth column CFD-DEM is most suitable for the ore process modelling of jigging with acceptable fundamental particle physics and reasonable computational effort.

Table 2–2. Typical models for particle-fluid flow and their relative merits (Zhu et al., 2007).

Model type	Length scale for fluid phase	Sub-particle (discrete or continuum)	Pseudo-particle (discrete)	Computational cell (continuum)	Computational cell (continuum)
	Length scale for particle phase	Particle (discrete)	Particle (discrete)	Particle (discrete)	Computational cell (continuum)
	Nature of coupling	Discrete + discrete or continuum + discrete	Discrete + discrete	Continuum + discrete	Continuum + continuum
	Example	LB-DEM or DNS-DEM	PPM-DEM	CFD-DEM	TFM
Closure of equations		Yes (but may experience numerical difficulty for systems with strong particle–particle interactions)	No (difficulty to determine physical properties of a pseudo-particle)	Yes	No (constitutive relation for solid phase and phase interactions not generally available)
Incorporation of distribution effects of dispersed, solid phase		Yes	Yes	Yes	No
Computational effort		Extremely demanding	Very demanding	Demanding	Acceptable
Suitability for engineering application in relation to process modelling and control		Extremely difficult	Very difficult	Difficult	Easy
Suitability for fundamental research in relation to particle physics		Most acceptable (particle–fluid interaction forces can be determined and used for CCDM)	Acceptable (but only valid for well-defined PPM system)	Acceptable	No

2.3.2.6 Summary of limitations of past DEM-CFD numerical studies

Each study in this area has lacked in certain aspects. The short-comings of previous work include:

- Geometric simplifications (Asakura et al., 2007; Xia et al., 2007; Xia and Peng, 2007);
- One-way coupling (Dong et al., 2009);
- A limitation of fluid-particle physics and discussion (Asakura et al., 2007; Dong et al., 2009; Xia et al., 2007; Xia and Peng, 2007);
- One study modelled an alternative profile to the sinusoidal waveform (Dong et al., 2009);
- One study pursued experimental validation which was performed for only one scenario—it is unclear how accurate the model will be for other parameters. (Dong et al., 2009)

The simplistic geometries selected in previous work limits the usefulness of the models. Xia and Peng (2007) developed a 2D column model, Asakura et al. (2007) a 3D column model, and Dong et al. (2009) produced a 3D geometrically close-to realistic model of an InLine Pressure jig. A geometrically simple model such as a column is helpful on a fundamental level and has merits, but it negates many real operating conditions including: bed cross flows; hutch flows; uneven particle feed distribution and fluid pulsion; screen partitions; sieves; complex particle transportation from feed inlet through to top layer, the presence of the roughing layer and separation layer; and particle transportation to the tailing and concentrate discharge chutes. Further, regardless of the geometric complexity a 2D investigation will minimally resolve interstitial trickling which is strongly a 3D phenomenon.

Secondly, particle-fluid coupling, or in other words DEM-CFD coupling, is a critical step in establishing the relationship and influences between the particles and the fluid. Xia and Peng (2007) and Asakura et al. (2007) both developed a two-way coupled model. Alternatively, Dong et al. (2009) used a less sophisticated technique, where in lieu of two-way coupling, they produced a one-way coupled model with a static area

of porosity accounting for the particles influence on the fluid. It is unknown how much this technique decreases model performance.

Thirdly, liquid-particle forces determine particle forces, trajectories, and consequently the fluid flow field. The drag due to porosity is crucial in modelling dense liquid-particle flow. Xia and Peng (2007) and Asakura et al. (2007) did not consider porosity, while Dong et al. (2009) did consider porosity in relation to drag force although used a monosize drag force correlation for a multisize particle system. Additionally, other liquid-particle forces can be important. All the existing studies have neglected the lubrication force. Only Asakura et al. (2007) included the following forces: pressure gradient, virtual mass, Basset, Magnus, and Saffman—although no resultant force values or examination was included in the article. Xia and Peng (2007) modelled the same forces with exception to the Basset force. However, the results are open to doubt. The values for these forces plotted against increasing particle size or density display frequent random large outlier data points several magnitudes larger than closely neighbouring values. No explanation is offered for these inconsistencies thus one may deduce these forces have potentially been improperly implemented. Dong et al. (2009) did not include liquid-particle forces beyond drag and buoyancy.

Fourthly, all the studies have used a sinusoidal pulsation profile with the exception of Dong et al. (2009) which used a saw tooth cycle. Hence, no numerical investigation has studied what effect the jigging pulsation profile shape has on concentration mechanics. This is true not only for DEM-CFD models but all numerical studies of jigging.

Lastly, there is a lack of experimental validation with only one attempt by Dong et al. (2009) for one set of parameters.

The previous jigging DEM-CFD models have all made excellent steps forward in simulating and understanding jigging. However, as discussed above they have lacked in certain areas. Each model developed certain aspects but the potential for improvement exists if all these aspects are incorporated into one model.

The literature would benefit from a numerical jigging model investigation including the following: two-way coupling; 3D model of either simple column or complex geometry; porous media drag force function; liquid particle forces as stated in the BBO (Basset (1888), Boussinesq (1885) and Oseen (1927)) equation together with Magnus, Saffman and lubrication forces, and an examination of these forces in a jigging context; attempts at experimental validation; and finally an investigation of different pulsation profile shapes on concentration mechanisms.

2.4 THEORY OF DEM-CFD

The DEM-CFD approach was firstly proposed by Tsuji et al. (1993) and was rationalized by Xu and Yu (1997, 1998b). There are different methods of implementing DEM-CFD which can be categorized into three aspects: governing equations, schemes of coupling fluid and solid phases, and correlations to calculate the particle-fluid interaction force.

2.4.1 Governing equations

Two model formulations, Model A and Model B are typically used in DEM-CFD (Gidaspow, 1994). Three different schemes have been used to couple the fluid and solid phases through the particle interaction force, which is a link between particle and a local averaged computation cell. Additionally, different correlations have been used to calculate the particle interaction force. Model A and Model B are also known as the Pressure Gradient Force (PGF) model and the Fluid Density-Based (FDB) model, respectively. Model A assumes that the pressure drop is shared between the fluid and solid phases while Model B assumes it applies to the fluid phase only. The governing equations for the fluid phase of both models are as follows:

Conservation of mass

$$\frac{\partial \varepsilon_f}{\partial t} + \nabla \cdot \left(\varepsilon_f \mathbf{u}_f \right) = 0 \tag{2–5}$$

Conservation of momentum

Model A

$$\frac{\partial \rho_f \varepsilon_f \mathbf{u}_f}{\partial t} + \nabla \cdot \left(\rho_f \varepsilon_f \mathbf{u}_f \mathbf{u}_f \right) = -\varepsilon_f \nabla P - \mathbf{F}^{\mathrm{A}} + \nabla \cdot \left(\varepsilon_f \boldsymbol{\tau} \right) + \rho_f \varepsilon_f \mathbf{g} \tag{2–6}$$

Model B

$$\frac{\partial \rho_f \varepsilon_f \mathbf{u}_f}{\partial t} + \nabla \cdot \left(\rho_f \varepsilon_f \mathbf{u}_f \mathbf{u}_f \right) = -\nabla P - \mathbf{F}^{\mathrm{B}} + \nabla \cdot \left(\varepsilon_f \boldsymbol{\tau} \right) + \rho_f \varepsilon_f \mathbf{g} \tag{2–7}$$

where $\mathbf{u}_f$ and P are the fluid velocity and pressure, respectively, and $\boldsymbol{\tau}$, ε_f, ρ_f and ΔV are the fluid viscous stress tensor, fluid volume fraction, fluid density, and computational cell volume, respectively. $\mathbf{F}^A$ and $\mathbf{F}^B$ are the volumetric particle-fluid interaction forces for the two models. There is a link between $\mathbf{F}^A$ and $\mathbf{F}^B$ given by $\mathbf{F}^B = \mathbf{F}^A / \varepsilon_f - \rho_f \varepsilon_s \mathbf{g}$. (Gidaspow, 1994)

The solid phase is treated by a discrete approach involving translational and rotational motion. The forces acting on a particle include gravity, contact forces between particles and wall, and interaction forces between particles and fluid. The particle-fluid interaction forces include: drag force, virtual mass, Basset, Magnus, Saffman, lubrication. Others forces exist depending on the system being wet, dry, fine or coarse.

The contacts between particles incur deformations and so the particles are allowed to over lap slightly in DEM. The interparticle forces act at the contact point not the centre of mass and torque will be generated from rotating the particle. Currently rolling friction torque is very difficult and is still an open study (Zhu et al., 2007). The most common linear model is the linear spring-dashpot model proposed by Cundall and Strack (1979) where the spring is used for elastic deformation and the dashpot accounts for viscous dissipation. More theoretically sound is the Hertz-Mindlin and Deresiewicz model, where Hertz (1882) coined a theory to describe the elastic contact between two spheres in the normal direction where the relationship between normal force and normal displacement was nonlinear. Due to the computational effort required adopting the Hertz-Mindlin and Deresiewicz model it is not so popular in the application of DEM (Zhu et al., 2007). A list of various simplified models based on

the Hertz-Mindlin and Deresiewicz theories and a table of equations can be found in (Zhu et al., 2007) and detailed theory can be found in (Cundall and Strack, 1979). Currently, there are only very simplified non-spherical DEM-CFD modelling techniques. These assume particles of different spherical sizes or of irregular shapes, such as ellipsoid, polygon, and cylinders which are constructed from spherical particles (Hilton and Cleary, 2011). The governing equations for spherical particle i can be expressed as follows:

Translational motion

$$m_i \frac{d\mathbf{u}_{\mathrm{p,i}}}{d\,\mathrm{t}} = \mathbf{f}_{\mathrm{p-f,i}} + \sum_{j=1}^{k_i} \left(\mathbf{f}_{c,ij} + \mathbf{f}_{d,ij} \right) + \rho_{p,i} V_{p,i} \mathbf{g} \tag{2–8}$$

Rotational motion

$$I_i \frac{d\boldsymbol{\omega}_i}{dt} = \sum_{j=1}^{k_i} \mathbf{T}_{ij} \tag{2–9}$$

where m_i, I_i, k_i, $\mathbf{u}_{p,i}$, and $\boldsymbol{\omega}_i$ are the mass, moment of inertia, number of contacting particles and translational and rotational velocities of particle *i*, respectively. While $\mathbf{f}_{c,ij}$, $\mathbf{f}_{d,ij}$, $\mathbf{T}_{ij}$ are the contact force, viscous contact damping force, and torque, respectively between particles *i* and *j*. These interparticle forces and torques are summed over k_i particles in contact with particle *i*. $\mathbf{f}_{p-f,i}$ is the total particle-fluid interaction force on a particle, which includes fluid drag force $\mathbf{f}_{drag,i}$, the buoyancy force, and others mentioned previously. For simplicity the buoyancy and fluid drag forces will be shown here to highlight the fundamentals of the formulae.

Corresponding to different ways to treat pressure drop, the particle-fluid interaction force $\mathbf{f}_{p-f,i}$ is calculated using two approaches. Consistent with the fluid phase these are referred to as Model A and Model B and are obtained at different time and length scales. The equations are as follows:

Model A

$$\mathbf{f}_{p-f,i} = -V_{p,i} \nabla P_i + \mathbf{f}^{A} \tag{2–10}$$

Model B

$$\mathbf{f}_{p-f,i} = \rho_f V_{p,i} g + \mathbf{f}^B \tag{2–11}$$

Feng and Yu (2004a) explain in detail the differences in both models A and B. As for the fluid phase there is a relationship between $\mathbf{f}^A$ and $\mathbf{f}^B$, given by $\mathbf{f}^B = \mathbf{f}^A / \varepsilon_f$. Models A and B for fluid and solid phase must correctly match in order to generate correct quantitative results (Xu and Yu, 1998a). In Model A the first term is the buoyancy force related to the total pressure drop ∇P_i, while the second term $\mathbf{f}^A$ is the fluid drag force multiplied by the fluid volume fraction $\varepsilon_f f_{drag,i}$. Alternatively, in Model B the first term represents the buoyancy force only related to the static pressure drop ∇P_o and the second the sum of fluid drag force $\mathbf{f}_{drag,i}$. The total pressure drop consists of ∇P mainly consists of three parts: the hydrostatic pressure drop due to gravity of the fluid ∇P_o, the dynamic pressure drop aka piezometric or manometric pressure drop ∇P_d, due to relative motion between fluid and particles, and the pressure drop due to friction between the fluid and wall usually ignored ∇P_w. The equations can be rewritten as follows:

Model A

$$\mathbf{f}_{p-f,i} = -V_{p,i}\rho_f \mathbf{g} + V_{p,i}\nabla P_{d,i} + \varepsilon_f \mathbf{f}_{drag,i} \tag{2–12}$$

Model B

$$\mathbf{f}_{p-f,i} = -V_{p,i}\rho_f \mathbf{g} + \varepsilon_s \mathbf{f}_{drag,i} + \varepsilon_f \mathbf{f}_{drag,i} \tag{2–13}$$

Feng and Yu (2004a) explained that for a system composed of monosized particles where both phases are uniformly distributed without acceleration, the pressure drop is only the static pressure drop ∇P_o and the dynamic pressure drop ∇P_d .The values of dynamic pressure for every particle are identical and can be described with a local average value, ∇P_d. The particle volume $V_{p,i}$ can be expressed as ε_s / n, where n is the number of particles per unit volume. The relationship between pressure drop and drag force acting on a particle is $\nabla P_d = n\mathbf{f}_{drag,i}$. Hence, the second term in equation (2–12) $V_{p,i}\nabla P_{d,i}$ can be replaced by $(\varepsilon_s / n)nf_{drag,i} = \varepsilon_s f_{drag,i}$. Therefore in a simple system

Models A and B are the same. However, during fluidization particles are not uniformly distributed in space and have different velocities in magnitude and direction and so the individual values of dynamic pressure $\nabla P_{d,i}$ are not identical and not equal to the local-average value of ∇P_d obtained using DEM-CFD. Feng and Yu (2004a) attributed the significant differences of Model A and B results of a binary mixture of multiple sizes to the distribution of the force related to dynamic pressure drop at local-average scale to individual particles in Model A. They concluded that Model B is more consistent with experimental evidence. Differences can be reduced by distributing forces in Model A according to surface area rather than volume of particles. For monosized particles there is no differences in particle surface and volume fractions and therefore little difference has been found between Model A and B in CFD-DEM (Feng and Yu, 2004b; Kafui et al., 2004), and also using TFM (Bouillard et al., 1989).

Kafui et al. (2002) examined the differences between the PGF and FDB models. The results show a minor difference in qualitative fluidization behaviour but a significant difference in the first wave of bed expansion. Kafui et al. (2004) later attributed the differences in initial porosity of the pre-fluidized beds and further stated that despite this, in slightly higher bed expansion the differences did not subside suggesting that the initial packing condition was irrelevant at this time of the simulation and that there is definitely a difference between models. An aspect of their study which deserves attention is the inclusion of a viscous stress gradient term, $\boldsymbol{\tau}_f$ replacing total pressure drop ∇P_i. In conclusion their results found that Model A results were most consistent with observations and empirical correlations.

2.4.2 Coupling schemes between discrete solid and continuum fluid phase

The three coupling schemes are described by Feng and Yu (2004a) for DEM-CFD along with their deficiencies. A list of study examples adopting these schemes have been listed by Zhu et al. (2007). The coupling between phases is achieved through the particle-fluid interaction force. The fluid phase is at a local-averaged computational

cell level ($\mathbf{F}^A$ or $\mathbf{F}^B$) and an individual particle level for the solid phase ($\mathbf{f}^A$ and $\mathbf{f}^B$). The following schemes have been proposed:

Scheme 1: The force from the particles to the fluid phase is calculated by a local-average method as used in the TFM, while the force from the fluid phase to each particle is calculated separately according to individual particle velocity. This scheme cannot guarantee Newton's third law—for every action, there is an equal and opposite reaction.

Scheme 2: The force from the particles to the fluid phase is calculated first with a local-average method as used in scheme 1. This value is then distributed to individual particles according to a certain average rule. An example of the average rule is as follows:

$$\mathbf{f} = \frac{\mathbf{F}\Delta V}{k_c} \tag{2–14}$$

where k_c is the number of particles in a computational cell, $\mathbf{F}$ is the volumetric particle-fluid interaction force, ΔV is the volume of the computational cell, and $\mathbf{f}$ is the force on an individual particle. This scheme can satisfy Newton's third law. However, it uniformly distributes the interaction force amongst the particles in a computational cell irrespective of the different behaviours of the particles in the cell. In addition the calculation of the particle fluid interaction force uses a mean particle velocity which is still an open question, particularly for multisized systems.

Scheme 3: At each time step the particle fluid interaction forces on individual particles in a computational cell are calculated first, the values are then summed to produce the particle-fluid interaction force at the cell scale, as follows:

$$\mathbf{F} = \frac{\sum_{i=1}^{k_c} \mathbf{f}}{\Delta V} \tag{2–15}$$

where ΔV is the volume of the computational cell. This scheme satisfies Newton's third law and is widely accepted overcoming the previous schemes issues, it was introduced by Xu and Yu (1997, 1998a).

Figure 2–15 illustrates diagrammatically the numerical coupling of DEM-CFD (Xu et al., 2001). At each time step DEM will give information of positions and velocities of individual particles for the evaluation of porosity and volumetric fluid drag force in a computational cell. CFD will then use this data to determine the fluid flow field then yields the fluid drag forces acting on individual particles. Incorporating the resulting forces into DEM will produce information about the motion of individual particles for the next time step.

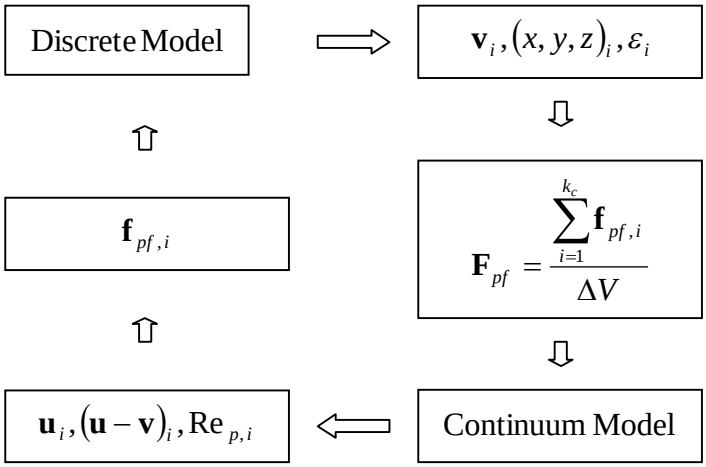

Figure 2–15. Coupling and information exchange between continuum (CFD) and discrete (DEM) models
(Xu et al., 2001).

2.4.3 Hard sphere vs. Soft sphere

Hard-sphere and soft-sphere are two types of particle dynamic modelling used to describe the interactions between particle-particle and particle-wall. These contact models and others were reviewed by Zhou et al. (2002). It was concluded the particle dynamic model is the most realistic method of dynamic simulation of granular flow

because of its first principle approach where particle motion is based on Newton's second law and particle contact mechanics.

The hard-sphere method assumes contacts are instantaneous and binary. Each collision is processed one at a time according to the order in which events occur consequently multiple collisions at the same instant will not be accounted for. This approach is event driven where particles are moved up until the next collision. In dilute systems the hard sphere approach is more efficient than the soft-sphere approach, although if the particles lock together the method breaks down. Therefore, particle systems which are dense or have a low coefficient of restitution resulting in a dramatic decrease of kinetic energy cannot be handled with the hard-sphere approach. (Deen et al., 2007)

In the soft-sphere method contacts are enduring rather than distinct. This method is time-step driven and all the particles are moved together within a fixed time-step. The method does not assume contacts are instantaneous and more than one contact at a time is possible. This model allows multiple slight overlaps (<0.5%) and contact forces are calculated from a deformation history of contact using a linear spring-dashpot model (Cundall and Strack, 1979). This approach can be used for both dilute and dense systems. Particulate flow in jigging is dense hence the soft-sphere method is the appropriate choice for modelling.

2.4.4 Correlations used for particle-interaction forces

The particle-fluid interaction force is determined using correlations derived from empirical evidence or numeral models. An accurate representation of the fluid drag force is necessary for a quantitative analysis of a particulate system. Due to the complexity of the problem a precise analytical solution at all Reynolds numbers is not available. Drag force correlations have been developed from numerous means including: packed-bed measurements (Ergun, 1952; Macdonald et al., 1979); settling experiments (Richardson and Zaki, 1954; Syamlal and O'Brien, 1994); fluidized-bed experiments (Wen and Yu, 1966); and Lattice-Boltzmann methods (Benyahia et al., 2006; Koch and Sangani, 1999).

The most common equations used is a combination of Ergun equation (Ergun, 1952) in the dense regime for porosities less than 0.8 and Wen and Yu's correlation (Wen and Yu, 1966) in the dilute regime for porosities greater than 0.8. Separately the Di Felice correlation across all porosities is used (Di Felice, 1994). For higher porosities see Enwald et al. (1996). The Ergun-Wen and Yu technique has the deficiency of a discontinuous prediction in drag force at porosity greater than 0.8 which results in a step like plummet in drag force values as seen in Figure 2–16. The Di Felice correlation is continuous and therefore has gathered much popularity. To avoid discontinuity of the Ergun-Wen and Yu technique, Xiang et al. (2010) introduced a switch function to give a smooth transition in drag force values from the dilute regime to the dense regime. Other techniques have also been used (Happel, 1958; Hill et al., 2001a; Koch and Sangani, 1999).

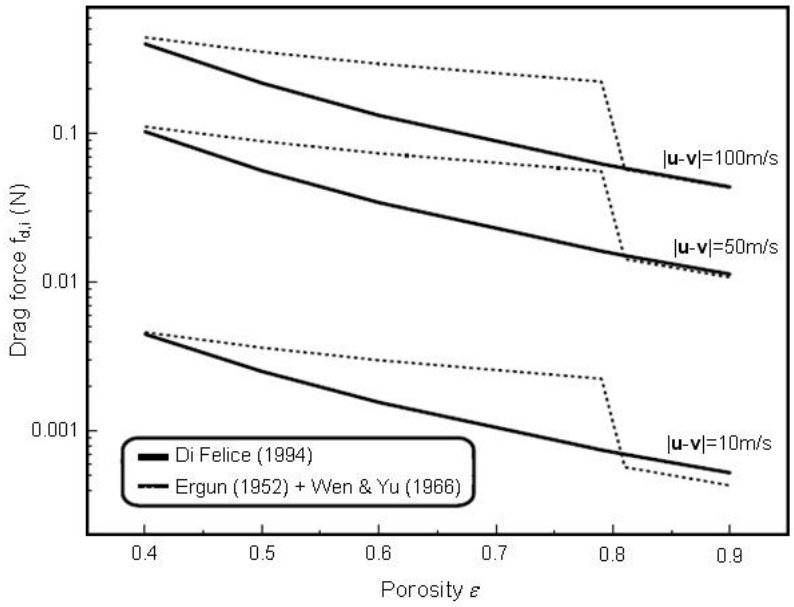

Figure 2–16. Drag forces acting on a 4mm diameter particle as predicted using a combination of the (Ergun, 1952) and (Wen and Yu, 1966) correlations compared with the prediction of (Di Felice, 1994) correlation for a range of porosities at three superficial slip velocities
(Kafui et al., 2002).

Bokkers et al. (2004) compared the empirical Ergun and Wen and Yu drag correlations to simulations using a drag relation that was derived from LBM

simulations by Hill et al. (2001a). The latter equation was shown to give results that are in better agreement with experiments as compared to simulations where empirical models were used. Beetstra et al. (2007a) derived another drag relation from LBM results which is claimed to be slightly more accurate than the relation of Hill et al. Hill et al. (2001a) and valid over a wider range of Reynolds numbers. Figure 2–17 below shows how the drag force model by Beetstra et al. (2007b) compares.

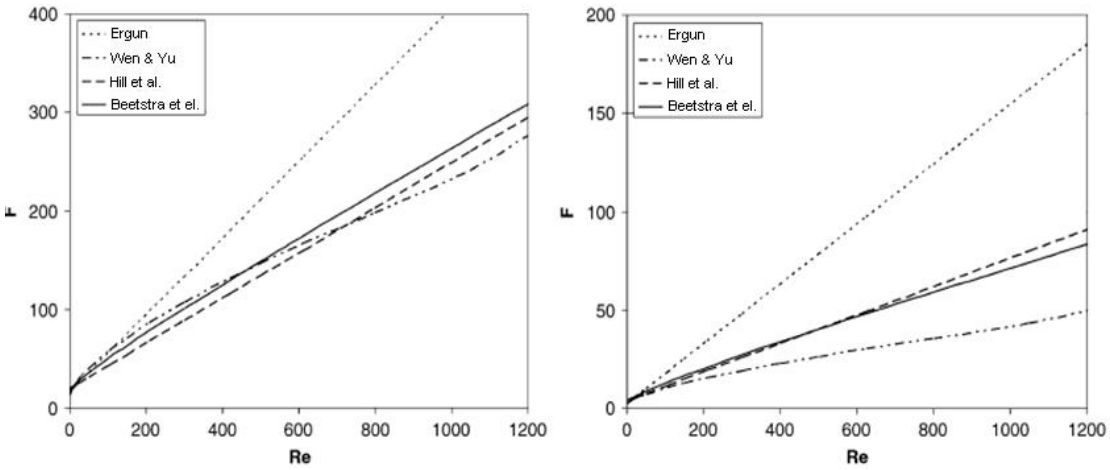

(a) (b)

Figure 2–17. Predictions for the normalised drag force as a function of Reynolds number calculated with the various equations: (a) ε =0.5; (b) ε =0.8 (Beetstra et al., 2007b).

Other modifications listed by Sarkar et al. (2009) that have been suggested for the Ergun equation include: (i) a correction should be made in order to get the correct limiting form for porosities approaching 1 (Gibilaro et al., 1985; Hoef et al., 2005); (ii) the coefficient 150 should be changed to 180 (Hill et al., 2001a; Hoef et al., 2005; Maier et al., 1999); (iii) the coefficient 1.75—in case a linear scaling with *Re* is assumed—should be replaced by a function depending on the porosity (Hill et al., 2001b).

Currently, many equations have been derived for monosized particle systems and have been used in an *ad hoc* approach to solve binary systems yielding qualitative results (Bokkers et al., 2004; Feng and Yu, 2007; Hoomans et al., 2000), and in jigging (Asakura et al., 2007; Dong et al., 2009; Xia et al., 2007; Xia and Peng, 2007). Polydisperse configurations cannot be treated as a monodisperse system because the

local porosity of the smaller particles is higher than the average porosity of a system, and of course that of the larger particles. Thus using an average porosity the small particles experience a smaller drag force than expected while the force on the larger particles is larger.

Pirog (1998) developed a drag force correlation for polydisperse systems based on a voidage-velocity correlation obtained from settling and creaming experiments in liquid-solid systems. The analysis was done for systems with a continuous size distribution and hence this correlation cannot be used for a general binary-size system as the size distributions in a usual binary system vary. Based on theoretical considerations Hoef et al. (2005) developed a drag force correlation for polydisperse systems based on LBM simulations of fluid flow a past random arrays of stationary bidisperse spheres. This work developed a correction factor for the effect of polydispersity which depends on the porosity, diameter ratio, and composition of the mixture. Simulations were done for Reynolds numbers up to 1 for solid volume fractions ranging from 0.1 to 0.6 and for diameter ratios ranging from 1 to 4. Beetstra et al. (2007b) later confirmed that the correction proposed by Hoef et al. (2005) holds for particle Reynolds numbers up to 1000. Beetstra et al. (2007b) further investigated gas-particle drag laws and found that the correction factor for polydispersity gives a significant improvement over drag models without this correction, the results were validated experimentally. Sarkar et al. (2009) proved with an analysis how significant it is to treat the particle-fluid interaction force with considerations to the binary nature of a system. Sarkar et al. (2009) found that the force on a particle may reduce by a factor of two when the particle size ratios are changed from 1:3 to 1:5.

2.4.5 Particle motion in fluids

2.4.5.1 General particle motion equation

The motion of particles in fluids give rise to additional forces which can be relevant but are less dominant than the drag force within a fluidization or jigging system. The BBO equation considers the general forces acting on particle. It was named after the pioneering work of Basset (1888), Boussinesq (1885) and Oseen (1927). Neglecting

Faxen terms the equation proposed by Maxey and Riley (1983) for small particle Reynolds number is as follows:

$$\mathbf{f}_{p-f,i} = \mathbf{f}_{drag} - \mathbf{f}_{inertial} + \mathbf{f}_{virtial\ mass} + \mathbf{f}_{basset} + \mathbf{f}_{gravity} \tag{2–16}$$

$$\begin{aligned} m_p \frac{d\mathbf{u}_p}{dt} = \frac{18\mu_f}{\rho_p d_p^2} m_p \left(\mathbf{u}_f - \mathbf{u}_p\right) - m_f \frac{D\mathbf{u}_f}{Dt} + 0.5 m_f \left(\frac{D\mathbf{u}_f}{Dt} - \frac{d\mathbf{u}_p}{dt}\right) \\ + 9\sqrt{\frac{\rho_f \mu_f}{\pi}} \frac{m_p}{\rho_p d_p} \int_0^t \frac{\dfrac{D\mathbf{u}_f}{D\tau} - \dfrac{d\mathbf{u}_p}{d\tau}}{(t-\tau)^{1/2}} d\tau + \left(m_p - m_f\right)\mathbf{g} \end{aligned} \tag{2–17}$$

where $\mathbf{f}_{p\text{-}f}$, $\mathbf{f}_{drag}$, $\mathbf{f}_{inertial}$, $\mathbf{f}_{virtual\ \mathrm{mass}}$, $\mathbf{f}_{basset}$ and $\mathbf{f}_{gravity}$ are the total particle-fluid interaction force, drag force, inertial (pressure-gradient) force, virtual mass force, basset (history) force and gravity force. Further, m_p, m_f, $\mathbf{u}_p$, $\mathbf{u}_f$ are the particle mass, fluid mass, particle velocity, fluid velocity, respectively. While ρ_p, μ_f, d_p, t and τ are the particle density, dynamic viscosity, particle diameter, time and time-scale, respectively.

2.4.5.1.1 Inertial force

The inertial force, $\mathbf{f}_{inertial}$, considers the acceleration of the carrier phase. It is only relevant if the fluid acceleration is strong. The inertial force can be re-written as:

$$\mathbf{f}_{inertial} = m_p \frac{\rho_f}{\rho_p} \left(\frac{D\mathbf{u}_f}{Dt}\right) \tag{2–18}$$

It can be seen that in gas-solid flows the inertial force can be neglected as $\rho_f/\rho_p << 1$. In liquid-solid flows this force can be relevant if $\rho_f/\rho_p \approx 1$.

2.4.5.1.2 Virtual mass force

The Virtual mass force (or added mass force), $\mathbf{F}_V$, is present when a particle is in rectilinear unsteady motion. This dynamic force is exerted by the fluid on a submerged object if the relative velocities between the two change with time. The

force is required to accelerate the surrounding fluid and is equivalent to adding a mass to a particle. This is due to the particle boundary which prevents mass flux through the surface. The Virtual mass force (or Added mass force) on a sphere accelerating in a viscous fluid is found as follows:

$$\mathbf{f}_{virtual\ mass} = \frac{1}{2} C_{vm} \rho_f V_p \left(\frac{D\mathbf{u}}{Dt} - \frac{d\mathbf{v}}{dt} \right) \tag{2–19}$$

Odar and Hamilton (1964b) and Odar (1966b) experimentally studied the force on a guided sphere rectilinearly oscillating in an otherwise stagnant fluid. A numerical coefficient was derived to account for the inertial effect at high Reynolds numbers, where C_{VM} determined empirically is formulated as:

$$C_{VM} = 2.1 - \frac{0.132}{A_c^2 + 0.12} \tag{2–20}$$

The parameter, A_c, is called the acceleration number and is defined by:

$$A_c = \frac{(\mathbf{u} - \mathbf{v})^2}{d_p \left(\frac{D\mathbf{u}}{Dt} - \frac{d\mathbf{v}}{dt} \right)} \tag{2–21}$$

In the above equations, **u** and **v** are the instantaneous fluid flow and particle velocities, ρ_f is the fluid density, V_p is the volume of the particle, and D/D*t* denotes the material derivative.

2.4.5.1.3 Basset force

The Basset force is caused by lagging boundary layer development on a particle where there is a changing relative velocity between the particle and carrier phase. This acceleration force arises when viscous stresses on a particle surface are unsteady. As it depends on temporal development of the flow it is also referred to as the history

force. Based on Odar and Hamilton (1964b) who studied the motion of a single sphere in simple harmonic motion, the Basset force is expressed as:

$$\mathbf{f}_{basset} = 9\sqrt{\frac{\rho_f \mu_f}{\pi}}\frac{m_p}{\rho_p d_p} C_B \left\{ \int_0^t \frac{\frac{D\mathbf{u}_f}{D\tau} - \frac{d\mathbf{u}_p}{d\tau}}{(t-\tau)^{1/2}} d\tau + \frac{(\mathbf{u}_f - \mathbf{u}_p)_0}{\sqrt{t}} \right\} \qquad (2\text{–}22)$$

The second term in the Basset force accounts for an initial slip velocity at t = 0 (Reeks and Mckee, 1984). The coefficient C_B was obtained experimentally by Odar and Hamilton (1964b) expressed as:

$$C_B = 0.48 + \frac{0.52}{(A_c + 1)^3} \qquad (2\text{–}23)$$

The basset force is time consuming to solve because it has to be integrated over the entire particle trajectory. Therefore, this force is often neglected. Numerical calculations of Sommerfeld (1996) have shown the inclusion of the Basset force increases the computational time by a factor of ~10. Fortunately, the history force tends to be negligible when $Re_p >> 1$, when $\rho_p/\rho_f >> 1$, or when the relative acceleration between the particle and fluid phase is small (Sommerfeld, 2000).

2.4.6 Additional forces

Aside from the general forces of particle motion based on translational particle and/or fluid movement, other forces may be significant in solid-liquid flow. These relate to the fluid velocity field, particle rotational movement, and neighbour particle trajectories.

2.4.6.1 Magnus force

A particle will rotate either when the fluid flow is not uniform at various locations, or it faces a collision with a rotating particle.

As a spinning particle moves through the fluid, it spins a boundary layer of fluid that clings to its surface due to viscous friction forming a thin vortex. On one side of the particle the vortex collides with oncoming free-stream fluid. The collision causes the fluid close to the surface of the particle to decelerate, creating a high-pressure area. On the opposing side, the vortex is moving in the same direction as the oncoming free-stream fluid, there is no collision and the fluid collectively moves faster. This sets up a low-pressure area. The pressure differential, high on one side and low on the other creates a lift force (the Magnus force) that causes the particle to move in the direction of the pressure differential which is perpendicular to both the objects spin axis and direction of travel (see Figure 2–18). The more spin, the greater the Magnus effect and the greater the resulting curve trajectory. When the particle spin axis is perfectly parallel to its velocity, the Magnus effect is null and no part of the boundary layer opposes or compliments the surrounding fluid flow.

The application of Bernoulli's principle provides an approximation of the Magnus phenomenon. A more accurate model would include unsteady viscous effects driven by laminar and turbulent boundary layer separation, and the influence of the separated wake behind a particle.

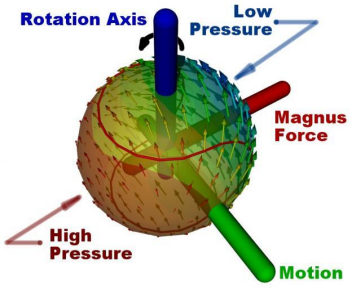

Figure 2–18. Pressure distribution due to Magnus rotational force.

The Magnus force due to particle rotation can be expressed as follows:

$$\mathbf{f}_{magnus} = \frac{1}{2}\rho_f v_r^{\,2}\frac{\pi d^2}{4}C_{LM}\frac{\boldsymbol{\omega}_r \times \mathbf{v}_r}{|\boldsymbol{\omega}_r||\mathbf{v}_r|} \qquad (2\text{–}24)$$

A number of Magnus lift coefficients C_{LM} exist depending on the Reynolds number regime. The following authors Rubinow and Keller (1961), Oesterle et al. (1991), and Tsuji et al. (1985), developed expressions for the regimes, $\mathrm{Re}_p < 1$, $10 < \mathrm{Re}_p < 60$, and $550 < \mathrm{Re}_p < 1600$, respectively. Utilizing these results Lun and Lui (1997) developed a correlation for the Magnus lift coefficient which is applicable for a wider intermediate range of Re_p and can be expressed as follows:

$$C_{LM} = \frac{d|\boldsymbol{\omega}_r|}{|\mathbf{v}_r|} \quad (\mathrm{Re}_p \le 1) \tag{2–25}$$

$$C_{LM} = \frac{d|\boldsymbol{\omega}_r|}{|\mathbf{v}_r|}(0.178 + 0.822\,\mathrm{Re}_p^{-0.522}) \quad (1 < \mathrm{Re}_p < 1000) \tag{2–26}$$

In the above equations the quantities $\mathbf{v_r} = \mathbf{u} - \mathbf{v}$ and $\boldsymbol{\omega_r} = \boldsymbol{\Omega_f} - \boldsymbol{\omega}$ are the instantaneous relative linear and angular velocities between the local fluid and the particle, respectively. Where, **u** and **v** are the instantaneous linear velocities of the fluid and the particle, respectively. The instantaneous particle angular velocity is defined as $\boldsymbol{\omega}$ while the local mean angular velocity of the fluid is defined as $\boldsymbol{\Omega_f} = 0.5\nabla \times \mathbf{U}$, where **U** is the mean fluid velocity.

2.4.6.2 Saffman force

A velocity gradient develops when either fluid flow moves around a particle, local porosity changes, or when fluid travels along a wall. Particles in a shear flow as shown in Figure 2–19 experience a lift force (the Saffman lift force) perpendicular to the direction of flow. The lift force is caused by the pressure distribution induced by the resultant velocity gradient.

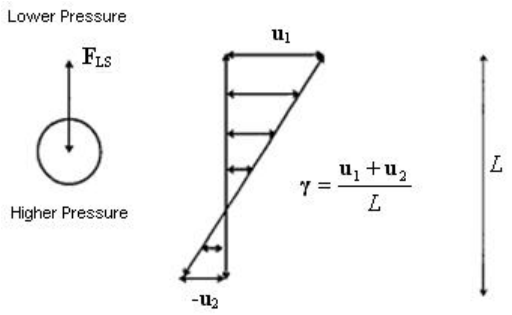

Figure 2–19. Shear field giving rise to Saffman lift force.

The Saffman lift force (Saffman, 1965, 1968) is due to a translating particle in a velocity gradient, where the translation velocity is parallel to the streamlines of the fluid, which can be expressed as follows:

$$\mathbf{f}_{saffman} = \frac{1.615 d^2 C_{LS} \sqrt{\rho_f \mu_f}}{\sqrt{|\boldsymbol{\gamma}|}} (\mathbf{u} - \mathbf{v}) \times \boldsymbol{\gamma} \tag{2–27}$$

Three different particle Reynolds numbers point out the necessary conditions for validity of equation 2–27:

$$\mathrm{Re}_p = \frac{|\mathbf{v}_r| d}{\nu} \text{ (Slip)} \tag{2–28}$$

$$\mathrm{Re}_\omega = \frac{|\boldsymbol{\omega}| d^2}{\nu} \text{ (Shear slip)} \tag{2–29}$$

$$\mathrm{Re}_\gamma = \frac{|\boldsymbol{\gamma}| d^2}{\nu} \text{ (Spin slip)} \tag{2–30}$$

In the above equations, **u** and **v** are the instantaneous fluid flow and particle velocities, $\mathbf{v}_r$ and **ω**, are the instantaneous particle relative velocity and angular velocity, respectively. The magnitude of the velocity gradient is defined as **γ**, ν is the kinematic viscosity, μ_f is the dynamic viscosity, and d the particle diameter. The equation is valid when the following condition are met:

$$\mathrm{Re}_p, \mathrm{Re}_\gamma, \mathrm{Re}_\omega < 1 \text{ and } \mathrm{Re}_\gamma / \mathrm{Re}^2 > 1$$

These restrictive conditions imply three alternatives, where either very low shear and particle linear and angular velocities are present, or the viscosity of the fluid is extremely high, or the particles are sub-micron.

A computational three-dimensional uniform shear flow around a non-spinning sphere analysis conducted by Dandy and Dweyer (1990) obtained values for the lift force in a wide range of Reynolds numbers based on the particle diameter $(0.1 < \mathrm{Re}_p < 100)$. Referring to these results Mei (1992) obtained a corrective factor to the lift force based on the particle Reynolds number and the local shear rate in the flow. The coefficient is expressed as follows:

$$C_{LS} = (1 - 0.3314\sqrt{\alpha})\exp(-\mathrm{Re}_p/10) + 0.3314\sqrt{\alpha} \quad (\mathrm{Re}_p \le 40) \qquad (2\text{–}31)$$

$$C_{LS} = 0.0524\sqrt{\alpha\,\mathrm{Re}_p} \quad (\mathrm{Re}_p > 40) \qquad (2\text{–}32)$$

where

$$\alpha = \frac{\mathrm{Re}_\gamma}{2\,\mathrm{Re}_p} \qquad (2\text{–}33)$$

2.4.6.3 Lubrication force

When two particles suspended in a viscous fluid approach each other, the motion of each particle is influenced by the other. The velocity field generated by the motion of one particle is transmitted through the fluid medium and influences the motion of (as well as the hydrodynamic force and torque) of the other particle (see Figure 2–20). The dominant contributions to the force and torque may be determined by the methods of lubrication theory. The lubrication force arises from hydrodynamic pressure in the interstitial fluid being squeezed out from the space between two solid surfaces. This hydrodynamic interaction between the two particles retards their motion.

There are several modes of lubrication force interactions between hard spheres. The most well known “squeeze” mode accounts for forces that develop as two spheres

directly approach each other. This force is proportional to the velocity difference between the spheres and is inversely proportional to the surface-to-surface distance. There are lesser known modes which make contributions but are largely dominated by the squeeze mode. These are "rotation" mode which describes one sphere rotating relative to another sphere, and also, a "shearing" mode where a sphere is moving past a second stationary sphere, in a direction transverse to the sphere axis generating a shearing flow. On the other hand, for two separating particles in close proximity the lubrication force becomes attractive, which suppresses the separating velocities (Ten Cate et al., 2004).

To model realistic flows between neighbouring spheres in very close proximity would require a very fine resolution between the spheres which is too high to simulate over reasonable times. To avoid this problem, it is helpful to use explicit near-field approximations of the lubrication forces using the leading order term of the analytic expression in simulation. This force is calculated for pairs of particles that are closer than a threshold separation taken as $\delta = 0.1 d_p$.

If the lubrication force is the only force that dictates the motion of two approaching particles, then the relative velocity will be fully dissipated and a contactless collision due to infinite lubrication force will occur (stokes paradox). This behaviour is caused by the singularity in the lubrication model at zero separation. The paradox can be avoided by considering surface roughness and non-continuum fluid flow. As the separation becomes very small the continuum description of the lubrication model breaks down in the order of the molecular mean free path (Joseph et al., 2001) or surface roughness (Sundararajakumar and Koch, 1996). Different threshold separations have been employed to overcome this singularity this study uses (at $10^{-4} d_p$) at which the lubrication force peaks (Derksen and Sundaresan, 2007).

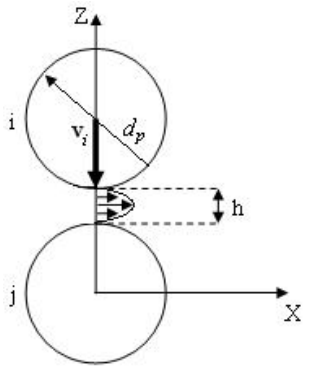

Figure 2–20. The developing velocity profile caused by the squeezing of fluid in particle collision.

For sufficiently small gap widths, the squeeze hydrodynamic force on a sphere moving perpendicular to a plane wall which acts to resist such motion is given by the expression (Cox and Brenner, 1967):

$$\mathbf{f}_{lubrication\ wall,\ i} = -\frac{3}{2}\pi\mu d_p^2 \mathbf{v}_i \frac{1}{h_{ij}} \tag{2–34}$$

For neighbouring particles in motion towards each other and along their line of centres, the net squeeze force on particle i is given by (Ball and Melrose, 1995):

$$\mathbf{f}_{lubrication\ p\text{-}p,\ i} = -\sum_{j=1}^{k_i}\left(\frac{3}{8}\pi\mu d_p^2 \frac{1}{h_{ij}}\right)\left\{\mathbf{v}_i - \mathbf{v}_j \bullet \mathbf{n}_{ij}\right\}\mathbf{n}_{ij} \tag{2–35}$$

In the above equations, μ is the viscosity of the fluid, d_p is the particle diameter, the sum is over nearest-neighbour particles *j*, h_{ij} is the gap between the surfaces, $\mathbf{n}_{ij}$ is the unit vector along the line of centres *i* to *j*, and $\mathbf{v}_i$, $\mathbf{v}_j$ are the particle velocities.

CHAPTER 3

SIMULATION METHOD AND EXPERIMENTAL COMPARISON

3.1 SIMULATION METHOD

3.1.1 Governing Equations

The DEM-CFD model has been well documented in the literature. For brevity, only the outline of the model structure is described below. The solid phase is treated as a discrete phase and solved using DEM. The translational and rotational motions of a particle at any time, t, in the bed are determined by Newton's second law of motion. These can be written as:

$$m_i \frac{d\mathbf{v}_i}{dt} = \mathbf{f}_{f,i} + \sum_{j=1}^{k_i} \left(\mathbf{f}_{c,ij} + \mathbf{f}_{d,ij} \right) + \mathbf{f}_{g,i} \tag{3–1}$$

and

$$I_i \frac{d\boldsymbol{\omega}_i}{dt} = \sum_{j=1}^{k_i} \mathbf{T}_{ij} \tag{3–2}$$

where m_i, I_i , k_i, $\mathbf{v}_i$ and $\boldsymbol{\omega}_i$ are, respectively, the mass, moment of inertia, number of contacting particles, translational and rotational velocities of particle *i*, and $\mathbf{f}_{f,i}$, $\mathbf{f}_{g,i}$ are fluid drag force, gravitational force respectively. $\mathbf{f}_{c,ij}$, $\mathbf{f}_{d,ij}$ and $\mathbf{T}_{i,j}$ are the contact force, viscous contact damping force and torque between particles *i* and *j*. These inter-particle forces and torques are summed over the k_i particles in contact with particle *i*. The particle-particle and particle-wall contact force is based on the soft-sphere method. The particle fluid interaction force is calculated using the Di Felice drag force correlation (Di Felice, 1994), and Model B formulation is adopted (Feng and Yu, 2004a).

The liquid phase is treated as a continuous phase moving through a porous medium created by the particles, and is modelled similarly to conventional two fluid models in which porosity (or liquid volume fraction) modifies the standard single phase Navier-Stokes equations. The governing equations are then the conservations of mass and momentum in terms of the local mean variables over a computational cell, given by:

$$\frac{\partial \varepsilon}{\partial t} + \nabla \cdot (\varepsilon \mathbf{u}) = 0 \tag{3–3}$$

and

$$\frac{\partial (\rho_f \varepsilon \mathbf{u})}{\partial t} + \nabla \cdot (\rho_f \varepsilon \mathbf{u}\mathbf{u}) = -\nabla P - \frac{\sum_{i=1}^{k_c} \mathbf{f}_{f,i}}{\Delta V} + \nabla(\varepsilon \boldsymbol{\tau}) + \rho_f \varepsilon \mathbf{g} \tag{3–4}$$

where ρ_f, $\mathbf{u}$ and P are, respectively, the fluid density, velocity and pressure; $\boldsymbol{\tau}$, ε and ΔV are the fluid viscous stress tensor, porosity and volume of a computational cell.

DEM is solved numerically with an in-house code using an explicit time integration method using established geometrical and flow boundary conditions (Feng and Yu, 2004a). The continuous liquid phase is readily solved using a commercial CFD software package (ANSYS CFX 10.0). The coupling between DEM and CFD is achieved as follows. At each time step DEM will give information of positions and velocities of individual particles for the evaluation of porosity and volumetric fluid drag force in a computational cell. CFD will then use this data to determine the fluid flow field, which in turn is used to determine the fluid drag forces acting on individual particles. Incorporating the resulting forces into DEM will produce information about the motion of individual particles for the next time step. The fluid drag force acting on an individual particle will react on the fluid phase from the particles, so that Newton's third law of motion is satisfied.

3.1.2 Simulation Conditions

The characteristics of feed entering a jig vary tremendously as does the product requirements of the ore being processed. The feed is composed of a multivariable particle distribution including size, density, and purity which constantly change with excavation sites, feed batches, and ore material being mined. Further, the particle system ranges from dense ($\varepsilon \approx 0.36$) to dilute ($e \approx 0.8$) regimes spatially and temporally, depending on operational circumstances. To simplify the system particles were divided into 565 light particles and 565 heavy particles with respective densities of 2540 kg/m^3 (glass) and 4630 kg/m^3 (ceramic), the liquid used was water 1000

kg/m^3 in density. A typical jigging system will contain millions of particles which at present is computationally prohibitive in terms of simulation time. With consideration to time constraints scaling down to 1130 particles has proven useful to model particle flow phenomena and helpful in analysis. The current case best represents a close particle size and density distribution of coarse particles.

Detailed model settings are shown in Table 3–1. The model consists of a rectangular domain (refer to Figure 3–1) filled with a binary-density spherical particle system and liquid. The structured mesh consists of 216 uniform hexahedral elements. The Finite Volume Method technique is used with a second-order high-resolution advection scheme. Time integration was performed using the second-order implicit Euler-Backward method. A time step size of $1x10^{-3}$ was adopted with a residual target (RMS) of $1x10^{-5}$. The DEM is run in serial and using a Intel(R) Core(TM) 2 Duo CPU @ 3.00GHz. The side walls were treated with no-slip boundary conditions. The bottom was considered as a wall for the particle phase, so that so they cannot fall through, but as an inlet for liquid. The top exit was treated with a zero normal gradient opening condition. Periodic boundary conditions were applied to the front and rear surfaces of the flow domain effectively creating infinite thickness and economically reducing the number of particles required to produce 3D results. Figure 3–1 illustrates the mesh and boundary conditions. Figure 3–2 shows an example of a jig particle bed cross-sectional cut numerically modelled. Other types of jigs, either through-the-screen or over-the-screen, could also be used for illustration purposes.

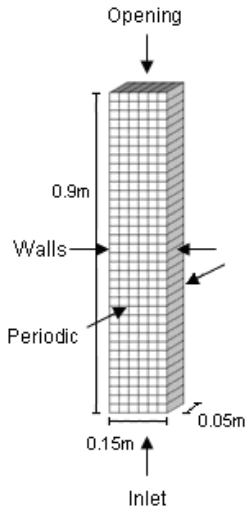

Figure 3–1. Jig model geometry and boundary conditions.

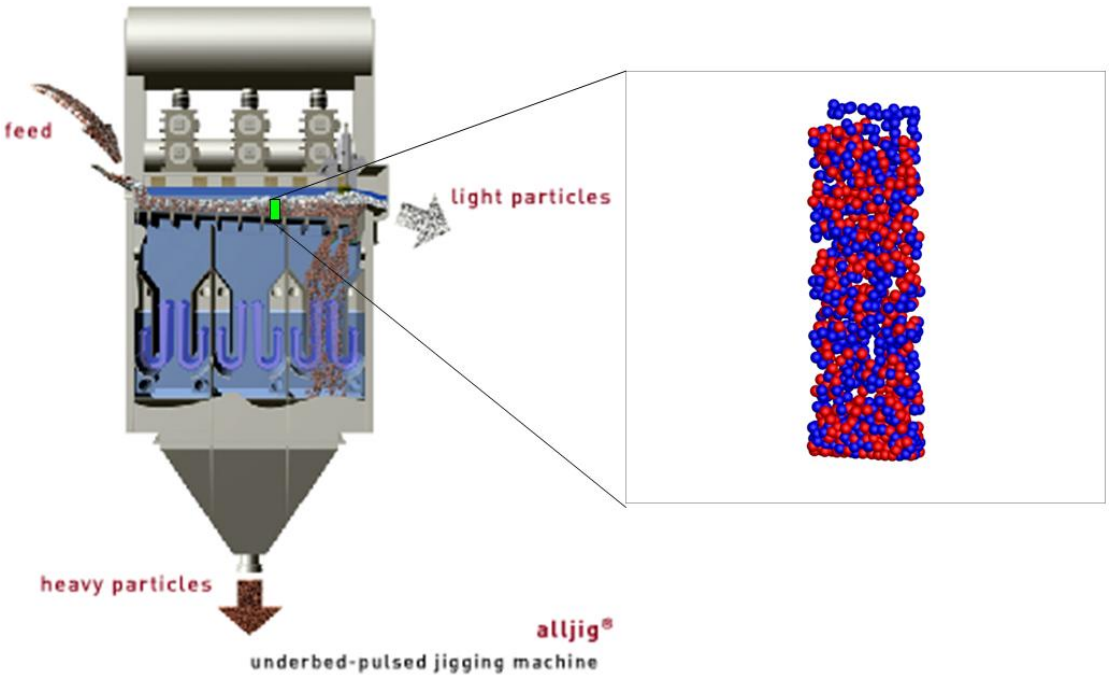

Figure 3–2. Example of jig particle bed cross-sectional cut numercially modelled. Alljig image from Allmineral (2010) adapted.

The liquid flow was considered in 2D using only one cell in the thickness direction and hence does not resolve detailed flow fields in this direction, while DEM modelling of the particles was in 3D, with a bed thickness equal to five particle diameters. Two-dimensional simulations can represent cases were the flow is by

nature two dimensional, i.e. where the flow variations (space and time) are significant in two directions and negligible in the third direction. Significant differences have been shown in the literature of numerical simulations of circulating fluidization units for the same numerical parameter, between 2D and 3D simulations, as the instantaneous local flow physics is highly three dimensional (Peirano et al., 2001). It has also been found that two dimensional Cartesian systems can be used to successfully simulate and predict a bubbling regime of low bed circulation, requiring lower computational resources which is common practice (Xie et al., 2008). As the current model incorporates short pulsations at the velocity inlet and bed circulation does not have sufficient time to highly develop or be present, three dimensional effects are kept to a minimum. However, caution must be exercised when using 2D Cartesian coordinates and a future 3D study of this model will be helpful in elucidating differences. As all pulsation profiles are studied with a two dimensional model, the results remain acceptable for comparison.

Uniform liquid flow was injected through the inlet and varied with time according to the pulsation profile being simulated. The inlet flow for the sinusoidal pulsation profile was established using a sine wave equation, while the other profiles used the heavy side step function. The amplitudes of the profiles simulated, *A*, are represented in litres not distance as the water/air free surface is not numerically resolved (i.e. the domain at anytime is completely filled with water). The simulation begins with the random generation of particles without overlaps, followed by a period of gravitational settling to form an initial mixed packed bed (see Figure 3–3). During the settling process, the buoyancy force to particles is switched off and particles fall only due to gravity. This is done to help prevent segregation and achieve a better mixed packing before the start of the jigging. After settling, liquid is injected through the bottom following the appropriate pulsation profile, and jigging begins. It is important to begin with a well mixed density distribution of particles to ensure that jigging performance is independent of initial conditions. The cumulative frequency distribution (CumFD) taken along the bed height as well as the associated differential cumulative frequency distribution (DCFD) indicate the bed is almost evenly mixed (see Figure 3–4).

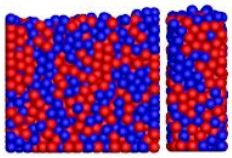

Figure 3–3. Front and side view of a well mixed initial packed state.

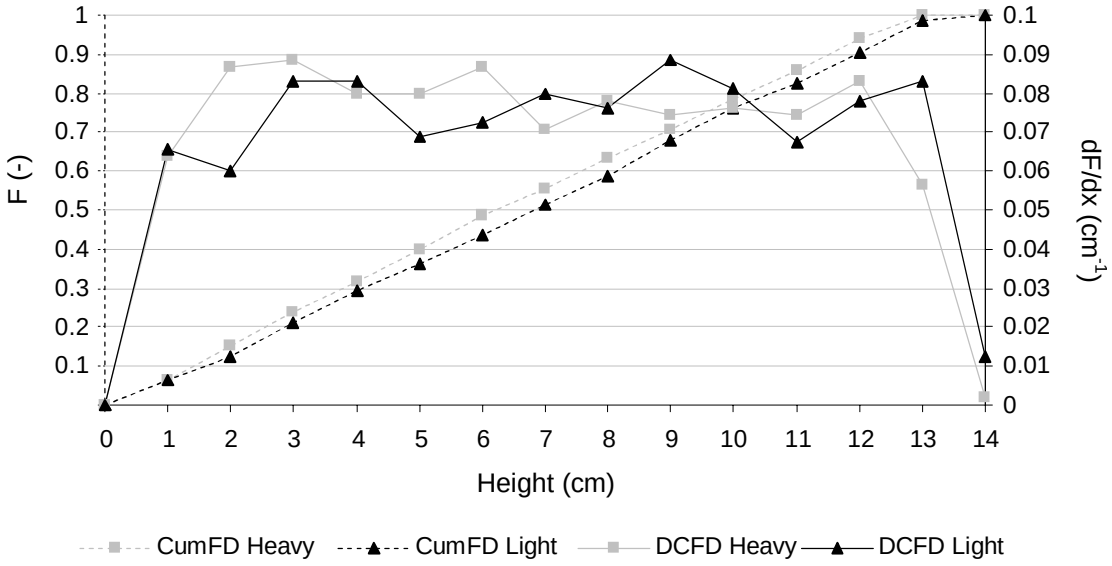

Figure 3–4. Cumulative frequency distribution and associated differential of DEM random packing. An almost perfectly mixed particle arrangement is shown.

Table 3–1. Jig model specifications.

Particle phase			**Liquid phase**		
Density (kgm^{-3})	Light	2,540	Viscosity ($kgm^{-1}s^{-1}$)		1×10^{-3}
	Heavy	4,630			
Young's Modulus (Nm^{-2})		1.0×10^{8}	Density (kgm^{-3})		1000
Poisson ratio (Nm^{-2})		0.3	CFD	Width (m)	0.025
Sliding friction coefficient (-)		0.3	Cell	Height (m)	0.025
Damping coefficient (-)		0.2	Bed	Width (m)	0.15
Particle diameter (m)	Light	0.01	Geometry	Height (m)	0.9
	Heavy	0.01		Thickness (m)	0.05
Number of particles (-)	Light	565	Bed distributor		Uniform
	Heavy	565	Convergence criteria (RMS)		1×10^{-5}
Time step (s)		1×10^{-5}	Time step (s)		1×10^{-3}

3.2 EXPERIMENTAL COMPARISON

Model specifications were based on past experiments performed by Mukherjee et al. (2005) (see Chapter 2, section 2.3.1 for details). These numerical parameters were used with a view of validating the numerical model against experimental results. The experiments adopted a 15cm diameter U-tube batch scale pilot jig. The jig used an air compressor and compensator (to store pressurized air). This system is effectively an air pulsed water jig. Key separation data was obtained using a nucleonic density gauge fixed at 75% of the bed height which recorded the bulk density—which includes both water and particles—along the horizontal plane intermittingly while the particles are at rest during jigging. The bulk density reduces over jigging cycles due to highly dense particles migrating to a lower portion of the tube while less dense particles increasingly populate the top. The reduction in bulk density over successive jig cycles was used by the authors as a measure of separation. The experiments applied a sinusoidal jig cycle with three variations of water level peak-to-peak amplitudes (a=0.15, 0.1, and 0.05 m) and frequency of 50 cycles/min. The amplitudes in terms of the numerical model are also represented in meters, a (m), (refer to Figure 3–5) although it is more correct to represent amplitude in litres as the simulation does

not resolve the water/air free surface (i.e. the domain at anytime is completely filled with water). The results remain comparable, as the experimental water level at anytime is considerably higher than the particles, however, it may misguide the reader as to whether the air/water interface is resolved. In all subsequent studies the amplitude will be defined as, *A*, which is in units of litres (L) (as mentioned in section 3.1.2). The numerical model amplitudes, *A*, of 1.125, 0.75, and 0.375 L are used as equivalents to experimental amplitude values, *a*, of 0.15 m, 0.1 m, and 0.05 m.

Figure 3–5 displays the both the experimental results by Mukherjee et al. (2005) and numerical model results. The bulk density values are compared over 10 jigging cycles. Considerable differences can be seen between experimental and numerical results reaching up to 23%. In order to explain the differences the experimental results are examined and three important issues arise.

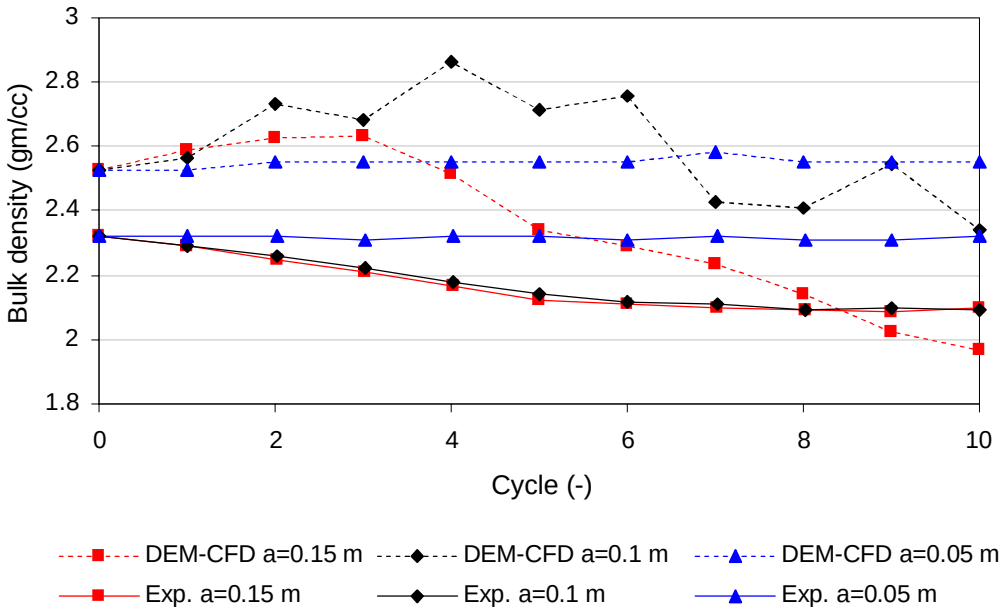

Figure 3–5. Comparison of experimental and numerical jigging results for three variations of water level peak-to-peak amplitude (*a*).

Firstly, the initial value of the experimental bulk density where the particles are presumed well mixed is quite low—indicating that the particle bed is already partially segregated. Alternatively, a quick calculation shows the DEM results are almost completely evenly mixed using the formula:

$$\rho_b = \frac{M_t}{V_t} \tag{3–5}$$

which can be expressed as

$$\rho_b = \left(\left(\frac{\rho_{p,h} + \rho_{p,l}}{2} \right) \times (1 - \varepsilon) \right) + (\rho_f \times \varepsilon) \tag{3–6}$$

where ρ_b, M_t, V_t, are the bulk density, total mass (including particles and liquid), and volume as a whole, respectively. Further, $\rho_{p,h}$, $\rho_{p,l}$, ρ_f, ε are the densities of the heavy particle, light particle, fluid, and porosity respectively. Taking ε as 0.4 which is reasonable for a random loosely packed spherical particle bed, a bulk density of 2.55 gm/cm^3 is obtained, the DEM results give a difference of only 0.02 gm/ cm^3. If the experimental bed is evenly mixed, to obtain the initial experimental value of 2.32 gm/cc the value of porosity, ε, would need to equal ~0.5. It is improbable that such a high volume fraction is present thus it is more likely that the experimenters had difficulty in establishing a evenly mixed packed bed as an initial condition. This outcome accounts for an 8.2% difference between experimental and numerical results before jigging begins. Consequently, the experimental jig is expected to achieve segregation rather quickly.

Secondly, the temporal behaviour of bulk density values during jigging differ either in gradient or final values. Both the experimental and numerical results for, a=0.05 m, display an identical linear behaviour where no segregation is present, although the final values are different due to the initial conditions. Here the inlet velocity is too weak to fluidise the bed. The numerical results for variants of a=0.1 m and a=0.15 m do not follow the same gradient or reach the same final values. Interestingly, the experimental results for these variants almost travel on the same continuously linear descending line. Therefore, increasing the amplitude by 50% has shown experimentally to almost give no change in the bulk density values. Alternatively, the numerical model bulk density results fluctuate while descending. A number of heavy particles—in the upper portion of the bed—due to particle-particle contact forces either circulate, push upwards, or stagnate as the entire particle system rearranges

itself, and while numerous heavy particles are descending from above. This causes bulk density values to increase even though segregation is progressing and heavy particles are continuously aggregating at the bottom of the bed. Taking bulk density values at 75% of the bed height gives a very localised view, and cannot detect this segregation which is a major limitation of this type of measurement for representing segregation. This complex particle behaviour is mentioned in Chapter 2, section 2.3.1. It has been verified through particle tracking experiments that during jigging both particle circulation and particle fluctuating leaps are present. These are attributed to circulation flows, particle collisions and turbulence and consequently impose mixing motions (Clarke et al., 1997; Kellerwessel, 1998; Schubert, 1994). Further, given the localised quantitative measurement it is unknown how the bulk behaviour of the numerical and physical models compare. Unfortunately, the experimenters have not published photographs of the lab jig in operation so qualitative comparisons cannot be discussed in terms of particle motions during jigging e.g. particle maximum height, transient solid distributions, and solid flow patterns.

Finally, perhaps the most crucial difference between the physical and numerical models is the shape of the pulsation profile. Figure 3–6 shows both the experimental attempt at a sinusoidal profile and the analytical result used for the numerical model. The authors experimental analysis of water profiles during jigging clearly shows that the water motion is cyclic but not symmetric and fairly poorly follows a sinusoidal shape. Further, about every 4 jigging cycles the authors observed that a measurable loss of air from the compensator had taken place which required to be automatically pressurised to the desired level. This gives reason to assume the 3^{rd} and 4^{th} jigging cycles may differentiate more than that presented in Figure 3–6. It is apparent that a subsequent pursuit into performing a laboratory jig experiment for the purpose of numerical validation would be very helpful. Due to a lack of resources this is not possible within this study.

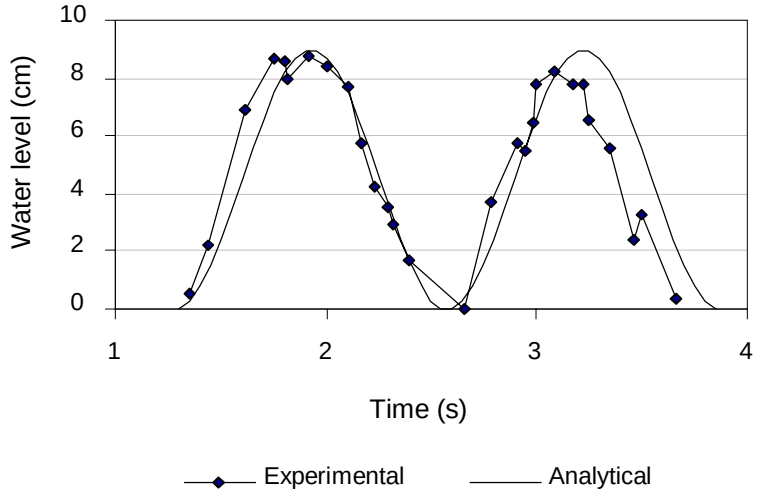

Figure 3–6. Comparison of the Mukherjee et al. (2005) experimental sinusoidal pulsation profile shape and the analytical version adopted in the numerical model.

3.3 ANALYSIS OF PARTICLE FLUID INTERACTION FORCES

The importance of various particle fluid interaction forces were analysed using the numerical model in order to elucidate their influences on the bulk behaviour of the particle system. The lubrication, Magnus, Saffman, virtual mass, and inertial forces are investigated. Details of the various forces can be found in Chapter 2, section 2.4.5 and 2.4.6. These are quantitatively compared to the drag force which is reasonably assumed to be dominant in this system. This study has excluded the Basset force because it is time consuming to solve as it has to be integrated over the entire particle trajectory. Consequently, this force is often neglected. Fortunately, the history force tends to be negligible when $Re_p >> 1$, which is the case in this system (Sommerfeld, 2000). The forces are examined using a sinusoidal profile with a period, *T*, of 2 seconds, (or 30 cycles/min) and amplitude, *A*, of 3 L input and exhaust of water.

3.3.1 Lubrication force

The lubrication force was examined, but only in terms of the "squeeze" mode because of its dominance over the "rotation" and "shear" modes. The force was considered in the scenarios when particles directly approach each other, and also when particles approach a wall. Figure 3–7 and 3–8 display lubrication particle-particle and particle-wall force contours over one jig cycle, respectively. The particle-particle lubrication force is seen to be highest when particles are falling back into a packed bed between the middle and end of the pulsation cycle. During pulsion particles fluidize with no strong interaction between one another. In suction particles fall at high velocity "crashing" down on the particles which have settled beforehand giving rise to high lubrication force values. It can also been seen many particles are effected by this force. Alternatively, the particle-wall lubrication force displays more consistent values throughout the cycle, and only a few particles in the vicinity close to the wall are effected. The magnitude of the particle-particle and particle-wall forces can be seen over 6 jigging cycles in Figure 3–9 (a) and (b), respectively. The particle-particle lubrication force is shown to be far greater than the particle-wall force. The stronger particle-particle lubrication force is approximately less than 2.5% of the drag force (refer to Figure 3–9 (c)).

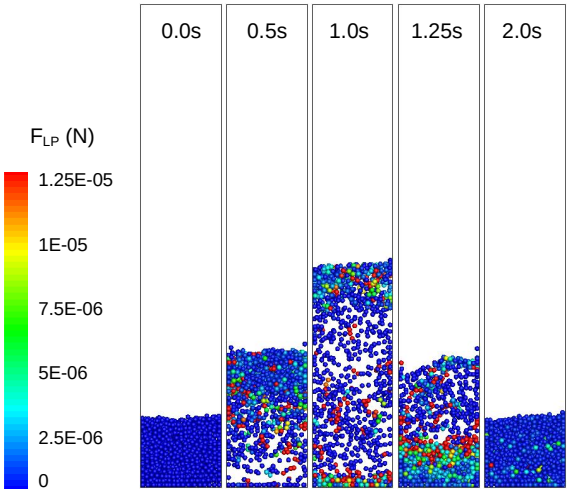

Figure 3–7. Particle-particle squeeze lubrication force.

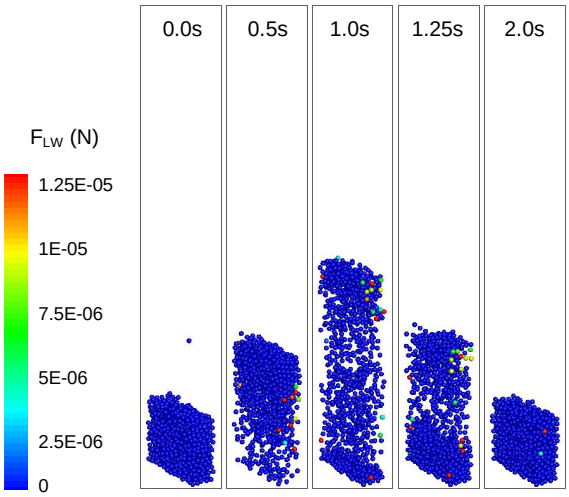

Figure 3–8. Particle-wall squeeze lubrication force.

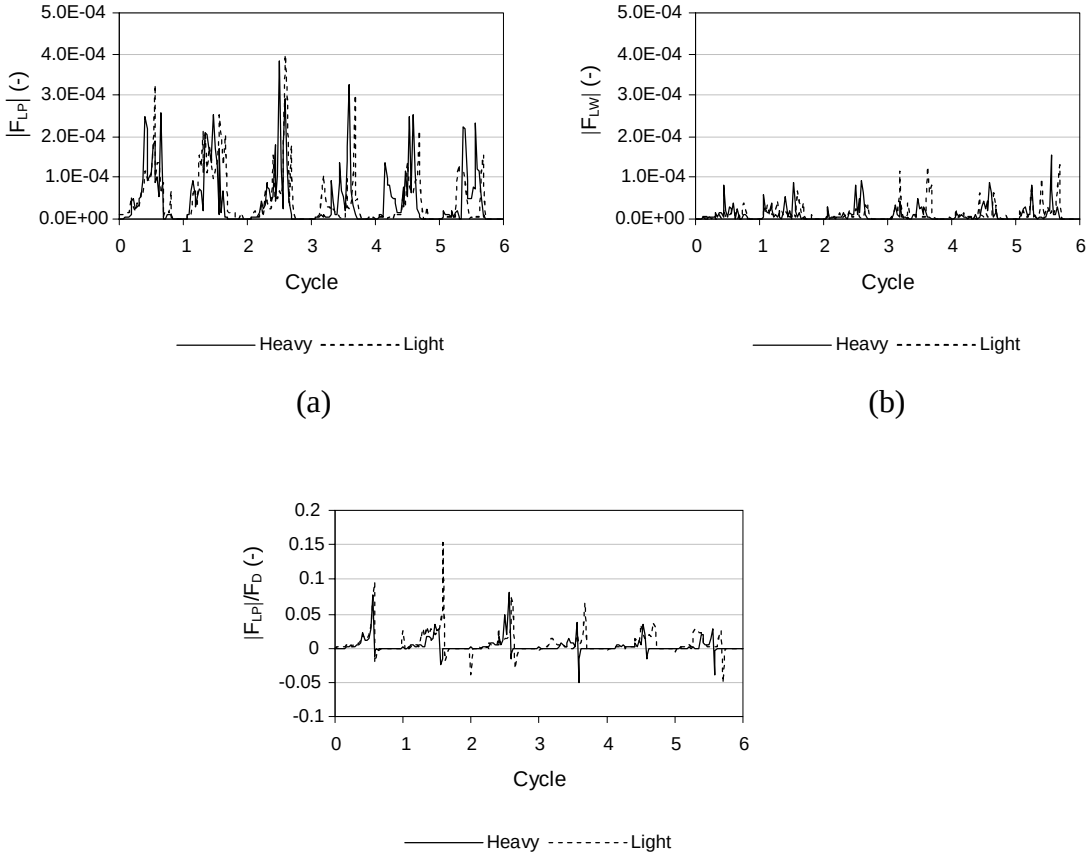

Figure 3–9. (a) magnitude of particle-particle squeeze lubrication force, (b) magnitude of particle-wall squeeze lubrication force, (c) comparison of particle-particle squeeze lubrication and drag force.

3.3.2 Magnus force

The Magnus lift force due to particle rotation was shown to have an even presence throughout pulsion and suction portions of the cycle. This force is approximately less than 0.25% of the drag force over the jig cycle. Refer to Figure 3–10, Figure 3–11 (a) and (b), respectively.

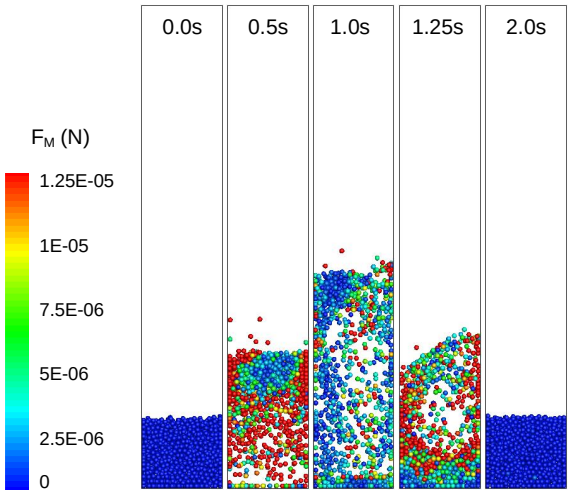

Figure 3–10. Magnus lift force.

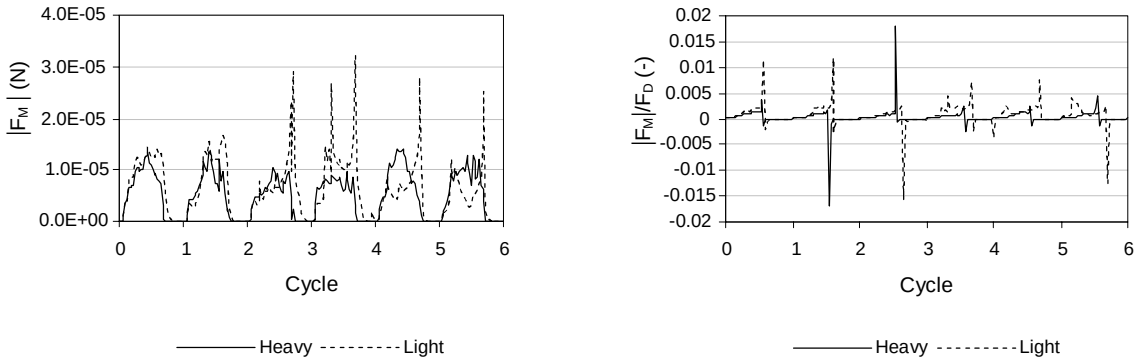

(a) (b)

Figure 3–11. (a) magnitude of Magnus lift force, (b) comparison of Magnus and drag force.

3.3.3 Saffman force

The Saffman lift force arises from a particle's presence in a velocity gradient. The force reaches its highest values during suction while particles experience a strong downwards velocity while in a packed configuration. The force drops to zero in the middle of the cycle when a zero inlet velocity is present. This force is approximately less than 2.5% of the drag force. Refer to Figure 3–12, Figure 3–13 (a) and (b), respectively.

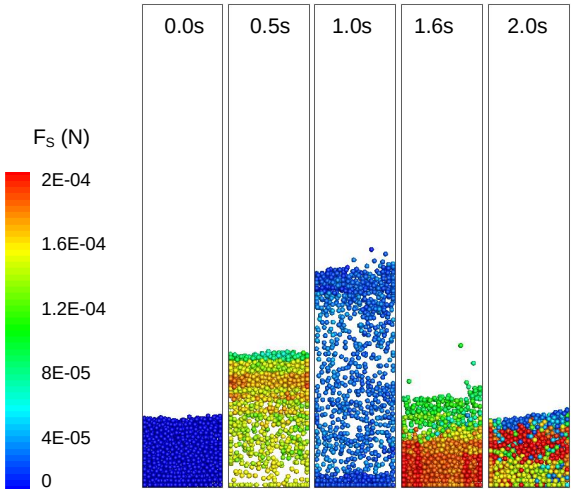

Figure 3–12. Saffman lift force.

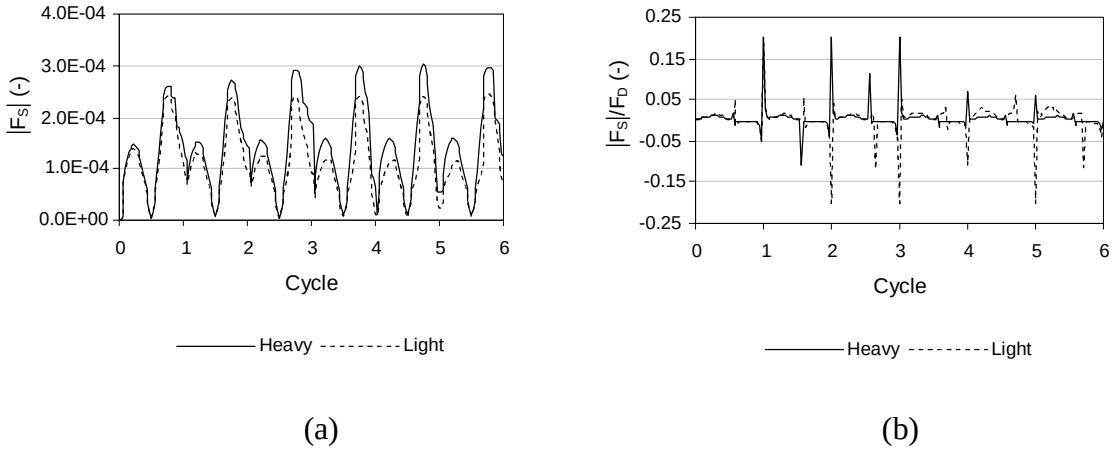

(a) (b)

Figure 3–13. (a) magnitude of Saffman lift force, (b) comparison of Saffman and drag force.

3.3.4 Virtual mass force

The virtual mass force is present if the relative velocities between a submerged object and fluid carrier phase change with time. It can be seen the force is highest as the particles are falling in the suction portion of the cycle. This force is approximately less than 2% of the drag force. Refer to Figure 3–14, Figure 3–15 (a) and (b), respectively.

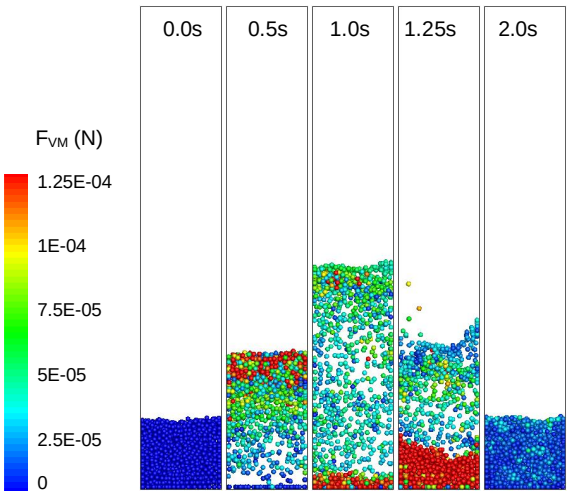

Figure 3–14. Virtual mass force.

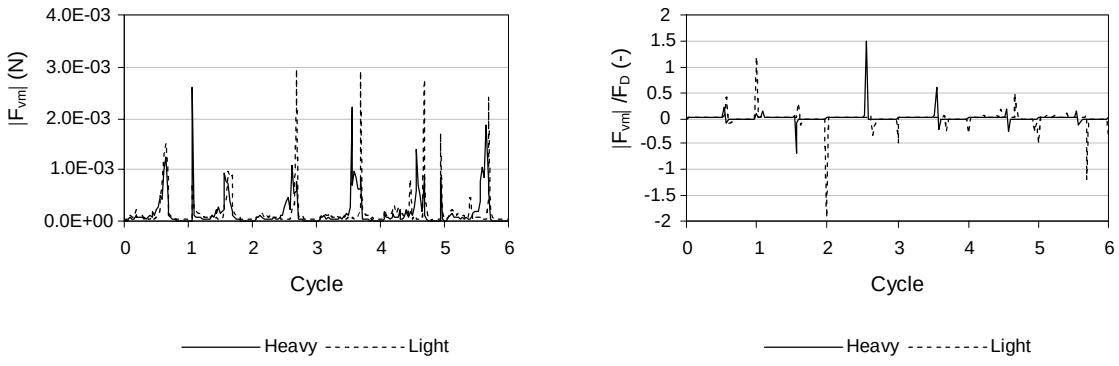

(a) (b)

Figure 3–15. (a) magnitude of virtual mass force, (b) comparison of virtual mass and drag force.

3.3.5 Inertial force

The inertial force due to the acceleration of the carrier phase, arises from a tendency of a physical object to resist any change in its motion. This force is greatest when acceleration is greatest within the sinusoidal profile (both in pulsion and suction). This force is approximately less than 1% of the drag force. Refer to Figure 3–16, Figure 3–17 (a) and (b), respectively.

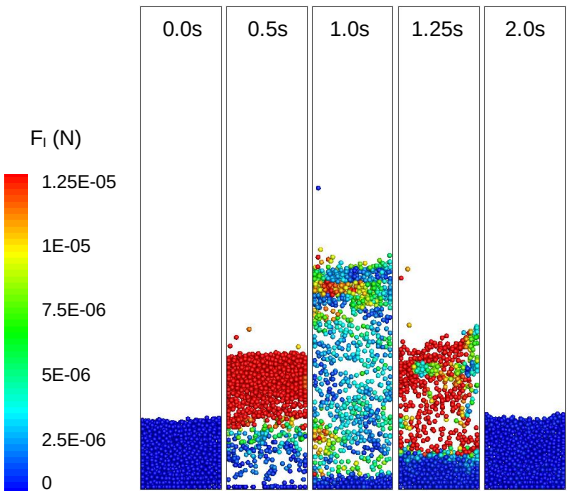

Figure 3–16. Inertial force.

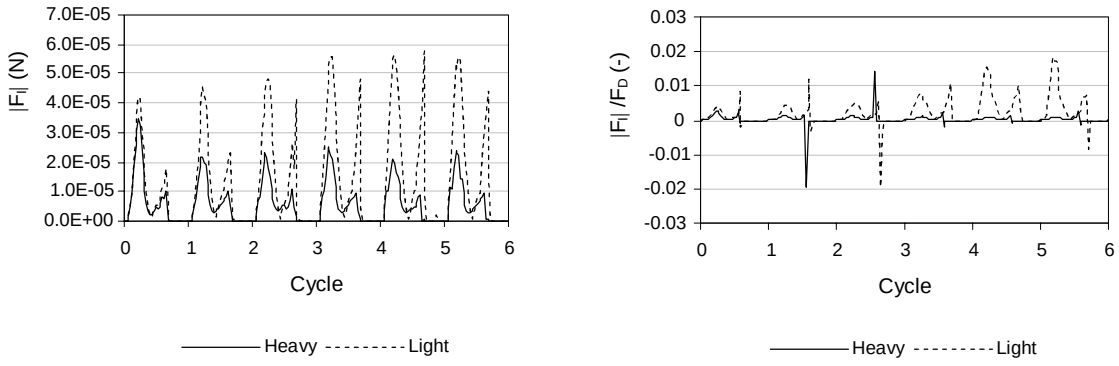

(a) (b)

Figure 3–17. (a) magnitude of inertial force, (b) comparison of inertial and drag force.

3.3.6 Amalgamation of particle fluid interaction forces

The isolated studies of the lubrication, Magnus, Saffman, virtual mass, and inertial forces have shown that the magnitude of these forces are extremely small compared to the drag force. It can also be seen through force contours superimposed on the solid flow pattern distributions that the bulk behaviour of the particles remain almost unchanged despite the inclusion of these forces (refer to Figure 3–7, 3–8, 3–10, 3–12, 3–14, and 3–16). Although these forces have shown to be insignificant on their own, amalgamating them into one model may display a culmination of forces in a certain direction which significantly alters the motion of the particles. After combining these forces the solid flow patterns show the drag force is indeed still dominant with miniscule changes in particle motions and segregation (see Figure 3–18 and 3–19). This is also found in variations of the sinusoidal pulsion profile and other profiles studied which characteristically have greater acceleration and where unsteady forces are greater e.g. virtual mass and inertial. Therefore, in subsequent studies the lubrication, Magnus, Saffman, virtual mass, and inertial force have been excluded in the numerical model for favour of reducing computational time.

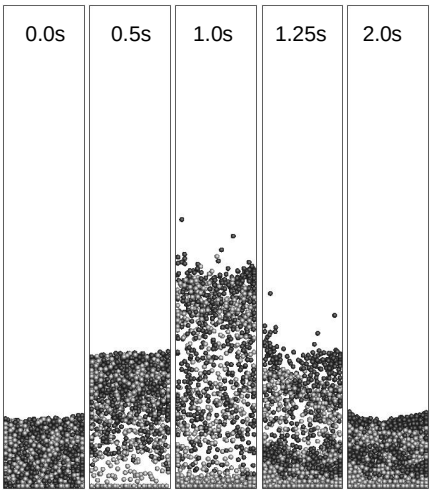

Figure 3–18. Jig model including drag and buoyancy forces.
Sinusoidal pulsation profile of T=2 s, A=3 L adopted.

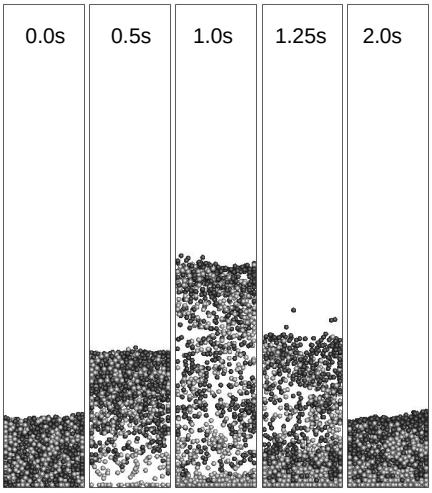

Figure 3–19. Jig model including drag, buoyancy, lubrication, Magnus, Saffman, virtual mass, and inertial forces. Sinusoidal pulsation profile of T=2 s, A=3 L adopted.

3.4 BED WIDTH EFFECTS ON SEGREGATION

It is necessary to understand whether segregation is influenced by changes in bed width before selecting a bed width for the simulation studies. Using the same numerical model properties as in Table 3–1, the bed width was increased by a multiple of 2 and 4 of the original. This is accompanied by a multiplication of the particle number in proportion to the extension of the bed width. The coordination number is used to measure segregation over 15 jigging cycles using a sinusoidal profile with a period (T) of 2 seconds (or 30 cycles/min), and amplitude (A) of 3 litres input and exhaust of water. The coordination number represents the average sum of contacts of a particle type, with either similar or different particle types, e.g. the heavy particles average contact number with light particles. The heavy-light coordination number is a good indication of particle segregation. The coordination number fluctuates as the bed expands under pulsion and compacts under suction. The value gradually reduces as the bed moves from a mixed state through to complete segregation. A high value indicates minimal segregation i.e. the light particles are in intimate contact with the heavy particles. A low value means the light particles are surrounded and in contact by mostly light particles indicating segregation of the bed. The heavy-light coordination number can be written as:

$$C_{h-l} = \frac{1}{k_l} \sum_{l=1}^{kl} x_l \tag{3–7}$$

where for each light particle l the sum of contacts with heavy particles x_l gives the coordination number for each light particle, which is averaged over the number of light particles k_l.

Segregation phenomenon was found to change with bed width. Firstly, irrespective of the bed width, segregation is present but is not necessarily steady (see Figure 3–20). The model of the original bed width gradually induces segregation, which when complete the bed assumes a segregated state for the remaining jigging cycles i.e. steady. Alternatively, increasing the bed width results in segregation becoming unsteady. Wider particle beds induce separation and complete separation in almost an identical rate and time, however, in subsequent cycles the particles begin to mix.

For the purpose of this thesis in which pulsation profiles are compared, a steady segregation behaviour is highly desirable as it gives an absolute time taken to complete separation and reduces complexities of an already elaborate system. The segregation rate for all three bed widths are almost identical up to when separation is complete (which is before subsequent mixing in beds wider than the original length). This indicates the bed width effects are not significant at or before this point. Therefore, to ensure steady separation while being satisfied bed width effects are not significant (in terms of separation completion time) the original length was chosen. However, caution must be taken using the original bed width, as the validity of the simulation will be limited if segregation behaviour is studied beyond the point in time which segregation is complete (this is not pursued in this PhD project).

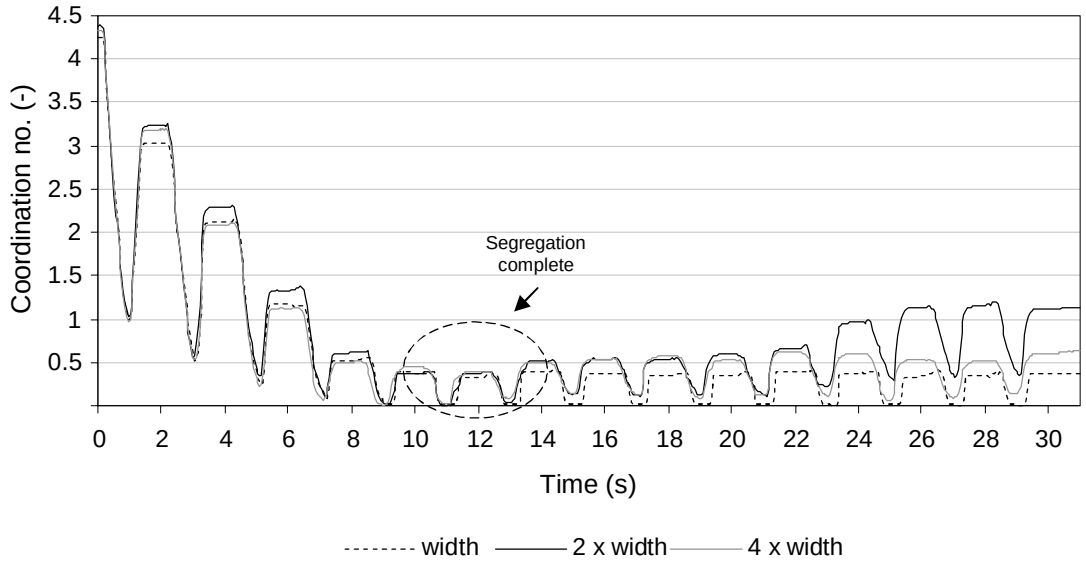

Figure 3–20. Steady and unsteady segregation shown using the coordination number values for three different bed widths. Modelled using a sinusoidal profile T=2 s, A=3 L.

CHAPTER 4

DISCRETE PARTICLE SIMULATION OF SOLID SEPARATION IN A JIGGING DEVICE

4.1 INTRODUCTION

Previous studies using the DEM-CFD model have used a sinusoidal pulsation profile with the exception of Dong et al. (2009), who used a forward leaning sawtooth cycle. No numerical investigations (including all various modelling techniques) have studied what effect the pulsation profile shape has on concentration mechanics. Many types of pulsation profiles historically exist and are implemented by numerous jigs (see Appendix A, Table A–2). This study investigates five popular industry jigging profiles (see Figure 4–1) using a mono-size binary-density system, and two way coupling (model specifications are found in Chapter 3 in section 3.1). The aim is to—through a range of criteria—elucidate on the different segregation behaviours when separating a mono-sized system of particles with a binary density distribution.

The pulsation profiles are compared using a fixed peak-to-peak amplitude and pulsation period. These are 3 litres of water intake/exhaust and 2 seconds pulsion duration (or 30 cycles/min), respectively. The amplitudes are represented in litres not distance as the water/air free surface is not resolved, otherwise the amplitude would be equivalent to 0.4m. Only the shape of the profile which satisfies these conditions is varied. The profiles adopted and their abbreviations are: sinusoidal (SINE), triangular (TRI), sawtooth-backward (STB), sawtooth-forward (STF), and trapezoidal (TRA). Each profile includes a pulsion period with an upward liquid motion (positive value in velocity) and a suction period with a downward liquid motion (negative value in velocity). To ensure comparable results independent of mesh size, the same mesh dimensions were used in all cases.

The relative performances are compared in terms of solid flow patterns, separation kinetics, energy, and mean particle position. The underlying mechanisms are explained in terms of particle-fluid interaction force. These quantitative comparisons demonstrate significant differences in the segregation rate and energy used for various pulsation profiles.

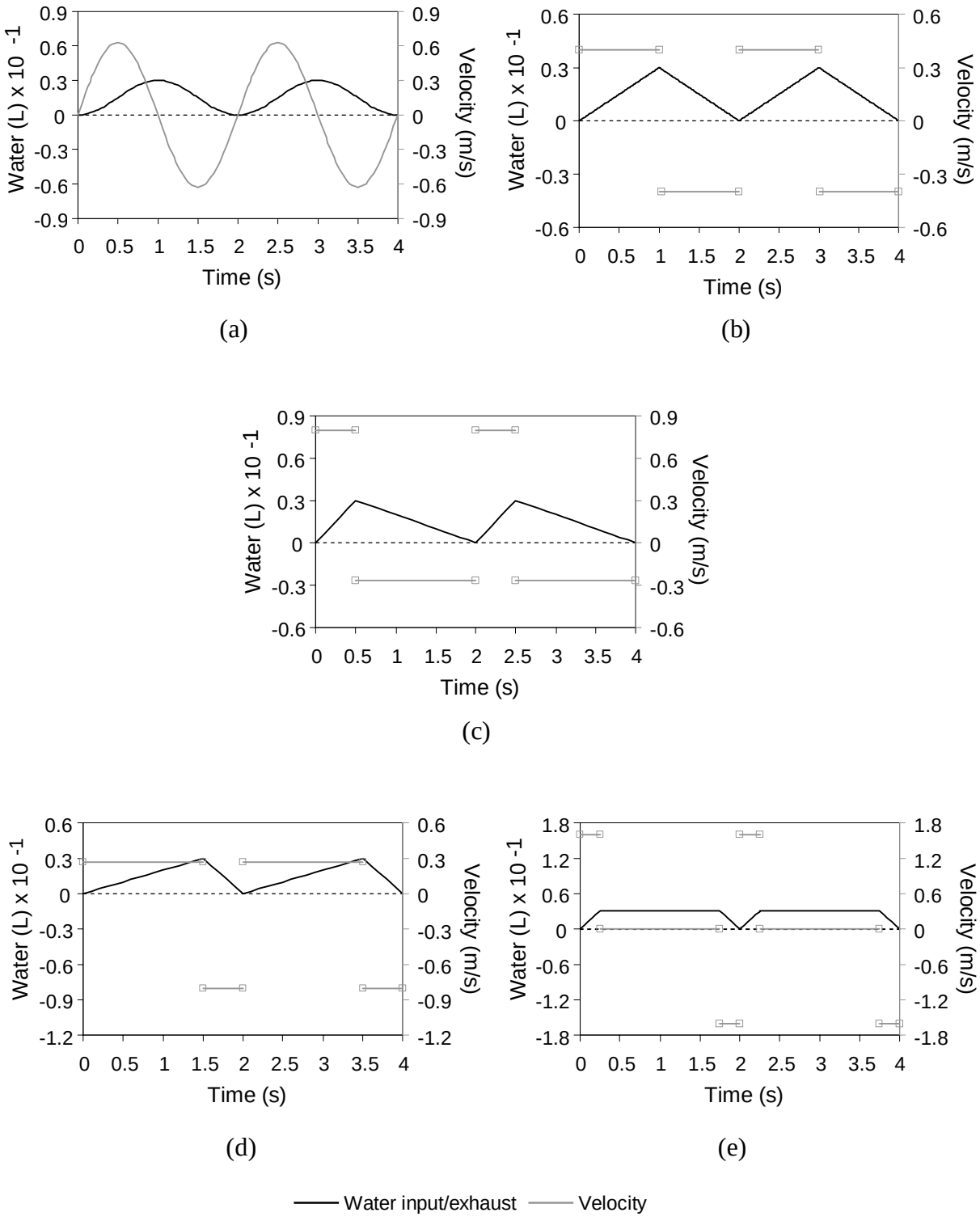

Figure 4–1. Variety of pulsation profiles applied at inlet boundary condition (a) Sinusoidal, (b) Triangular, (c) Sawtooth-backward, (d) Sawtooth-forward, (e) Trapezoidal.

4.2 RESULTS AND DISCUSSION

4.2.1 Solid Flow Patterns

Solid flow patterns are checked first to obtain a visual understanding of the stratification process. Figure 4–2 shows the particle positions during jigging for all the five jigging profiles. The maximum and minimum particle displacements can be visualized. The light particles are coloured black and heavy particles grey. For each pulsation profile, only the 1^{st}, 3^{rd}, 4^{th} and 6^{th} jigging cycles are plotted. Three snapshots are plotted at each cycle which corresponds the following moments: before pulsion, middle of pulsion, and end of suction, respectively. The profiles display very different phenomena.

The initial cycle of the sinusoidal profile (see Figure 4–2 (a)) begins well mixed and expands vertically in a uniform manner. As segregation progresses the particles cluster together and lift increasingly as one whole and to greater heights—this behaviour is apparent in all profiles except the sawtooth-forward profile. The triangular profile (see Figure 4–2 (b)) exhibits slugging which increases with segregation, and also—not seen in the figure but present—a short period of re-expansion near the end of pulsion. The sawtooth-backward (see Figure 4–2 (c)) and trapezoidal (see Figure 4–2 (e)) profiles both completely lift the bed off the bottom of the jig to large heights. The sawtooth-forward profile (see Figure 4–2 (d)) shows almost no expansion and produces minimum fluidization. Segregation can be seen gradually progressing in all cases at different rates.

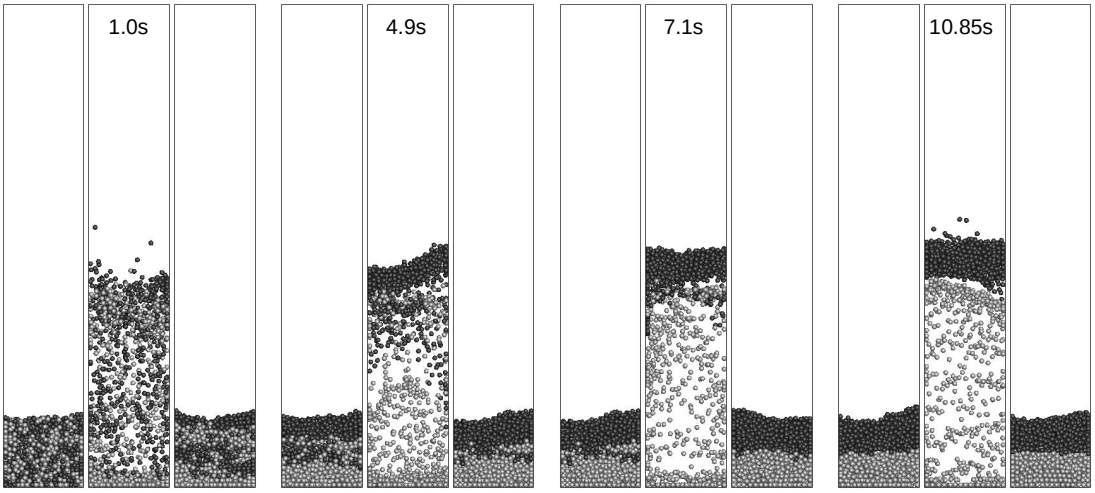

(a) Sinusoidal

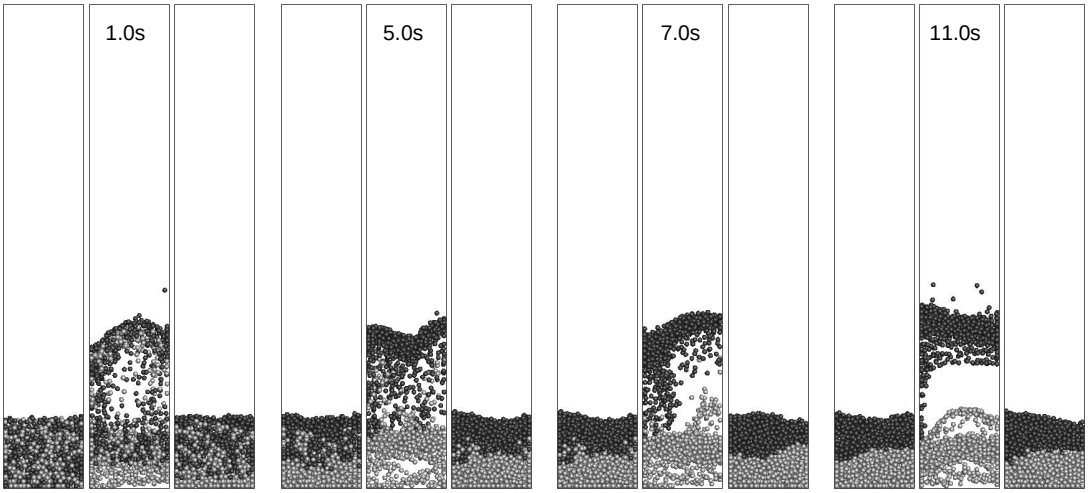

(b) Triangular

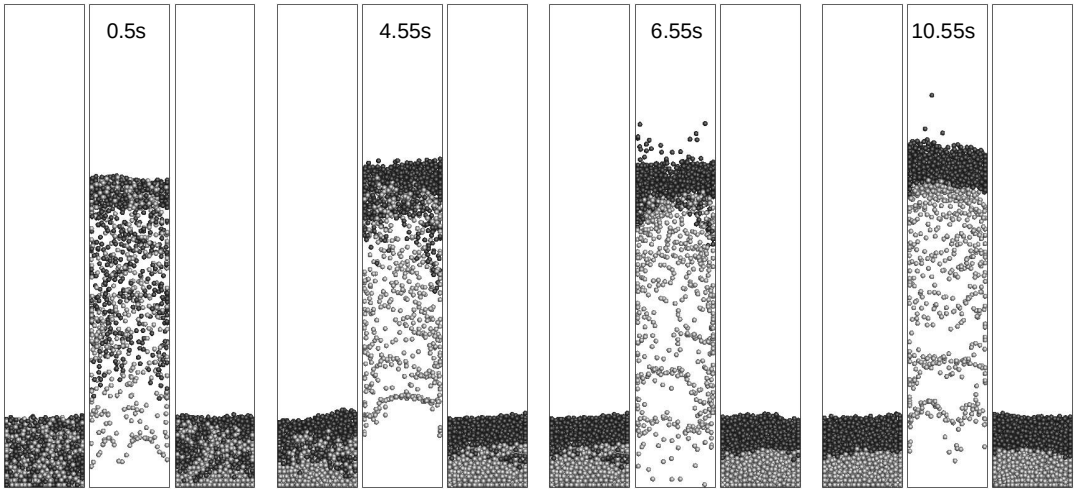

(c) Sawtooth-backward

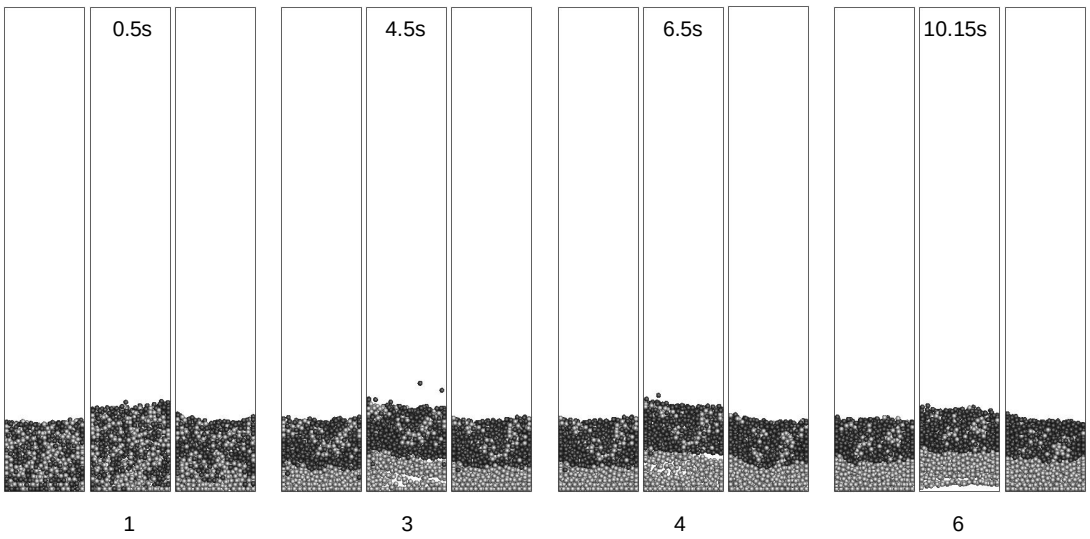

(d) Sawtooth-forward

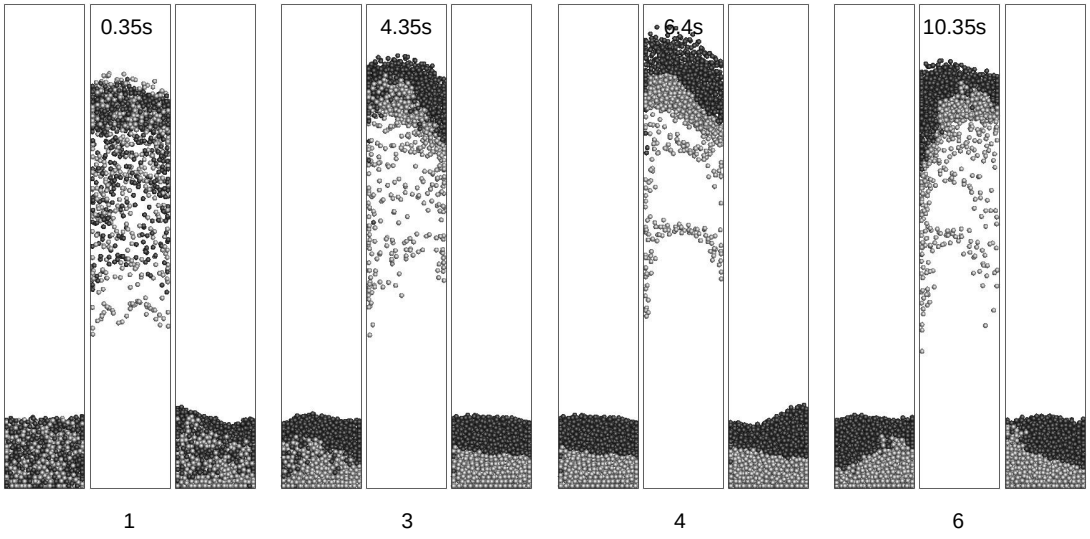

(e) Trapezoidal

Figure 4–2. Solid flow patterns shown by particle position under different pulsation profiles at 1st, 3rd, 4th, and 6th cycle. Heavy and light particles are coloured grey and black respectively. (a) Sinusoidal, (b) Triangular, (c) Sawtooth-backward, (d) Sawtooth-forward, (e) Trapezoidal.

4.2.2 Mean Particle Position

The mean displacement positions (see Figure 4–3) quantify the jigging behaviour by illustrating the average height of both particle types separately. All profiles display

gradual segregation shown by the gradual increase in differences between the heavy and light particle mean positions at the conclusion of each cycle. The mean positions reveal that particles reach peak mean heights from highest to lowest in the following order: trapezoidal (79cm), sawtooth-backward (60cm), sinusoidal (41cm), triangular (29cm), and sawtooth-forward (12.5cm). The mean peak heights particles reach is shown to be directly proportional to maximum pulsion inlet velocity.

The mean position of each type of particle gives a good understanding of the separation process. Starting from a well mixed state where each type of particle has a similar mean position, the light particles move upwards faster than the heavy particles during the pulsion period. During the suction period, both types of particles fall down, but the heavy particles fall faster than the light particles. Following separation, more and more light particles aggregate on top of the heavy particles. The light particles receive less constrain from the heavy particles, and move higher during the pulsion period as demonstrated by their mean position until a dynamically stable state is reached. The mean positions remain at a constant value for a significant period during the suction process for the SINE, TRI, STB, STF profiles, indicating that the particles fall down quickly to form a fixed bed. The results imply an opportunity to optimise the profiles to improve the jigging performance—as the period corresponding to the fixed bed is a waste of time and energy.

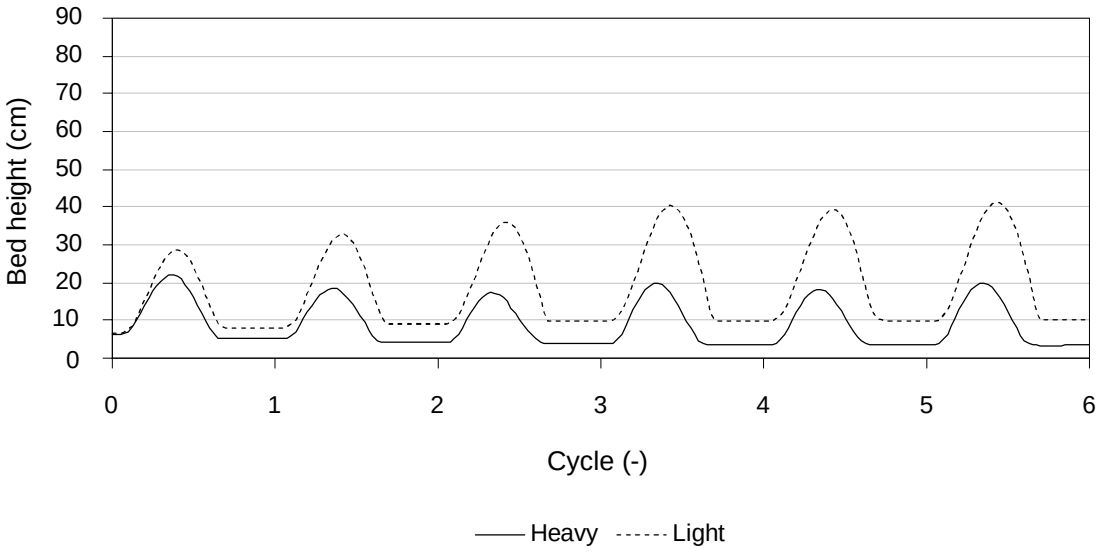

(a) Sinusoidal

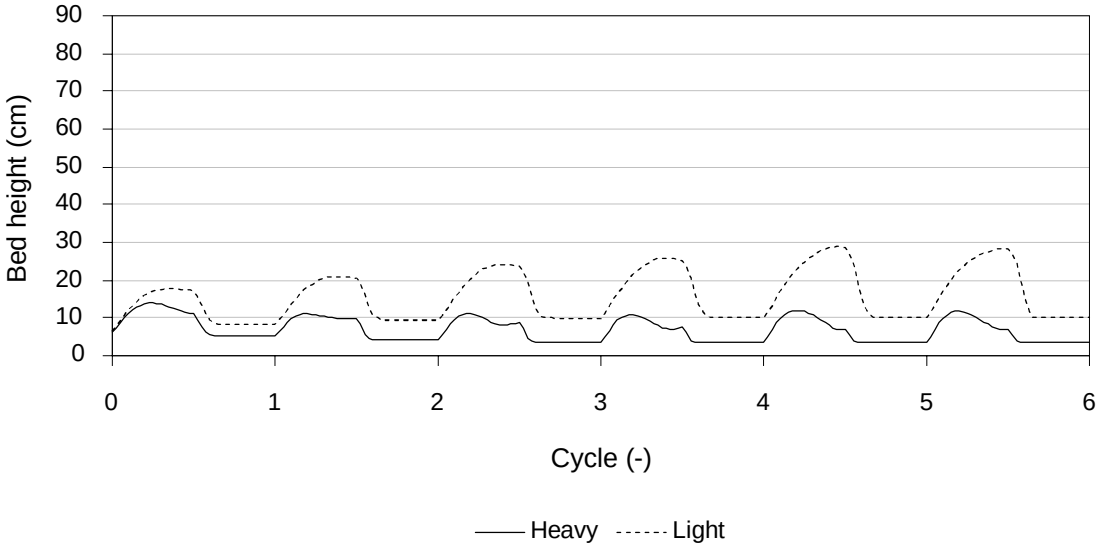

(b) Triangular

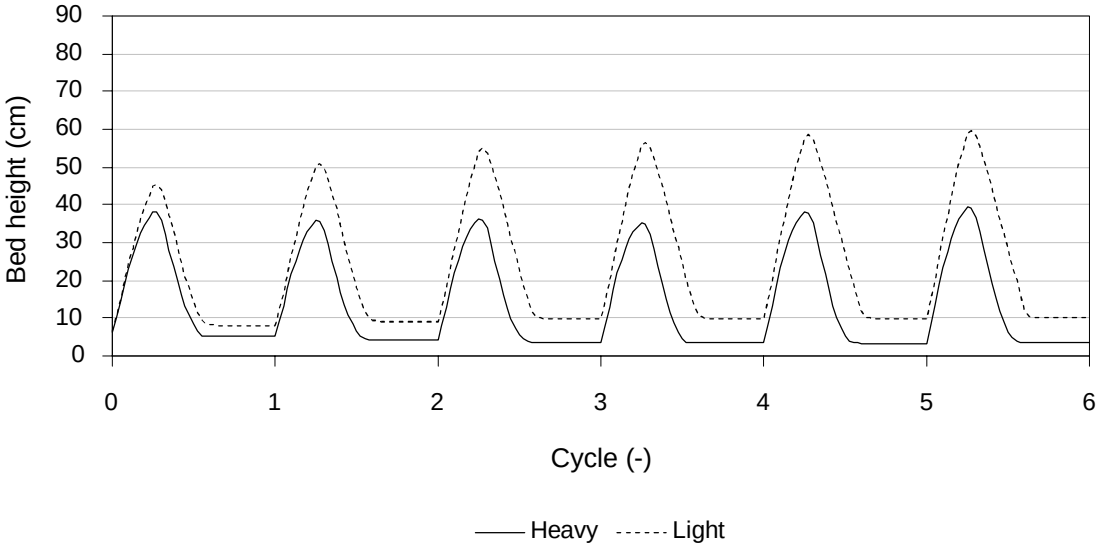

(c) Sawtooth-backward

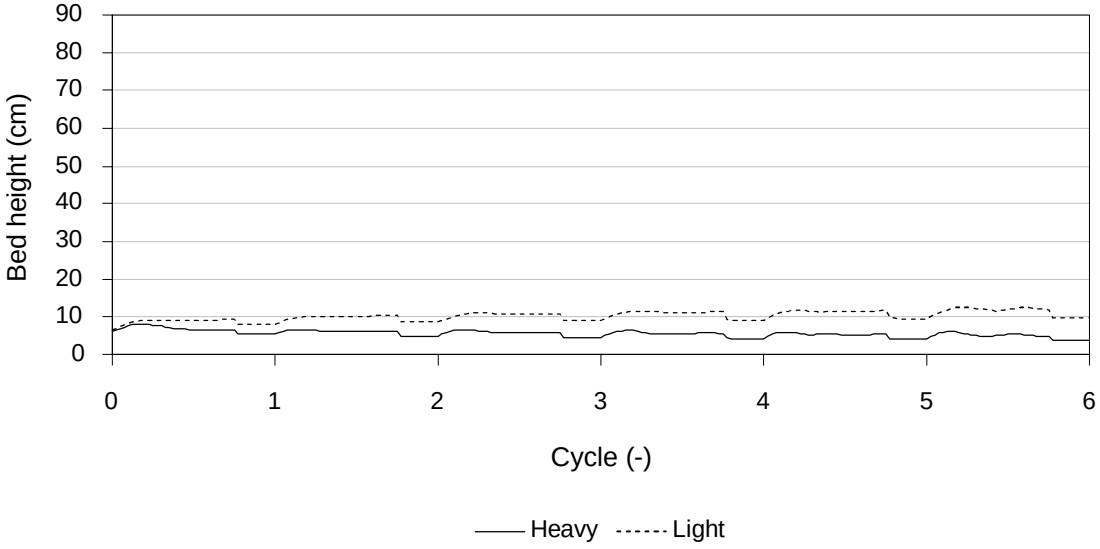

(d) Sawtooth-forward

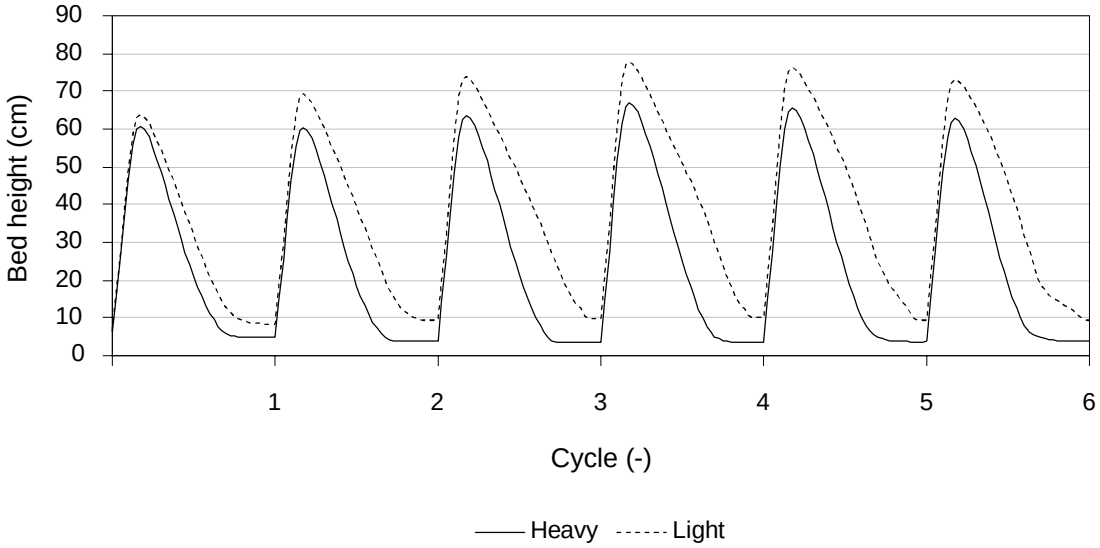

(e) Trapezoidal

Figure 4–3. Mean particle position (a) Sinusoidal, (b) Triangular, (c) Sawtooth-backward, (d) Sawtooth-forward, (e) Trapezoidal.

To highlight the difference in segregation between profiles Figure 4–4 plots the difference in distance between the mean particle displacement for light and heavy particles for each profile. These values are taken while the bed is at rest at the end of each cycle. The larger the average distances between the light and heavy particles the greater the bed separation. (Figure 4–4 (a)) indicates that all the profiles excluding trapezoidal and sawtooth-forward segregate the bed by approximately the forth cycle. The trapezoidal profile is unique in its response as re-mixing begins at the forth cycle showing decreasing values in the mean particle position difference which indicates inversion conditions have been reached. (Figure 4–4 (b)) focuses on the final cycle. It can be seen after the sixth cycle of jigging very little difference in the degree of separation exists between the sinusoidal, triangular, and sawtooth-backward profiles, while the trapezoidal and sawtooth-forward profiles performed poorly in comparison.

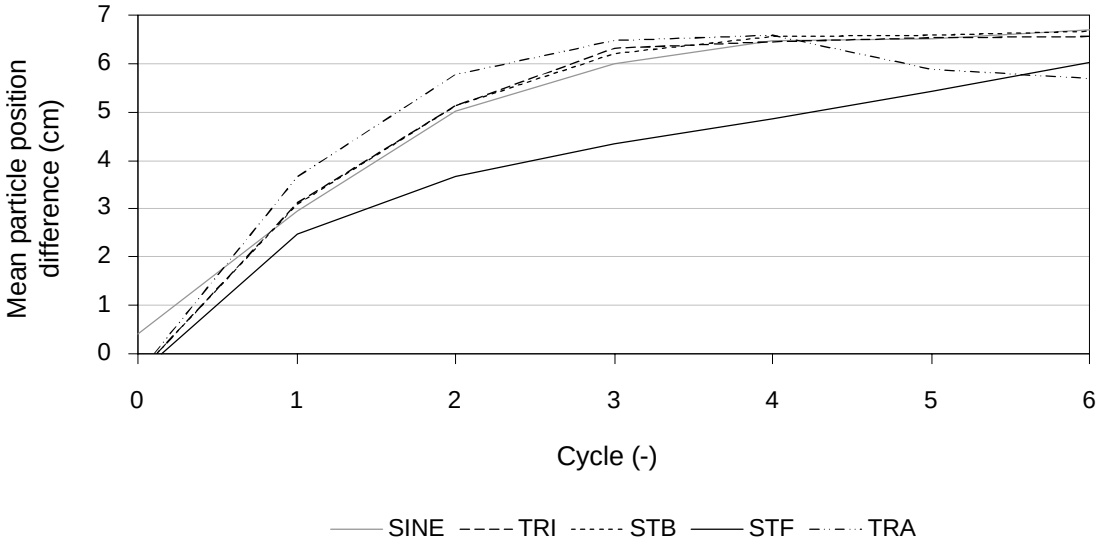

(a)

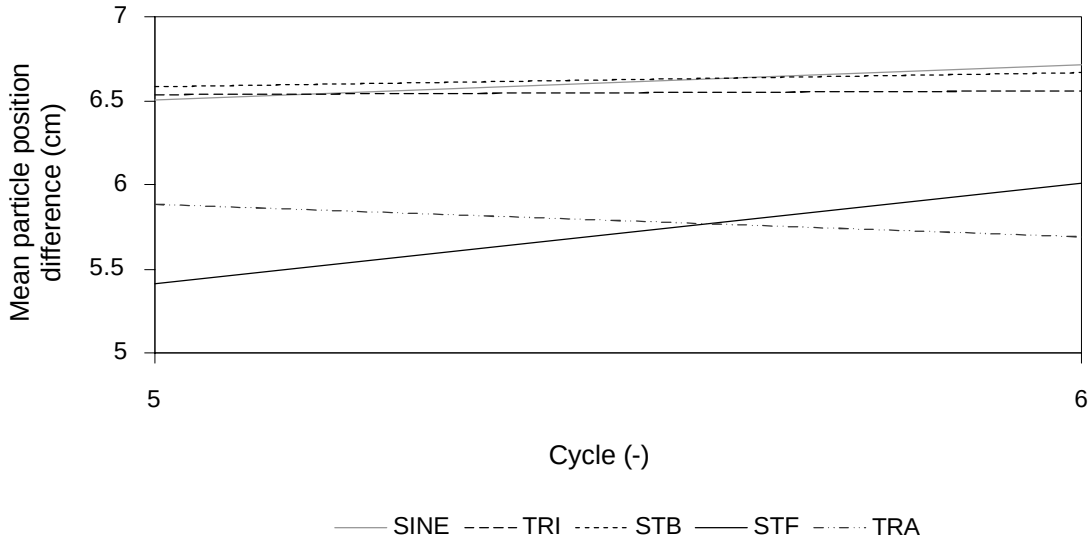

(b)

Figure 4–4. Distance between light and heavy average mean particle position for all profiles (a) 6 cycles, (b) final cycle.

4.2.3 Concentration profile

The concentration profile helps visualize and quantify the degree of separation achieved by each profile after 6 cycles of jigging (see Figure 4–5). The concentration profile measures the average particle density vertically along the bed height. The values represent a vertical line when particles along a given height are of the same

density. A subsequent slope ensues when a mixture of particle densities are present. The gradient of this slope represents the degree of separation along the vertical plane with a low gradient indicating greater separation.

The values in Figure 4–5 are taken when jigging is complete (i.e. end of cycle 6) and particles have settled in their final state. The triangular, sawtooth-backward, and sinusoidal profiles all achieve a sharp gradient indicating almost complete segregation. The trapezoidal profile displays segregation to a lower degree, however, it is noticed that this profile displays inversion behaviour i.e. mixing after the fourth cycle, and hence could provide the most segregation if values were taken from the fourth cycle. Lastly, the sawtooth-forward profile displays the lowest degree of segregation due to poor jigging dynamics.

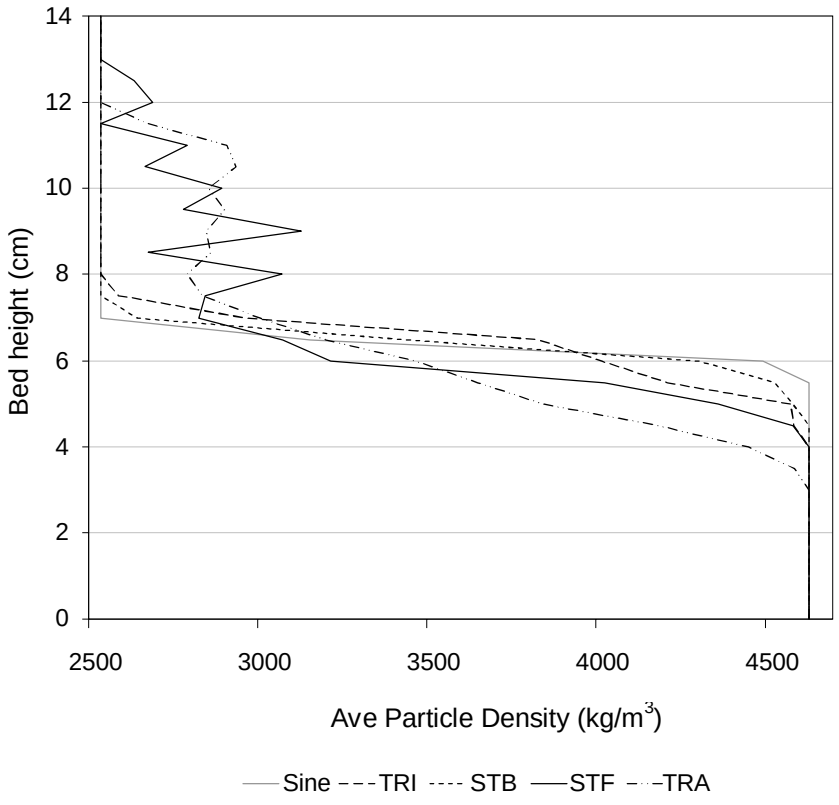

Figure 4–5. Average particle density along height of bed for all profiles in final rested state.

4.2.4 Particle-Fluid Interaction Force

The non-dimensional average particle-fluid interaction force values shown for example in Figure 4–6 indicate whether the light or heavy particles have sufficient particle-fluid interaction force upon them to overcome their respective gravitational force and achieve movement. This non-dimensional force can be expressed as:

$$\mathbf{f}_{p-f,i} = \frac{1}{k_i}\sum_{i=1}^{k_i}\left(V_{p,i}\rho_f \mathbf{g} + \mathbf{f}_{f,i}\right)/\, m_i \mathbf{g} \qquad (4\text{–}1)$$

where $V_{p,i}$, ρ_f, g , $\mathbf{f}_{f,i}$ and m_i are the volume of particle, i, fluid density, acceleration due to gravity, fluid drag force, and particle mass, respectively. The differences between the non-dimensional average particle-fluid interaction force for heavy and light particles in a system indicates which particles have greater acceleration.

4.2.4.1 Sinusoidal

In the pulsion stage the light particles have a larger upward force overcoming their gravitational force whilst the heavy particles have only slightly more (see Figure 4–6). As the cycles progress this gradually reverses because the light particles move further to the top of the bed where the porosity gradually becomes higher and less drag is experienced. Initially, the bed is in a well mixed state and the light particles have $f_{p\text{-}f} > 1$ resulting in acceleration upwards, while the heavy particles have $f_{p\text{-}f} = 1$ resulting zero acceleration and static suspension. This situation results in light particles propelling both themselves and heavy particles upwards. As each particle has the freedom to move the particles of high $f_{p\text{-}f}$ values (light particles) interact with particles with lesser $f_{p\text{-}f}$ and rearrangement begins. This interaction causes light particles to lift heavy particles or pass them by and move to the top of the bed, resulting in both bed agitation (through interaction) and segregation.

In the initial cycles the light particles contribute to more of the total bed lift but later the heavy particles are the main contributors. As the bed segregates, the heavy particles descend to the tightly packed portion of the bed and experience a greater

drag. At this point, the light particles are residing at the loosely packed portion on top of the bed and have an insufficient force ratio to create lift and hence are lifted using support from the heavy particles beneath. The heavy particles cannot penetrate back through to the top of the bed. As they collect toward the lower portion of the bed they become susceptible to a loosening wave which begins from the bottom of the bed and travels vertically to the top, additionally they also have higher settling velocities. The loosening wave arises from the interfacial instability at the bottom of the bed and fluid interface which causes particles to 'rain' down.

In the 1st cycle in Figure 4–6, the heavy particles have $f_{p\text{-}f} = 1$ which means they are suspended and the light particles have $f_{p\text{-}f} > 1$ which drives the bed upwards. As jigging progresses through the cycles this then switches gradually and heavy particles drive the bed as a result of the developing porosity gradient.

During suction in the first jigging cycle, the light particles have the greatest negative $f_{p\text{-}f}$. After successive jigging cycles, these values reverse due to the developing porosity gradient during segregation. Further, total $f_{p\text{-}f}$ values exhibit similar behaviour to the average vertical drag force.

The particle fluid interaction force is further illustrated in Figure 4–7 using solid flow patterns of the first and last jigging cycles.

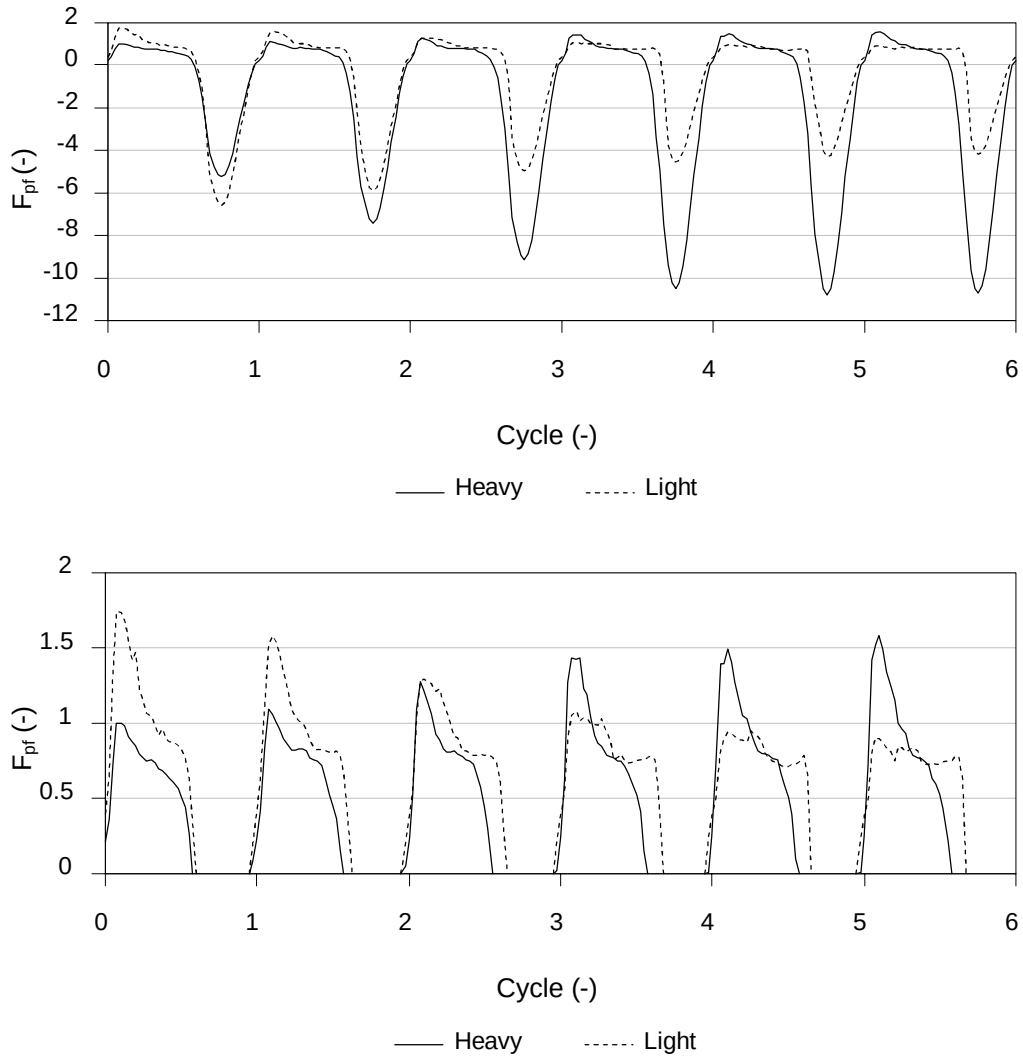

Figure 4–6. Non-dimensional average particle-fluid interaction force. Full view (top) magnified view (bottom) (SINE).

Since heavy particles have comparatively high drag values when they are in a densely packed state, and light particle are loosely packed, the heavy particles are driven into the light particles during pulsion, squeezing the light particles between themselves and the top fluid interface. This decreases the voidage between the light particles and locally increases the overall drag. The behaviour is very visible in profiles with high pulsion velocities, such as the sawtooth-backward and trapezoidal profiles. This behaviour can be described as a drag wave moving upwards though the bed, as shown in Figure 4–8.

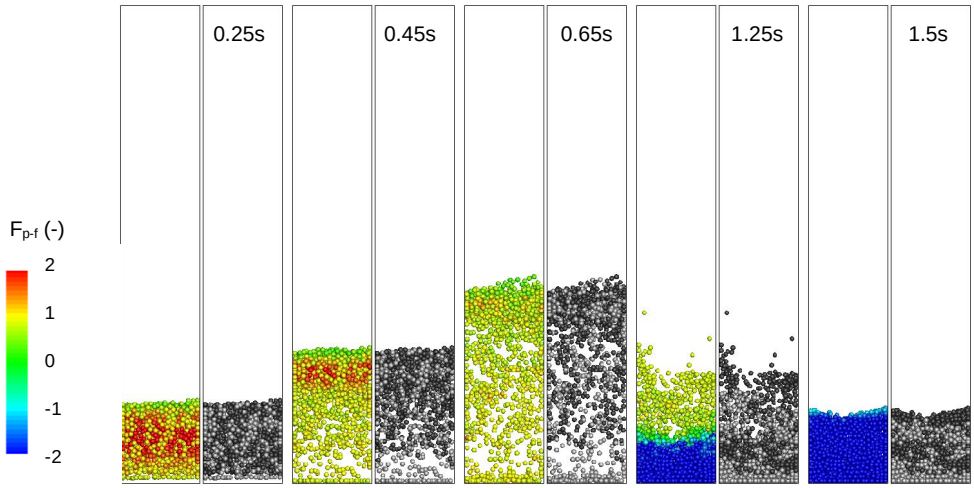

(a)

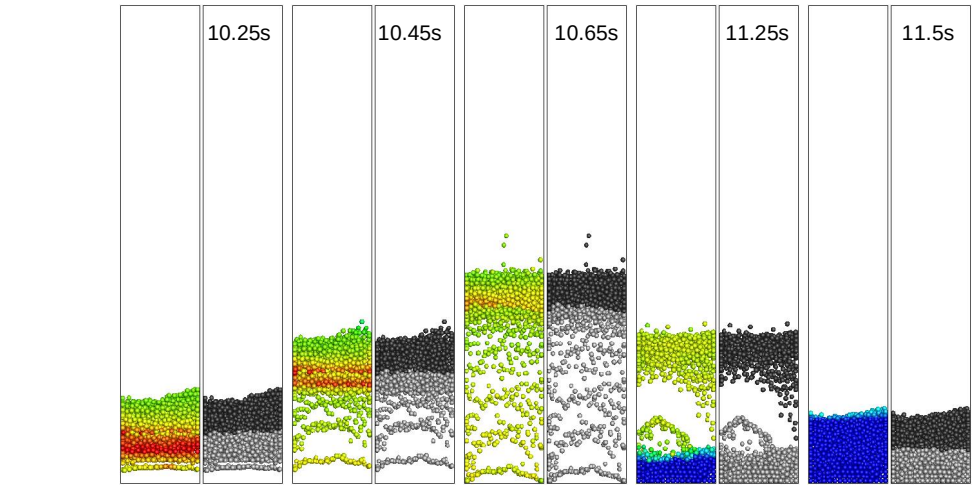

(b)

Figure 4–7. Solid flow patterns showed by particle fluid interaction force (left) and particle position (right) for the sinusoidal profile (a) first cycle, (b) final cycle. Heavy and light particles are coloured grey and black respectively.

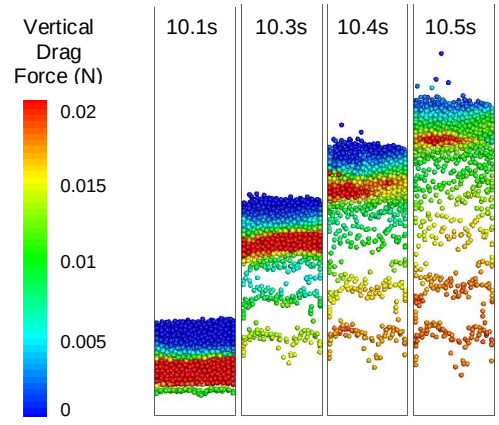

Figure 4–8. Drag wave up through bed (STB final cycle).

4.2.4.2 Other profiles

All the pulsation profiles react differently when considering the non-dimensional particle fluid interaction force. In the triangular profile, the heavy particles $f_{p\text{-}f}$ values are much lower than the sinusoidal profile because the lower inlet velocity produces less drag (see Figure 4–9). The differences between heavy and light particles $f_{p\text{-}f}$ values are small for the triangular profile, indicating that both types of particles almost equally displace as in a fluidized bed. The particles at the bottom of the bed form a packed bed very early during pulsion which increases the bed drag force and causes a re-expansion. This behaviour leads to an S-shaped pulsion drag profile (horizontally along pulsion peak), seen in Figure 4–9.

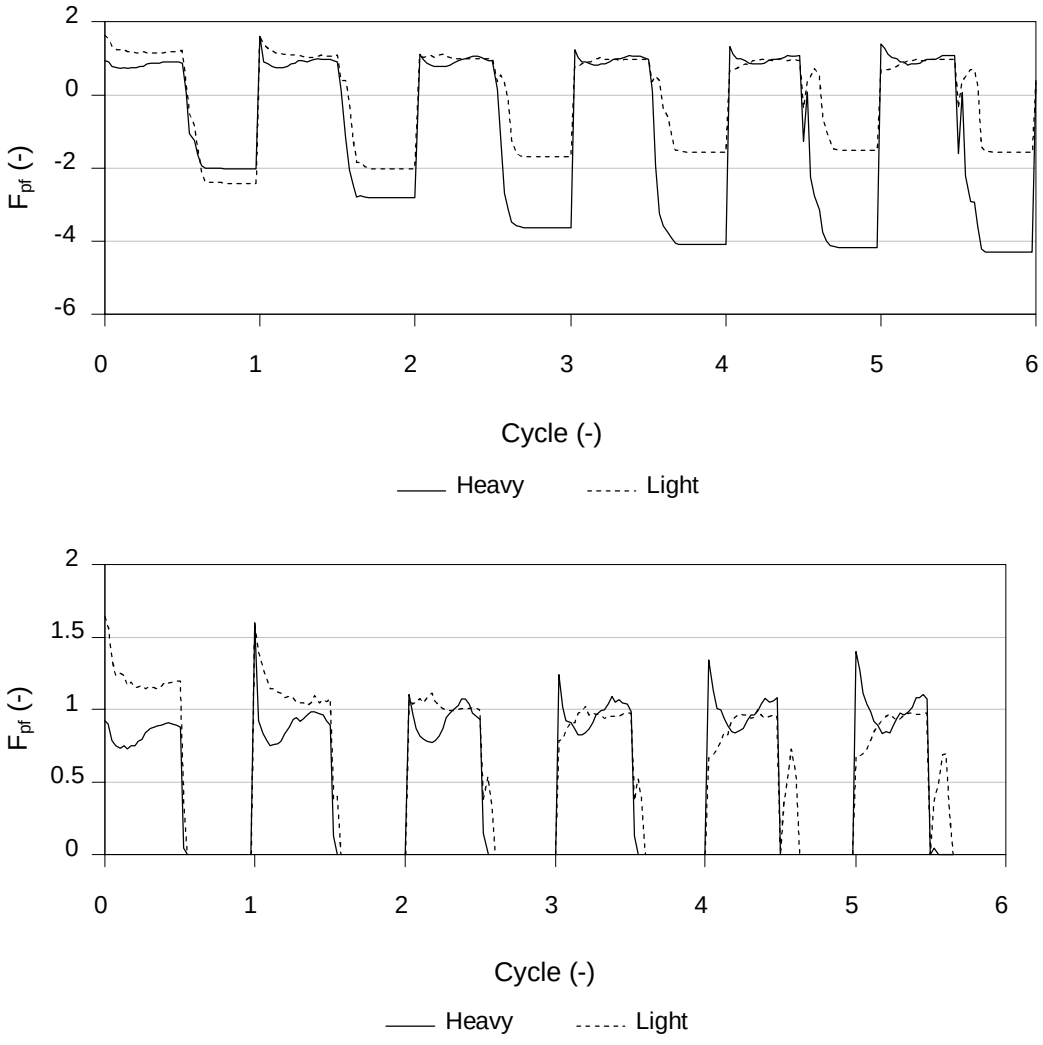

Figure 4–9. Non dimensional average particle-fluid interaction force.
Full view (top) magnified view (bottom) (TRI).

Using the Sawtooth-backward profile (see Figure 4–10) the suction force is so weak during settling that the particles experience high positive viscous drag resistance in decent. Consequently, as the light particles are more buoyant they experience a higher positive force when falling compared to heavy particles. This occurs throughout every cycle and gives rise to a deeply upward propagating loosening wave and very large expansion of the bed. Importantly, the heavy particles due to the large bed expansion are less hindered and have a greater opportunity to move past the light particles and settle, promoting efficient segregation.

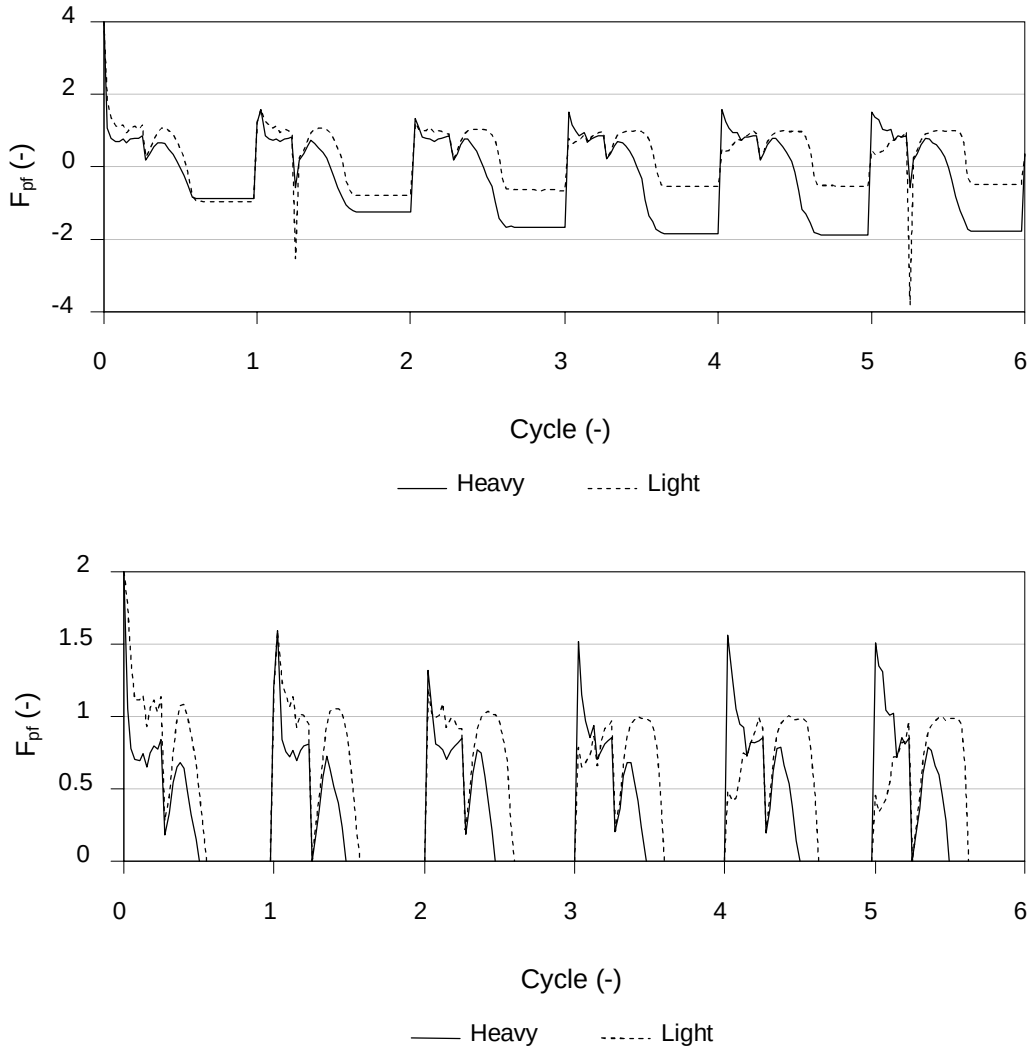

Figure 4–10. Non dimensional average particle-fluid interaction force. Full view (top) magnified view (bottom) (STB).

The Sawtooth-forward profile $f_{p\text{-}f}$ values results in Figure 4–11 are typical of a combined fluidized bed and jigging system. All particle-fluid interaction values

fluctuate around a mean. Light particles consistently have an almost linear and constant $f_{p\text{-}f} > 1$ where heavy particles do not. This drives the light particles up through the particle bed. Heavy particles are generally forced to move either laterally or downwards to make way for the upward flux of light particles. It is easy to imagine the suction portion of this cycle is redundant as the bed only takes a small fraction of a second to fall to rest—almost instantaneously.

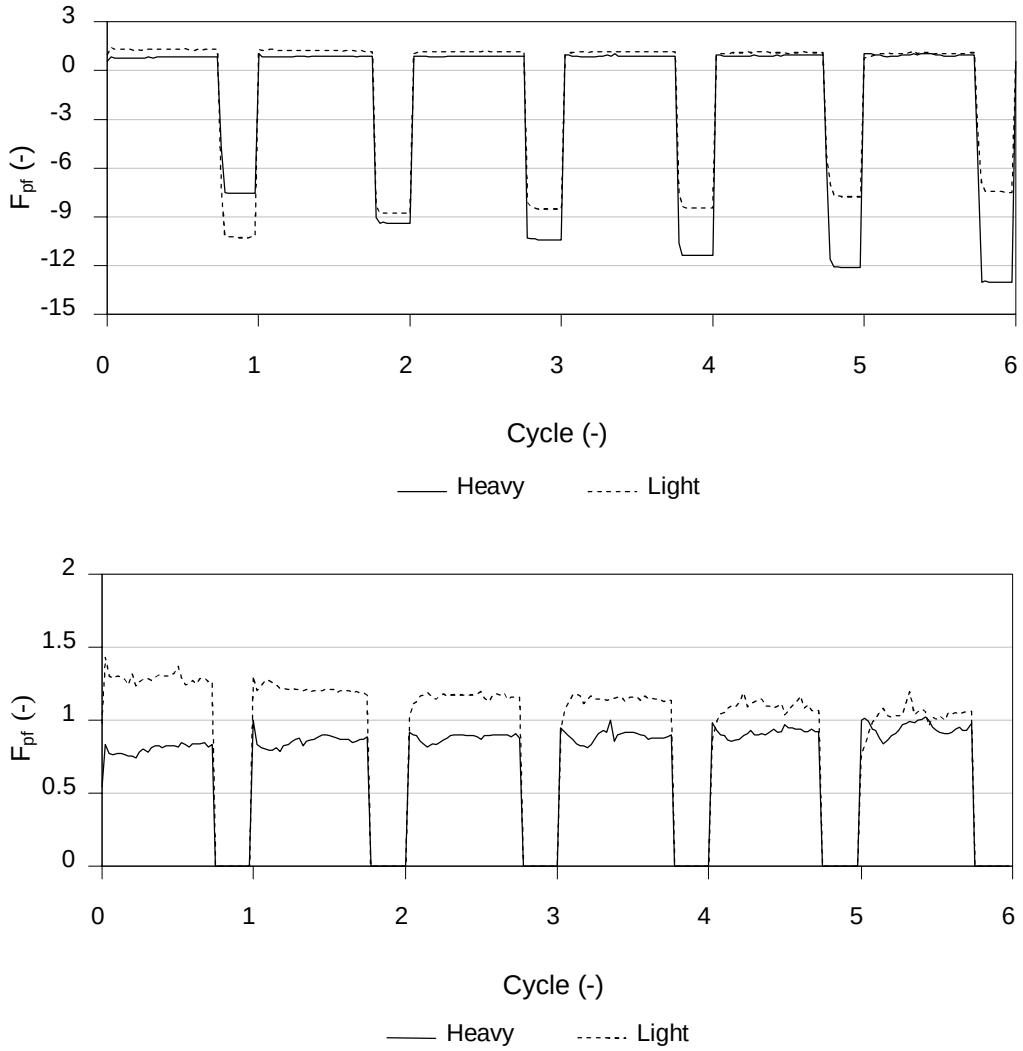

Figure 4–11. Non dimensional average particle-fluid interaction force. Full view (top) magnified view (bottom) (STF).

Finally, the trapezoidal pulsation profile unlike other profiles studied shows some unsteadiness in $f_{p\text{-}f}$ values (see Figure 4–12). In this profile the inversion velocity is reached and the bed begins to re-mix in the 5th and 6th cycle. When particles are segregated and fall freely without inhibiting each other, both heavy and light particles

eventually achieve peak values of $f_{p\text{-}f} \sim 1$. This shows both particle types fall for long enough on average to achieve terminal velocity, where their weight force is equal to drag and buoyancy forces (i.e. acceleration is zero). The heavy and light particles have different terminal velocity values which promotes segregation.

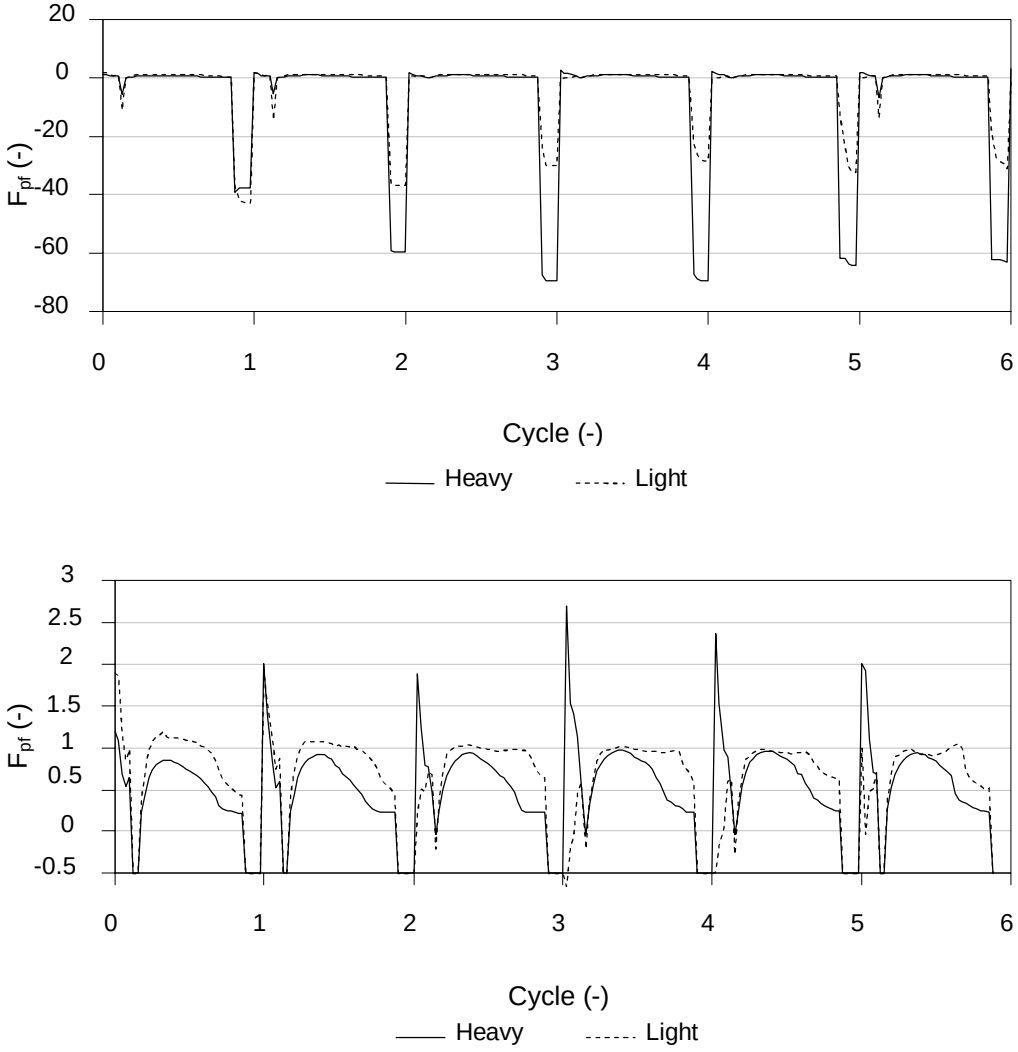

Figure 4–12. Non dimensional average particle-fluid interaction force. Full view (top) magnified view (bottom) (TRA).

4.2.5 Mean Particle Contact Force

The contact forces for the sinusoidal profile are shown in Figure 4–13. During each jig cycle the lower section of bed becomes progressively more tightly packed and populated by heavy particles. This causes the total average contact force to increase. As the heavy particles increasingly reside in a tightly packed state their contact force values increase, and this reverses for light particles as they move to a loosely packed state. High contact forces are experienced when particles land, and these forces move upward as the bed reforms (see Figure 4–14). Most significantly, contact forces peak when the particles are at rest in the throes of suction where the negative liquid velocity causes drag that squeezes the bed together (see 4th particle bed image in Figure 4–14). This is undesirable as high peak contact forces may cause particle fragmentation and blockages during jigging operation.

The STB, TRI, STF and TRA profiles perform similarly to the sinusoid profile. The average contact force in pulsion is similar in all five profiles with values ranging from 2 N to 5 N. The peak values arise in suction and are the most important to consider as they are much higher and vary greatly with the choice of pulsation profile. The trapezoidal profile shows extremely high contact force values with the highest 70 N which can easily lead to fragmentation.

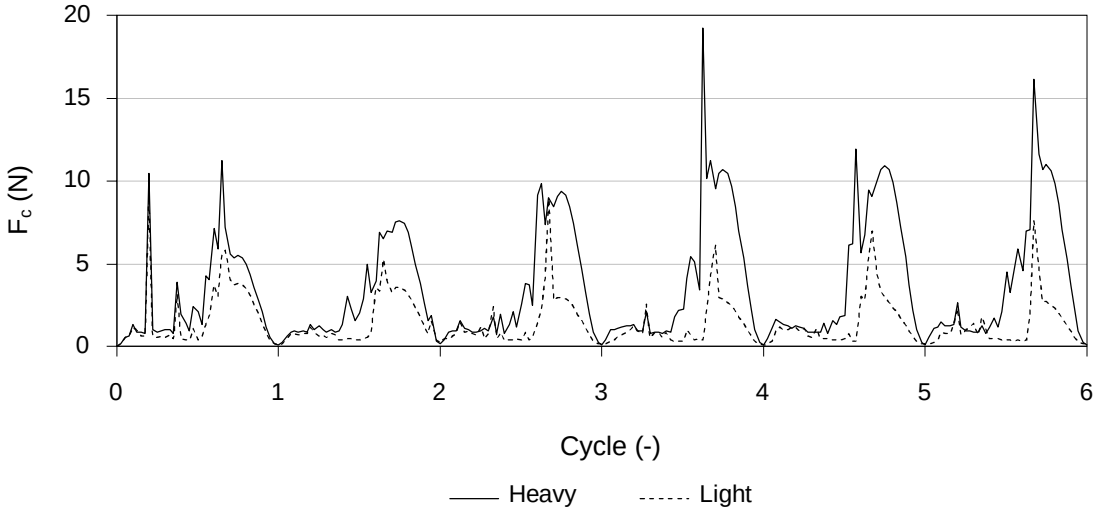

Figure 4–13. Mean particle contact force (SINE).

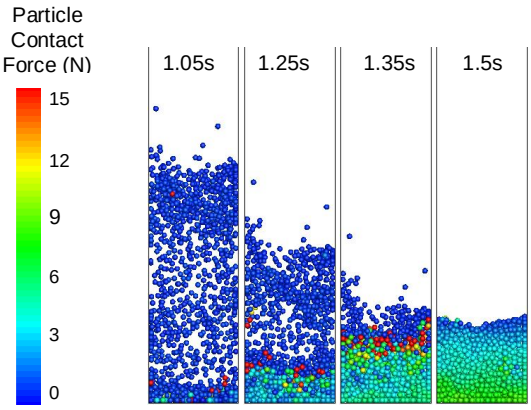

Figure 4–14. Particle contact forces travelling upwards while the particle bed is compiling and highest average contact forces found during suction (SINE first cycle).

4.2.6 Coordination number

The coordination number represents the average sum of neighbouring particle contacts. These can be of a particle type with its own or other type, or the total number of contacts in the system. The total coordination number represents how particles on average are in contact with other particles, irrespective of the particle type. While the bed is in suction and in a packed rested state the peaks of the total coordination number, seen in Figure 4–15 (a), consistently return to similar values of close to eight as expected for all monosize spherical systems. On the other hand the trough values coincide with particle expansion returning a low number of contacts.

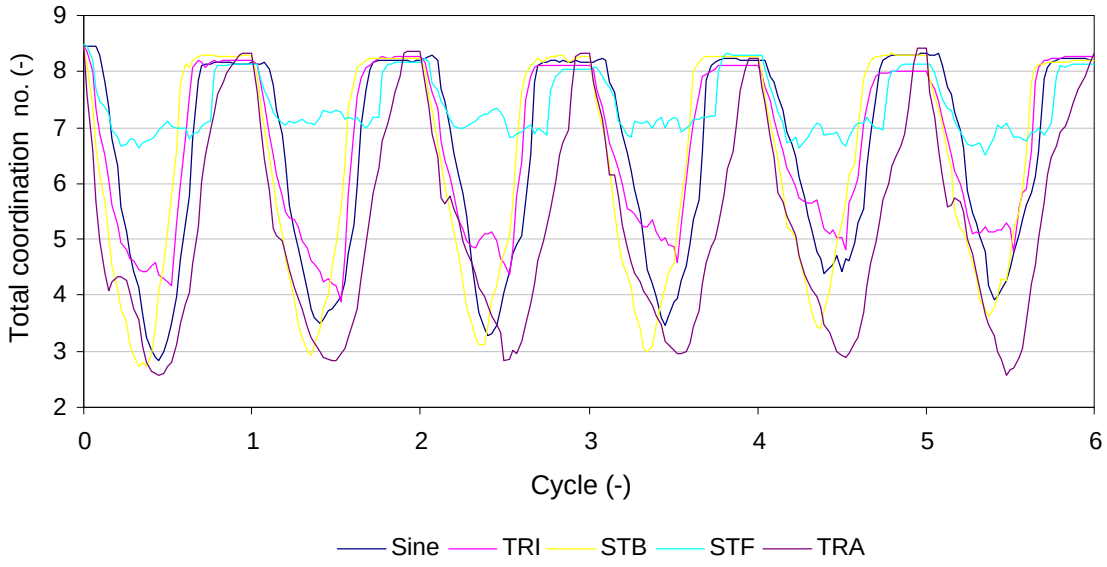

(a)

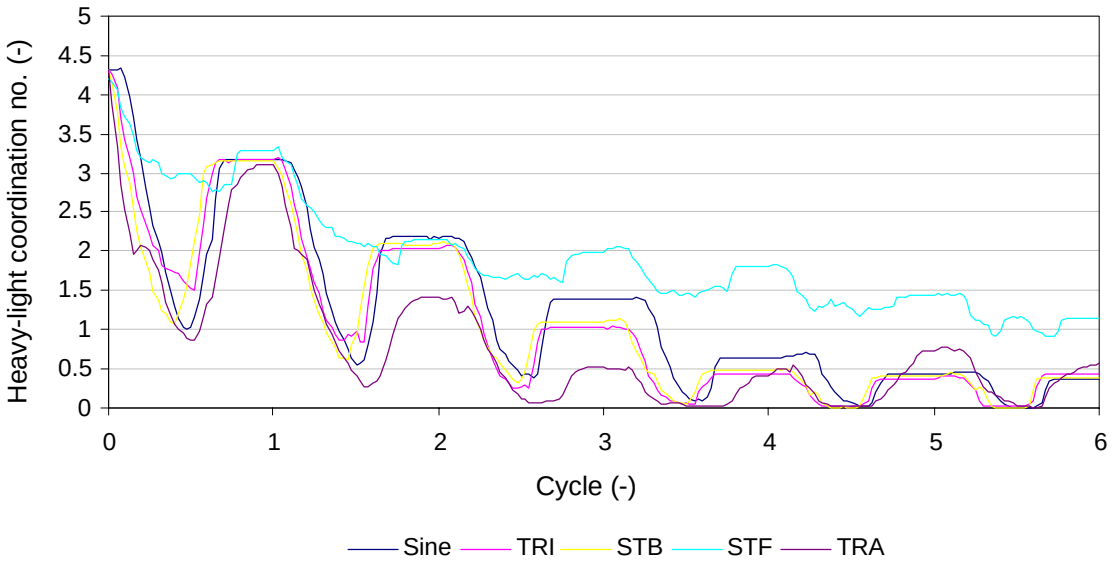

(b)

Figure 4–15. Profile comparison of (a) Total coordination number, and (b) Heavy-Light coordination number for all profiles.

As mentioned in Chapter 3, section 3.4, the Heavy-Light coordination number, seen in Figure 4–15 (b), is a good ‘one line’ representation of segregation. In the beginning in a mixed state there are an equal number of four heavy particles in contact with four lights. As jigging progresses there are less contacts with the opposite particle type and the coordination number reduces. This indicates that jigging is successfully separating

the particles. When segregation is complete the minimum coordination number is only affected by interfacial contact at the boundary between the segregated particles. Therefore, the coordination number can never be zero when particles are at rest, but will sit just below 0.5 when segregation is complete.

4.2.6.1 Coordination number comparison

Figure 4–15 (b) shows the sawtooth-forward profile provides incomplete segregation. The trapezoidal profile performs exceptionally as it segregates the quickest (3rd cycle), however, re-mixing proceeds after this cycle. Nonetheless the trapezoidal profile segregates one full cycle quicker than other profiles. In all other profiles the bed is highly segregated and to a high degree by the 4th cycle, and therefore the trapezoidal profile separates 25% faster. Reductions in coordination number beyond the 4th cycle can be discounted due to small fluctuations at the particle type interface arising from small particle rearrangements.

This indicates that firstly, the trapezoidal profile clearly (within these profiles) has the most potential for fast segregation. Secondly, the sawtooth-forward profile has very poor performance in this monosize system, but it cannot be disregarded as literature states this profile is tailored to fine particle segregation which was not simulated here. Finally, all other profiles perform similarly and segregate the particles despite their different pulsation profile shapes.

The two main contributing factors to segregation in a monosize system are: the expansion duration, and the magnitude of expansion of the whole particle system. Comparing Figure 4–15 (a) and (b) it is clear that maximum total expansion (i.e. maximum porosity) is not directly proportional to segregation. For example the triangular profile provides less expansion than the sawtooth-backward and sinusoidal profiles (refer to Figure 4–15 (a)) but constantly yields more separation (as shown in Figure 4–15 (b)). Unlike a fluidized bed, the difference of $f_{p\text{-}f}$ between particle types is not directly proportional to segregation either. Comparing the same profiles, the differences in the $f_{p\text{-}f}$ for the sawtooth-backward and sinusoidal profiles are greater than in the triangular profile, yet the triangular profile consistently induces more

segregation. So how can the triangular profile give less expansion and have a lower difference in $f_{p\text{-}f}$ between particle types yet still induce higher segregation per cycle?

The duration of expansion (time particle bed is expanded) is however directly proportional to segregation (see Figure 4–16). The time the particles are in suspension dictates how much time is present for differential settling. The particles only need *sufficient expansion* to segregate, whereby any further expansion is redundant and the bed is *over expanded* yielding no benefit by reducing particle congestion in settling. Conversely, if the particles expand below a critical level, segregation is far more difficult due to a high level of particle congestion and associated particle contacts causing hindrance to rearrangement. The respective acceleration of each particle is different due to their respective $f_{p\text{-}f}$ in either direction, up or down. When particle suspension time increases, the difference in particle velocities continually increases with time until the terminal velocity is reached. Therefore, greater expansion duration leads to greater differences in distance between particle types i.e. segregation. Regardless of the difference in $f_{p\text{-}f}$ between profiles, the expansion duration of each profile is shown to be more influential in this study i.e. the differences in $f_{p\text{-}f}$ do not out-weigh the differences in expansion duration. Uniquely, the sawtooth-forward profile does not provide sufficient expansion, and consequently large particle hindrance is present and segregation through most cycles is poor.

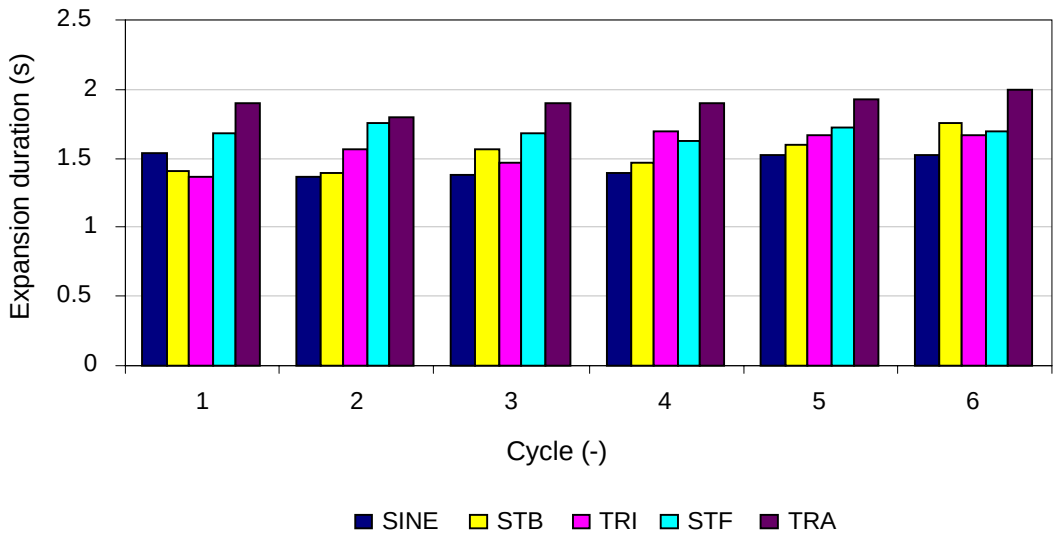

Figure 4–16. Expansion duration for all profiles.

From here a cycle-by-cycle explanation will proceed excluding the sawtooth-forward profile. In the first cycle the segregation is similar for all profiles regardless of expansion time however as cycles progress differences are found (refer to Figure 4–15 (b)). The 2nd cycle displays a large drop in heavy-light coordination number and a very high expansion time for the trapezoidal profile. The sawtooth-backward profile expands to the same level and has a similar difference in $f_{p\text{-}f}$ between particle types however the coordination number does not drop as far because the expansion duration is far less. In the 2nd cycle, the triangular profile provides a larger drop in coordination number than the sawtooth-backward profile even though the bed expands significantly less and the difference in $f_{p\text{-}f}$ between particle types is similar. However, the expansion time is slightly greater and therefore so is segregation. This cycle also shows that the sinusoidal profile provides more expansion than in the triangular profile and similar difference in $f_{p\text{-}f}$ between particle types but because the expansion time is less the segregation is reduced.

The third cycle again shows the trapezoidal profile coordination number greatly drop while expansion is similar to the sawtooth-back profile and only a very slight difference in $f_{p\text{-}f}$ exists between particle types, but because expansion duration is far greater so too is the segregation. This is a great example to show that segregation is by far most sensitive to expansion time. The sawtooth-backward and triangular profiles values drop but also come closer together. Interestingly, the triangular profile expands far less and has far less $f_{p\text{-}f}$ difference compared to the sawtooth-back profile. Despite this the triangular profile still holds its place as second most segregated thus far and greater than the sawtooth-back profile. This is because even though the bed is slightly more segregated from the previous cycle, the sawtooth-backward profile only very slightly reduces the difference because its expansion duration is slightly higher. The sinusoidal profile again shows relatively poor segregation even though the bed expands more and has the same difference in $f_{p\text{-}f}$ between particle types than the triangular profile, the expansion duration is far less. This again is an example highlighting the high sensitivity in segregation due to expansion time.

In the fourth cycle the trapezoidal profile begins to mix the particles because the inlet flow velocity is too high to allow the bed to gently fall. Instead the bed fully segregates whilst suspended but lands erratically. Here the triangular profile has far

less expansion and difference in $f_{p\text{-}f}$ than the sawtooth-back profile but still leads to a more segregated state because the expansion duration is again greater. The sinusoidal cycle trails behind the other profiles consistently yielding small expansion duration values.

In the fifth cycle the trapezoidal profile continues to cause mixing. The sinusoidal profile makes up differences in segregation to the other profiles as they are already segregated.

4.2.7 Power

There are various parameters to judge the performance of a jigging device. In addition to the separation speed and the final degree of separation as already discussed, the power input is one important concern in industrial processes. The following formula is used to calculate the input power, where power is a product of total pressure drop ΔP_t, and volumetric flow rate **Q**:

$$Power = \Delta P_t \mathbf{Q} \tag{4–2}$$

and

$$\Delta P_t = \Delta P_{fa} + \Delta P_{pa} + \Delta P_{fw} + \Delta P_{sw} + \Delta P_{shs} + \Delta P_{shf} \tag{4–3}$$

where the total pressure drop ΔP_t is a summation of various pressure drops due to, ΔP_{fa}, fluid acceleration, ΔP_{pa}, particle acceleration, ΔP_{fw}, fluid-to-wall friction, ΔP_{sw}, solid-to-wall friction, ΔP_{shs}, static head of solids, and, ΔP_{shf}, static head of fluid. The contributions of wall effects are not resolved in high resolution using the current model due to the computational effort and complexity. Although these effects do contribute they are relatively small. The following power values are calculated using ANSYS CFX 10.0 commercial software.

The power values calculated are not absolute power values and only yield qualitative results. In particular, the model does not consider the fluid pushing through a distributor plate at the inlet which would cause substantial drag on the fluid. Table 4–

1 shows power values, and ranks the amount of energy used to achieve segregation placed in decreasing order. Note that the trapezoidal profile total energy values are taken over all 6 cycles, opposed to 3 (when the bed is segregated), because it exhibits unsteady segregation behaviour i.e. subsequent mixing.

Table 4–1. Maximum power, average power, and total energy for segregation of all profiles.

Pulsation profiles (-)	Max power (Watts)	Average power (Watts)	Total energy for Segregation (Joules)
Trapezoidal	1732.4	199.7	1198.2*
Sinusoidal	71.7	24.4	243.8
Triangular	33.5	16.5	132.3
Sawtooth-backward	68.6	16.2	129.9
Sawtooth-forward	124.4	44.3	-

*The trapezoidal profile value is taken over all 6 jigging cycles. Even though the profile is shown to segregate by the 3rd cycle, subsequent mixing ensues.

The amount of energy consumed during jigging depends on the type of profile and how many jigging cycles have occurred. Power values for the sinusoidal profile can be seen in Figure 4–17. As jigging progresses the porosity development (heavy particles in the lower portion of the bed gradually compacting tighter over each cycle) coincides with an increase of power (see Figure 4–17). During pulsion, beyond the minimum fluidisation velocity the particles are suspended by the liquid flow, a further increase in liquid velocity will have little effect on the particle friction pressure drop owing to sufficient percolation of the liquid flow because the particle system will expand proportionally. Alternatively, during suction the bed cannot expand, so an increase in liquid velocity will increase the drag as the porosity is constant. The power in suction grows as the bed experiences high flow velocity whilst in an increasingly tightly packed state. A further consideration is whether the profile has a high or low flow rate in suction. Figure 4–17 shows suction portions in every cycle where zero power is used. This is because the flow rate is very small and the hydrostatic fluid pressure is sufficient to supply this flow rate without the addition of power. The

sawtooth-backward and triangular profiles take advantage of this and require virtually zero power in suction. Alternatively, profiles with a high flow rate in suction such as the sawtooth forward and trapezoidal profile are penalised with high power consumption.

During pulsion two parameters are the most influential in terms of power requirements. The first parameter is the mean pressure drop in pulsion which is approximately the same for all profiles. The second and most influential parameter is the flow rate which is multiplied with the almost constant pressure drop to yield power. All pulsion pressure drop values are similar but the injection velocities vary greatly.

There are two ways of evaluating power. Firstly, maximum values are important to find the maximum requirements needed for operation. Secondly, because instantaneous power values change the average value is important. For example a profile may have a high maximum power peak but other values in the profile may be quite low. Focusing on peak power values in Table 4–1, the trapezoidal profile has a value almost fourteen times higher than second highest sawtooth-forward profile, followed by the sinusoidal, sawtooth-backward and triangular profiles. The average power values are ordered as follows, trapezoidal, sawtooth-forward, sinusoidal, triangular, and sawtooth-backward. The average power values show a change in order and a reduction in the magnitude of differences between profiles as compared to maximum power values.

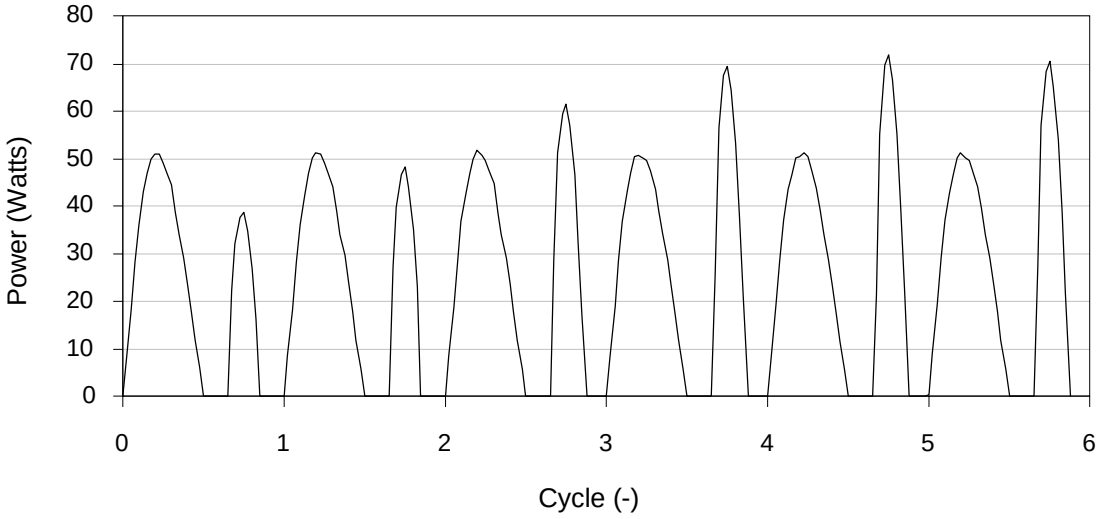

Figure 4–17. Instantaneous power values (SINE).

It is not sufficient to focus solely on power and the number of cycles to reach segregation. A profile which requires high power consumption may need only a few cycles to achieve separation and will prove more favourable than a profile using little power over many cycles. Table 4–1 summarises the energy required by each profile to reach a fully segregated state. The sawtooth-forward profile was not included as it did not produce sufficient segregation. The sawtooth-backward profile is shown to use the least energy to achieve segregation, followed by triangular, sinusoidal, and lastly the most energy inefficient trapezoidal profile.

4.3 CONCLUSIONS

The particle separation process in a jigging device under five pulsation profiles has been studied using a DEM-CFD model. The present study selected one amplitude and cycle period. With these settings all the five pulsation profiles demonstrated potential for particle separation, but subject to different separation rate, final degree of separation, and power usage.

Solid flow patterns indicate that different phenomena exist according to the pulsation profile adopted. The inlet velocity affects particle movement. If a high inlet velocity is present at the onset of pulsion the bed will move as a whole, and will either display

slugging or complete transport behaviour. If the inlet velocity develops slowly i.e. sinusoidal profile, the particles will not lift as a whole and the loosening wave will dominate in the beginning of the cycle. Further, if a low and constant inlet velocity is adopted fluidization is present, e.g. sawtooth-forward profile.

Both the solid flow patterns and mean particle displacement values show that all pulsation profiles exhibit segregation. The particles remain in a fixed bed position for a significant time during the suction period in all of the pulsation profiles with exception to the trapezoidal profile, demonstrating potential opportunities to improve the jigging process using an optimised pulsation profile, e.g. reducing the suction period of the profile.

Non-dimensional particle fluid force values confirm the solid flow pattern behaviour. Further, drag force values for heavy and light particles change with jigging due to porosity developments. As local porosity changes occur, the bottom of the bed becomes more tightly packed and the drag force on heavy particles increases.

Within the selected profiles, segregation is shown to be far more sensitive and therefore proportional to expansion duration, rather than expansion magnitude, or non-dimensional particle fluid interaction force differences between heavy and light particle types. This holds true provided that the particles are expanded up to a critical porosity whereby sufficient particle-particle hindrance is avoided and also inversion velocities are not present making it difficult for particles to land uniformly causing mixing.

The contact forces show peak values occurring when the particles are at rest and in the throes of suction where maximum negative liquid velocity and drag is experienced. These high contact forces of up to 70 N may cause particle fragmentation and blockages during jigging operation.

The most influential parameter related to power during pulsion was the inlet flow rate. All pressure drop values were similar but the injection velocities varied greatly. It was found that power values gradually increased during suction in conjunction with gradual local porosity developments.

The present study based on one set of peak-to-peak amplitude and period can not fully assess the relative performance of different pulsation profiles. However, the work demonstrates the usefulness of DEM-CFD model as an effective numerical model, to study the jigging process. Chapter 5 considers different amplitudes and periods of the four pulsation profiles, as well pulsation profile optimisation, to fully clarify this issue in detail. The sawtooth-forward profile has been excluded as the profile principally induces segregation by fluidization, which has been commonly studied.

CHAPTER 5

DEM-CFD INVESTIGATION OF VARIOUS JIGGING PROFILES

5.1 INTRODUCTION

Past studies using the DEM-CFD model have used a sinusoidal pulsation profile with the exception of Dong et al. (2009), which adopted a forward leaning saw tooth cycle. No numerical investigations (including all various modelling techniques) have studied what effect the sinusoidal, triangular, sawtooth-backward, and trapezoidal profiles have on concentration mechanics by using two-way coupling in conjunction with a porous drag force model. Further, these studies have not investigated jigging aspects such as separation time, energy, and profile optimisation. The aim of this study is to elucidate how the profile induces segregation, and how variations of frequency and amplitudes affect performance based on a range of criteria. The sawtooth-forward profile has not been investigated here as the profile principally induces segregation through regular fluidization (see Chapter 4, section 4.2.1). Segregation by fluidization has been commonly studied and hence will be excluded from this section.

This study investigates the sinusoidal, triangular, sawtooth-backward, and trapezoidal jigging profiles (see Figure 4–1) using a mono-size binary-density system, and two-way coupling (model specifications are found in Chapter 3, section 3.1). The inlet flow for the sinusoidal pulsation profile was established using a sinusoidal function, while other profiles employed the heavy-side step function. Whilst chapter 4 used constant conditions of amplitude, A=3 litres, and wave period, T= 2 seconds, each pulsation profile is compared by holding the shape of the profile constant and using three variations of period (T) and three volumetric water input/exhaust amplitudes (A). These are 1, 2, and 3 second periods (or 60, 30, and 20 cycles/min), and, 1.5, 2.25 and 3 litres water amplitudes. The amplitudes are represented in litres not distance as the water/air free surface is not resolved (i.e. the domain at anytime is completely filled with water), otherwise the amplitudes would be equivalent to 0.2, 0.3 and 0.4m. A further study is performed with broader amplitude and frequency values to establish and investigate operational limits of these parameters. The particles were processed using 60 seconds of jigging concluding with 1 second of settling after the last jigging cycle.

The performance of profile variants are compared in terms of solid flow patterns, separation kinetics, energy consumption, and mean particle position. These quantitative comparisons demonstrate significant differences in the segregation rate, energy consumption, and solid flow phenomena, helping find an alternative optimum operating setting for the system. In addition, boundaries of operation are found in terms of frequency and amplitude limits and the concentration mechanics are investigated in these regions.

5.2 RESULTS AND DISCUSSION

5.2.1 Solid flow patterns

The maximum particle displacements for all variants (of each profile shape) during the first cycle can be visualized in Figures 5–1 to 5–4, together with the particles in a rested state once segregation is achieved. The results show large differences in the maximum heights the particles reach during pulsion and also bed expansion. Profiles with volumetric water inputs of, A=1.5 L, have low velocity and therefore little drag to lift the bed upwards. Consequently, there is less opportunity for bed expansion which facilitates particle rearrangement. The A=1.5 L variants comparatively require a lot of time to segregate the particle bed. As the volumetric input increases, the bed maximum particle height and expansion increases. This is advantageous to segregation and these profiles segregate much faster. Decreasing the cycle period from T= 3s to T= 1s is shown to increase maximum particle height and expansion (see Figure 5–1 for example).

The trapezoidal profile uniquely shows particles settle very slowly due to a zero inlet velocity present in the midst of the cycle. When a high frequency and high volumetric input is adopted—despite a short period of suction—particles do not form a fixed bed before pulsion in the following cycle (see variant A=2.25 L and A=3 L on the bottom of Figure 5–4 (a), where particles are shown to be far from settled at the end of suction). Consequently, the particles undergo pulsion in an already highly suspended and relatively high voidage state which leads to bed circulation and mixing. These

variants cannot successfully induce segregation. Similar behaviour can be seen in the sinusoidal profile, but due to suction being more predominate throughout the cycle the particles are partially settled at the end of suction preventing bed circulation (see variant *A*=3 L on the bottom of Figure 5–1 (a)).

Further, it is found in all pulsation profile shapes that a high frequency profile must lift the bed to a large height which therefore increases differential settling time. This allows time for rearrangement before the particles are quickly sucked back down. A moderate or low frequency profile does not have to lift a bed to such great heights as the duration of the cycle is longer allowing more time for rearrangement. Therefore two important criteria must be met for segregation: a profile must sufficiently lift the bed to a height where expansion and loosening can proceed, but also allow enough time for particles to rearrange.

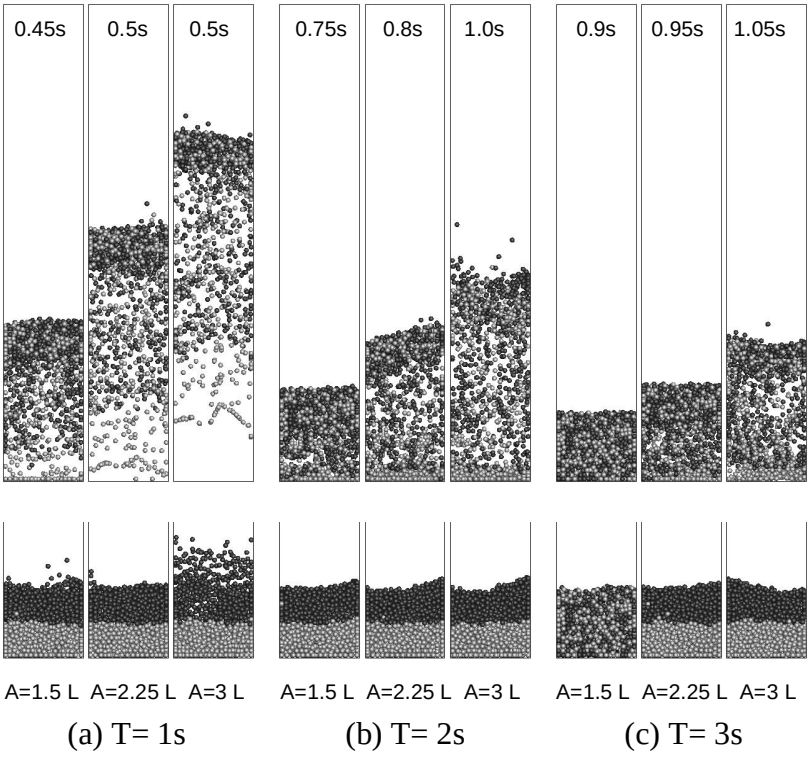

Figure 5–1. Solid flow patterns of the sinusoidal profile at maximum particle height in the first cycle for all variants (top) and snapshots at a rested state on completion of separation (bottom). Heavy and light particles are coloured grey and black respectively (a) *T*=1 s, (b) *T*=2 s, (c) *T*=3s.

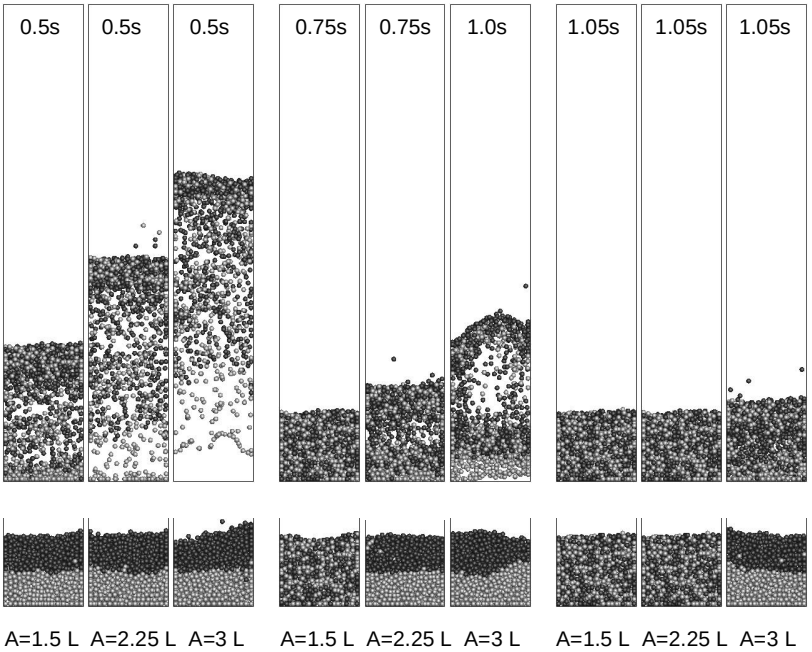

Figure 5–2. Solid flow patterns of the triangular profile at maximum particle height in the first cycle for all variants (top) and snapshots at a rested state on completion of separation (bottom). Heavy and light particles are coloured grey and black respectively (a) *T*=1 s, (b) *T*=2 s, (c) *T*=3 s.

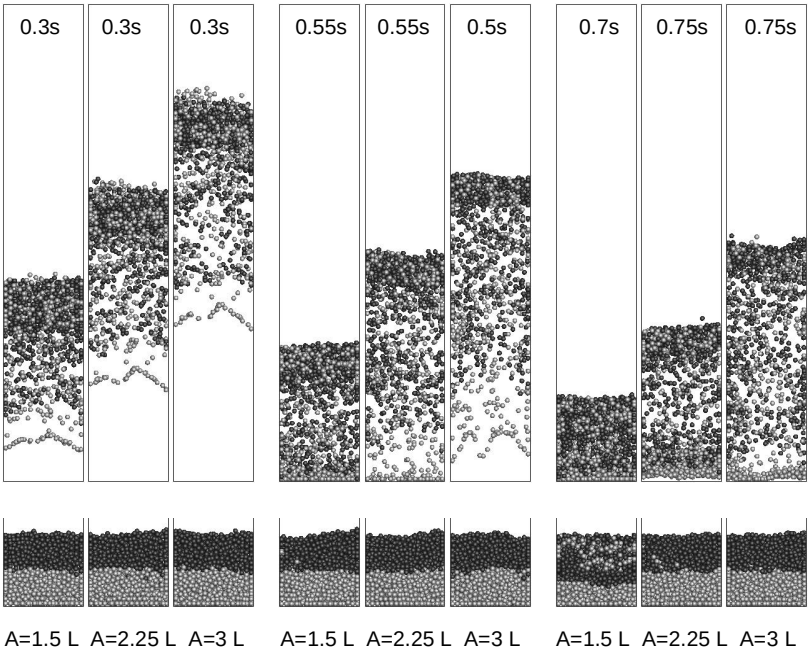

Figure 5–3. Solid flow patterns of the sawtooth-backward profile at maximum particle height in the first cycle for all variants (top) and snapshots at a rested state on completion of separation (bottom). Heavy and light particles are coloured grey and black respectively (a) T=1 s, (b) T=2 s, (c) T=3 s.

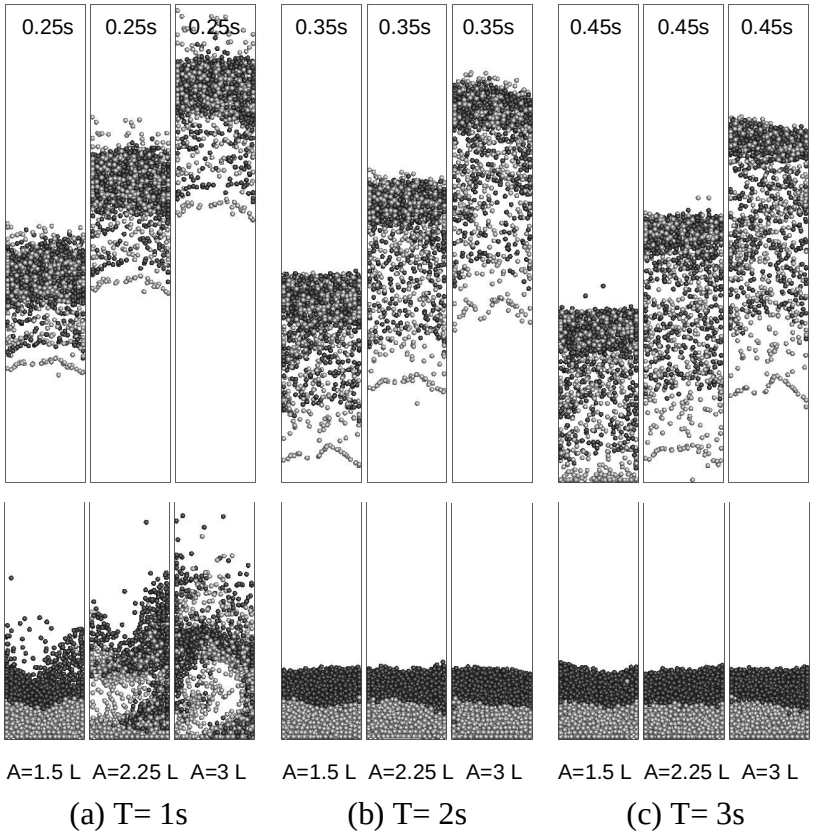

Figure 5–4. Solid flow patterns of the trapezoidal profile at maximum particle height in the first cycle for all variants (top) and snapshots at a rested state on completion of separation (bottom). Heavy and light particles are coloured grey and black respectively (a) *T*=1 s, (b) *T*=2 s, (c) *T*=3 s.

5.2.2 Particle separation time

5.2.2.1 Coordination number

The heavy-light coordination number is a good indication of particle segregation (for details see Chapter 3, section 3.4). Only values when the bed is at rest are considered here which coincides with the state of the final product. The lower the value the higher the segregation i.e. the less light particles are in contact with heavy particles.

Of the nine sinusoidal profiles investigated, eight completely segregated the particle bed within 60 seconds of jigging time. Complete segregation is indicated by coordination numbers beginning to plateau after approximately a value of 0.5, slight

differences under this value are insignificant (see Figure 5–5). Steady separation is critical for a reliable jigging process. The separation process can be unsteady and may reverse and re-mix in subsequent cycles. In this situation the coordination number of a rested bed will fluctuate (see Chapter 4, subsection 4.2.6.1). In this study the sinusoidal profile is found to provide steady segregation for all variants. Figure 5–5 shows the steady segregation for the eight variants which induce segregation.

The triangular profile completely segregated the particle bed within 60 seconds of jigging time for six variants. Figure B–1 in Appendix B shows the steady segregation for the six variants which induce segregation.

The sawtooth-backward profile completely segregated the particle bed within 60 seconds of jigging time for eight variants. Figure B–2 in Appendix B shows the steady segregation of all nine variants which induce segregation.

The trapezoidal profiles completely segregated the particle bed within 60 seconds of jigging time for seven variants. In this study the trapezoidal profile is found to provide steady segregation for only four of the seven variants which induced segregation (see Figure B–3 in Appendix B).

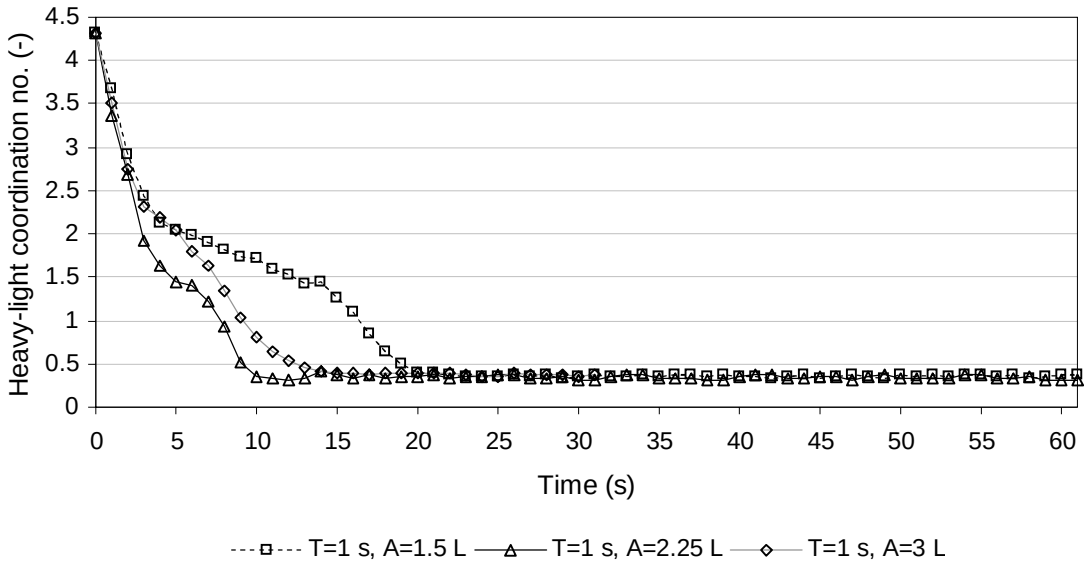

(a) T= 1s

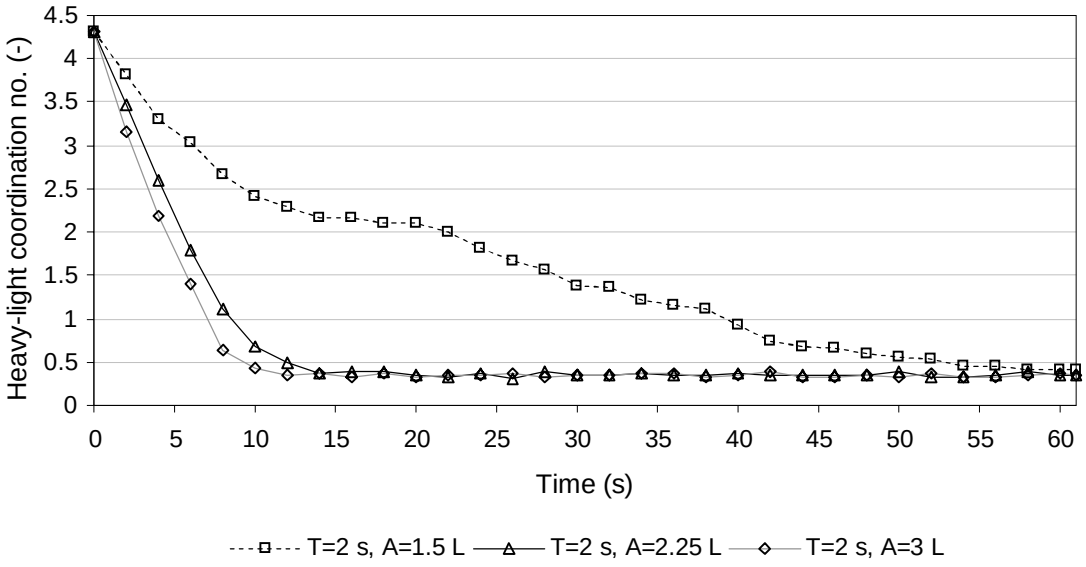

(b) T= 2s

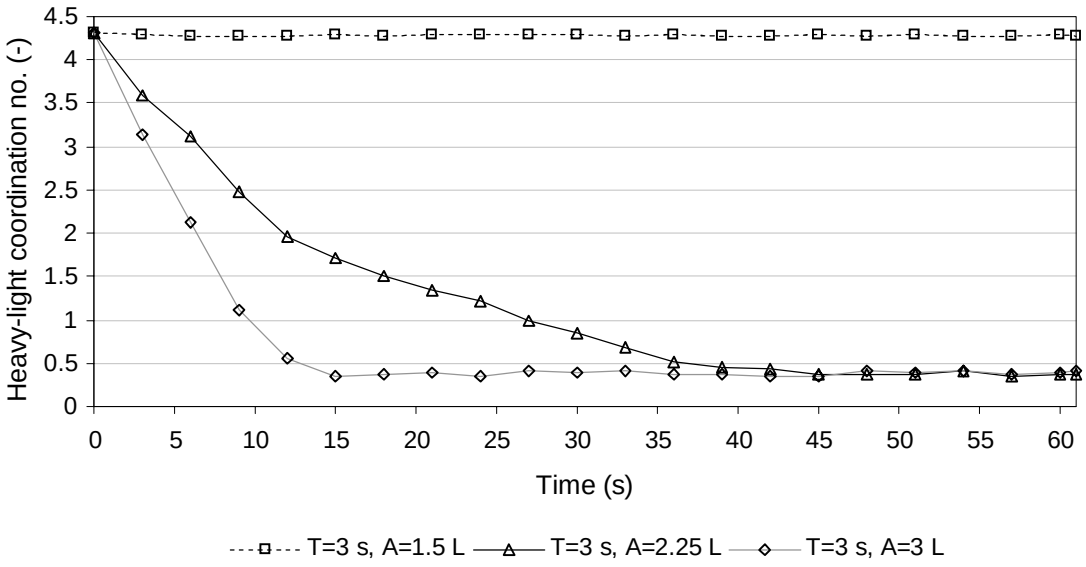

(c) T= 3s

Figure 5–5. Packed bed coordination number values for all sinusoidal profile variants (a) = T=1 s, (b) T=2 s, (c) T=3 s.

A consistently low coordination number indicates stable separation and a segregated bed. However, it does not characterize in which way particles have settled. Desirable settling occurs when particles are stratified vertically with one particle type directly

on top of another, this ensures separate delivery to the launders in a real jig. In addition to segregation the settling also needs to be stable. Inconsistent settling is undesirable and unreliable in jig processing even if the bed is perfectly segregated. The solid flow patterns, as in Figure 5–1, help visualize the stratification behaviour. Similar to the coordination number, the solid flow pattern is tracked through all the jigging cycles. If a tendency of undesirable settling is present, the variant is deemed impractical for particle processing of this system. All variants of the sinusoidal, sawtooth-backward, and triangular profiles which induced segregation were found to behave steadily in both coordination number and settling configuration. Only three successfully segregating variants of the trapezoidal profile were found to behave steadily in both coordination number and settling configuration.

5.2.2.2 Pulsation profile parametric effects

The effects of volumetric water input and cycle period on the separation time is shown in Figure 5–6 to 5–9. Here a broader range of cycle profile parameters are used to illustrate the complete particle separation time phenomenon in terms of amplitude and frequency selection. Here only profile variants are considered which are both stable in particle coordination number and settling configuration.

5.2.2.2.1 Sinusoidal

A strong relationship between volumetric input, *A*, and separation time is seen in all but one variant of frequency (see Figure 5–6 (a)). As the volumetric input increases the separation time reduces. An exception is the profile setting of *T*=1s and *A*=3 L. Unlike other frequency variants, segregation is faster at an intermediate amplitude. This is caused by particles being far from settled at the end of suction before pulsion begins in the following cycle (see variant *A*=3 L on the bottom of Figure 5–1 (a) where particles are shown not to be fully settled at the end of suction). In this variant, a portion of the light particles are still settling during pulsion in the subsequent cycle. These light particles under pulsion have a downwards momentum and low drag force upwards (due to high porosity) resulting in a deceleration of the particle downwards. Alternatively, the heavy particles settled in the previous cycle. These heavy particles which have no momentum while in a packed bed state and higher drag force (due to

low porosity) move upwards with an opportunity to penetrate back through the bed slowing down segregation. It is expected that further increases in amplitude for variants T=2 s, and T=3 s, would eventually result in the same situation.

The relationship between period, T, and separation time is shown in Figure 5–6 (b). Reducing the cycle period has a similar effect of increasing amplitude. As the cycle period is reduced, the resulting higher inlet velocity substantially increases particle expansion reducing separation time. The reduction in particle separation time reaches a maximum and beyond this point any further reduction in cycle period slows separation. The separation slows for the same reason as explained previously, for these variants separation is faster until the bed can no longer expand and settle within one cycle. Therefore, for each variation in amplitude an intermediate frequency provides the fastest separation.

It can be concluded from the results that an optimal amplitude and frequency exists in terms of separation time.

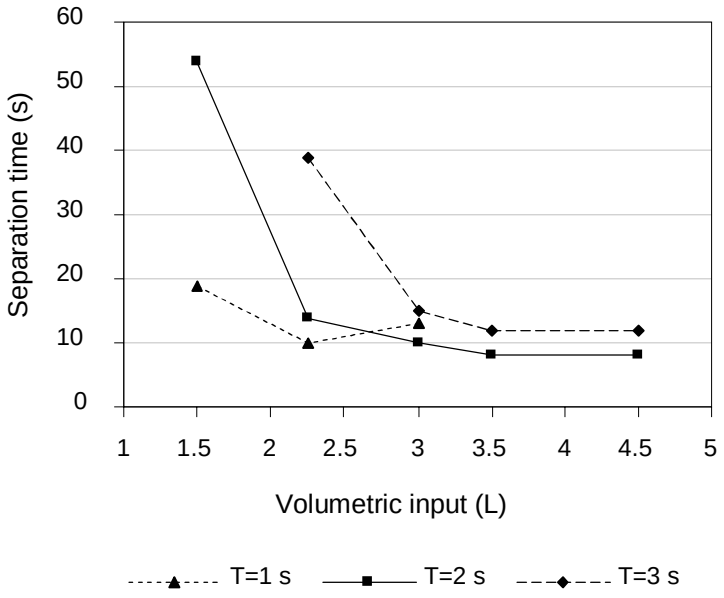

(a)

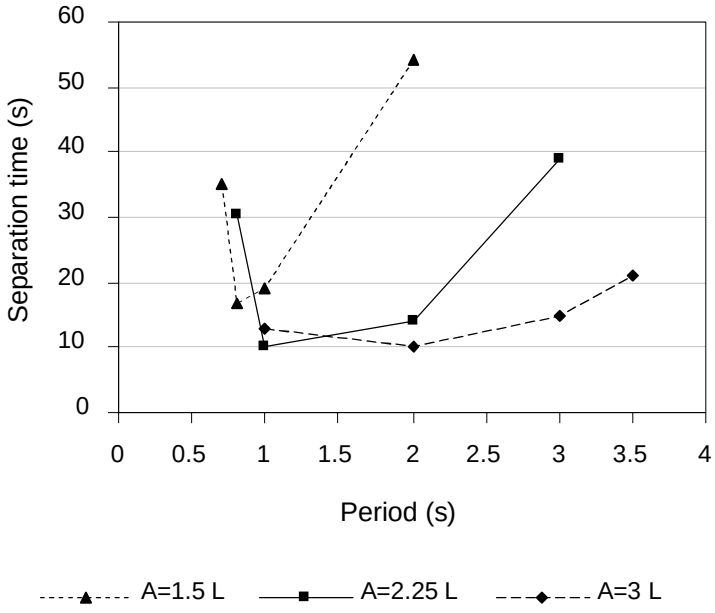

(b)

Figure 5–6. The effect of separation time against pulsation profile input parameters for the sinusoidal profile (a) volumetric input and (b) cycle period.

5.2.2.2.2 Triangular

A strong relationship between volumetric input, *A*, and separation time is seen in all variants of cycle period (see Figure 5–7 (a)). As the volumetric input increases the separation time reduces. Alternatively, the relationship between period, *T*, and separation time does not correspond in strength for all variants of volumetric input (see Figure 5–7 (b)). Increasing the frequency reduces separation time for all volumetric input variants, however, further increase results in slower separation. A high frequency results in the bed not having time to expand and segregate before being sucked immediately back down, while a low frequency imparts a low velocity and therefore lower drag force producing insufficient bed expansion slowing segregation. The intermediate values provide the right balance of porosity and expansion time.

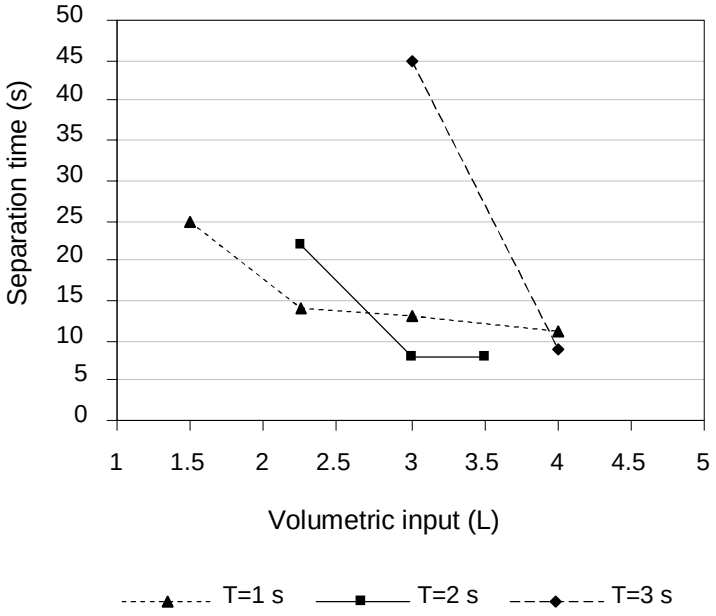

(a)

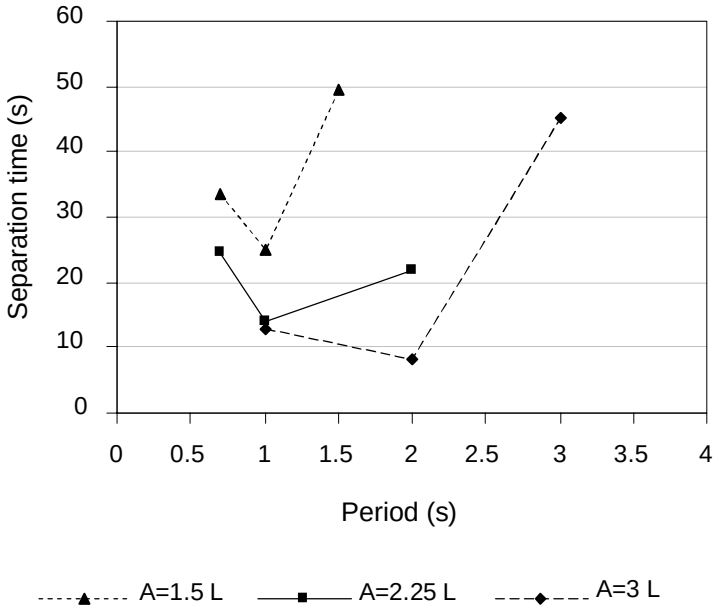

(b)

Figure 5–7. The effect of separation time against pulsation profile input parameters for the triangular profile (a) volumetric input and (b) cycle period.

5.2.2.2.3 Sawtooth-backward

The sawtooth-backward and triangular profiles behave similarly. A strong relationship between volumetric input, *A*, and separation time is seen in all variants of frequency (see Figure 5–8 (a)). As the volumetric input increases the separation time reduces. Alternatively, the relationship between period, *T*, and separation time does not correspond in strength for all variants of volumetric input (see Figure 5–8 (b)). The variant of *A*=1.5 L performs relatively poorly, even a short period where a high inlet velocity is present results in low bed lift and expansion. Consequently, as the period is increased the inlet velocity reduces and the bed struggles to expand. At a period of *T*= 3 s the particles largely remain compact and require an extremely long jigging time to separate thus the results are omitted. Alternatively, variants *A*=2.25 L and *A*=3 L do provide substantial lift and expansion over all frequencies. An intermediate period of *T*=2 s results in the fastest separation for these variants. A high frequency (*T*= 1s) results in the bed not having time to expand and segregate before being sucked immediately back down, while a low frequency (*T*= 3s) imparts a low velocity and therefore lower drag force producing insufficient bed expansion. The intermediate values provide the right balance of porosity and expansion time.

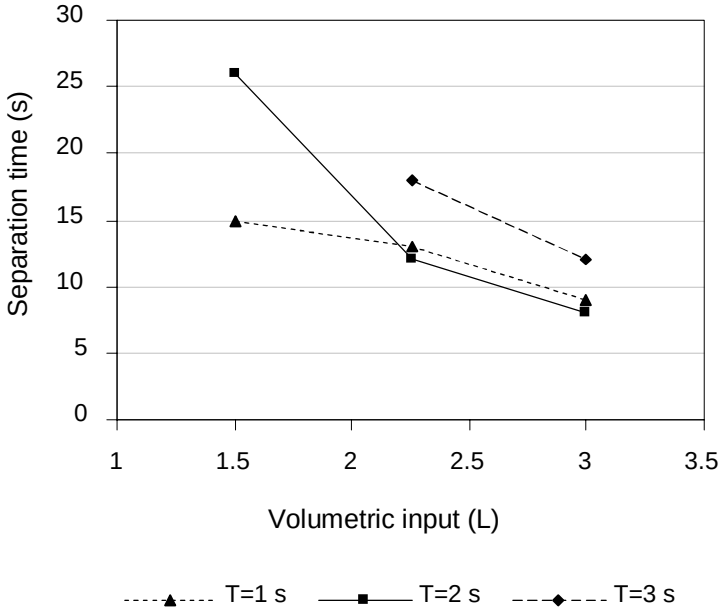

(a)

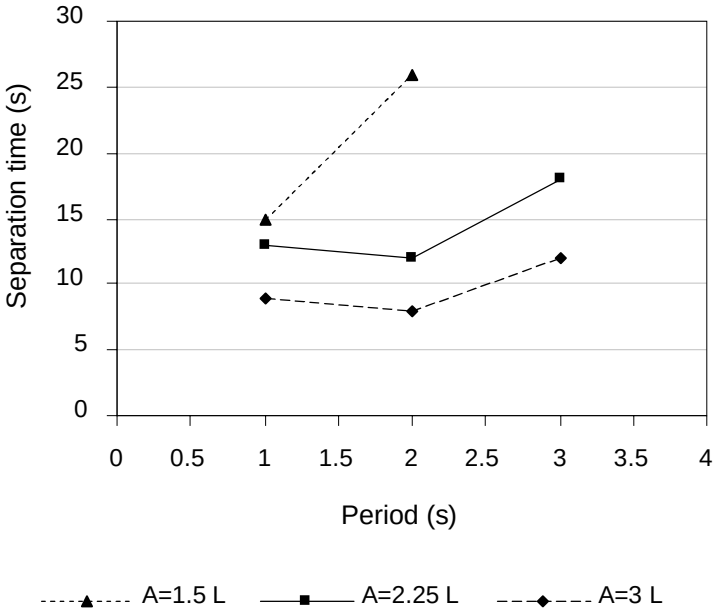

(b)

Figure 5–8. The effect of separation time against pulsation profile input parameters for the sawtooth-backward profile (a) volumetric input and (b) cycle period.

5.2.2.2.4 Trapezoidal

A strong relationship between volumetric input and separation time is seen in all variants of frequency (see Figure 5–9 (a)). As amplitude increases the separation time almost linearly reduces. Increasing frequency has a similar effect of increasing amplitude, separation time almost or does linearly reduce (see Figure 5–9 (b)). Conversely, reducing, *A*, or increasing, *T*, will slow segregation up until the inlet velocity is insufficient to dilate the particle bed. The optimal amplitude and frequency exist at the highest amplitude or frequency which allow for a stable particle settling configuration.

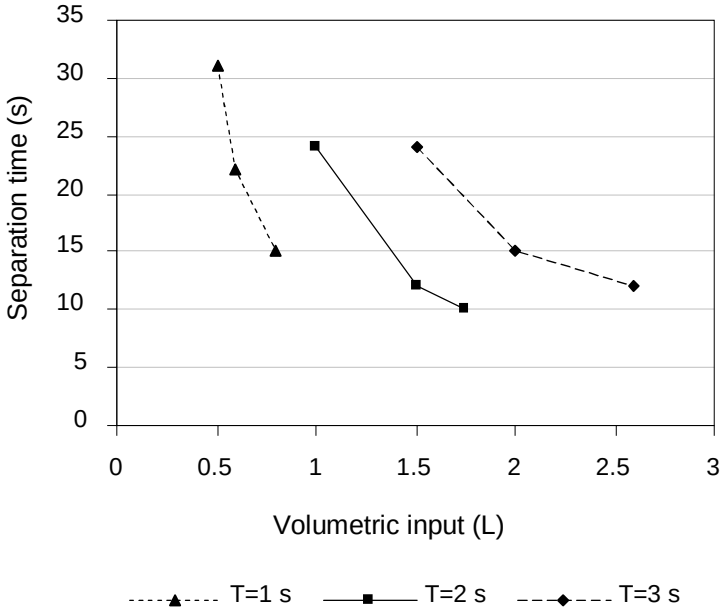

(a)

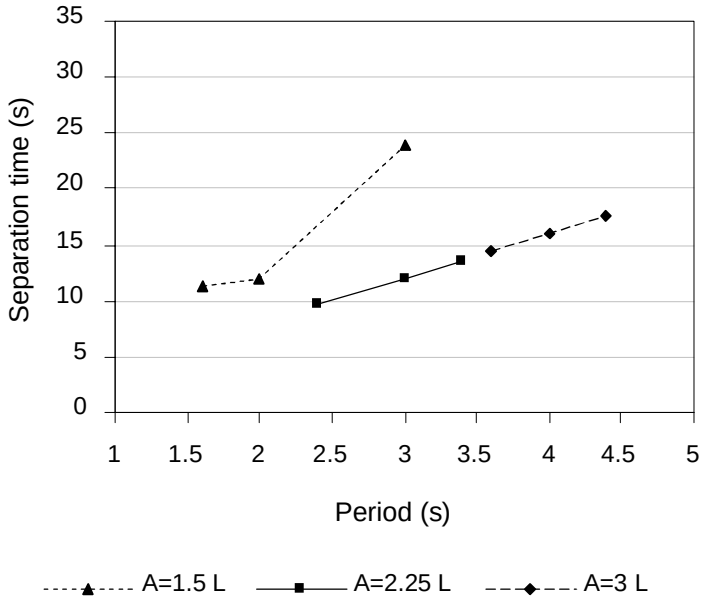

(b)

Figure 5–9. The effect of separation time against pulsation profile input parameters for the trapezoidal profile (a) volumetric input, (b) cycle period.

5.2.3 Cycle numbers

The number of jigging cycles used to achieve segregation can be important in terms of operating wear and fatigue. High cycle numbers may cause certain mechanical damages earlier.

The two equal fastest sinusoidal profile variants of frequency, T=1 s, and intermediate value of, T=2 s, separate after 10 seconds of jigging. However, the high frequency variant of, T=1 s, requires 5 additional cycles, that is 100% more cycles.

The fastest sawtooth-backward profile variant of intermediate frequency, T=2 s, requires 4 cycles to achieve separation in 8 seconds, the second fastest profile of high frequency, T= 1 s, segregates in 9 seconds which slower by only 1 second but to perform it requires 5 additional cycles, that is 125% more cycles. In addition, the third and forth fastest profiles separate in an equal time of 12 seconds and have a 2 cycle difference.

The two equal fastest triangular profile variants of intermediate frequency, T=2 s, require 4 cycles to separate after 8 seconds of jigging. The second fastest profile of period, T=3 s, separates in 9 seconds, which slower by only 1 second but to perform it requires 1 less jig cycle, that is 25% less cycles.

The two trapezoidal profile variants, T=1 s and A=0.8 L, and, T=3 s and A=2 L, both segregate in 15 seconds. However, the high frequency profile of T=1 s requires 10 additional cycles to perform, that is 200% more cycles.

5.2.4 Jigging profile optimisation

With exception of the high frequency variant of, T=1 s, the mean particle positions for all other variants remain at a constant value for a significant period. These moments correspond to a fixed bed which is a waste of time and energy and show an opportunity to improve jigging performance by modifying the profile settings. Figures 5–10 (a) to 5–13 (a) for each profile shape display the mean particle position for a high frequency variant of T=1 s. For all profile types the mean particle position is constant for almost an instant. Figures 5–10 (b) to 5–13 (b) for each profile shape display the mean particle position for a low frequency profile of T= 3 s. For all profile types the bed is shown to remain in a static state for a significant duration of time. Using mean particle position data to identify at what point in the cycle the bed comes to rest, this point is made the beginning of the following cycle. As a consequence the water input is not completely exhausted at the conclusion of the cycle. This has no influence on results, but can be a consideration for jig design, the inlet and exit water velocity remain the same (this issue is addressed in Chapter 6). It is found common in all profiles shapes that with exception of the high frequency variant of, T=1 s, all other profiles have the ability to increase performance in terms of segregation time, while the cycle numbers remain the same.

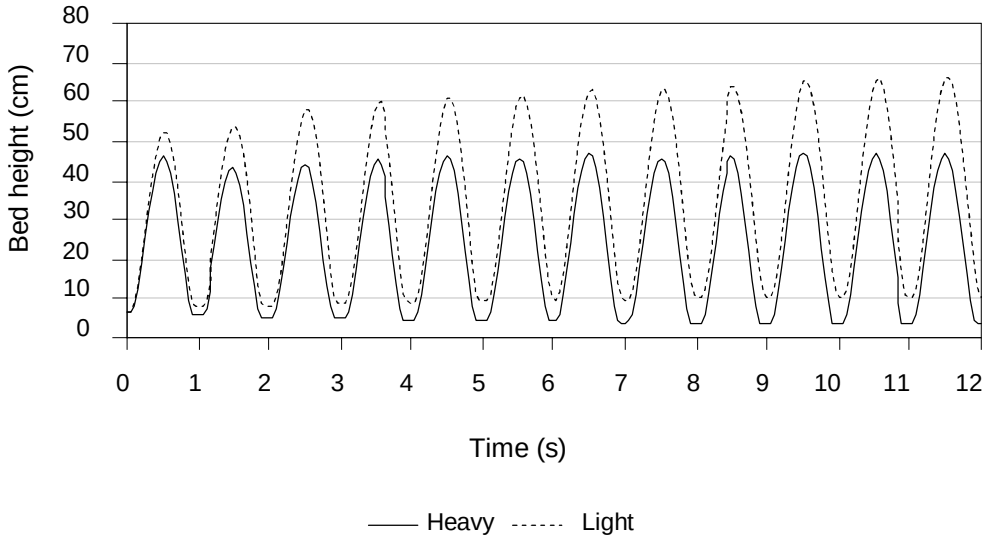

(a)

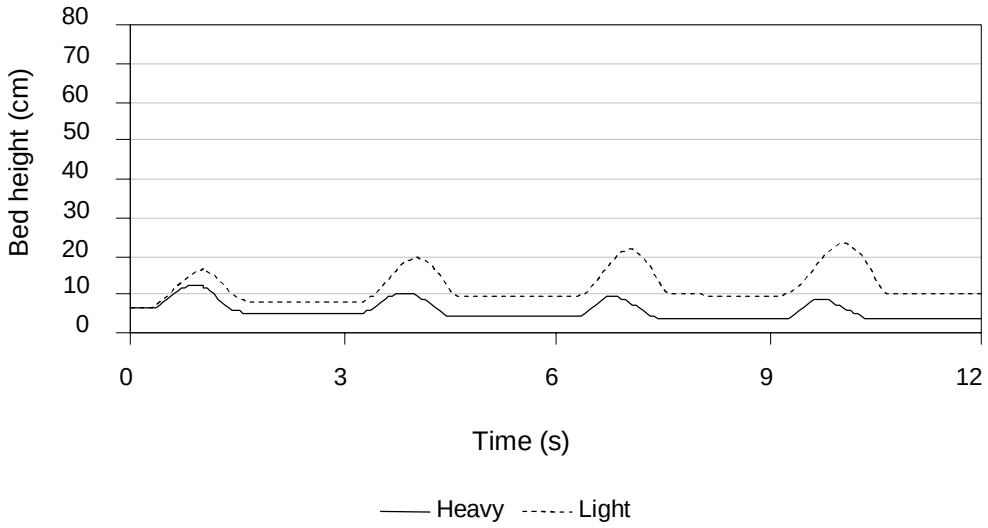

(b)

Figure 5–10. Sinusoidal mean particle position showing where profile improvements can be made (a) T=1 s, A=3 L (b) T=3 s, A=3 L.

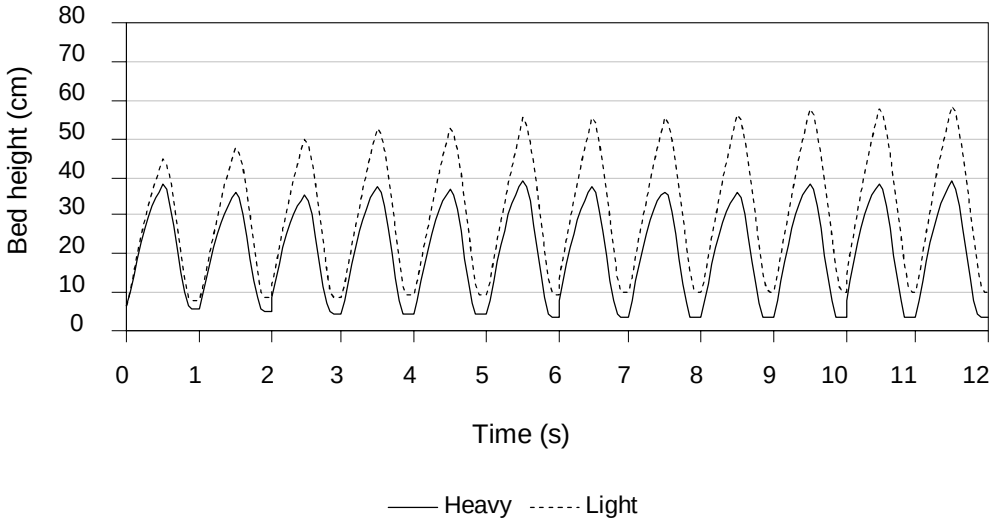

(a)

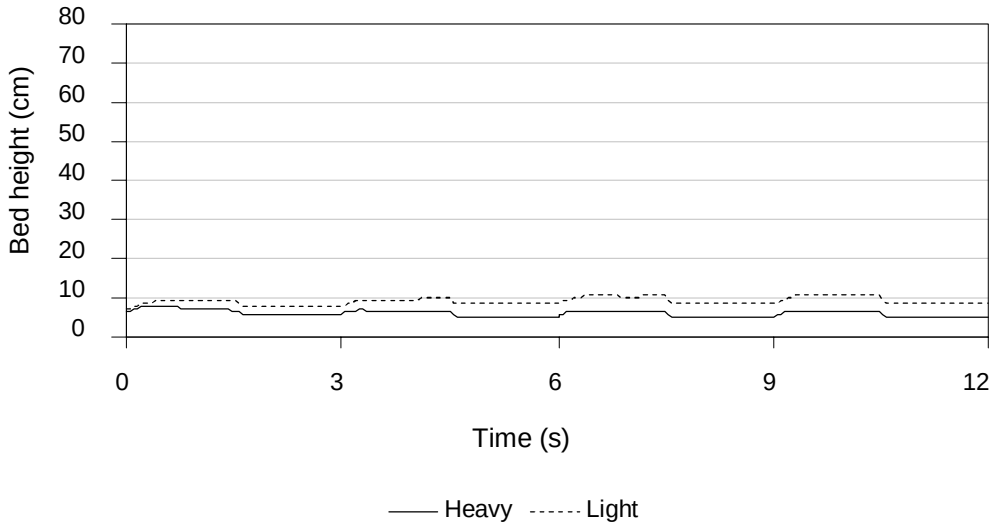

(b)

Figure 5–11. Triangular mean particle position showing where profile improvements can be made (a) T=1 s, A=3 L (b) T=3 s, A=3 L.

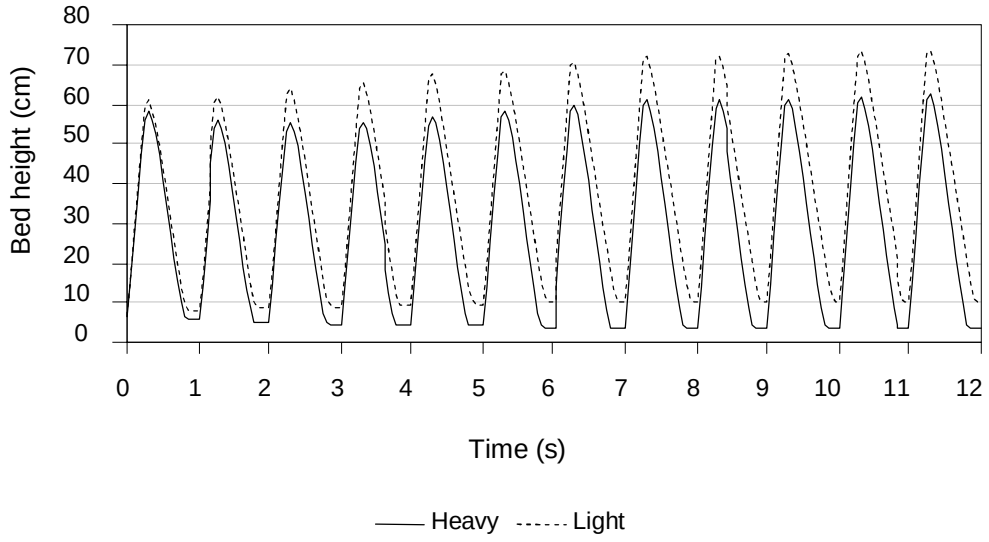

(a)

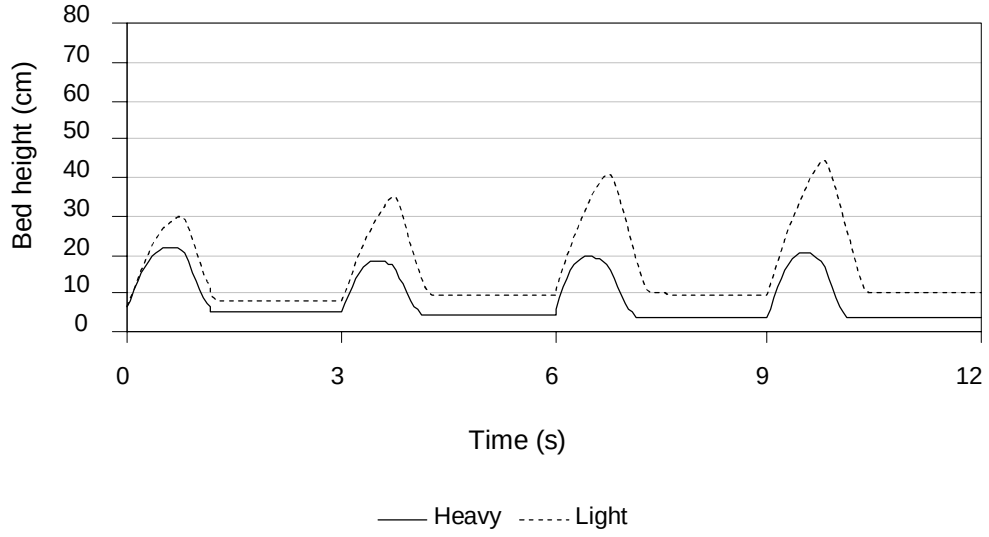

(b)

Figure 5–12. Saw-tooth backward mean particle position showing where profile improvements can be made (a) *T*=1 s, A=3 L (b) *T*=3 s, *A*=3 L.

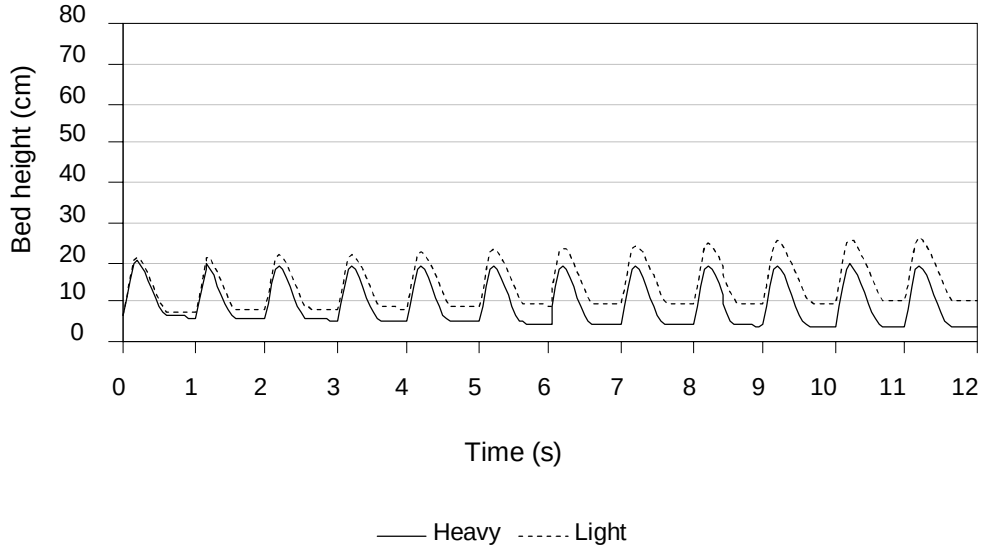

(a)

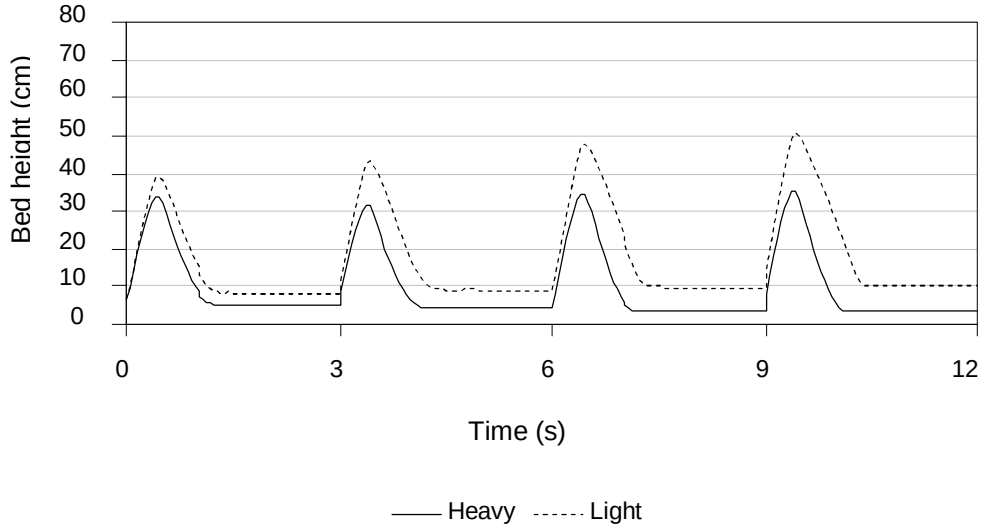

(b)

Figure 5–13. Trapezoidal mean particle position showing where profile improvements can be made (a) T=1 s, A=0.8 L, (b) T=3 s, A=2.25 L.

5.2.4.1 Sinusoidal

To illustrate how the profile setting can be improved the settings were changed for the original variant of T= 2 s and A= 3 L (see Figure 4–1 (a)). The period, T= 2 s, was changed to 1.7 seconds. Figure 5–14 (a) shows the modified profile setting. The resulting mean particle position is shown in Figure 5–14 (b) which displays a reduction in time the bed is at rest when compared to Figure 4–3 (a). After modification the sinusoidal profile separated after 8.5 seconds, which is 1.5 seconds (15%) faster. Applying the same treatment to the fastest profile of T=2s and A=3.5 L (which one would expect to have a minimal time that the bed is at rest) the separation time is reduced from 8 s to 6.8 s, again 15% faster.

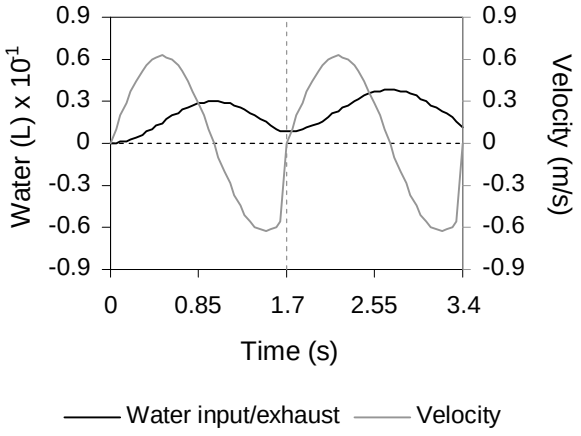

(a)

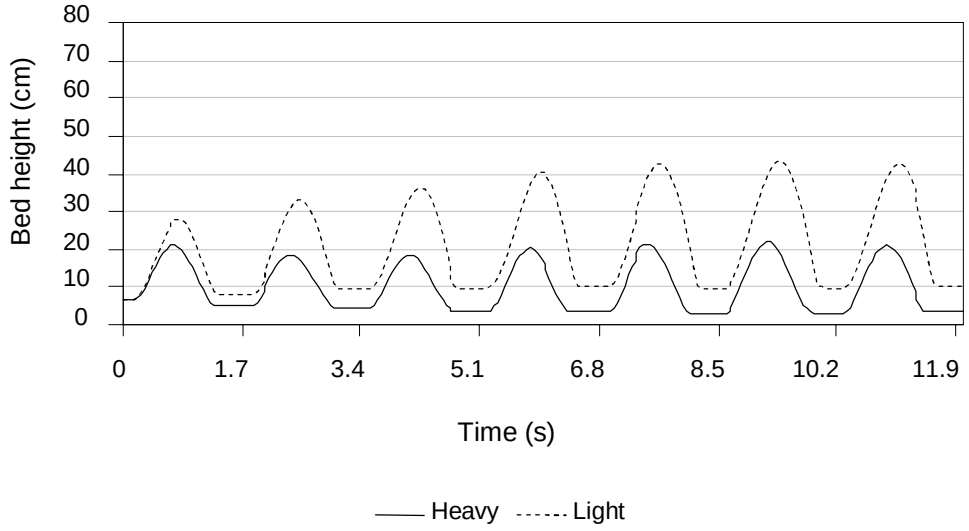

(b)

Figure 5–14. Alternative sinusoidal profile

(a) improved profile setting, (b) mean particle position of improved profile.

5.2.4.2 Triangular

The period, *T*, of the original and fastest variant, *T*=2 s and *A*=3 L, (see Figure 4–1 (b)) was changed to 1.6 seconds. Figure 5–15 (a) shows the modified profile setting. The resulting mean particle position is shown in Figure 5–15 (b) and displays a reduction in time the bed is at rest when compared to Figure 4–3 (b). After modification the profile separated after 6.4 seconds, which is 1.6 seconds that is 20% faster.

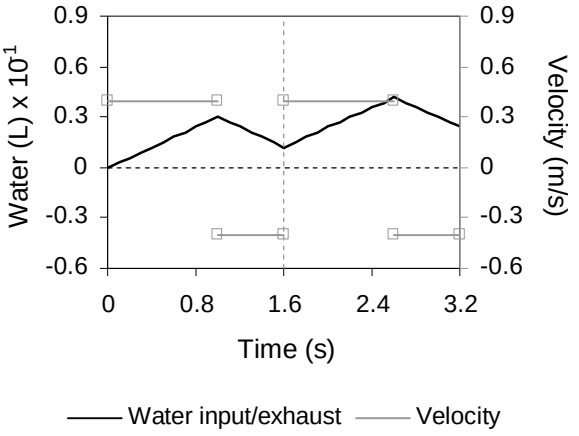

(a)

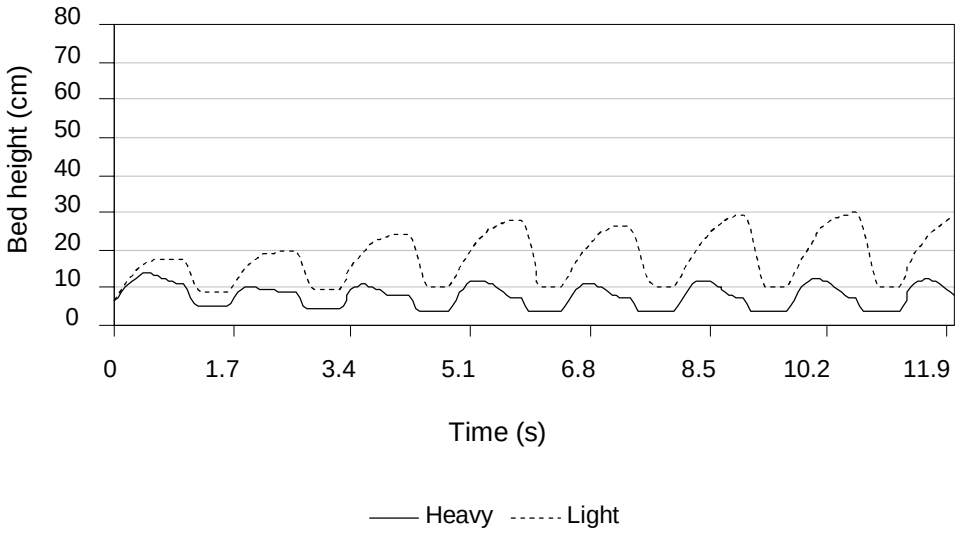

(b)

Figure 5–15. Alternative triangular profile

(a) improved profile setting, (b) mean particle position of improved profile.

5.2.4.3 Sawtooth-backward

The period, *T*, of the original and fastest variant, *T*=2 s, (see Figure 4–1 (c)) was changed to 1.5 seconds. Figure 5–16 (a) shows the modified profile setting. The resulting mean particle position is shown in Figure 5–16 (b) and displays a reduction in time the bed is at rest when compared to Figure 4–3 (c). After modification the profile separated after 6 seconds, which is 2 seconds or 25% faster.

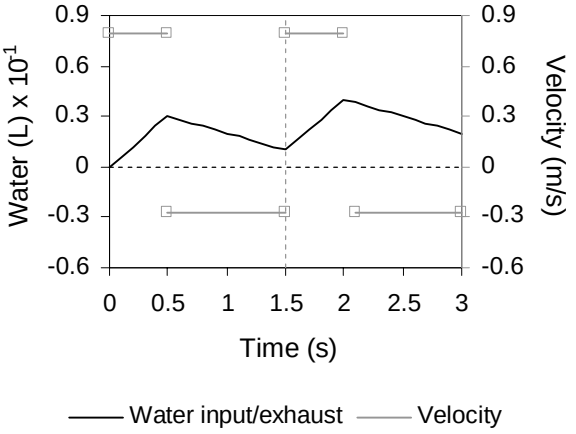

(a)

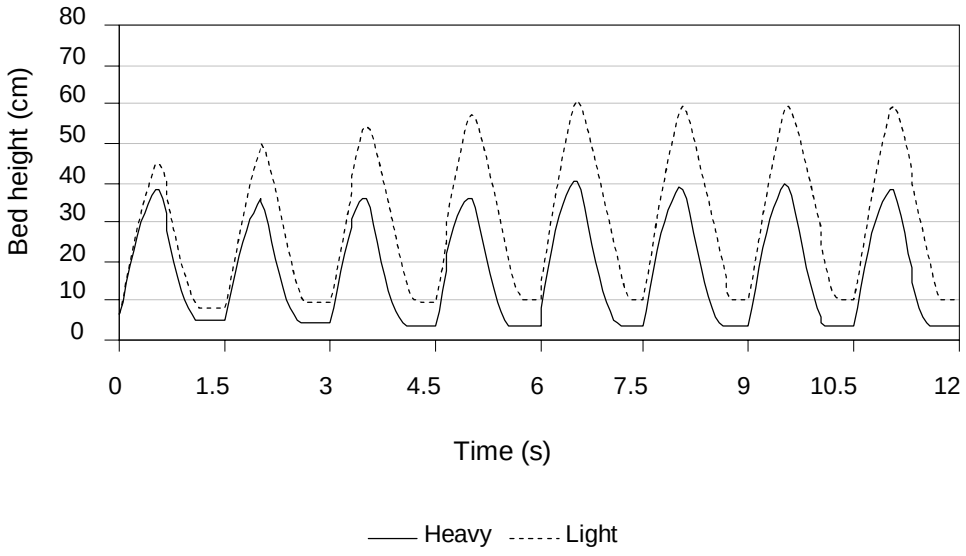

(b)

Figure 5–16. Alternative sawtooth-backward profile
(a) improved profile setting, (b) mean particle position of improved profile.

5.2.4.4 Trapezoidal

The original variant was not used due to unstable segregation. The period, *T*, for the profile of *T*=3 s and *A*=2.25 L was changed to 1.75 seconds. Figure 5–17 (a) shows the modified profile setting. The resulting mean particle position is shown in 5–17 (b) where there is a reduction in time the bed is at rest when compared to Figure 5–13 (b). After modification the profile separated after 7 seconds, which is 5 seconds (42%) faster. It would be expected that the fastest profile is the most efficient segregator in terms of time. Applying the same treatment to the fastest profile of *T*=2.4 s and *A*=2.25 L, the profile separated 2.8 seconds (29%) faster.

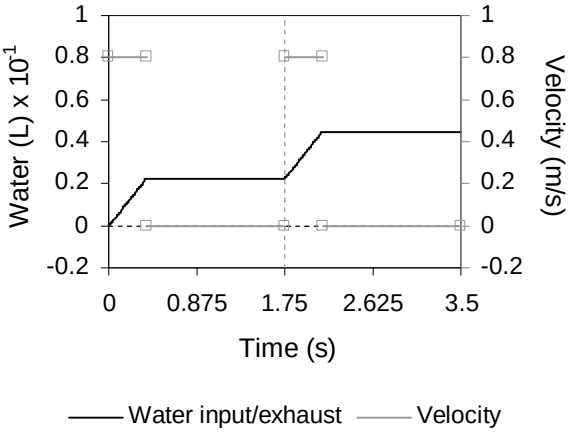

(a)

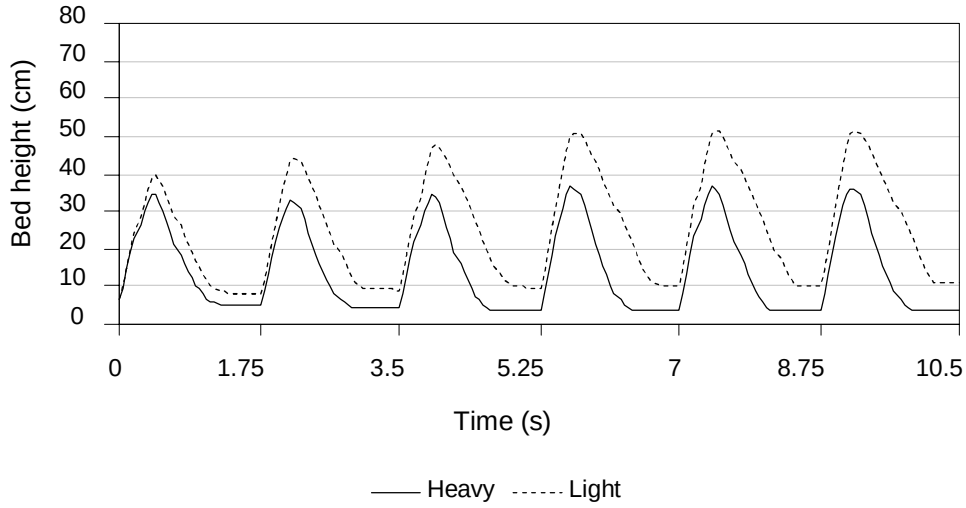

(b)

Figure 5–17. Alternative trapezoidal profile
(a) improved profile setting, (b) mean particle position of improved profile.

5.2.5 Power

In addition to the separation speed, number of cycles to achieve segregation, and the final particle settling configuration as already discussed, the energy input is an important concern in industrial processes. The method to calculate power was detailed in Chapter 4, section 4.2.7. By integrating power over the jigging time the total energy can be calculated shown in Figure 5–18 for the sinusoidal profile. Cumulative energy graphs for all other profiles can be found in Appendix B, Figure B–4 to B–6.

The results show energy per cycle is proportional to water volumetric input for all profile types. Further, the energy required to complete segregation is shown not to be dependent on the time taken to achieve segregation. A profile can use a little or large amount of energy and segregate either quickly or slowly. Each profile has individual characteristics and reasons which describe the energy required to achieve segregation. There is no correlation between the profiles which can be used as a quick aid for power evaluation. For example, neither: litres input, segregation speed, pulsion or suction velocities or duration, alone correlate to energy. It is a combination of all these variables which decide the energy outcome.

It is found power is used during suction which varies upon the profile shaped adopted and also the wave period and volumetric input. This occurs in situations when the bed falls into a packed or partially-packed bed while a high suction velocity and pressure drop is present.

In six of the nine sinusoidal profiles considerable power is found to be used in suction. Relatively minor power is used in four of the triangular profile variants. The sawtooth-backward profile has a relatively low suction velocity which results in very minor and insignificant energy consumption in two high frequency variants of T=1 s. In comparison to other profile shapes the trapezoidal profile provides very large energy consumption in almost every variant due an exceptionally high suction velocity.

Optimising the profile as shown previously by immediately beginning the following pulsion cycle once the bed comes to rest can reduce or remove this redundant power

usage. This reduction depends on how high the suction velocity and low the average porosity is in the remainder of the jigging cycle. Another method is to use hutch water addition (discussed in Chapter 6). This involves introducing water from the bottom of the column with a positive upwards velocity nullifying the high negative suction velocity. Hutch water addition is not a new concept in relation to controlling the dilation of the bed (see Chapter 2, subsection 2.2.3.4), however, no references have been made to controlling energy usage.

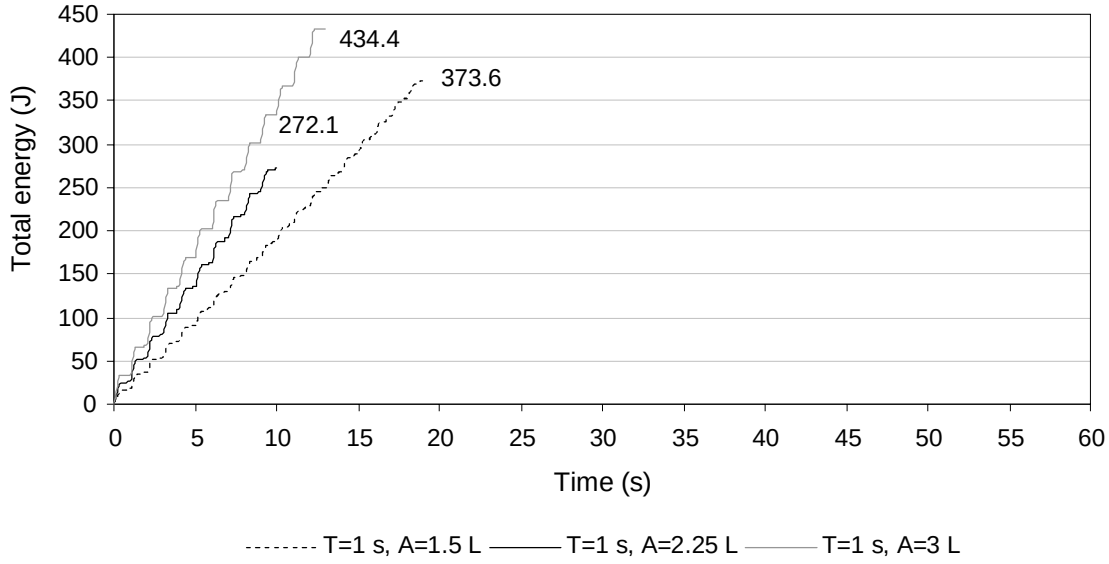

(a)

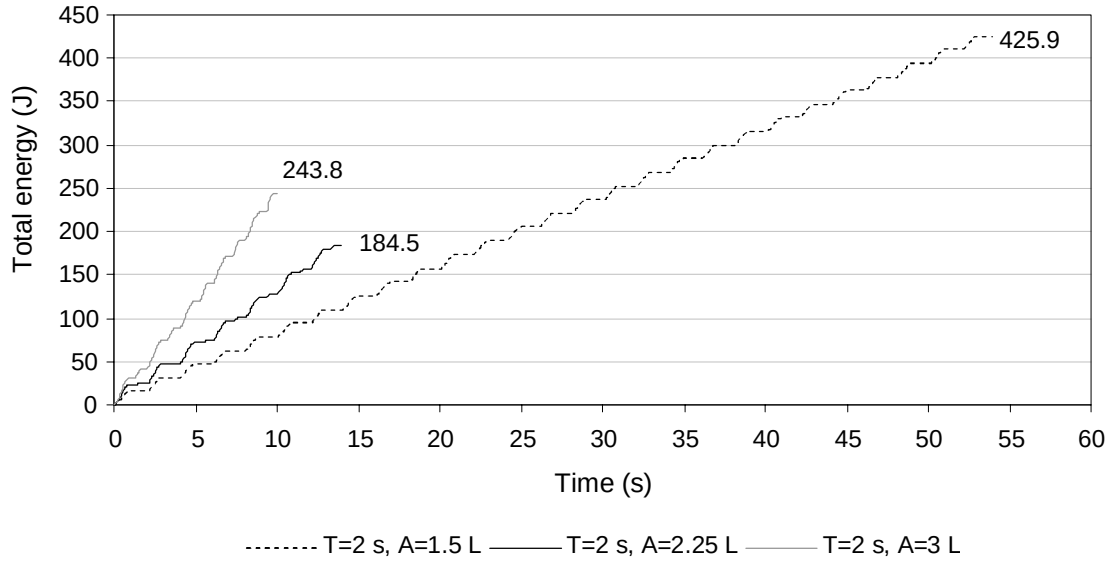

(b)

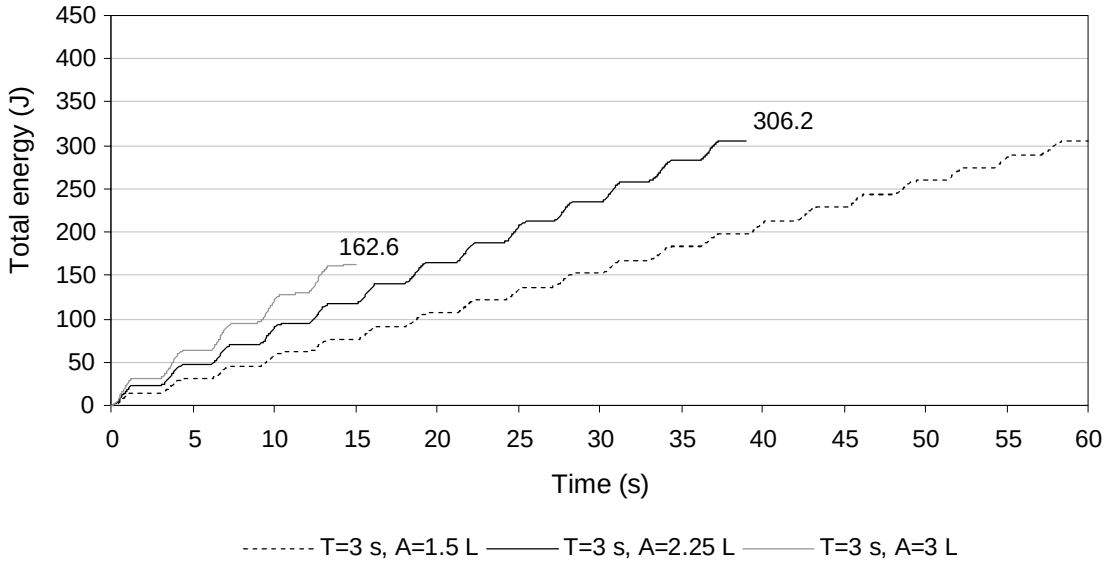

(c)

Figure 5–18. Total energy for all sinusoidal profile variants
(a) *T*=1 s, (b) *T*=2 s, (c) *T*= 3s.

5.3 CONCLUSIONS

A DEM-CFD model was used to investigate the particle separation process in a jigging device using a sinusoidal, triangular, sawtooth-backward and trapezoidal profile. The study selected three variations in amplitude and applied those over three frequencies. Complete separation was represented by a plateau in the coordination number. Not every variant induced particle separation, and those that displayed separation did so at different rates and energy usage.

A broader jigging profile parametric study in terms of amplitude and frequency values was performed for the purpose of a deeper investigation and to establish operational limits of these parameters. Broadening the study to more variations in amplitude and frequency it was found an optimal amplitude and frequency exists in terms of separation time for the sinusoidal profile. Increasing the amplitude will decrease the separation time up to a point where the bed ceases to settle before the proceeding cycle. At this point the bed undergoes pulsion in an unsettled state which

slows separation. Alternatively, increasing frequency has a similar effect of increasing amplitude. Separation time reduces until the bed can no longer settle before the beginning of pulsion in the proceeding cycle resulting in slower separation.

The triangular and sawtooth-backward profiles behaved similarly. Increasing amplitude induces faster separation regardless of the frequency adopted. However, it was shown that an intermediate frequency performed best. This is due to the highest frequencies not allowing the bed to expand and segregate before being quickly sucked back down to form a packed bed.

Finally, the trapezoidal profile (similarly to other profile shapes) showed that increasing amplitude induces faster separation regardless of the frequency adopted. However, an upper limit to the amplitude adopted exists when particle bed settling becomes unstable. Here the particles do not stratify vertically with one particle type directly on top of another, and thus does not ensure separate delivery to launders. Alternatively, reducing the amplitude will increase separation time until the inlet velocity provides insufficient drag to dilate the bed. Increasing frequency displayed the same effects as increasing amplitude.

The number of cycles used to complete separation is found to be vastly different and could be a consideration in operation. For example, the two equal fastest sinusoidal profiles where found to separate in an equal time of 10 seconds, but with a large 5 cycle difference, which is 100% more cycles. Similar observations were found for all other profile shapes. The largest difference was found using the trapezoidal profile. Here two profiles which both complete segregation in 15 seconds were found to do so with a 200% difference in jigging cycle numbers.

The mean particle position for all profile shapes indicate the particle bed falls to rest in the midst of the cycle and remains at rest for some time during suction. This varies depending on the shape of the profile and amplitude and frequency conditions being simulated. The moment corresponding to a static particle bed is a waste of processing time, by eliminating this period the separation time is found to reduce significantly. Investigating the fastest sinusoidal profile variant (which one would expect to have a minimal time that the bed is at rest) the separation time is reduced from 8 s to 6.8 s,

that is 15% faster. The fastest triangular, sawtooth-backward, and trapezoidal profile variants separated 20%, 25%, and 29% faster, respectively.

Finally, the total energy required to complete separation is shown not to be dependent on the time taken to achieve segregation. It is a combination of many factors which contribute to the final energy outcome e.g. water velocity, pulsion duration, and separation time. Further, power is found to be used in suction, which can range from being absent to very large depending on profile shape and variant. As particles can completely fall to rest before suction commences, the suction imparts a high negative liquid velocity on a packed bed resulting in a large pressure drop and energy consumption. This redundant power usage can be reduced or removed by immediately beginning pulsion in the following cycle once the bed comes to rest. Another possible method is to use hutch water addition to eliminate the high negative suction velocity.

CHAPTER 6

DESIGN AND OPERATION RECOMMENDATIONS

6.1 INTRODUCTION

The conventional jig is a very useful mechanical device for relatively coarse particle stratification of a variety of materials. Jigs have a very long standing history in the mining industry, from the first reported jigging device for the beneficiation of metal ores in the 1560s (Agricola, 1950), to the first commercial jig, the Neil Jig (1914) (Burt, 1984), to the present 21st century jigs. This study has proven improvements in jigging technology via process control are still possible. The DEM-CFD studies performed in this thesis have given qualitative information and added to our mechanistic understanding of jigging profiles through numerical experimentation. The results have given rise to insights and new ideas for jig operation and engineering design. Chapter 2, section 2.2.6, elucidates that process control in the past has concentrated mainly on improving particle separation, and doing this in minimal time. The areas of focus have been automatic reject gate control, and adjustments of a continuous jigging stroke. Here the objectives of jig control are different and include: reduction in energy consumption using hutch water addition, and utilization of the entire processing time by jig cycle truncation. Chapters 4 and 5 have explained how these methods would improve jigging via numerical simulation. However, it is important to describe how they can be applied in a practical sense as well. Hutch water addition for the reduction of energy consumption is straight forward, and can readily be applied by modifying the jig operation. At the present time, mechanical execution of jig cycle truncation to shorten separation time requires a new jig design. This study examines how these two new methods can be implemented practically in real jigging.

6.2 NOVEL JIGGING CONTROL METHODS

6.2.1 Hutch water addition for energy minimisation

As mentioned previously a significant contribution to energy usage in all the pulsation profile shapes (least being the sawtooth-backward profile) arises from the fluid being forced at high velocity through an already packed bed. To counter this redundantly high negative fluid velocity 'hutch water addition' can be used—which is in addition to normal operating water addition. By injecting water into the hutch when the suction becomes redundant the net fluid velocity will reduce. If the injection rate matches the suction rate, the fluid velocity will become zero, and consequently so will the power (excluding minor power used to add hutch water). Before the subsequent pulse, this extra fluid can be drained from a discharge mechanism e.g. tailings launder or discharge pipe, and maybe recycled for the following stroke (see schematic illustration in Figure 6–1). An example of a pulsation profile with hutch water addition during suction is shown in Figure 6–2.

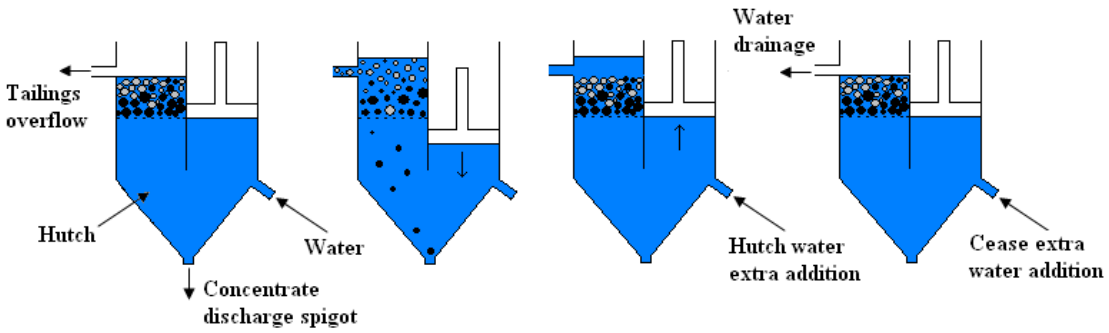

Figure 6–1. Hutch water addition to minimise energy usage.

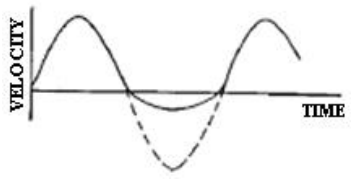

Hutch water addition Velocity

Figure 6–2. Sinusoidal profile with hutch water addition during suction.

To identify a condition of redundant suction, pressure drop sensors or impact sensors can be used to help notify of excessive suction on a packed-bed. This information can then be used as a trigger to introduce hutch water or cease suction. Hutch water addition is not a new concept in relation to controlling the dilation of the bed (see Chapter 2, subsection 2.2.3.4), however, no references have been made to controlling energy usage.

Another method of minimising power loss from suction through a packed bed is to begin the next cycle at the point in time of excessive suction. This is discussed in the following section.

Note air pulsator jigs which induce suction by opening air valves to relieve pressure in the air chamber will not benefit from this technique. In these devices solely gravity is utilized to reduce the water level thus mechanical power is not used during suction.

6.2.2 Cycle truncation for time efficient jigging

Even the cycle settings (of amplitude and frequency) found to induce the minimal particle separation time for each profile shape result in the particle bed being in a rested state for a redundant and considerable amount of time (see Chapter 5, section 5.2.4). This may result in power wastage—depending on the profile shape and settings—due to strong suction imparted on a rested bed, and in all profiles wastes processing time. Once all the particles are at rest the bed is ready for the proceeding pulse.

In Chapter 5, section 5.2.4 the mean particle position data was used to indicate at what point in the cycle a packed bed is formed. The wave period for the profiles which segregated in minimal time were changed to make this point the beginning of the following cycle. As a result the litres of water introduced into the jigging vessel were more than that which was exhausted. The method of using equal water volume intake/exhaust gives a good indication on how profiles compare (as shown in Chapter 4) but does not allow for optimum operation. However, the currently popular jigs including mechanical piston and air pulsators rely on equal water intake and exhaust

and thus a practical engineering design issue is raised when considering cycle truncation for optimisation.

In practice, a novel twin-pulsator air jigging concept shown schematically in Figure 6–3 is completely flexible in terms of profile manipulation. An air pulsator is chosen as it is benchmark jigging technology in terms of profile shape flexibility—rather than an eccentric motor sinusoidal driven piston.

Firstly, Figure 6–3 (a) shows the jig at rest with both chambers full of water and the discharge gate on the right pulsator open and the left pulsator closed. The pulsion stroke proceeds shown in Figure 6–3 (b). The air relief valve on the right pulsator is closed and air is injected displacing the water downwards, around the u-tube and up through the jigging screen fluidizing the bed. A majority of light particles move through the tailings overflow while heavy particles travel through the jigging screen and towards the concentrate discharge spigot. Suction shown in Figure 6–3 (c) draws water back through the particle bed forcing the particles back into a packing. Suction refills the jigging chamber although does not exhaust all the water because the profile is stopped short (truncated). Consequently, a void of air in the right jigging chamber is present. Due to this void the same pulsator cannot proceed in numerous more pulsations as the void will grow and eventually leave no water to displace. For this reason a second pulsator full of water is needed for the subsequent pulse. During the following pulse shown in Figure 6–3 (d) the gate on the right pulsator closes and the air relief valve opens, this allows water to be added into the chamber to be refilled. Simultaneously, once the gate on the right pulsator is shut, the left pulsator gate opens and drives the following pulse mirroring the process of the partner pulsator.

In a usual system hutch water addition is generally used to refill the system as water pours out through the tailings and concentrate discharge spigot. The water lost in this system is supplemented through chamber water addition.

Switching pulsator allows time for chamber water addition. The various profile jigging periods are cut short only by a fraction of a second (0.4 to 0.7 seconds depending on the profile type and settings). If one pulsator is used there is not enough time to promptly begin another pulse as the chamber needs to be refilled. The pause

needed for the jig to refill will potentially take more time than the time saved cutting the profile short, this eliminates any time saving benefits.

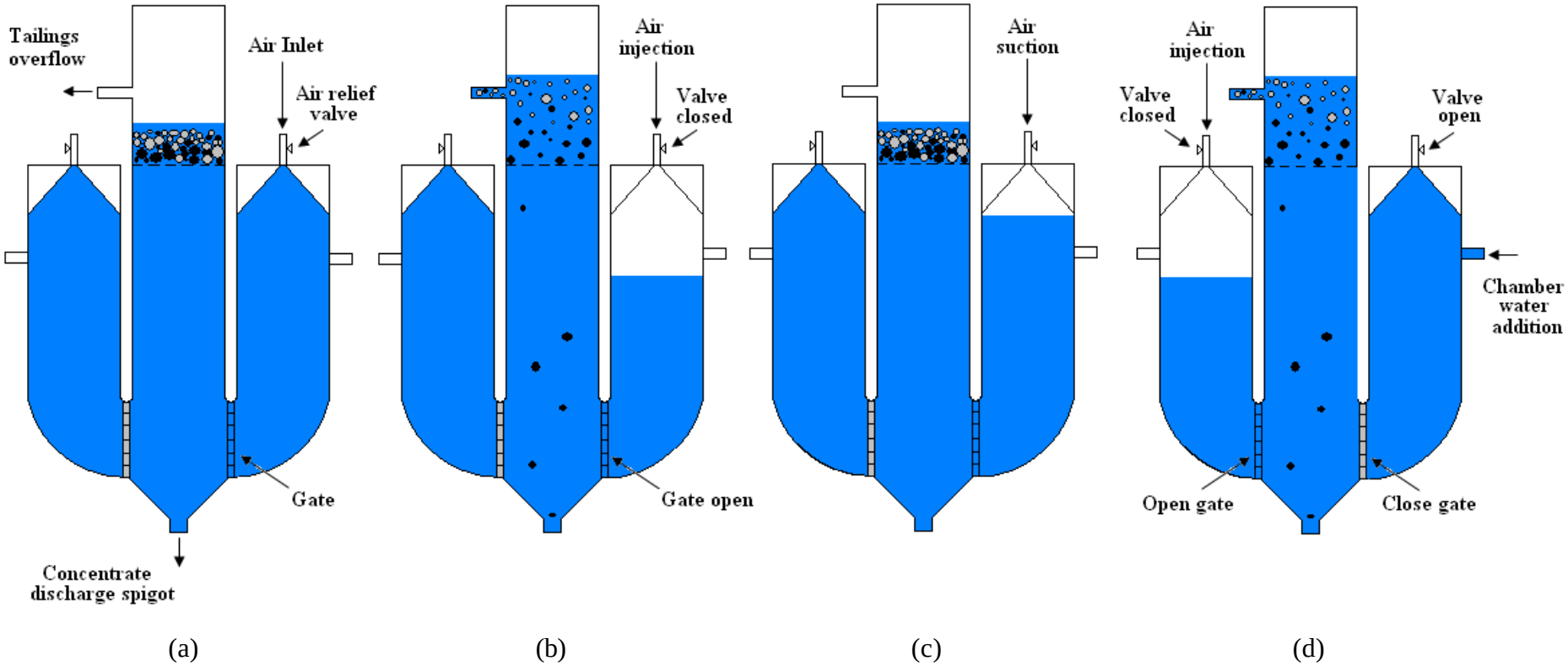

Figure 6–3. Novel twin-pulsator air jigging.

Light and heavy particles are coloured grey and black, respectively.

6.2.3 The importance of suction

The characteristics of feed entering a jig vary tremendously as does the product requirements of the ore being processed. The feed is composed of a multivariable particle distribution including size, density, and purity which constantly change with excavation sites, feed batches, and ore material being mined. The jigging product requirements vary from high or intermediate recovery, coarse fine or heavies, light fine or heavies, or a range in between. Therefore, there are numerous profiles adopted in practice which attempt to factor in the feed characteristics and address the product requirements. This study has not fully explored the importance of suction. Suction is very important in a polydisperse particle system when an operator seeks to segregate by accentuating differential acceleration and interstitial trickling. Extended suction can also be of use after the majority of the bed has come to rest to bring down the smallest fines instead of losing them to in the tailings. Therefore, cutting the profile short may not be appropriate with some feed characteristics and product requirements although is beneficial in the current case. The current case best represents a close particle size and density distribution of coarse particles.

CHAPTER 7

SUMMARIES AND FUTURE WORK

A numerical study of gravity separation behaviour of particle mixtures in wet jigging has been made by the use of a combined Discrete Element Method and Computational Fluid Dynamics model (DEM-CFD) during the course of this PhD project. Firstly, a comprehensive review has been undertaken of the venerable mineral processing technology of jigging. This has discussed many areas: economics of mineral processing; theories of jigging; an historical account on types of jigs; design and operation aspects; control systems; experimental and numerical studies; and DEM-CFD and particle motion in fluids theory. Secondly, a comparison between numerical and physical experiments was conducted, and particle fluid interaction forces were examined. Thirdly, based on the numerical model, gravity separation phenomena of particle mixtures was studied with the consideration of five popular jigging pulsation profiles (sinusoidal, triangular, sawtooth-forward, sawtooth-backward, and trapezoidal). Finally, given insight by means of the numerical model two original propositions are made for the future operation and design of jigs. The following conclusions/summaries can be made from this study:

1. Solid flow patterns indicate that different phenomena exist according to the pulsation profile shape adopted. The inlet velocity affects particle movement. If a high inlet velocity is present at the onset of pulsion the bed will move as a whole, and will either display slugging or complete transport behaviour, as in the triangular, sawtooth-backward, and trapezoidal profiles. If the inlet velocity develops slowly e.g. sinusoidal profile, the particles will not lift as a whole and a loosening wave will dominate in the beginning of the cycle. Further, if a low and constant inlet velocity is adopted fluidization is present, e.g. sawtooth-forward profile.

2. Both the solid flow patterns and mean particle displacement values show that if the inlet velocity exceeds the minimum fluidisation velocity then all pulsation profiles exhibit segregation. The particles remain in a fixed bed position for a significant time during the suction period in all of the pulsation profiles with exception to the trapezoidal profile, demonstrating potential opportunities to improve the jigging process using an optimised pulsation profile, e.g. reducing the suction period of the profile.

3. Non-dimensional particle fluid force values confirm the solid flow pattern behaviour. Further, drag force values for heavy and light particles change with jigging due to segregation induced porosity developments. As local porosity changes occur, the bottom of the bed becomes more tightly packed and the drag force on heavy particles increases.

4. For the selected profile shapes segregation is shown to be far more sensitive and therefore proportional to the bed expansion duration, rather than expansion magnitude, or non-dimensional particle fluid interaction force differences between heavy and light particle types. This holds true provided that the particles are expanded up to a critical porosity whereby sufficient particle-particle hindrance is avoided; and also inversion velocities are not present making it difficult for particles to land uniformly causing mixing.

5. The contact forces show peak values occurring when the particles are at rest and in the throes of suction where maximum negative liquid velocity and drag is experienced. These high contact forces of up to 70 N—and greater depending on pulsation profile parameters adopted—may cause particle fragmentation and blockages during jigging operation.

6. The most influential parameter related to power during pulsion was the inlet flow rate. All pressure drop values were similar but the injection velocities varied greatly. Power values gradually increased during suction in conjunction with gradual local porosity developments.

7. Broadening the study to more variations in amplitude and frequency it was found an optimal amplitude and frequency exists in terms of separation time for the sinusoidal profile. Increasing the amplitude will decrease the separation time up to a point where the bed ceases to settle before the proceeding cycle. At this point the bed undergoes pulsion in an unsettled state which slows separation. Alternatively, increasing frequency has a similar effect of increasing amplitude. Separation time reduces until the bed can no longer settle before the beginning of pulsion in the proceeding cycle resulting in slower separation.

The triangular and sawtooth-backward profiles behaved similarly. Increasing amplitude induces faster separation regardless of the frequency adopted. However, it was shown an intermediate frequency performed best. This is because the highest frequencies did not allow the bed to expand and segregate before being quickly sucked back down to form a packed bed.

Finally, the trapezoidal profile showed that increasing amplitude induces faster separation regardless of the frequency adopted. However, an upper limit to the amplitude adopted exists when particle bed settling becomes unstable. Here the particles do not stratify vertically with one particle type directly on top of another, and thus does not ensure separate delivery to launders. Alternatively, reducing the amplitude will increase separation time until the inlet velocity provides insufficient drag to dilate the bed. Increasing frequency displayed the same effects as increasing amplitude and *vice versa*.

8. The number of cycles used to complete separation is found to be vastly different and could be a consideration in operation in terms of equipment wear and fatigue. For example, the two equal fastest sinusoidal profiles were found to separate in an equal time of 10 seconds, but with a large 5 cycle difference, which is 100% more cycles. Similar observations were found for all other profile shapes. The largest difference was found using the trapezoidal profile. Here two profiles which both complete segregation in 15 seconds were found to do so with a 200% difference in jigging cycle numbers.

9. The mean particle position for all profile shapes indicate the particle bed falls to rest in the midst of the cycle and remains at rest for some time during suction. The moment corresponding to a static particle bed is a waste of processing time, by eliminating this period the separation time is found to reduce significantly. Investigating the fastest sinusoidal profile variant (which would be expected to have a minimal time that the bed is at rest) the separation time is reduced from 8 s to 6.8 s, that is 15% faster. The fastest triangular, sawtooth-backward, and trapezoidal profile variants separated 20%, 25%, and 29% faster, respectively.

10. The total energy required to complete separation is shown not to be dependent on the time taken to achieve segregation. It is a combination of many factors which contribute to the final energy outcome e.g. water velocity, pulsion duration, and separation time. Further, power is found to be used in suction, which can range from being absent to very large depending on profile shape and variant. As particles can completely fall to rest before suction commences, the suction imparts a high negative liquid velocity on a packed bed resulting in a large pressure drop and energy consumption.

11. A significant contribution to energy usage in all the pulsation profile shapes (least being the sawtooth-backward profile) arises from the fluid being forced at high velocity through an already packed bed. To counter this redundantly high negative fluid velocity 'hutch water addition' can be used—which is in addition to normal operating water addition. By injecting water into the hutch when the suction becomes redundant the net fluid velocity will reduce. With an injection rate matching the suction rate the fluid velocity will become zero, and consequently so will power (excluding minor power used to add hutch water). Hutch water addition is not a new concept in relation to controlling the dilation of the bed however no references have been made to controlling energy usage (see Chapter 2, subsection 2.2.3.4).

12. Even the cycle settings (of amplitude and frequency) found to induce the minimal particle separation time for each profile shape result in the particle bed being in a rested state for a redundant and considerable amount of time. This will result in power wastage if strong suction is imparted on a rested bed, and in all profiles wastes processing time. Once all the particles have rested the bed is ready for the proceeding pulse. The mean particle position data was used to indicate at what point in the cycle a packed bed is formed. The wave period for the profiles which segregated in minimal time were changed to make this point the beginning of the following cycle i.e. truncating the jig cycle. This was shown to reduce separation time significantly.

    As a result the litres of water introduced into the jigging vessel are more than that which is exhausted. Currently popular jigs including mechanical piston and air

pulsators rely on equal water intake and exhaust and thus a practical engineering design issue is raised when considering cycle truncation for optimisation.

In practice, a novel twin-pulsator air jigging concept presented in this study is completely flexible in terms of profile manipulation. An air pulsator is chosen as it is benchmark jigging technology in terms of profile shape flexibility—in favour of eccentric motor sinusoidal driven piston.

This project is largely preliminary work in the gravity separation jigging area. However, the DEM-CFD model has proved helpful in fundamental research and qualitative understanding of the highly complicated liquid solid system. Highlighting the complexities of the system will help in appreciating the challenges posed for numerical modelling and help justify the model used in this project.

The characteristics of feed entering a jig vary tremendously as does the product requirements of the ore being processed. The feed is composed of a multivariable particle distribution including size, density, and purity which constantly change with excavation sites, feed batches, and ore material being mined. Further, the particle system ranges from dense to dilute regimes spatially and temporally, depending on operational circumstances i.e. jig type, feed, and operational settings. Particle transport varies tremendously with jig type. Jig types include through-the-screen and over-the-screen, which come in an assortment of complex vessel geometries, pulsion and discharge mechanisms. A typical jigging system will contain millions of particles which at present is computationally prohibitive in terms of simulation time. With consideration to time constraints scaling down to 1130 particles has proven useful to model particle flow phenomena and helpful in analysis. The current case best represents a close particle size and density distribution of coarse particles. Further, a simple column geometry was used with the aim to isolate a fundamental active and dominant stratification portion common of all jig beds. This ensures that conclusions may apply to a broader range of jig types.

In the future, additional work will be done to validate the model experimentally. However, the conclusions drawn from qualitative results are believed not to require high model fidelity to be helpful in the elucidation of jigging phenomena. Further, the

segregation study can be extended to a fully polydisperse particle system. Composing of different solid concentrations, size/density ratios (including coarse and fine particle mixtures), and also bed thicknesses and widths. Extending the current 3D DEM and 2D CFD model to a full 3D model with complicated bed geometries would also be of significance.

Two-dimensional CFD simulations can represent cases were the flow is by nature two dimensional, where the flow variations (space and time) are significant in two directions and negligible in the third direction. Although significant differences have been shown in numerical simulations of circulating fluidization units for the same numerical parameter, between 2D and 3D simulations, as the instantaneous local flow physics is highly three dimensional (Peirano et al., 2001). It has also been found two dimensional Cartesian systems can be used to successfully simulate and predict the bubbling regime economically lowering computational resources which is common practice (Xie et al., 2008). As this model incorporates short pulsations at the velocity inlet and bed circulation is minimum three dimensional effects are kept to a minimum, however, caution must be exercised when using 2D Cartesian coordinates and a future 3D study of this model will be helpful elucidating differences.

REFERENCES

ABS, 2010. 2009–2010 Year Book Australia. Australian Bureau of Statistics Canberra.

Agricola, G., 1950. De Re Metallica, Translated by H.C. and L.H. Hoover, Dover reprint of 1912 edition, New York.

Ahmed, M.M., 2011. Optimization of A Jigging Process Using Statistical Technique. International Journal of Coal Preparation and Utilization 31, p. 112–123.

Allmineral (2010). Retrieved 12Dec 2009, from www.allmineral.com.

Anderson, M. (2010). Gravity Separation. Retrieved 22 Jul 2009, from http://www.faculty.uaf.edu/ffrg/min313/Handout_9_Min313.pdf.

Anderson, T.B., Jackson, R., 1967. A fluid mechanical description of fluidized beds: Equations of motion. Industrial and Chemistry Engineering Fundamentals 6, p. 527–539.

Asakura, K., Mizuno, M., Nagao, M., Harada, S., 2007. Numerical Simulation of Particle Motion in a Jig Separator, 5th Joint ASME/JSME Fluids Engineering Conference, San Diego, California USA.

Ball, R.C., Melrose, J.R., 1995. Lubrication breakdown in hydrodynamic simulations of concentrated colloids. Advances in Colloid and Interface Science 59, p. 19–30.

Bartelt, D., 1962. Regulating jig discharge by means of radio-isotopes, 4th Int. Coal Prep. Cong.. Paper B2, p. 89–97.

Basset, A.B., 1888. On the motion of a sphere in a viscous liquid. Phil. Trans. Roy. Soc A179, p. 43–69.

Basset, A.B., 1961. Treatise on hydrodynamics. Deighton, Bell and Co., Cambridge.

Beck, A.J.G., Holtham, P.N., 1993. Computer simulation of particle stratification in a two-dimensional batch jig. Minerals Engineering 6, p. 523–532.

Beetstra, R., Hoef, M.A.v.d., Kuipers, J.A.M., 2007a. Drag force from lattice Boltzmann simulations of intermediate Reynolds number flow past mono- and bidisperse arrays of spheres. A.I.Ch.E. Journal 53, p. 489–501.

Beetstra, R., Hoef, M.A.v.d., Kuipers, J.A.M., 2007b. Erratum to “Drag force of intermediate Reynolds number flow past mono- and bidisperse arrays of spheres” A.I.Ch.E. Journal 53, p. 489–501.

Beetstra, R., van der Hoef, M.A., Kuipers, J.A.M., 2007b. Numerical study of segregation using a new drag force correlation for polydisperse systems derived from lattice-Boltzmann simulations. Chemical Engineering Science 62, p. 246–255.

Benyahia, S., Syamlal, M., O'Brien, T.J., 2006. Extension of Hill–Koch–Ladd drag correlation over all ranges of Reynolds number and solids volume fraction. *Powder Technol.* 162, p. 166–174.

Bokkers, G.A., van Sint Annaland, M., Kuipers, J.A.M., 2004. Mixing and segregation in a bidisperse gas-solid fluidised bed: a numerical and experimental study. Powder Technology 140, p. 176–186.

Bouillard, J.X., Lyczkowski, R.W., Gidaspow, D., 1989. Porosity distributions in a fluidized bed with an immersed obstacle. A.I.Ch.E. Journal 35, p. 908–922.

Boussinesq, J.V., 1885. Sur la resistance d'une sphere solide. C.R. Hebd. Seanc. Acad. Sci. Paris 100, p. 935.

Burt, R.O., 1984. Gravity Concentration Technology, Vol 5. Elsevier, Amsterdam, Netherlands.

Chen, W.L., 1980. Batac cleaning in five U.S Plants. Min. Eng. , p. 1346–1350.

Clarke, A.J., Jia, X., Williams, R.A., Parker, D.J., 1997. Verification of distinct element modelling of particle segregation in laboratory jigs using positron emission tomography. , Frontiers in Industrial Process Tomography II, Engineering Foundation/Technical University of Delft, New York., p. 91–96.

Coggin, H.M. (2006). Jig Recovery Systems. Retrieved 22 Sept 2009, from http://www.admmr.state.az.us/Publications/circ052jig.html.

Cook, B.K., Noble, D.R., Willams, J.R., 2004. A direct simulation method for particle-fluid systems Eng. Computations 21, p. 151–168.

Cope, L.W., 2000. Jigs: THE FORGOTTEN MACHINE. Engineering & Mining Journal 201, 30.

Cox, R.G., Brenner, H., 1967. The slow motion of a sphere through a viscous fluid towards a plane surface—II Small gap widths, including inertial effects. Chem. Eng. and Sci. 22, p. 1753–1777.

Cundall, P.A., Strack, O.D.L., 1979. A discrete numerical model for granular assemblies. Geotechnique 29, p. 47–65.

Dandy, S.D., Dweyer, H.A., 1990. A sphere in a shear flow at finite Reynolds number: effect of particle lift, drag and heat transfer. J. Fluid Mech 216, p. 381–410.

Das, B., Prakash, S., Das, S.K., Reddy, P.S.R., 2007. Effective beneficiation of low grade iron ore through jigging operation. Journal of Minerals & Materials Characterization & Engineering 7, p. 27–37.

Deen, N.G., Van Sint Annaland, M., Van der Hoef, M.A., Kuipers, J.A.M., 2007. Review of discrete particle modeling of fluidized beds. Chemical Engineering Science 62, p. 28–44.

Derksen, J.J., Sundaresan, S., 2007. Direct numerical simulations of dense suspensions: wave instabilities in liquid-fluidized beds. 587, p. 303–336.

DFAT (2009). Direction of Merchandise Exports. Retrieved 18 Mar 2010 from www.dfat.gov.au/publications/stats-pubs/dme/Direction_of_Exports_2008-09.pdf.

Di Felice, R., 1994. The voidage function for fluid-particle interaction systems. International Journal of Multiphase Flow 20, p. 153–159.

Dieudonne, V., Jonkers, A., Loveday, G., 2006. An approach to confidently predicting jigging performance. The Journal of The Southern African Institue of Mining and Metallurgy 106, p. 733–739

Ding, J., Gidaspow, D., 1990. Bubbling fluidization model using kinetic theory of granular flow. AIChe Journal 36, p. 523–538.

Dong, K.J., Kuang, S.B., Vince, A., Hughes, T., Yu, A.B., 2009. Numerical simulation of the in-line pressure jig unit in coal preparation. Minerals Engineering 23, p. 301–312.

Du, W., Bao, X., Xu, J., Wei, W., 2006. Computational fluid dynamics (CFD) modeling of spouted bed: Influence of frictional stress, maximum packing limit and coefficient of restitution of particles. Chemical Engineering Science 61, p. 4558–4570.

Enwald, H., Peirano, E., Almstedt, A.E., 1996. Eulerian two-phase flow theory applied to fluidization. International Journal of Multiphase Flow 22, p. 21–66.

Ergun, S., 1952. Fluid flow through packed columns. Chem. Eng. and Proc. 48, p. 89–94.

Feng, Y., 2004. Discrete particle simulation of gas solid flow of particle mixtures in gas fluidization. PhD thesis, p. 26–32.

Feng, Y.Q., Yu, A.B., 2004a. Assessment of model formulations in the discrete particle simulation of gas-solid flow. Industrial and Engineering Chemistry Research 43, p. 8378–8390.

Feng, Y.Q., Yu, A.B., 2004b. Comments on "Discrete particle-continuum fluid modelling of gas-solid fluidised beds" by Kafui et al. [Chemical Engineering Scinece 57 (2002) 2395-2410]. Chemical Engineering Science 59, p. 719–722.

Feng, Y.Q., Yu, A.B., 2007. Microdynamic modelling and analysis of the mixing and segregation of binary mixtures of particles in gas fluidization. Chemical Engineering Science 62, p. 256–268.

Fernandez, J.W., Cleary, P.W., Sinnott, M.D., Morrison, R.D., 2011. Using SPH one-way coupled to DEM to model wet industrial banana screens. Minerals Engineering 24, p. 741–753.

Ge, W., Li, J.H., 2003. Macro-scale phenomena reproduced in microscopic systems - pseudo-particle modelling of fluidization. Chem. Eng. Sci. 58, p. 1565–1585.

Gekko Systems, 2003. Successful Applications Of The InLine Pressure Jig With Particular Reference To The Recovery Of Gold and Diamonds, SAIMM Gravity Conference.

Gibilaro, L.G., Di Felice, R., Waldram, S.P., Foscolo, P.U., 1985. Generalized friction factor and drag coefficient correlations for fluid-particle interactions. Chemical Engineering Science 40, p. 1817–1823.

Gidaspow, D., 1994. Multiphase flow and fluidization. Academic Press, San Diego.

Gray, A.H., 1997. InLine Pressure Jig - An Exciting, Low Cost Technology with Significant Operational Benefits in Gravity Separation of Minerals

Gupta, C.K., 2003. Chemical Metallurgy: Principles and Practice, Chapter 2: Mineral Processing. Weinheim: Wiley-VCH.

Han, K., Fuerstenau, M.C., 2003. Principles of Mineral Processing. SME, Littleton, Colorado, USA.

Handley, D., Doraisamy, A., Butcher, K.L., N.L.;, F., 1966. A study of the fluid and particle mechanics in liquid-fluidized beds. Trans. Inst. Chem. Eng., 44, p. T260–T273.

Happel, J., 1958. Viscous flow in multiparticle systems: slow motion of fluids relative to beds of spherical particles. J. AIChE 4, p. 197–201.

Hasse, W., Wasmuth, H.D., 1988. Use of Air Pulsated BATAC Jigs for Production of High Grade Lump Ore and Sinter Feed from Intergrown Hematite Iron Ores

XVI Mineral Processing Congress, Stockholm, Sweden, (Ed.) KSE Forssberg, p. 1053–1064.

Hentzschel, W., 1958. Die Bewegungsvorgänge monodisperser homogener Kugelschüttungen unter dem Einfluß vertikaler harmonischer Schwingungen des Mediums. Freiberger Forsch, Akademie-Verl.

Hertz, H., 1882. Über die Berührung fester elastischer Körper. *Journal fur die reine und angewandte Mathematik* 92, p. 156–171.

Hiens, R.A., Grady, P.M., Langa, R.L., 2006. Measurement systems for gravity circuit performance: A new approach. The Southern African Institute of Mining and Metallurgy, DMS and Gravity Concentration Operations and Technology in South Africa, 2006.

Hill, R.J., Koch, D.L., Ladd, A.J.C., 2001a. The first effects of fluid inertia on flows in ordered and random arrays of spheres. J. Fluid. Mech. 448, p. 213–241

Hill, R.J., Koch, D.L., Ladd, J.C., 2001b. Moderate-Reynolds-numbers flows in ordered and random arrays of spheres. J. Fluid Mech 448, p. 243–278.

Hilton, J.E., Cleary, P.W., 2011. The influence of particle shape on flow modes in pneumatic conveying. Chemical Engineering Science 66, p.231–240.

Hoef, M.A.v.d., Beetstra, R., Kuipers, J.A.M., 2005. Lattice-Boltzmann simulations of low-Reynolds-number flow past mono- and bidisperse arrays of spheres. J. Fluid Mech. 528 528, p. 233–254.

Holland-Batt, A.B., 1998. Gravtity separation: A revitalised technology. Mining Engineering, p. 43–48.

Hoomans, B.P.B., Kuipers, J.A.M., van Swaaij, W.P.M., 2000. Granular dynamics simulation of segregation phenomena in bubbling gas-fluidised beds. Powder Technology 109, p. 41–48.

Hu, H.H., 1996. Direct simulation of flows of solid-liquid mixtures. International Journal of Multiphase Flow 22, p. 335–352.

Humboldt-Wedag (2009). Retrieved 22 Sept 2009, from http://www.humboldtwedag.co.za/separation.php.

Jenkins, J.T., Savage, S.B., 1983. A theory for the rapid flow of identical, smooth, nearly elastic, spherical particles. Journal of fluid mechanics 30, p. 187–202.

Jinnouchi, Y., Kawashima, S., 1979. How to predict and optimise the pulsation in the air-pulsated jigs, 8th Int. Coal Prep. Cong. (Donetz Doue), Paper B5.

Jinnouchi, Y., Kita, S., Sawada, Y., Tanaka, M., 1984. New trends in theory and technology of the air-pulsated jigs in Japan. Minerals and Metallurgical Processing, p. 76–81.

Jong, d.T.P.R.d., Witteveen, H.J., Dalmijn, W.L., 1996. Penetration velocities in a homogeneous jig bed. International Journal of Mineral Processing 46, p. 277–291.

Jonkers, A., Lyman, G.J., 1997. Application of modern sensor technology to air-pulsated jigs, Innovation in physical separation thechnologies, Richard Mozley Memorial Symposium, Institution of Mining and Metallurgy, London.

Joseph, G.G., Zenit, R., Hunt, M.L., Rosenwinkel, A.M., 2001. Particle–wall collisions in a viscous fluid. J. Fluid Mech. 433, p. 329–346.

Kafui, K.D., Thornton, C., Adams, M.J., 2002. Discrete particle-continuum fluid modelling of gas-solid fluidised beds. Chemical Engineering Science 57, p. 2395–2410.

Kafui, K.D., Thornton, C., Adams, M.J., 2004. Reply to Comments by Feng and Yu on "Discrete particle-continuum fluid modelling of gas-solid fluidised beds" by Kafui et al. Chemical Engineering Science 59, p. 723–725.

Kellerwessel, H., 1998. Concentration by jigging—current investigations, concepts and models. Aufbereitungs-Technik 39, p. 9–15.

Kelly, E.G., Spottiswood, D.J., 1982. Introduction to mineral processing. John Wiley and Sons

Kmiec, A., 1978. Particle distributions and dynamics of particle movement in solid--liquid fluidized beds. The Chemical Engineering Journal 15, p. 1–12.

Koch, D.L., Sangani, A.S., 1999. Particle pressure and marginal stability limits for a homogeneous monodisperse gas-fluidized bed: kinetic theory and numerical simulations. J. Fluid Mech 400, p. 229–263.

Lin, I.J., Knish-Bram, M., Rosenhouse, G., 1997. The benefication of minerals by magnetic jigging, Part 1. Theoretical aspects. International Journal of Mineral Processing 50, p. 143–159.

Lun, C.K., Savage, S.B., Jeffery, D.J., Chepurniy, N., 1984. Kinetic theories for granular flow: Inelastic particles in coquette flow and slightly inelastic particles in a general flow field. Journal of Fluid Mechanics 140, p. 223–256.

Lyman, G.J., 1992. Review of Jigging Principles and Control. Coal Preparation 11, p. 145–165.

Macdonald, I.F., Elsayed, M.S., Mow, K., Dullien, F.A.L., 1979. Flow through porous-media: Ergun equation revisited. Ind. Eng. Chem. Fundam 18, p. 199–208.

Maier, R.S., Kroll, D.M., Davis, H.T., Bernard, R.S., 1999. Simulation of Flow in Bidisperse Sphere Packings. Journal of Colloid and Interface Science 217, p. 341–347.

Maxey, M.R., Riley, J.J., 1983. Equation of motion for a small rigid sphere in a nonuniform flow. Phys. of Fluids 26, p. 883–889.

Mayer, F.W., 1964. Fundamentals of a Potential Theory of the Jigging Process. Proc. 7th Int. Miner. Proc. Cong. New York, p. 75–97.

Mei, R., 1992. An approximate expression for the shear lift force on a spherical particle at finite Reynolds number. Int. J. Multiphase Flow 18, p.145–147.

Miller, D.J., 1991. Design and operating experience with the Goldsworthy Mining Limited BATAC Jig and spiral separator iron ore beneficiation plant. Minerals Engineering 4, p. 411–435.

Minerals Council of Australia (2010). The Australian Minerals Industry and the Australian Economy. Retrieved 16 Jan 2012 from http://www.minerals.org.au/__data/assets/pdf_file/0017/32804/Aus_min_industry_fact_sheet_March_2010.pdf.

Minerals Council of Australia (2011). 2011–2012 Pre-Budget Submission. Retrieved 16 Jan 2012, from http://www.mineralscouncil.com.au/file_upload/files/submissions/MCA_Pre%20Budget_FINAL.pdf.

Minerals Information Institute (2011). Mii Mineral Baby. Retrieved 12 Jan 2012, from www.mii.org.

Mining Eng. (2003). Annual Review 2003. Retrieved 22 Jul 2009, from http://mrw.interscience.wiley.com.ezproxy.lib.monash.edu.au/emrw/9780471238966/kirk/article/minenaga.a01/current/pdf.

Mishra, B.K., Chakroborty, P., 1995. Explorations into fuzzy logic control of stratification in a jig, XIX International Mineral Processing Congress, San Francisco, USA, p. 273–276.

Mishra, B.K., Mehrotra, S.P., 1998. Modelling of particle stratification in jigs by the discrete element method. Minerals Engineering 11, p. 511–522.

Mishra, B.K., Mehrotra, S.P., 2001. A jig model based on the discrete element method and its experimental validation. International Journal of Mineral Processing 63, p. 177–189.

Mukherjee, A.K., Bhattacharjee, D., Mishra, B.K., 2006. Role of water velocity for efficient jigging of iron ore. Minerals Engineering 19, p. 952–959.

Mukherjee, A.K., Dwivedi, V.K., Mishra, B.K., 2005. Analysis of a laboratory jigging system for improved performance. Minerals Engineering 18, p. 1037–1044.

Mukherjee, A.K., Gupta, P., Sit, S.K., Thomas, M.C., Jha, H., Mishra, B.K., 2007. Role of feed characteristic in jigging plant optimisation—a case study, Iron Ore Conference, Perth, Australia, p. 353–360. .

Mukherjee, A.K., Mishra, B.K., 2006. An integral assessment of the role of critical process parameters on jigging. International Journal of Mineral Processing 81, p. 187–200.

Mukherjee, A.K., Mishra, B.K., 2007. Experimental and simulation studies on the role of fluid velocity during particle separation in a liquid-solid fluidized bed. International Journal of Mineral Processing 82, p. 211–221.

Nagaraj, D.R., 2005. Kirk-Othmer Encyclopedia of Chemical Technology, Minerals Recovery and Processing, Vol 16. New York: Wiley.

Odar, F., 1966a. Verification of proposed equation for calculation of forces on a sphere accelerating in a viscous fluid. Journal of Fluid Mechanics (1966) 25, p. 591–592.

Odar, F., 1966b. Verification of proposed equation for calculation of forces on a sphere accelerating in a viscous fluid. Journal of Fluid Mechanics 25, p. 591–592.

Odar, F., Hamilton, W.S., 1964a. Forces on a sphere accelerating in a viscous fluid. Journal of Fluid Mechanics (1964) 18, p. 302–314.

Odar, F., Hamilton, W.S., 1964b. Forces on a sphere accelerating in a viscous fluid. Journal of Fluid Mechanics 18, p. 302–314.

Oesterle, B., Dinh Tri, B., Vial, J., 1991. Measurements of lift and torque on a rotating sphere at intermediate Reynolds numbers. Mech. Res. Commun. 18, p. 145–150.

Oseen, C.W., 1927. Hydromechanik, Akademische Verlagsgem. Leipzig, 132.

Pan, T.-W., Joseph, D.D., Bai, R., Glowinski, R., Sarin, V., 2002. Fluidization of 1204 spheres: simulation and experiment. Journal of Fluid Mechanics 451, p. 169–191

Panda, L., Sahoo, A.K., Tripathy, A., Biswal, S.K., Sahu, A.K., 2012. Application of artificial neural network to study the performance of jig for beneficiation of non-coking coal. Fuel 97, p. 151–156.

Peirano, E., Delloume, V., Leckner, B., 2001. Two- or three-dimensional simulations of turbulent gas–solid flows applied to fluidization. Chemical Engineering Science 56, p. 4787–4799.

Pirog, T.W., 1998. Dynamics of destabilization of food emulsions. Measurement and simulation of gravity driven particle velocities in polydisperse dispersions. Ph.D. Dissertation, Purdue University.

Rasul, M.G., Rudolph, V., Wang, F.Y., 2000. Particles separation using fluidization techniques. International Journal of Mineral Processing 60, p. 163–179.

Reeks, M.W., Mckee, S., 1984. The dispersive effects of Basset history forces on particle motion in a turbulent flow. Physics of Fluids 27, p. 1573–1582.

Remennyi, A.P., Levchanko, I.I., 1972. Automated monitoring and control of coal jigging. Coke and Chemistry, USSR 3, 12.

Remer, W. (2010). Retrieved 23Jan 2010, from http://www.flsmidth.com/en-US/Products/Product+Index/All+Products/Classification/RemerJigs/RemerJigs.

Rhodes, M., 2008. Introduction to particle technology, 2nd ed.

. Hoboken, NJ : Wiley, 2008.

Richards, R., Goodwin, E., Bardwell, E., 1909. A text book of ore dressing. New York : McGraw-Hill.

Richards, R.H., 1894. Close Sizing before Jigging. Trans. Am. Inst. Min. Eng. 26.

Richards, R.H., 1896. The Cycle of the Plunger Jig. Trans. Am. Inst. Min. Eng. 26, p. 3–32.

Richards, W., Richard, S., 2007. Mining Engineering - Upgrading Coal Quality through Dry Jigging. p. 29–34.

Richardson, J.F., Zaki, W.N., 1954. Sedimentation and fluidisation: part 1. Trans. Am. Inst. Chem. Eng 32, p. 35–53.

Rowe, P.N., Nienow, A.W., Agbim, A.J., 1972. The mechanism by which particles segregate in gas fuidised beds-binary systems of near-spherical particles. Transactions of the Institution of Chemical Engineers 50, p. 310–323.

Rubinow, S.I., Keller, J.B., 1961. The transverse force on a spinning sphere moving in a viscous fluid. Journal of Fluid Mechanics (1961) 11, p. 447–459.

Saffman, P.G., 1965. Lift on a small sphere in a slow shear flow. Journal of Fluid Mechanics 22, p. 385–400.

Saffman, P.G., 1968. Corrigendum to “The lift on a small sphere in a slow shear flow”. Journal of Fluid Mechanics, 31, p. 624.

Sarkar, S., van der Hoef, M.A., Kuipers, J.A.M., 2009. Fluid-particle interaction from lattice Boltzmann simulations for flow through polydisperse random arrays of spheres. Chemical Engineering Science 64, p. 2683–2691.

Schubert, H., 1994. Review of the fundamentals of wet jigging. Aufbereitungs-Technik 35, p. 337–349.

Solnordal, C.B., Hughes, T., Gray, A.H., Schwarz, P.M., 2009. CFD Modelling of a Novel Gravity Separation Device, Seventh International Conference on CFD in the Minerals and Process Industries, CSIRO, Melbourne, Australia.

Sommerfeld, M., 1996. Modellierung und numerische Berechnung von partikelbeladenen turbulenten Strömungen mit Hilfe des Euler/Lagrange-Verfahrens. Habilitaionsschrift, Universität Erlangen-Nürnberg, Shaker Verlag, Aachen.

Sommerfeld, M., 2000. Theoretical and Experimental Modelling of Particulate Flows. Institut für Verfahrenstechnik, Fachbereich Ingenieurwissenschaften, Martin-Luther-Universität Halle-Wittenberg, D-06099 Halle (Saale), Germany.

Srinivasan, R., Mishra, B.K., Mehrotra, S.P., 1999. Simulation of particle stratification in jigs. Coal Prep. 20, p. 50–70.

Sun, W., Liu, J., Yang, D., 2005. Real time prediction of ash content of clean coal using Neural Network. Journal of China University of mining & technology 34.

Sundararajakumar, R.R., Koch, D.L., 1996. Non-continuum lubrication flows between particles colliding in a gas. Journal of Fluid Mechanics 313, p. 283–308.

Syamlal, M., O'Brien, T.J., 1994. The derivation of a drag coefficient formula from velocity–voidage correlations. U.S. Department of Energy, Office of Fossil Energy, Technical Report.

Taggart, A.F., 1967. Handbook of Mineral Dressing. John Wiley & Sons.

Tavares, L.M., 1999. Monte Carlo Simulations on the Potential Energy Theory of Jigging. Coal Preparation 20, p. 71–83.

Tavares, L.M., King, R.P., 1995. A Useful Model for the Calculation of the Performance of Batch and Continuous Jigs. Coal Preparation 15, p. 99–128.

Ten Cate, A., Derksen, J.J., Portela, L.M., Van den Akker, H.E.A., 2004. Fully resolved simulations of colliding spheres in forced isotropic turbulence. J. Fluid Mech. 519, p. 233–271.

Tsuji, Y., Kawaguchi, T., Tanaka, T., 1993. Discrete particle simulation of two-dimensional fluidized bed. Powder Technology 77, p. 79–87.

Tsuji, Y., Morikawa, Y., Mizuno, O., 1985. Experimental measurement of the Magnus force on a rotating sphere at low Reynolds numbers. ASME, J. Fluids Eng 107, p. 484 –488.

Vinogradov, N.N., et al., 1968. New trends in theory and technology of the jigging minerals [sic], 8th Int. Min. Proc. Cong., Leningrad, Paper C2.

Wen, C.Y., Yu, Y.H., 1966. A generalized method for predicting the minimum fluidization velocity. A.I.Ch.E. Journal 12, p. 610–612.

Wills, B.A., 1992. Mineral Processing Technology. Pergamon Press

Xia, Y., Peng, F.F., Wolfe, E., 2007. CFD simulation of fine coal segregation and stratification in jigs. International Journal of Mineral Processing 82, p. 164–176.

Xia, Y.K., Peng, F.F., 2007. Numerical simulation of behavior of fine coal in oscillating flows. Minerals Engineering 20, p. 113–123.

Xiang, L., Shuyan, W., Huilin, L., Goudong, L., Juhui, C., Yikun, L., 2010. Numerical simulation of particle motion in vibrated fluidized beds. Powder Technology 197, p. 25–35.

Xie, N., Battaglia, F., Pannala, S., 2008. Effects of using two- versus three-dimensional computational modeling of fluidized beds: Part II, budget analysis. Powder Technology 182, p. 14–24.

Xu, B.H., Feng, Y.Q., Yu, A.B., Chew, S.J., Zulli, P., 2001. A numerical and experimental study of gas–solid flow in a fluid-bed reactor. Powder Handling and Processing 13, p. 71–76.

Xu, B.H., Yu, A.B., 1997. Numerical simulation of the gas-solid flow in a fluidized bed by combining discrete particle method with computational fluid dynamics. Chemical Engineering Science 52, p. 2785–2809.

Xu, B.H., Yu, A.B., 1998a. Comments on the paper “Numerical simulation of the gas–solid flow in a fluidized bed by combining discrete particle method with computational fluid dynamics. Chem. Eng. Sci. 53, p. 2646–2647.

Xu, B.H., Yu, A.B., 1998b. Discussion. Chemical Engineering Science 53, 2646-2647.

Zhou, Y.C., Xu, B.H., Yu, A.B., Zulli, P., 2002. Experimental and numerical study of the angle of repose of coarse spheres. Powder Technol. 125, p. 45–54.

Zhou, Y.C., Yu, A.B., Stewart, R.L., Bridgwater, J., 2004. Microdynamic analysis of the particle flow in a cylindrical bladed mixer. Chemical Engineering Science 59, p. 1343–1364.

Zhu, H.P., Zhou, Z.Y., Yang, R.Y., Yu, A.B., 2007. Discrete particle simulation of particulate systems: Theoretical developments. Chemical Engineering Science 62, p. 3378–3396.

Zhu, H.P., Zhou, Z.Y., Yang, R.Y., Yu, A.B., 2008. Discrete particle simulation of particulate systems: A review of major applications and findings. Chemical Engineering Science 63, p. 5728–5770.

APPENDIX A

SUMMARY OF JIGS PAST AND PRESENT, JIGGING PROFILES, AND MODERN JIGS

Table A–1. Summary of jigging types past and present.

			JIGS PAST & PRESENT				
		MINERAL JIGS		COAL JIGS		MINERAL/COAL	
TYPE	**METHOD OF PULSATION**	**OVER**	**THROUGH**	**OVER**	**THROUGH**	**OVER**	**THROUGH**
Moveable Screen							
		James	Inline Pressure Jig	Wilmot Pan			
		Halkyn	Hancock	Rom			
			Humboldt				
			Hardy-Smith Circular Buddle				
Fixed Screen Mechanical							
	Plunger	Hodge Jig	Delta	Siever's Jig (1860)	Faust		
		McLanahan-Stone	YT12 Pulsator	Humboldt Nut/Fine coal washbox			
		Hartz	Cooley Jig	ORC			
		Stone	May Duplex	Elmore			
			Collom	Reading			
			Dee				
			New Century				
			Thielmann				
			Woodbury				
	Diaphram	Bendelari	Goldfield Duplex	Jeffrey			WEMCO Remer
			Goldfield Round				Dove
			IHC				
			Cleaveland Circular				
			Yuba-Richards				
			RMS Circular				
			Pan-American Placer				
			Pan-American Kraut				
			New Jersey Zinc				
			Southwestern-Kraut Hydromotor				
			Titan Twin Diaphram				
			Ruoss				
			Denver				
Pulsator	**Air**	OPM Series	Schiechel Circular	Tacub	Feldspar	Allmineral Alljig - SP	
			Feldspar	Baum	Cortex	Allmineral Alljig - UP	
			Cortex	Batac	Vissac	APIC	
				McNally-Norton jig			
	Soley Air		Rotary Air Concentrator	Allmineral Allairjig		Plumb Pneumatic	Krom Pneumatic (1874)
				Paddock (1888)			
	Water	Richards Pulsator	Pan-American pulsator				
	Vane		Hooper Vaning				
			Neil				

Table A–2. Summary of jigging profiles.

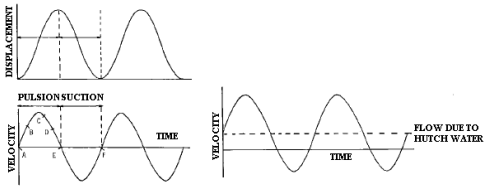	Fundamental plunger type jigging cycle & added hutch water addition version e.g. Hartz jig however variations of the jig were formed.	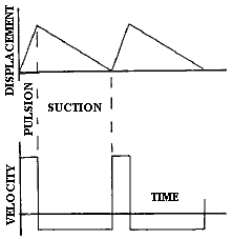	This method by IHC seeks to enhance differential acceleration and interstitial trickling phases and suppress the hindered settling phase. The short sharp pulsion brings the raises the entire bed as a whole. The flow suddenly stops and initial acceleration in combination of hindered settling occurs, since the upward flow breaks off sharply, this process only lasts a short time. The suction stoke is weak preventing compacting and giving ample time for interstitial trickling.
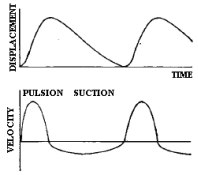	The Collom jigs early attempt at saw tooth cycle. Here differential acceleration and interstitial trickling is accentuated, while hindered settling is depressed.	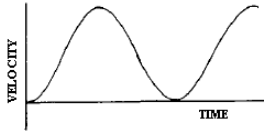	Richards pulsator jig (1916) is the first unit using a pulsation mechanism (water), and achieved complete mineral separation of closely sized material at a higher rate than pulsion-suction jigs.
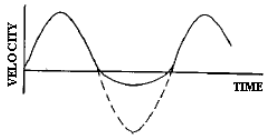	Bendelari Jig with hutch water addition on suction stroke to accentuate hindered settling. Denver jig has similar profile.	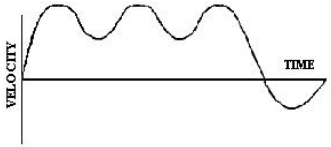	Allmineral claim their jig cycle sustains suspended bed fluidization which permits more complete differential settling.
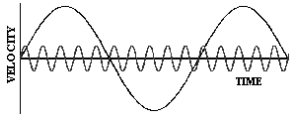	WEMCO-Remer and Cortex jig combines a medium stroke of harmonic motion with high frequency short stroke motion. The aim is to prevent complete bed closure during interstitial trickling phase. The resultant wave has not been fully described, and not fully understood.	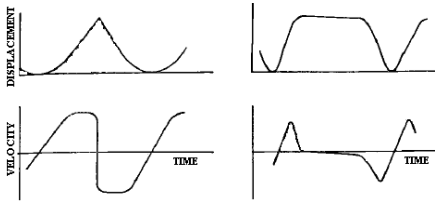	The bird cycle accentuates differential acceleration and interstitial trickling and minimizes hindered settling. Mayer's cycle begins with a fast upstroke to lift the bed as a whole, there after the water level remain constant to allow for hindered settling. K. Aso recommended a trapezoidal wave pattern. Armstrong (1964) pointed out using experimentation that the Bird cycle is superior. However Harris (1964) found Bird's mechanism gives fast stratification and enhanced jig capacity with high recovery, whilst the Mayer mechanism is more suited to enrichment.

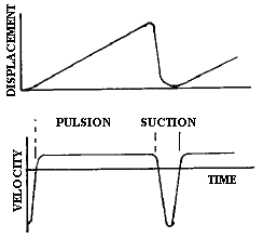

Panam-Kraut made an attempt to increase the range of jigging to finer sizes. Opposite to the IHC jig, similar stroke to IPJ. This profile seeks to enhance hindered settling and suppress interstitial trickling and differential acceleration phases.

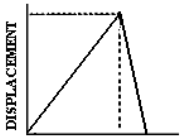

The Gekko IPJ uses a slow upstroke-quick downstroke wave pattern, recommended by Araki et al. and Lovel et al. This profile seeks to enhance hindered settling and suppress interstitial trickling plus differential acceleration phases.

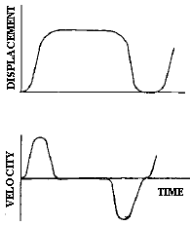

Combining principles of the Baum and Tacub jigs, eventuated in the more widely employed Batac jig. This jig cycle is very close to the one suggested by Mayer's principle of separation and seeks to lift bed as a whole and accentuate hindered settling.

* Jigging profile shapes found in (Burt, 1984), (Gray, 1997), (Remer, 2010), and (Holland-Batt, 1998).

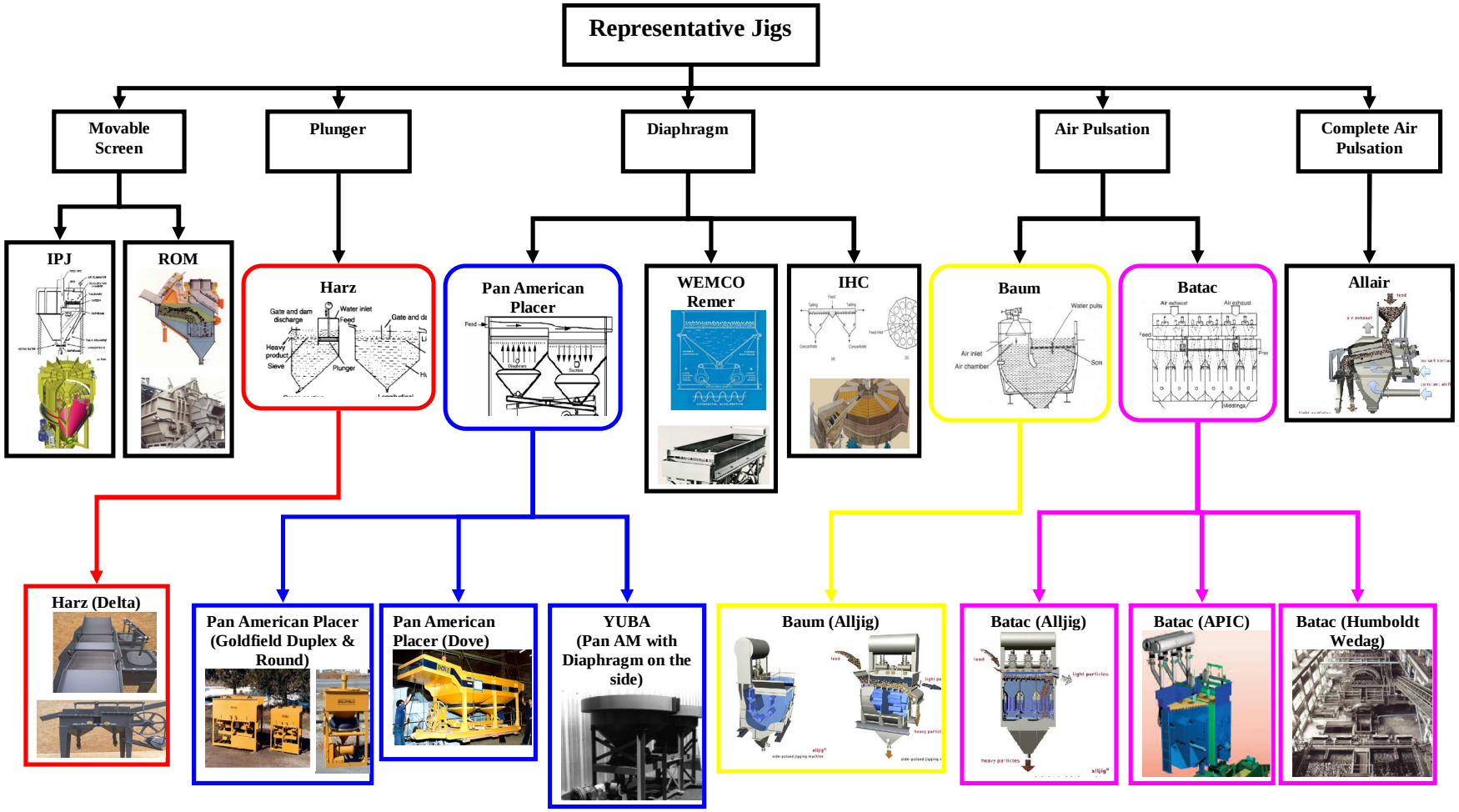

Figure A–1. Representation of jigs in modern times.

*The Harz, Ruoss, Yuba Pan American Placer, Batac and Baum Jigs are generic, with several manufactures of each (Burt, 1984).
*The rush to jigs inspired inventiveness of many individuals. A large number of jigs were patented and came on the market, many of them developed to treat a specific ore. However, the Harz, Yuba, Pan American, and Mineral jigs stood the test of time, and became the generally used units (Cope, 2000).

APPENDIX B

CORDINATION NUMBER AND TOTAL ENERGY

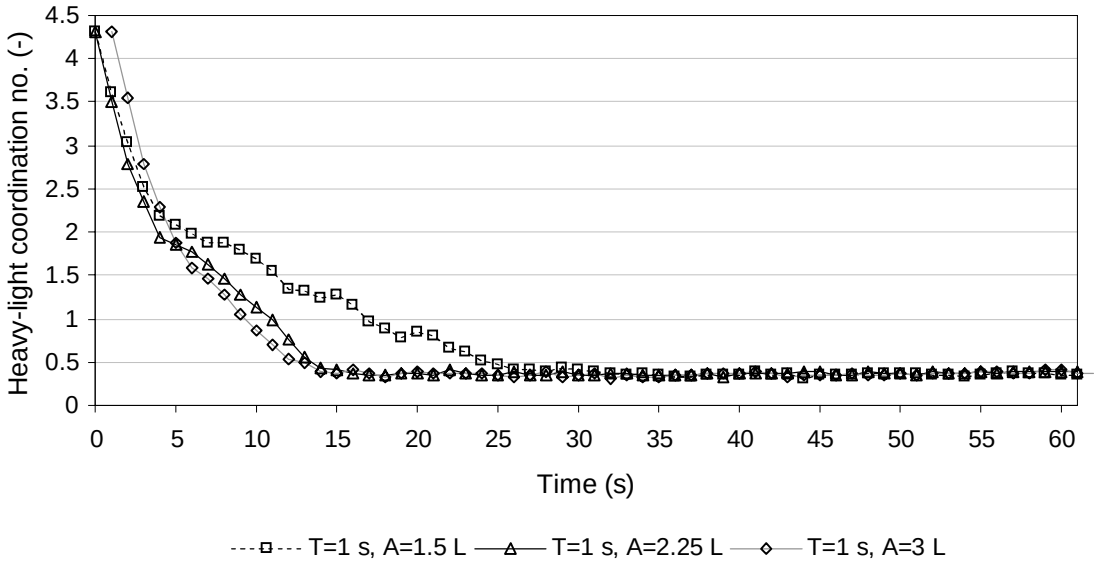
Heavy-light coordination no. (-)
Time (s)
T=1 s, A=1.5 L
T=1 s, A=2.25 L
T=1 s, A=3 L

(a)

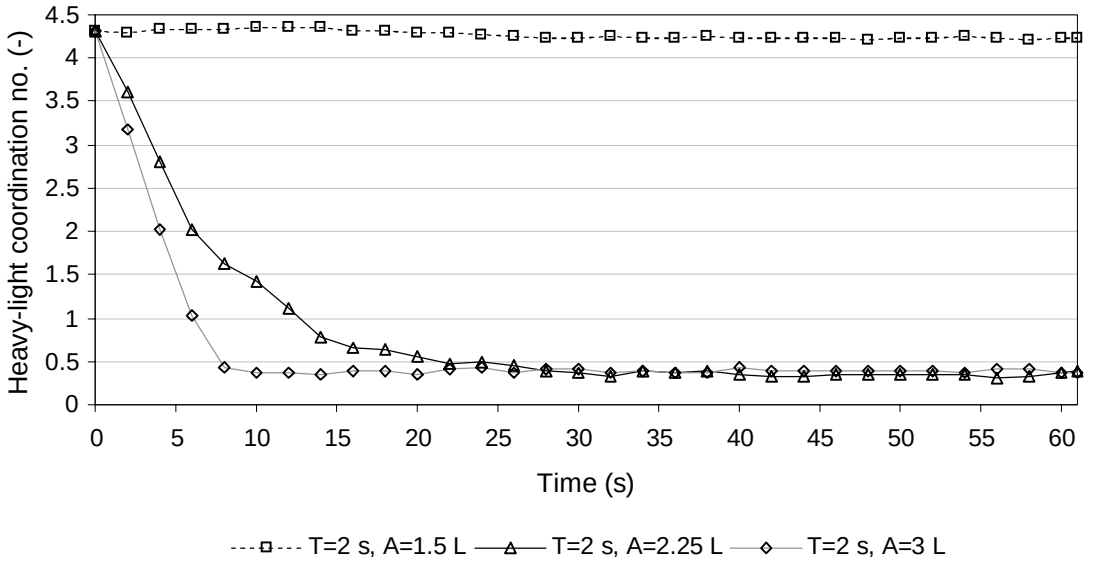
Heavy-light coordination no. (-)
Time (s)
T=2 s, A=1.5 L
T=2 s, A=2.25 L
T=2 s, A=3 L

(b)

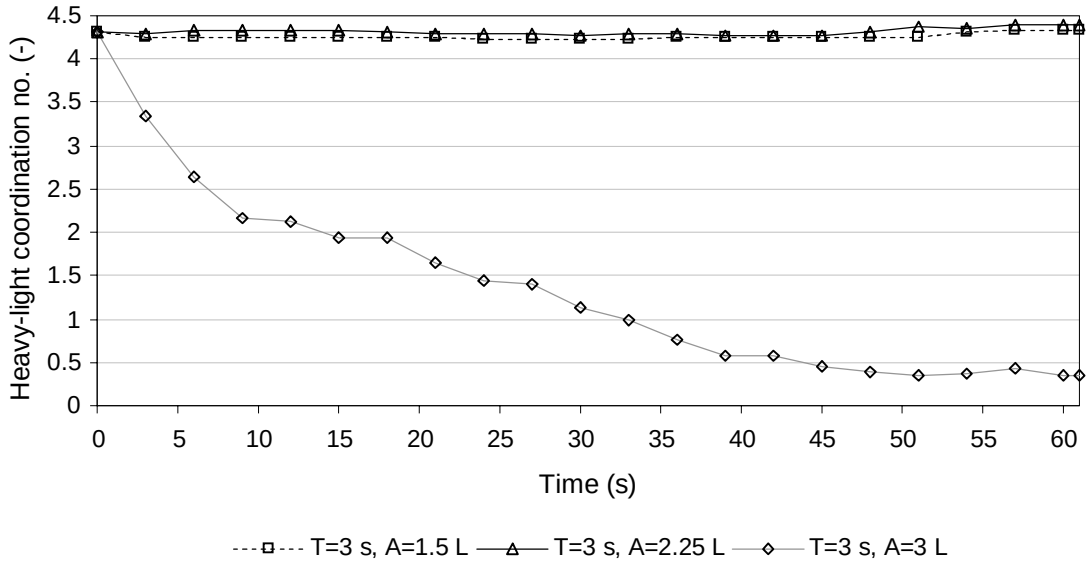

(c)

Figure B–1. Packed bed coordination number values for all triangular profile variants (a) T=1 s, (b) T=2 s, (c) T=3 s.

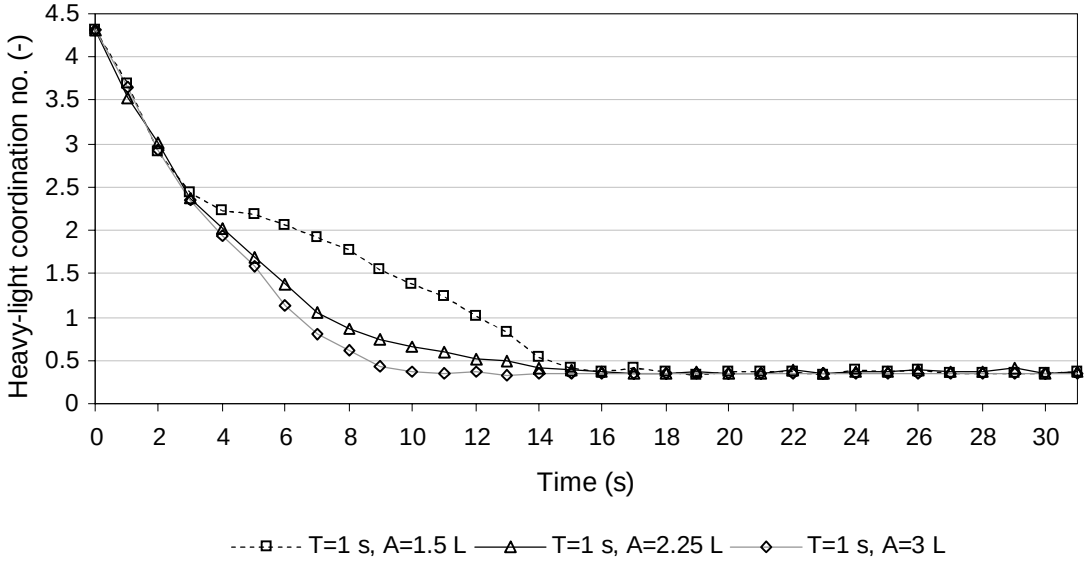
Heavy-light coordination no. (-)
Time (s)
T=1 s, A=1.5 L
T=1 s, A=2.25 L
T=1 s, A=3 L

(a)

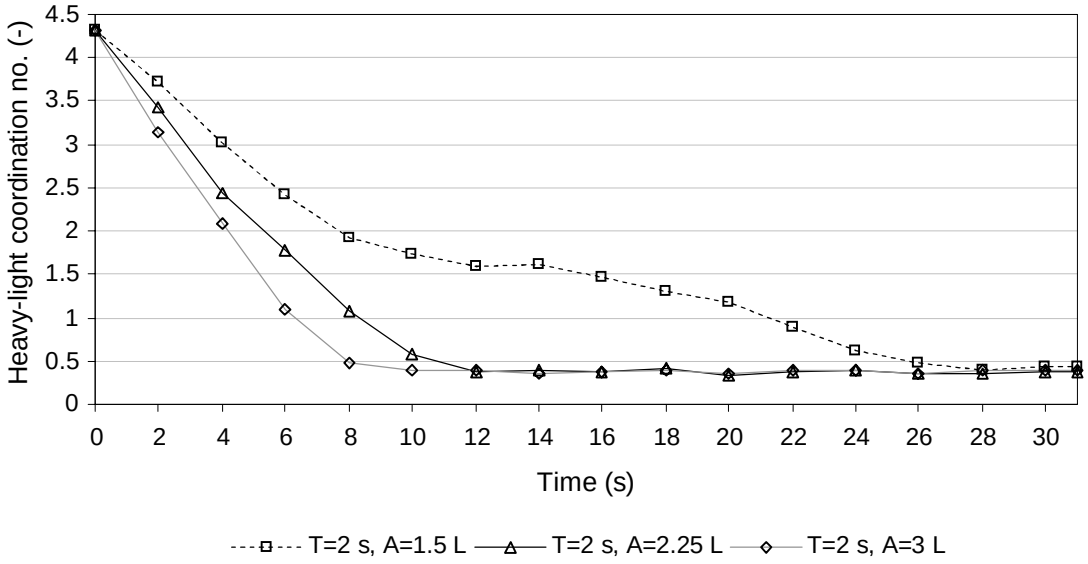
Heavy-light coordination no. (-)
Time (s)
T=2 s, A=1.5 L
T=2 s, A=2.25 L
T=2 s, A=3 L

(b)

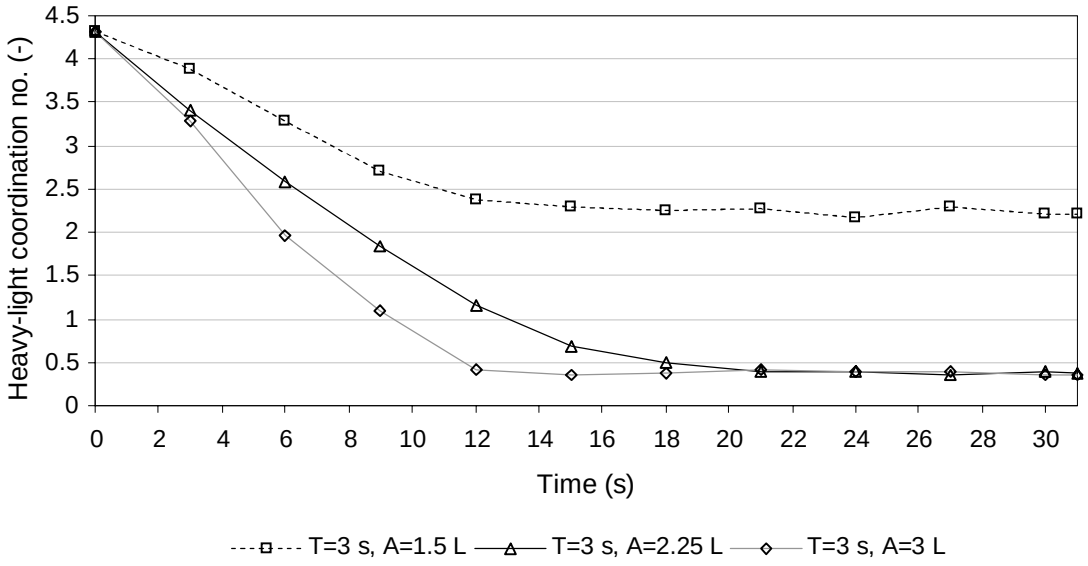

(c)

Figure B–2. Packed bed coordination number values for all sawtooth-backward profile variants (a) T= 1 s, (b) T=2 s, (c) T=3 s.

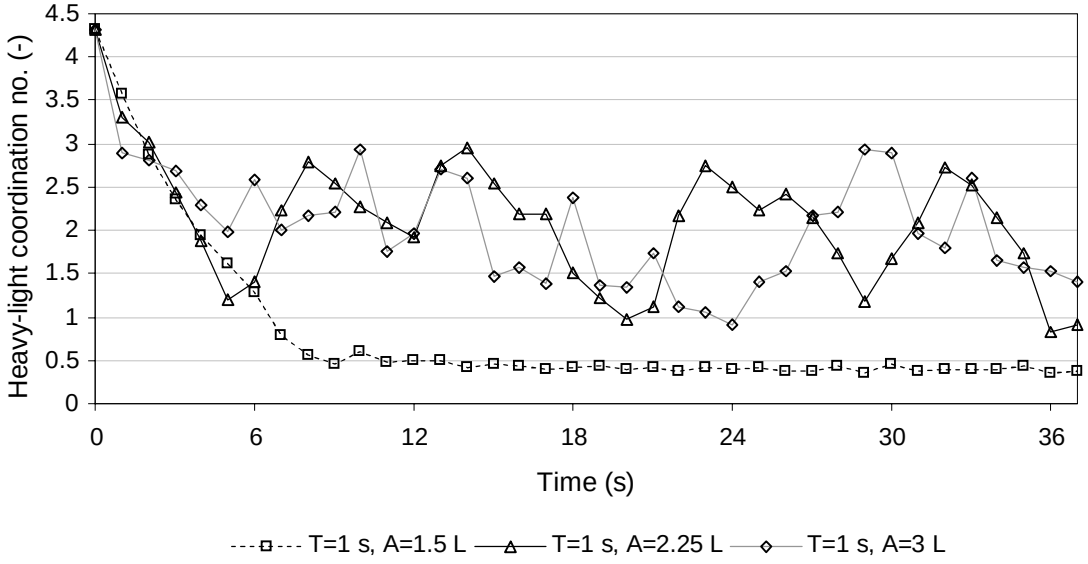
Heavy-light coordination no. (-)
4.5
4
3.5
3
2.5
2
1.5
1
0.5
0
0
6
12
18
24
30
36
Time (s)
T=1 s, A=1.5 L
T=1 s, A=2.25 L
T=1 s, A=3 L

(a)

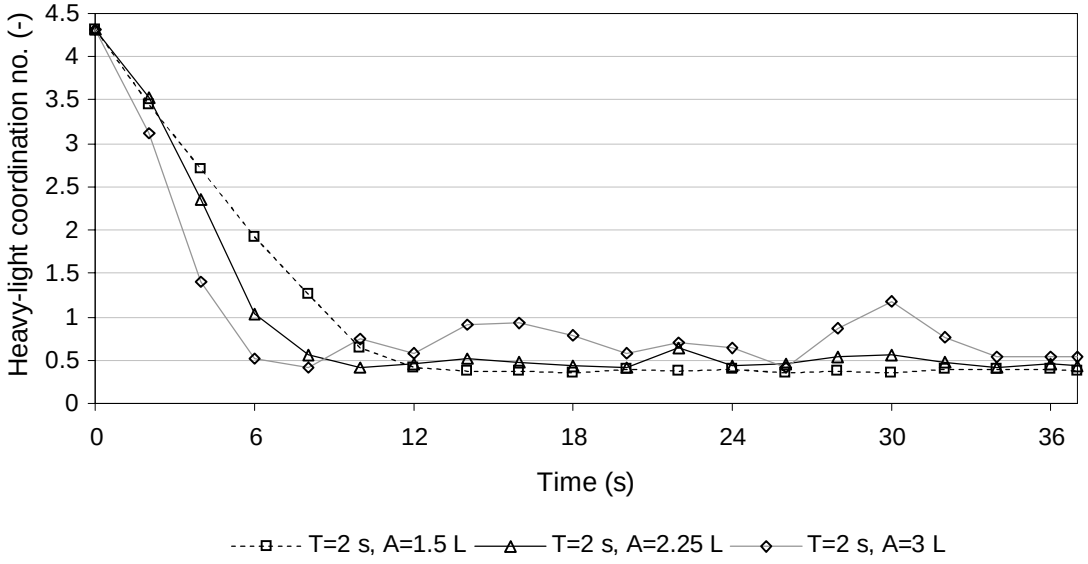
Heavy-light coordination no. (-)
4.5
4
3.5
3
2.5
2
1.5
1
0.5
0
0
6
12
18
24
30
36
Time (s)
T=2 s, A=1.5 L
T=2 s, A=2.25 L
T=2 s, A=3 L

(b)

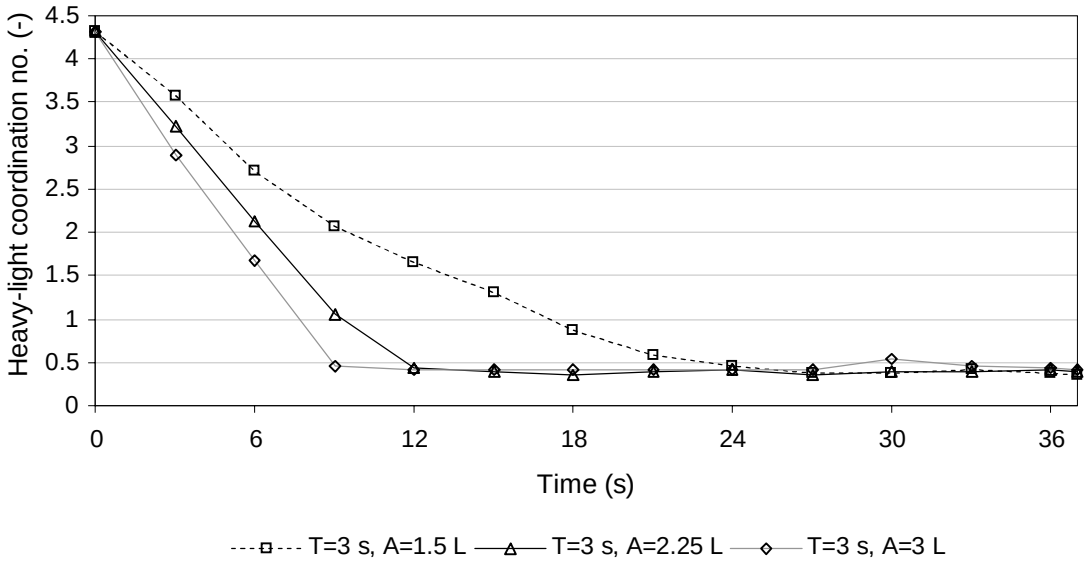

(c)

Figure B–3. Packed bed coordination number values for all trapezoidal profile variants (a) T=1 s, (b) T=2 s, (c) T=3 s.

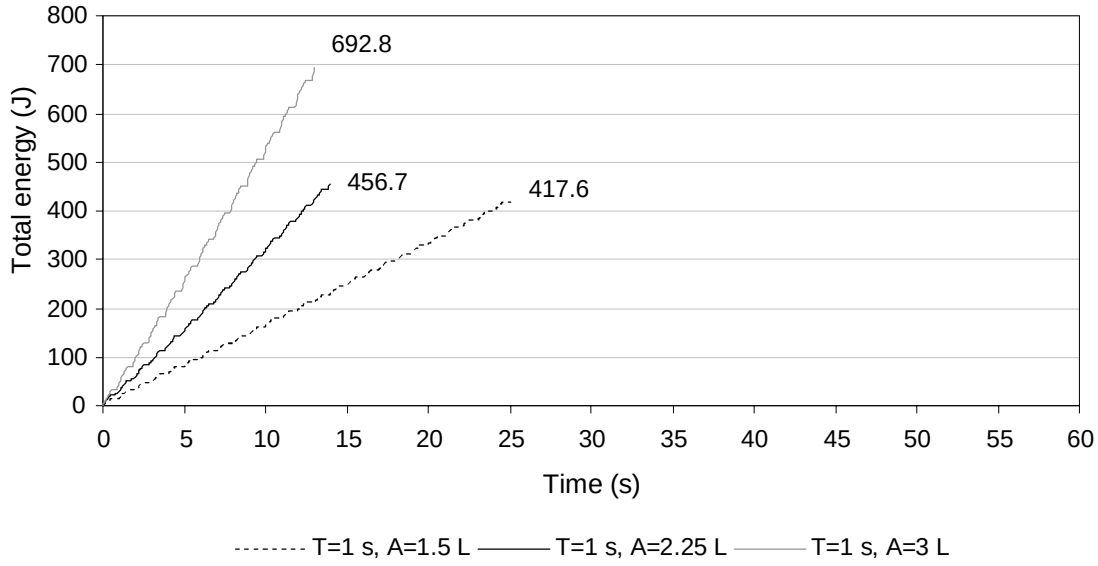
800
700
600
500
400
300
200
100
0
Total energy (J)
692.8
456.7
417.6
0
5
10
15
20
25
30
35
40
45
50
55
60
Time (s)
T=1 s, A=1.5 L
T=1 s, A=2.25 L
T=1 s, A=3 L

(a)

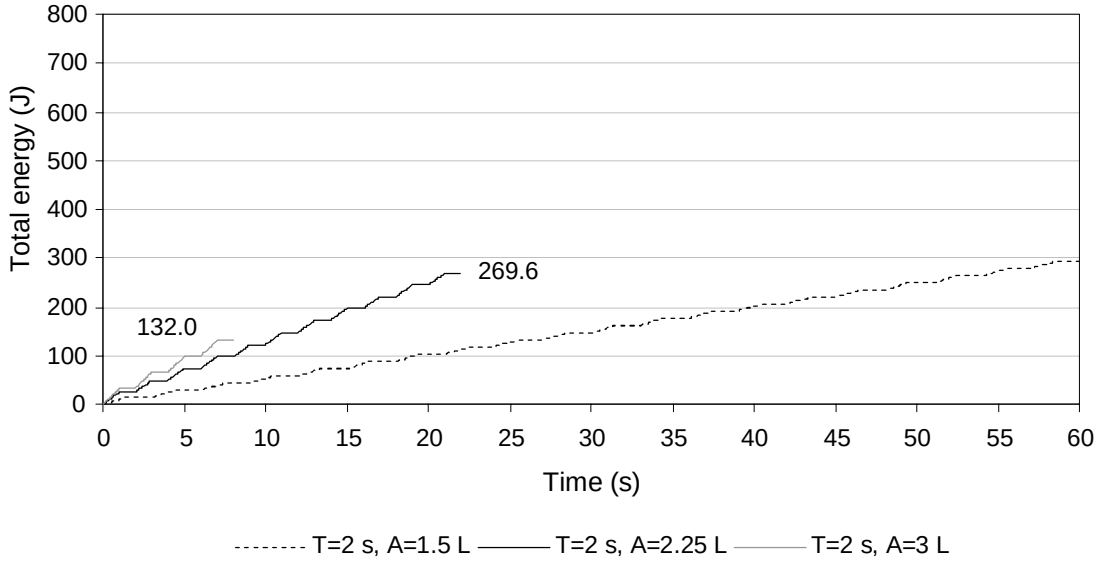
800
700
600
500
400
300
200
100
0
Total energy (J)
269.6
132.0
0
5
10
15
20
25
30
35
40
45
50
55
60
Time (s)
T=2 s, A=1.5 L
T=2 s, A=2.25 L
T=2 s, A=3 L

(b)

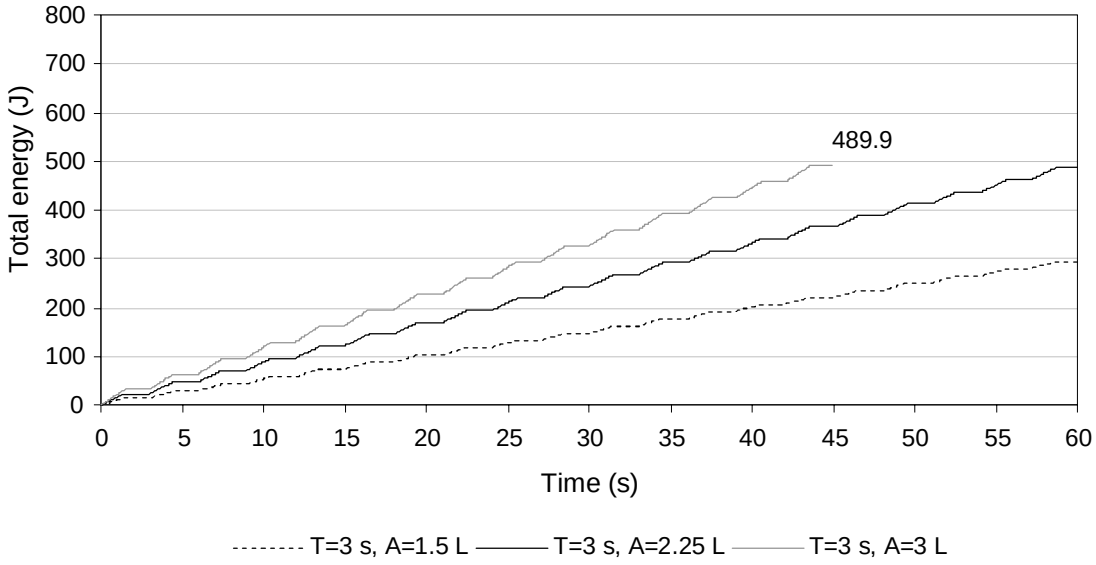

(c)

Figure B–4. Total energy for all triangular variants

(a) T=1 s, (b) T=2 s, (c) T= 3s.

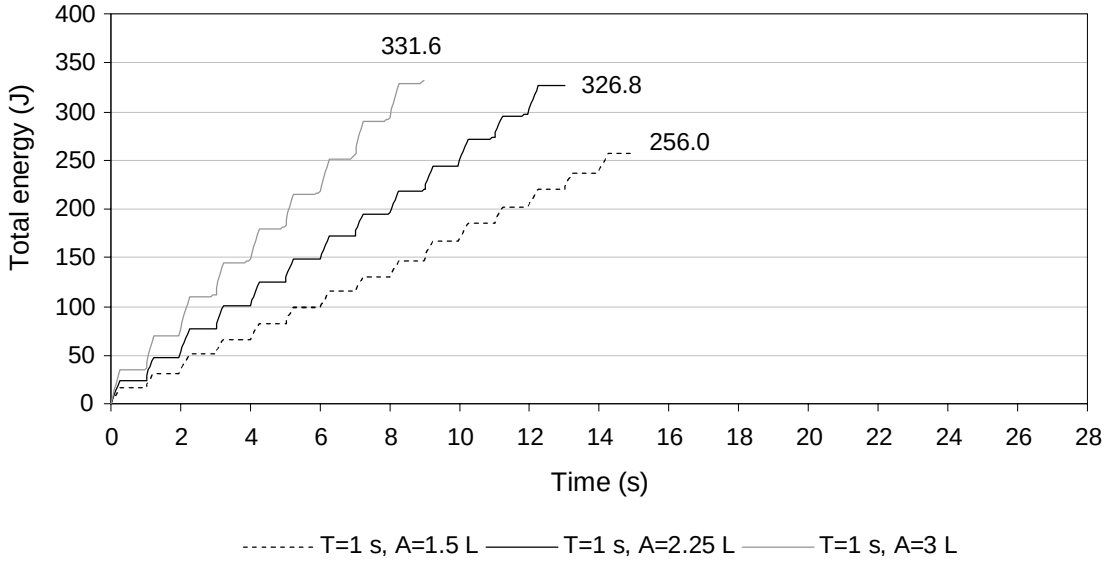
Total energy (J)
Time (s)
331.6
326.8
256.0
T=1 s, A=1.5 L
T=1 s, A=2.25 L
T=1 s, A=3 L

(a)

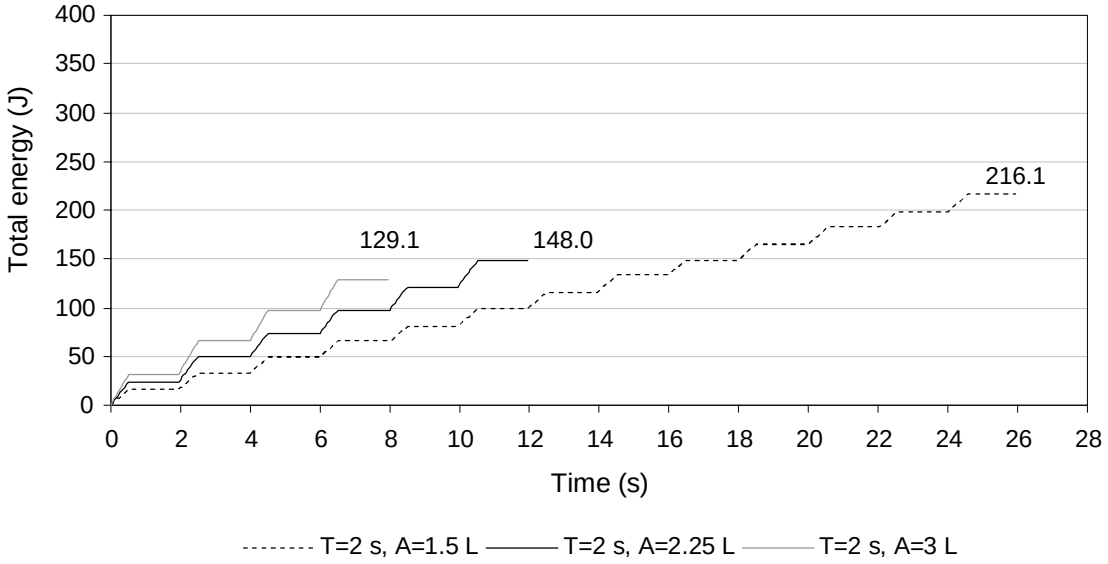
Total energy (J)
Time (s)
216.1
129.1
148.0
T=2 s, A=1.5 L
T=2 s, A=2.25 L
T=2 s, A=3 L

(b)

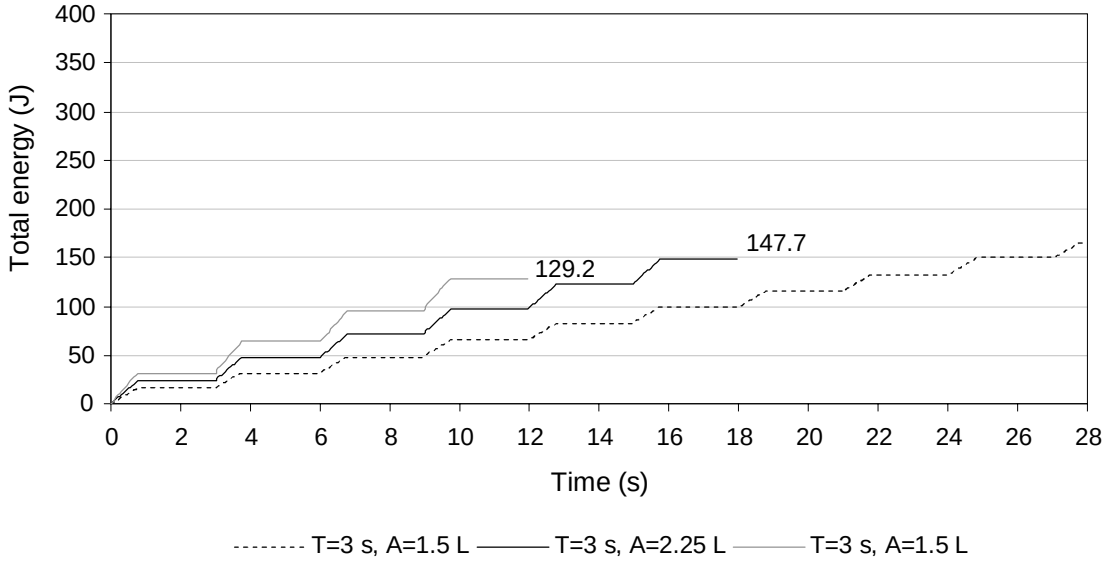

(c)

Figure B–5. Total energy for all sawtooth-backward variants
(a) T=1 s, (b) T=2 s, (c) T= 3s.

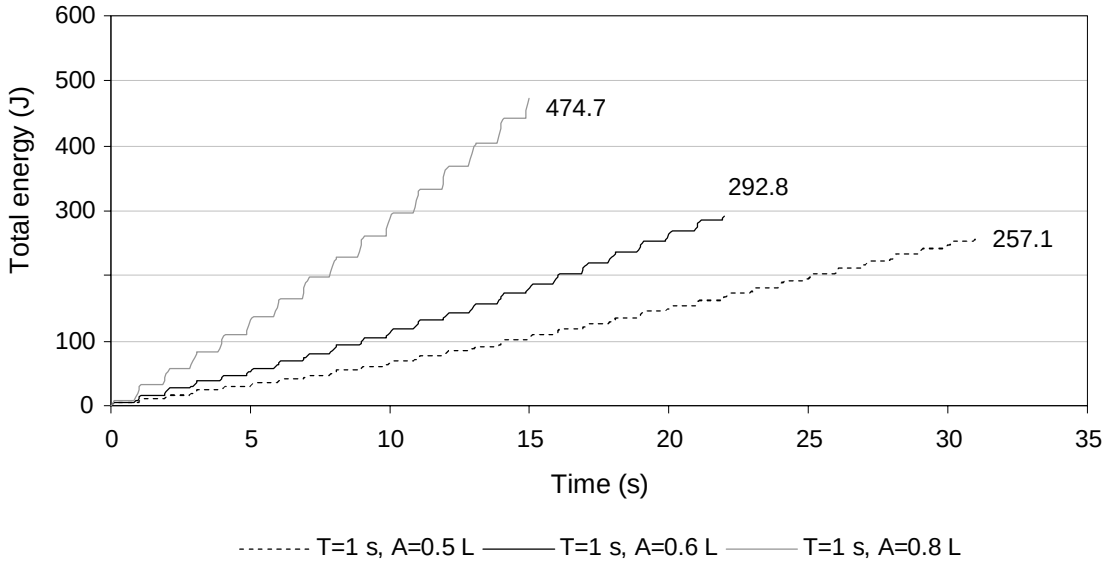
600
500
400
300
100
0
Total energy (J)
474.7
292.8
257.1
0
5
10
15
20
25
30
35
Time (s)
T=1 s, A=0.5 L
T=1 s, A=0.6 L
T=1 s, A=0.8 L

(a)

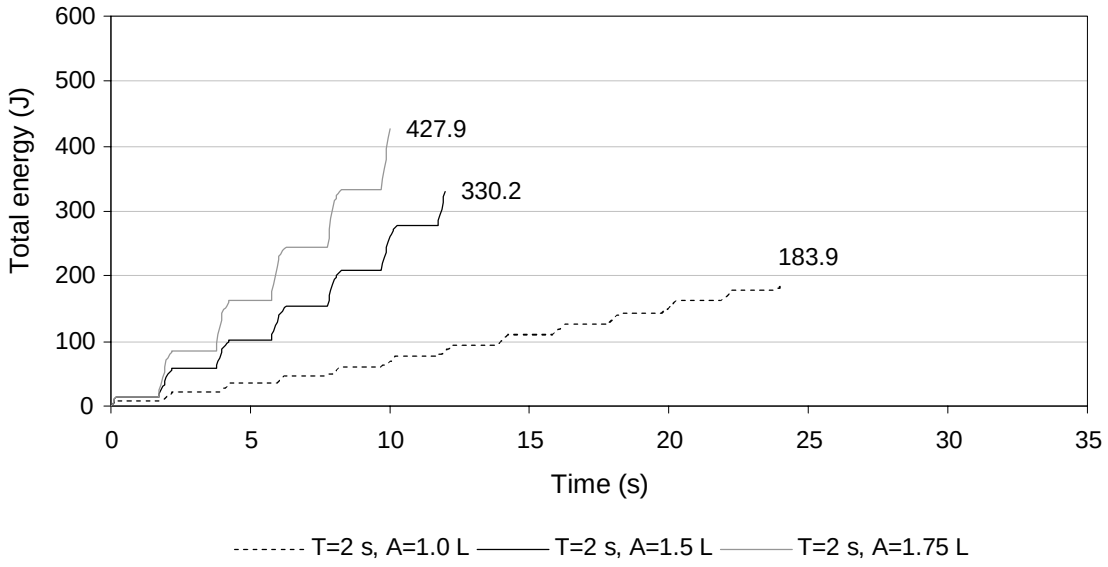
600
500
400
300
200
100
0
Total energy (J)
427.9
330.2
183.9
0
5
10
15
20
25
30
35
Time (s)
T=2 s, A=1.0 L
T=2 s, A=1.5 L
T=2 s, A=1.75 L

(b)

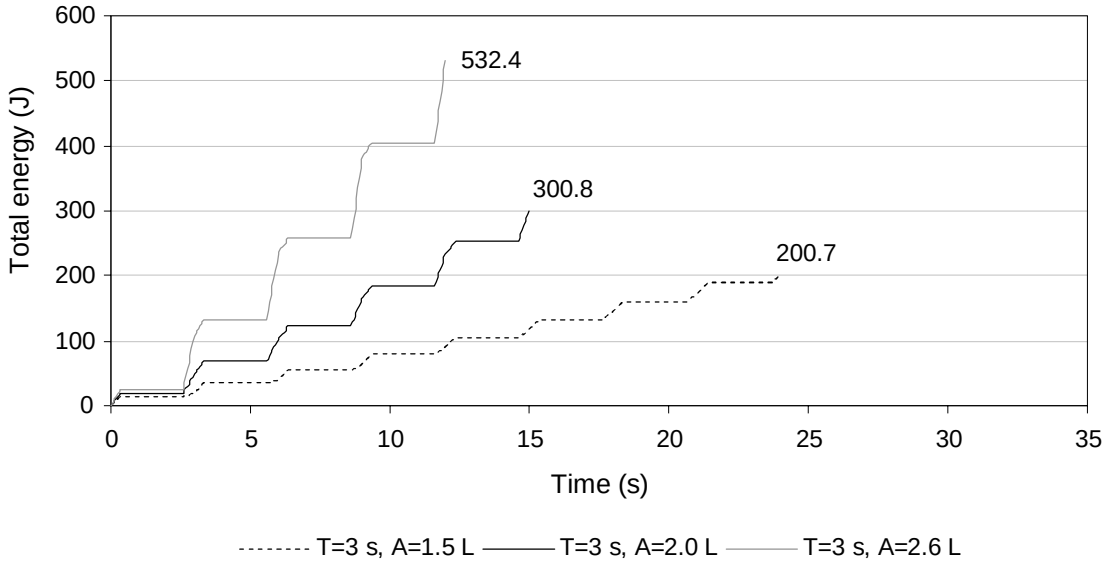

(c)

Figure B–6. Total energy for all trapezoidal variants
(a) T=1 s, (b) T=2 s, (c) T= 3s.

APPENDIX C

LIST OF PUBLICATIONS

JOURNAL PAPERS:

1. S. Viduka, Y. Feng, K. Hapgood and M.P. Schwarz, “CFD-DEM investigation of particle separations using sinusoidal jigging profile”, Advanced Powder Technology. (invited paper/accepted)

* Further papers will be or have been prepared for publication based on Chapter 2, 4 and 5. As the PhD candidature ceased after 3.5 years these could not be completed/accepted in time for inclusion.

CONFERENCE PAPERS (FULLY REFEREED):

2. S. Viduka, Y. Feng, K. Hapgood and M.P. Schwarz, “CFD-DEM investigation of particle separations using a trapezoidal jigging profile”, Proc. of the Ninth International Conference on CFD in the Minerals and Process Industries CSIRO, December 10-12, 2012, Melbourne, Australia. (accepted)

3. S. Viduka, Y. Feng, K. Hapgood and M.P. Schwarz, “CFD-DEM simulations of a sawtooth jigging profile on particle mixtures”, Proc. of the XXVI International Mineral Processing Congress, September 24-28, 2012, New Delhi, India, p. 1409–1022.

4. S. Viduka, Y. Feng, K. Hapgood and M.P. Schwarz, “CFD-DEM investigation of particle separations using sinusoidal jigging profile”, Proc. of the 5th Asian Particle Technology Symposium, July 2-5, 2012, Singapore, p. 328–342.

5. S. Viduka, Y. Feng, K. Hapgood and M.P. Schwarz, “Discrete particle simulation of particle separation in a jigging device”, Proc. of the 4th Conference on Industrial Fluidization-South Africa, November 15-17, 2011, Gauteng, South Africa, p. 175–191.

AWARDS:

2012 XXVI International Mineral Processing Congress Young Author Award.